In presenting the dissertation as a partial fulfillment of the requirements for an advanced degree from the Georgia Institute of Technology, I agree that the Library of the Institute shall make it available for inspection and circulation in accordance with its regulations governing materials of this type. I agree that permission to copy from, or to publish from, this dissertation may be granted by the professor under whose direction it was written, or, in his absence, by the Dean of the Graduate Division when such copying or publication is solely for scholarly purposes and does not involve potential financial gain. It is understood that any copying from, or publication of, this dissertation which involves potential financial gain will not be allowed without written permission.

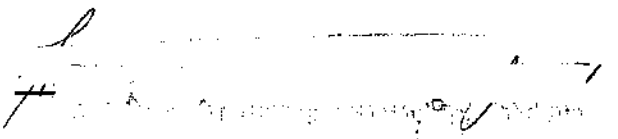

7/25/68

AN INVESTIGATION OF THE DEVELOPMENT OF SKIN FRICTION OF DRILLED PIERS IN DECOMPOSED ROCK

A THESIS

Presented to

The Faculty of the Division of Graduate

Studies and Research

by

Francis Xavier Watson

In Partial Fulfillment

of the Requirements for the Degree

Doctor of Philosophy

in the School of Civil Engineering

Georgia Institute of Technology

December, 1970

AN INVESTIGATION OF THE DEVELOPMENT OF SKIN FRICTION OF DRILLED PIERS IN DECOMPOSED ROCK

Approved:

Chairman

Date approved by Chairman: February 15, 1971

ACKNOWLEDGMENTS

The author would like to express his sincere appreciation to Dr. Richard D. Barksdale for his assistance and guidance as chairman of the thesis committee and as chairman of his Doctoral Program Committee. Special thanks are also due to Professors George F. Sowers and Billy B. Mazanti who served on the reading committee and who offered valuable advice throughout the investigation.

The efforts of many private concerns involved in this study are also greatly appreciated. McKinney Drilling Company provided the men and equipment necessary for the 12 piers used in the study. Law Engineering Testing Company performed the exploratory soil test borings. Dames and Moore provided sampling and laboratory equipment for the study and numerous test results from previous studies. MacDougald Warren provided the necessary quantities of concrete.

The author is also appreciative of the technical assistance provided by Mr. Roland Brown, Mr. Charles Pavey, and Mrs. Rena Bond during the course of this study.

This study was performed under a NDEA Title IV fellowship which provided the financial assistance that made the author's graduate study possible and for which he is very grateful.

Finally, the author wishes to thank the members of his family, especially his wife and daughters for their assistance, encouragement, and patience while performing graduate studies.

TABLE OF CONTENTS

LIST OF TABLES

LIST OF ILLUSTRATIONS

Figure Page

Figure | Page

SUMMARY

This investigation was made to study the load-carrying characteristics of drilled-in piers in decomposed rock with particular emphasis on the development of skin friction forces. Seven 18-inch diameter, straight shaft, instrumented test piers were installed in weathered rock to investigate the load distribution pattern throughout the length of the concrete piers.

The test site is located in Atlanta, Georgia, which lies in the Piedmont Physiographic Province of the eastern United States. The test piers were installed in heterogeneous weathered rock consisting of silty sands and sandy silts with stringers of less weathered rock. The parent material for the weathered rock is predominately gneiss, but had frequent intrusions of quartz seams and other rock types throughout. The average standard penetration resistance was found to be approximately 27 blows per foot to a depth of 35 feet. The ground water table was found to be approximately 28 feet below the ground surface.

Four of the piers tested were designed and constructed to develop their ultimate capacity in a combination of skin friction and end bearing. Two of these piers were 15 feet and the other two were 22 feet long. The remaining three piers were 20 feet long and were constructed to develop their ultimate capacity through skin friction alone. Two of the friction piers were tested with axial compressive forces and the remaining pier was tested in tension to determine the uplift capacity of a straight shaft drilled pier.

The review of literature indicates the lack of agreement between previous investigations and illustrates the many variables involved in the determination of the load carrying capacity and settlement relationships for deep foundations. The available theoretical and field test results are compared to the results obtained from prototype testing of drilled piers in decomposed rock and to those from an axisymmetric elastic finite element computer solution.

The manner in which the load was transferred from the drilled piers to the surrounding soil was investigated by the use of AS-9 concrete embedment strain gages placed at various locations in the open shaft prior to concreting. From these measurements the rate and amount of load transfer can be calculated for a particular load when the load at one of the gages is known. The load difference was used to determine the average shear stress along the circumference of the circular shaft, a portion of which is directly related to the lateral earth pressure. Once the lateral earth pressure was calculated, the lateral earth pressure coefficient was computed using the soil strength values determined from laboratory testing. The coefficient of lateral earth pressure was found to vary considerably throughout the length of the pier and was a function of applied load, number of loading cycles, magnitude of load during a load cycle, previous stress history and length of each pier. The average value of the coefficient of lateral earth pressure was found to decrease rapidly with depth and to be approximately inversely proportional to the square of the depth of embedment. These values for the coefficient of lateral earth pressure were checked

using a finite element computer program for an elastic material. The computer results showed similar variations for the coefficient of lateral earth pressure for stress levels in the elastic range.

The load tests performed for this study indicated that 80 per cent of the load, at approximately the ultimate pier capacity, or impending failure, is carried by skin friction. The finite element program and the review of literature shows that the percentage of the ultimate load carried by skin friction increases with depth to a certain point and then remains approximately constant. The results of the finite element analysis showed also that in the elastic range 80 per cent or more of the applied load was carried by skin friction for depth to diameter ratios greater than five. The results of the field tests and computer study show that the percentage of load carried by the base of the pier is a function of the pier geometry and deformation characteristics of the soil and pier. The base load is also influenced by the previous loading history of the pier and settlement characteristics of the soil directly beneath the pier.

This study showed that the settlement of drilled piers is a function of applied load, geometry and material properties. Most significantly, it was determined that pier settlement may be estimated if the ultimate and working loads are known for piers in weathered rock. The amount of settlement at the failure load for the field tests was less than 0.25 inches in all cases.

The field results indicate that piers deriving their load carrying capacity by a combination skin friction and end bearing do

not settle as much as piers deriving their load carrying capacity from skin friction alone. This study indicated that the bottom bearing capacity of small diameter piers could not be predicted adequately with existing theories since the bottom probably could not be cleaned properly in the 18-inch shafts prior to concreting.

The data obtained from this study was compared to previous research and a design procedure was established for determining the ultimate load carrying capacity and settlement of drilled-in piers in weathered rock. The design procedure for determining the ultimate capacity utilizes a field test procedure to determine the limiting average coefficient of lateral earth pressure and neglects the end bearing capacity for small diameter piers, which cannot be cleaned properly. Design curves are presented to correct for different length piers. The settlement is then computed utilizing the curves presented. The curves for the analysis of settlement are also compared to load deformation curves from drilled piers in other soils to establish a more general criteria.

CHAPTER I

INTRODUCTION

A drilled-in pier may be defined as a deep foundation which permits carrying a load imposed by a structure to firmer materials at some depth below the surface without displacing the soil during construction. The use of piers is a relatively new method of constructing foundations. Probably the first use of piers, also termed caissons or Chicago Wells, was for the Chicago Stock Exchange in 1894 (1)*. The design and construction of these piers was accomplished by General Sooy Smith using manual methods similar to those used at that time for well construction. For this reason this type of foundation was originally called excavation wells. "Caissons" are what the laborers used to call this kind of foundation and that term is still used today to denote a pier foundation which retains its casing after placement of the concrete.

At that time a caisson was defined as a foundation in which a shell, box or casing was placed into the ground as excavation proceeded (2). The method of constructing these caissons involved digging a hole with minimum diameter of four feet and placing sheeting as soon as five feet four inches had been excavated below the previous sheeting. The method of constructing caissons, described above, is now called the

---

*Numbers in parentheses and underlined refer to references given in the Bibliography.

Chicago Method and is essentially the same method used by General Sooy Smith. The Gow Caisson, originated in Boston by Charles R. Gow, is similar to the Chicago caisson except that a telescoping steel shell is used instead of wood lagging (3). Both Gow and Chicago caissons may be constructed with an enlarged base, called a bell, which resembles a truncated cone. Manual methods were employed for construction of both the Gow and Chicago caissons. For this reason they had to be large enough to accommodate at least one person. At the same time, the caisson had to be kept free of water. In most cases this limited the depth of excavation to the water table in permeable soils and to several feet below the water table when dewatering methods were not used in less permeable soils.

Since the advent of mechanical construction equipment, several other types of caissons have developed. For very large structures, such as bridges, the foundations may be built above ground and then sunk through the soft overlying soils by excavating the soil to form a hollow interior. The weight of the structure itself causes the sinking when the interior material has been excavated. This type of foundation is known by several names which vary according to the conditions during construction. A pneumatic caisson is one in which air pressure is used to keep the interior of the prefabricated structure dry to permit men and equipment to excavate the interior soil. When a caisson is placed entirely in water by this method it is called a floating caisson. A floating caisson may be excavated under water by clam shell buckets or cleaned out in the dry using men and machinery by continually pumping

out the water or by keeping out the water with increased air pressure. Floating and/or pneumatic caissons have been constructed in many parts of the world (cf., 4, 5, 6, 7, 8, 9, 10, 11).

A foundation similar to the floating caisson can be installed completely on land. This is done by erecting the exterior structural walls (foundation walls) as the interior soil material is excavated, causing the structure to sink into the ground. The slip forming method of constructing reinforced concrete has led to the successful application of this type of caisson construction in Europe and Asia (12, 13).

Recent innovations in construction equipment have led to the development of two other types of caissons. A Benoto caisson is constructed by forcing a steel shell into the ground with a combination of steady downward pressure and back and forth rotation about the caisson's longitudinal axis. When the shell has partially or completely penetrated into the ground the interior soil is removed by an orange peel bucket (14). A drilled-in pier is formed by rotating a cork screw type auger blade into the ground. When the auger blades become filled with the soil, the auger is lifted completely out of the ground and rotated at a high speed to remove the loose soil. In cases where the soil cannot be removed by rapid rotation, the auger is cleaned by a laborer. Drilled piers are excavated in this manner to the desired depth or until auger refusal is reached. A steel casing may be temporarily placed in the hole to prevent collapse of the sides or left uncased, depending on the soil conditions and the depth of the hole. With either the Benoto caisson or drilled pier the bottom may

enlarged to form a bell, or a socket may be cut into the underlying rock either manually or by special machinery.

The caisson and pier types of foundations have developed into a commonly used method of transmitting the structural load to a material capable of supporting the foundation loads, since its introduction in the late 19th century. The brief description above has shown the main types of caissons and similar foundations which are in use today. The innovation of mechanical equipment has increased the popularity of caisson and pier foundations and has made them an economic foundation alternative in many instances.

Since the beginning of the 20th century the trend has been to make buildings higher, insteader of wider, because of the cost of land and the lack of large areas in metropolitan centers. These larger buildings impose greater loads than ever before on the foundation. Fewer caissons or piers can be used to support these large superstructure loads than conventional piling. Caissons and piers offer many added advantages: They may be inspected at the bottom to visually determine the bearing material. They can be constructed manually in locations where vertical clearance is limited. They can also be constructed without any damaging ground vibrations with mechanical augering equipment. Caissons and piers are used to transit superstructure loads to a more desirable strata to reduce settlement, increase bearing capacity, or reduce the effect of swelling soils.

The drilled pier type of foundation has been used throughout the world for a variety of purposes. Although they are used chiefly to

support the load of a superstructure resting upon them they have also been successfully used for anchors for tie back bracing systems (15, 16), excavation retaining walls (17) and spikes or keys to halt earth movement (18).

Although the drilled pier is commonly used in many ways, its primary purpose is to support the structure. In areas where there are unusual or undesirable soil conditions, such as those found in the Atlanta area, the drilled pier provides a dependable, economic way to support the heaviest of structures.

Soil and Foundation Conditions in the Atlanta Area

Atlanta is located in the southern Piedmont geologic and physiographic region. The Piedmont region is a broad strip extending from central Alabama across Georgia, the Carolinas, and Virginia, and tapering out to an end in the vicinity of Baltimore and Philadelphia (19). The entire region is underlain by crystalline rocks formed by the metamorphism of igneous rocks and ancient sediments. Igneous rocks have repeatedly intruded the metamorphosed schists and gneisses, producing an "injection complex" (20). The intruded igneous rocks are generally granites, amphibolites and diabases which typically form bands 300 feet or greater in width (19). In most cases the intruded rocks form very irregular patterns in the parent rock. Because of the metamorphism and igneous injection, the rock minerals are separated into narrow bands which have been contorted by various geologic processes which include faulting and folding.

The soils in the Piedmont area are generally formed by the inplace weathering of the rock complex or by the deposition of materials eroded from higher elevations. The mild climate and high annual rainfall cause chemical weathering to proceed at a high rate. Chemical weathering is intensified by the many faults and fissures in the rock which permit the water to easily percolate along these discontinuities below the ground surface. The indigineous rock is extremely variable in composition due to intrusions, and has often left resistant dykes or stringers surrounded by a residual soil matrix of silty sand, or sandy silt.

The soil in the Atlanta area is generally less weathered at greater depths except for the stringers of materials which resist weathering. A general soil profile consists of three zones distinguished by the degree of weathering, with the two uppermost zones being completely weathered rock which are now discrete particles. The uppermost zone has undergone the most complete weathering with the soils in the uppermost zone being generally red sandy silts that are quite stiff because of leaching and dessication. Below this zone the soils are not completely weathered, as indicated by zones of partially decomposed feldspars and micas. The lower most zone is the least weathered of the soils before competent rock is encountered. In this zone frequent stringers and lenses of resistant rock, such as quartizite, are found in a matrix of softer decomposed rock which has weathered into a sandy silt or silty sand.

Foundations for structures can be placed in any of these zones or on competent rock. The loads from light structures may be placed on the uppermost zone, which is usually dessicated; but resulting settlement of the underlying compressible sandy silt layer may cause damage to the structure. The soil in the middle zone may be used to support very light structures. The soil in this zone can be quite variable, weak and compressible which may lead to harmful differential settlement for heavier structures. Heavier structures are usually supported by deep foundations which derive their support from the partially weathered zone or bear directly on bedrock. In Atlanta, the partially weathered zone or bedrock may be found at the surface but is generally at some variable depth below the surface.

Since the soil and bedrock in the Atlanta area is quite variable, drilled piers are often used to carry the superstructure loads to a competent material. The sound bedrock in the Atlanta area is very strong, and an allowable bearing stress of 100 KSF is not uncommon for this material. In many instances it is, however, necessary to cut through partially weathered and fractured rock before rock of sufficient quality is reached. This material cannot always be excavated with the auger, or even with different rock bits which have been developed, but must in many instances be excavated by hand with or without the use of explosives.

Different types of piles can also be used to support heavy structures, but it is impossible, in most cases, to be certain that these piles are not bearing on a thin resistant stringer of hard rock.

With the drilled pier and caisson type of foundations the bottom material and the material below can be inspected to assure that end bearing is not obtained on an isolated resistant dyke.

In the Atlanta area drilled piers are customarily designed to carry the ultimate load in end bearing on the inherently strong bedrock. The use of skin friction alone to support drilled piers has been made only occasionally in the Atlanta area (22). Drilled piers, supported primarily by skin friction, have been used in other locations in the Piedmont geologic region (21, 73) and on the west coast of the United States (23, 24).

The particular type of caisson most commonly constructed in the Atlanta area is called a drilled pier. It can be constructed most economically if the work is done by machine augering, using manual labor only to clean the auger trimmings from the bottom of the pier.

The purpose of this thesis is to evaluate the combined capacity of a drilled pier in skin friction and end bearing and to formulate a design procedure for drilled piers in the weathered rock zone immediately above bedrock. Particular emphasis is placed on the way the load is transferred from the pier to the soil as the pier is loaded to its ultimate capacity. The load distribution pattern and total capacity will be compared to theoretical results and past research for other soils since there has not been any previous work on this subject for soils in the Piedmont region.

The results will also be compared with an elastic finite element computer solution which is used to extend the field test results to

include length and diameters other than those tested as part of the field testing program for this thesis. The elastic finite element computer program also enables the elastic soil properties to be varied. This permits the load carrying capacity of piers to be estimated for other soils.

The load distribution pattern was investigated using electric strain gages placed in the concrete. As the drilled piers were loaded up to failure with a hydraulic jack the strain gages were read at certain time intervals for each load. Testing in this manner, both the ultimate load-carrying capacity and vertical stress distribution patterns were obtained. Using the vertical stress distribution pattern it is possible to determine the amount of load transferred to the soil through skin friction at each load level. This permits the evaluation of the skin friction capacity of a drilled pier in weathered rock.

This thesis presents the results of seven load tests on prototype drilled piers in weathered rock. The results are compared with existing theoretical solutions and a procedure is recommended to predict the ultimate capacity and short term settlement of drilled piers in weathered rock. The available theories and the elastic finite element computer solution will be used to extend the design procedure to drilled piers having lengths and diameters different from those tested as part of this thesis.

CHAPTER II

REVIEW OF LITERATURE

Introduction

Contractors and engineers have been using various types of open shaft deep foundations, including drilled piers to support heavy structures for the past 70 years. The increased use of drilled piers has fostered an increase in the amount of research being done to determine their ultimate capacity. Unfortunately, very little of this research has been done in saprolitic soils such as those found in the Atlanta area.

Little work has been performed to evaluate the distribution of the shearing stress along the sides of drilled piers. Some of the research (29, 36) has consisted of measuring the bottom load and the load applied to the top of the pier being tested. The difference between these two loads is then the load transmitted to the soil through skin friction. Tests to evaluate skin friction capacity have also been performed in which end bearing was not possible because of some compressible material such as sawdust, steelwool and mineral wool which was placed in the ground before pouring the pier (21, 23).

Frictional resistance of drilled piers has been estimated when the ultimate bottom load was predicted from plate load tests at the base level (25). This ultimate bottom load was obtained from plate bearing tests performed at the desired levels. The load transmitted to

the soil before it reached the bottom of the pier is then assumed to be equal to the ultimate load less the ultimate plate bearing load adjusted to consider the relationship between the diameter of the plate used and the diameter of the bottom of the caisson.

The approximate evaluation of the base carrying capacity of a deep circular foundation may be estimated by the following formulas (25):

For Clays:

$$Q_{bu} + W_b = A_b(N_c C_u + \bar{\gamma} D) \qquad (1)$$

where Q_{bu} = ultimate net applied load at base.

W_b = weight of caisson reaching base.

A_b = area of base.

N_c = bearing capacity factor.

C_u = undrained shear strength (cohesion of soil).

D = depth of embedment in soil.

$\bar{\gamma}$ = average effective soil density to depth D.

For Sands (26):

$$Q_D = A_b(1.3cN_c + \gamma_1 D_f N_q + 0.6R\gamma N) \qquad (2)$$

where Q_D = load on pier (weight of pier included) required to produce failure.

$N_c N_q N_\gamma$ = bearing capacity factors (after Terzaghi).

c = cohesion of soil.

D_f = depth of embedment.

γ = average effective density to depth D_f.

γ_1 = increased density due to shear stresses.

Equations 1 and 2 are for the short term end bearing capacity of a deep circular foundation. The development of these equations and the theoretical limitations are presented in Chapter III. The bearing capacity of a deep pier in soil, however, is not the only consideration. Deformation characteristics of the soil-pier system must also be evaluated to determine the desirability of drilled piers in soil, since very often the working capacity is determined on the basis of settlement limitations.

The method of determining the ultimate carrying capacity and settlement of a drilled pier depends on the soil and rock in which it has been placed. Decomposed rock such as found in the Atlanta area exhibits both cohesion and intergranular friction. There has been only a limited amount of research pertaining to deep foundations imbedded in soils which develop their strength through cohesion and internal friction and none on soils resembling those found in the Atlanta area. The discussion of pier investigations in both clays and sands will show some of the relevant factors for each material which must be considered when a soil exhibits internal friction and cohesion. For this reason the review of literature on straight shaft, drilled piers will be separated according to soil classification. The discussion of the theoretical capacity of different types of circular deep foundations

will be discussed in Chapter III since their theoretical analysis is similar. The discussion below pertains only to pertinent theoretical and emphirical studies for drilled piers.

Drilled Piers in Clay

Drilled piers are constructed to transmit the load to some depth below the structure and in many cases directly to rock. This type of drilled pier is common in the northern United States, Canada and in Great Britain. A majority of the research done in predicting the capacity of drilled piers in clay has been performed in London, England. In London the predominant soil is a stiff fissured clay overlain by recent deposits of sands and in some locations, gravels of limited depth. The results of a number of investigations in the London clay have been presented in two symposiums on drilled piers (large bored piles) in the London area (27, 28). The field testing of drilled piers in clay has often led to the use of design formulas which are practically identical. The formulas all use or imply the use of a term called the adhesion reduction factor to express the skin friction in terms of the unconfined compressive strength of the clay. The adhesion reduction factor, α, is defined as the ratio of the adhesion to the average cohesion over a given pier depth. The adhesion reduction factor has been found to be less than unity and is generally reported to be between 0.25 and 0.65. The reduction in strength is probably caused primarily by the migration of water from the surrounding clay to the drilled hole during drilling and also from the introduction of water from the concrete. The reduction in strength may also be caused in part by the

drilling operation which requires continuous insertion and removal of an auger and in some cases insertion of a steel shell to keep the hole open during construction. The soil surrounding of the open excavation also expands during the drilling process. Thus, the drilling operation itself probably causes much of the softening around the hole. Therefore the adhesion reduction factor is controlled primarily by the construction technique, soil type, and climatic conditions, all of which must be considered when designing a drilled pier. The effect of local softening, due to water migration, disappears with time (25, 29, 33).

Whitaker and Cooke (29) have measured the load reaching the bottom of drilled piers by means of an electrical load cell. By positioning the cell in the bottom, the load in end bearing could be measured. This permitted evaluation of both the bottom bearing capacity and the total load transferred to the soil through skin friction. They determined that the ultimate bearing capacity of drilled piers in London clay could be expressed by the formula:

$$P_u + W = \pi d_s \alpha \bar{C} + \frac{\pi}{4} d_b^2 (N_e \omega C_b + \bar{\gamma} D) \qquad (3)$$

where d_s = shaft diameter.

α = adhesion coefficient = $C_a/\bar{C}$.

C_a = adhesion between concrete and soil.

$\bar{C}$ = average cohesion over a given depth.

d_b = base diameter.

N_c = bearing capacity factor at the base.

ω = ratio of the fissured strength of the clay measured on shear planes of large area to the mean strength of fissured clay determined from triaxial tests.

W = weight of concrete shaft.

$\bar{\gamma}$ = average density of soil over depth D.

D = depth to the pile base.

D_b = cohesion of soil below the base.

From their full scale tests of caissons 24.5" to 37" in diameter and from 26.0 to 50.0 feet deep, they found the values of $\alpha = 0.44$ and $\omega = 0.75$ apply when N_c is taken as 9. The adhesion reduction factor (α), bearing capacity factor (N_c) and ω were found to vary from test to test. The values given above are average values obtained from the tests performed on straight shaft and under-reamed drilled piers. They have found that the ultimate capacity of a circular drilled pier could be estimated fairly accurately using Equation 3. Equation 3 is identical to Equation 1 with modifications for the fissured strength of the clay and for the developed resistance in skin friction.

Some of the factors which affect the adhesion coefficient in London clay were also discussed by Burland, Butler and Dunican (25). They recommended a value for the adhesion coefficient of 0.30 for under-reamed drilled piers and 0.45 for straight shaft piers. They analyze end bearing and skin friction separately and assume that in a great majority of the cases a settlement of 1/4" will yield a maximum value of skin friction. Burland, et al., assume that at vertical displacements greater than 1/4" the load-carrying capacity in skin friction remains constant while the base capacity increases to its ultimate value.

The method of design proposed by Burland, et al., considers both load-carrying capacity and settlement. This is accomplished by using the load settlement curves from plate load tests and an assumed shaft load having its maximum value at 1/4" settlement and having an adhesion coefficient of 0.3 or 0.45.

The load tests performed on large bored piles (25, 29) showed that settlement was only an important consideration with under-reamed piles. Furthermore, Skempton (30) has noted from observation of numerous load tests on drilled piers that when the diameter of the base exceeds six feet the working load should be evaluated from settlement considerations. These results imply that both settlement and ultimate bearing capacity are considerations in the design of drilled piers in soil.

Utilizing the records of ten load tests on drilled piers in London clay, Skempton (31) observed that α varies from 0.3 to 0.6. The higher values were characteristic of less local softening caused by natural elements or water from the concrete. By plotting the adhesion vs. the average shear strength, he determines that $\alpha = 0.45$ in probably the best value for the data, with a limiting value of 2000psf for shaft adhesion. The ultimate capacity of the caisson was expressed by Skempton using the following formula:

$$Q_u = Q_p + Q_s = 9C_pA_p + C_aA_s \qquad (4)$$

where Q_p = end bearing capacity.

Q_s = skin friction capacity.

C_p = average shear strength for 2/3 of pier diameter below base.

A_p = area base.

C_a = average adhesion.

A_s = surface area of pier.

The end bearing capacity expressed in Equation (4) is identical to Equation (1) assuming that the bearing capacity factor (N_c) equals nine and that the weight of the soil removed is approximately equal to the weight of the concrete which replaces it so there is generally no serious fault involved in neglecting the weight of the soil removed. For deep circular drilled piers the actual value of N_c is found to vary widely, but it is generally assumed to be equal to nine as determined by theoretical considerations and field observations (25, 29).

The basic method of analysis of drilled piers in London clay is similar from one investigator to another. The major difference is in the selection of the adhesion reduction coefficient (α). In addition to the values discussed previously, other investigators have also empirically determined the adhesion reduction coefficient for drilled piers in clay (32, 33). Golder and Leonards (32) suggest a value of 0.7 for the adhesion coefficient for caissons greater than 30 feet in length. Meyerhof and Murdock (33) recommend a value of 0.3 for the adhesion reduction coefficient. Woodward, Landgren and Boitano (34) suggest an adhesion reduction factor of 0.49 to 0.52 based on load tests on drilled piers in stiff clay located in Lemoore, California. This factor corresponds favorably with the value of 0.45 obtained by

others (25, 29, 31). From the available results it seems appropriate to use an average value of the adhesion reduction factor of 0.45 for drilled piers in stiff clay. The value of cohesion obtained from undrained triaxial tests is thus multiplied by 0.45 to determine the shaft adhesion in clay.

Meyerhof (35) has performed an analytical study to determined the theoretical capacity in both end bearing and skin friction of a deep circular foundation. His results are given by the expression:

$$q_r = cN_{cqr} + K_s \gamma D \tag{5}$$

where c = average shear strength.

N_{cqr} = bearing capacity factor for a circular foundation.

K_s = coefficient of earth pressure on shaft within failure zone.

γ = average unit weight of soil.

D = depth of pile tip below ground surface.

q_r = bearing capacity.

Equation (5) is identical to those presented previously. A discussion of the theoretical aspects and limitations of the Meyerhof method of computing the capacity of deep foundations is presented in Chapter III.

The bearing capacity of a drilled pier is dependent on the roughness of the shaft as shown in Figure 1 for a perfectly smooth and a perfectly rough shaft. Since Equation (5) is representative of the

end resistance only, a modification to consider skin friction must be added. This modification is represented by a change in the bearing capacity factor (N_{cqr}) as shown on the right-hand side of Figure 1.

DuBose (36, 37, 38) has also performed several field and laboratory tests on drilled piers and buried shafts in clay with diameters from 7 to 24 1/2 inches and length of up to 18 feet. His study revealed results which agreed fairly well with the values computed by the Terzaghi (26) equation:

$$Q_{tot} = \pi r^2(1.3cN_c + \bar{\gamma}D_fN_q + 0.6r\gamma N_\gamma) + 2\pi r f_s D_f \qquad (6)$$

where the values are described in Equation (2) with

f_s equal to the shearing resistance of the soil, and

r equal to the shaft radius for straight shaft, drilled piers.

The bearing capacity factors used are also from Terzaghi (26). DuBose also conducted a study to determine the effect of water migration through clay to an open hole. He determined that the strength loss due to water migration in the clay he used was insignificant.

According to Persons (24) the ultimate capacity of a pier may be computed with sufficient accuracy by formula six advocated by Terzaghi. This conclusion was reached by observing the test results of eight drilled piers in predominately clayey soils. Some of the piers utilized end bearing and skin friction for support, while others obtained their capacity through skin friction alone.

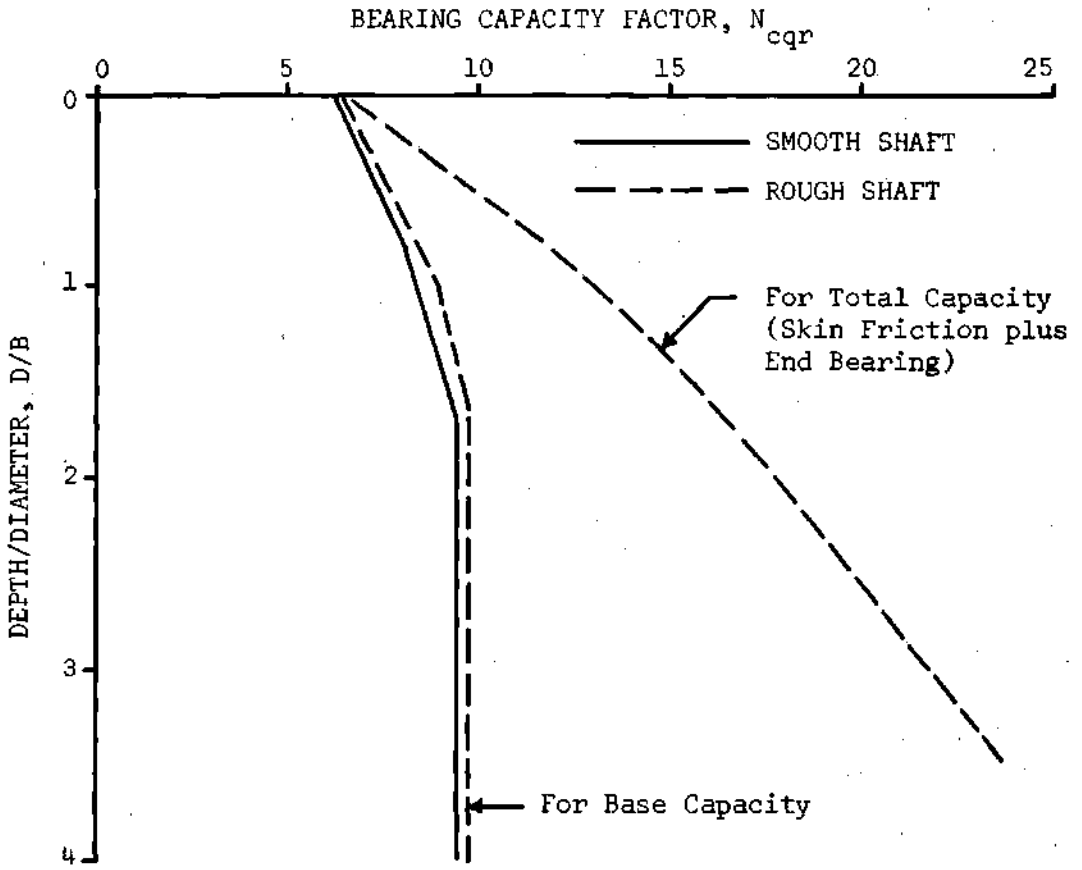

Figure 1. Theoretical Bearing Capacity Factors for Circular, Deep Foundations in Cohesive Soils (After Meyerhof (12)).

All of the methods discussed in determining the ultimate capacity of a drilled pier in clay are similar. For design considerations of a deep foundation of clay N_γ can be neglected, N_q can be assumed equal to unity, and N_c can be considered as having an average value of nine unless local conditions demand a modification (for example: fissured clay strength corrections). The ultimate base capacity is then expressed by Equation (2). The unit adhesion can be considered equal to 0.45 times the measured laboratory value for cohesion for computing the available skin friction resistance.

Drilled Piers in Sand

Meyerhof (35) has performed theoretical studies on piers in cohesionless soils. The resulting bearing capacity equation is:

$$q = \lambda \frac{\gamma D}{2} N_{\gamma q} \tag{7}$$

where $N_{\gamma q}$ is the resultant bearing capacity factor which depends on N_γ, N_q and the earth pressure coefficient. The shape factor, λ, depends on the angle of internal friction and the depth-diameter ratio of the pier.

Mohan, Jain and Kumar (39) have performed large scale instrumented load tests on cast-in-place concrete piles (drilled piers) in sands and silts of varied consistency. They observed:

> In the initial stages of loading, the load applied to the pile top is entirely taken up by skin friction, the top layers taking the maximum. As the load is generally increased, part of it is transferred to the toe. At a certain stage of loading, when the pile shears through the soil, any additional load applied to the

> top is directly transferred to the toe and the pile is then subjected to the maximum skin friction. This is also the state when friction is completely mobilized.
>
> It is observed that the frictional resistance offered to the pile in the initial stages increases to a certain depth, depending upon the load and then decreases. At the stage of ultimate friction, though the frictional resistance increases with depth, the rate of increase decreases approaching a negative value in the lower region near the pile toe. . . . A probable explanation for this reduction may be that the compression at the pile tip results in the development of a radial movement of the soil in the shear zone around the toe which reduces the lateral earth pressure.

The results of two tests performed are shown in Figure 2. These tests indicated that the coefficient of earth pressure is apparently unity at the toe and near the passive earth pressure value at the top. Based on their results they have developed an empirical method to predict the ultimate capacity of a drilled pier by use of the values obtained from the static cone test.

A theoretical correlation between the value of ultimate settlement and the extent of a sliding zone has been developed by Berezantev (40) to predict the failure load of deep (D/B > 4) foundation. Berezantev's theory showed that the boundary surfaces of a punching shear failure zone, which are inclined at an angle of 45° and cross the foundation edges, are reached by a horizontal sliding zone when the relative settlement (ratio of the settlement to the diameter) averaged 0.2 (Figure 5). Utilizing these data and plane strain theory for a long, deep foundation, he found the approximate allowable load for a deep circular foundation to be

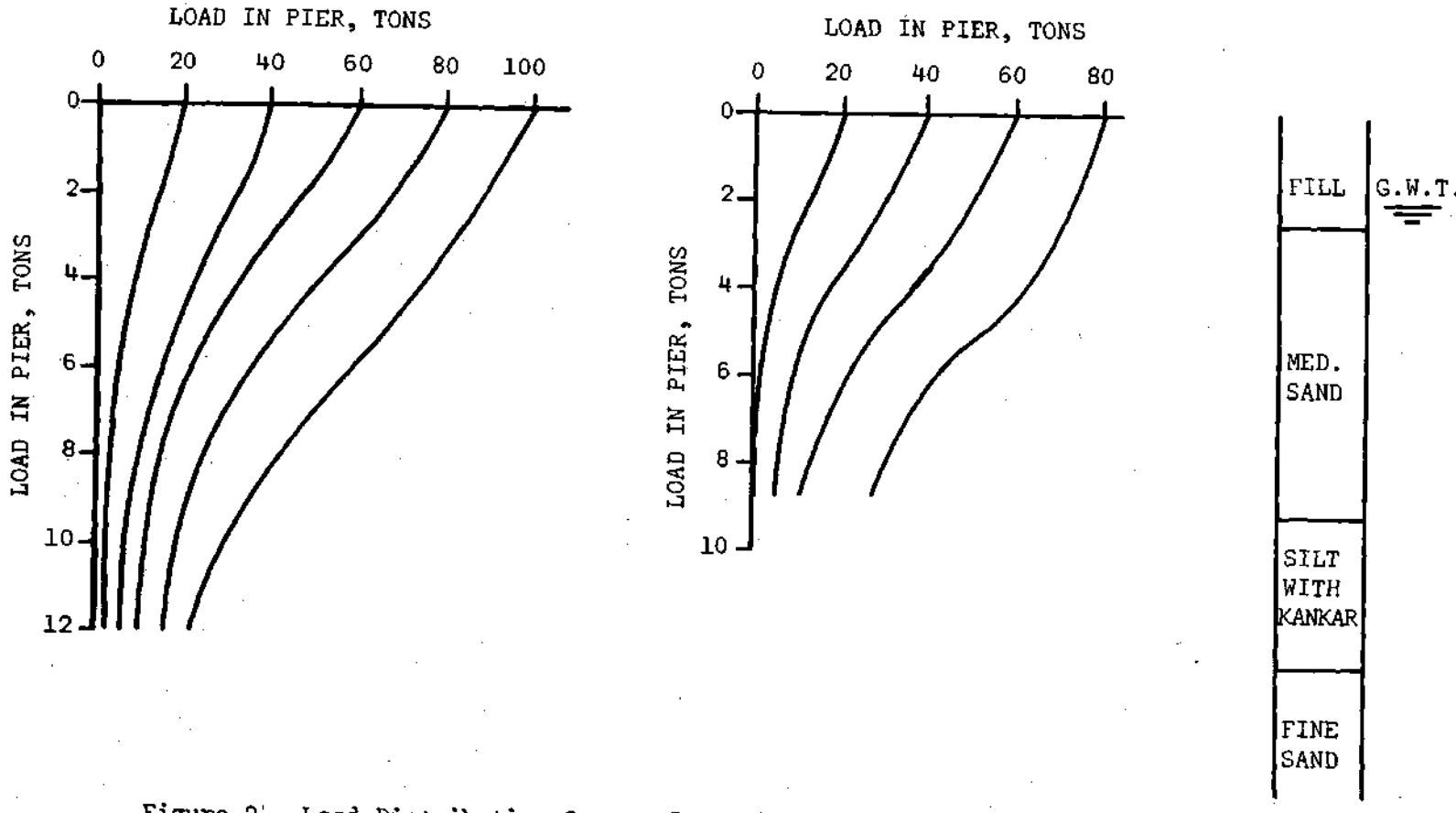

Figure 2. Load Distribution Curves for Drilled Piers (After Mohan et al., 39).

$$q_k = eN_k\gamma B \tag{8}$$

where q_k = allowable unit load.

e = reduction factor (0.6 to 0.7).

N_k = coefficient depending on depth to diameter ratio and the angle of internal friction.

γ = unit weight.

B = diameter of pier.

Berezantev's presentation assumes no skin friction and a horizontal boundary of the bearing capacity shear zone. This method is discussed more completely in Chapter III.

Vesic (41, 42, 43) has conducted theoretical, laboratory, and field studies on the bearing capacity of deep foundations in sand. The studies were performed using circular steel piles (buried and driven) up to four inches in diameter. He observed that the skin friction and bearing capacity increase linearly to some depth, after which the total capacity is dependent on the relative density of the sand alone. The skin friction was also found to reach a constant value at a depth exceeding approximately 15-20 diameters, depending on the relative density of the sand. According to Vesic this occurs because the overburden pressure at depths greater than about four diameters may be less than the unit stress caused by the overburden soil due to arching in the sand. At depths between 4 and 20 diameters the effect of arching may partially counteract the overburden stress. Vesic's tests show that at a depth of approximately 15 diameters the shear stress along

the side of the pile becomes essentially constant because the arching effect counteracts any increase in vertical stress caused by the overburden.

The work performed by Vesic (43) also shows some of the factors which influence the capacity of a deep foundation. He has developed relationships which show the effect of soil compressibility and volumetric strain of the soil. As the soil compressibility, expressed as the rigidity index, increases, the bearing capacity increases. An increase in the volumetric strain of the soil causes a decrease in the bearing capacity.

The effect of volume expansion and pile rigidity were studied in an effort to determine the scale effect in the study of model foundations. The studies done by Vesic are discussed in more detail in Chapter III and are analyzed in Chapter VII.

The research on bearing capacity of circular drilled piers in sand has shown that the bearing capacity is a function of the depth to diameter ratio, pier rigidity, and soil properties (weight, volumetric strain characteristics, relative density, and angle of internal friction). These and other aspects which effect the behavior and load-carrying capacity of drilled piers will be discussed in more detail in Chapters III, VI, and VII.

Drilled Piers in Other Soils and Rock

On a test pier drilled into weak and variable shale in San Francisco, Moore (23) investigated the development of skin friction. Using a lumped value, without considering stress distribution, he observed

that the allowable shaft adhesion was 10,000psf. This study was carried out using a false bottom on a pier drilled through the overlying Bay area mud into shale.

The stress distribution pattern along an 18-inch diameter drilled pier in weathered shale has been investigated by Henly (46). This study, utilizing concrete embedment gages, showed that the load remaining in pier decreases approximately lineally with depth as shown in Figure 3.

To date, very little work has been done on drilled piers in the Atlanta area. Walters (47) has investigated the end bearing capacity of small diameter (8 inch) drilled shafts in weathered rock similar to the soil used in the present study. His study showed close agreement with the formula presented by Sowers and Sowers (48) for deep circular foundations when shaft adhesion can be neglected. This formula is:

$$q_c = 5.20c + \gamma D_f \tag{9}$$

where q_c = critical unit base resistance.

c = 1/2 unconfined compressive strength = unit cohesion.

γ = effective weight of overburden.

D_f = depth of toe below ground surface.

These results are based on data from three tests with an indication of a settlement required to reach the ultimate load equal to greater than 50 per cent of the pier diameter. This settlement was probably caused by inadequate cleaning of the bottom of the 8-inch drilled shafts prior to concreting.

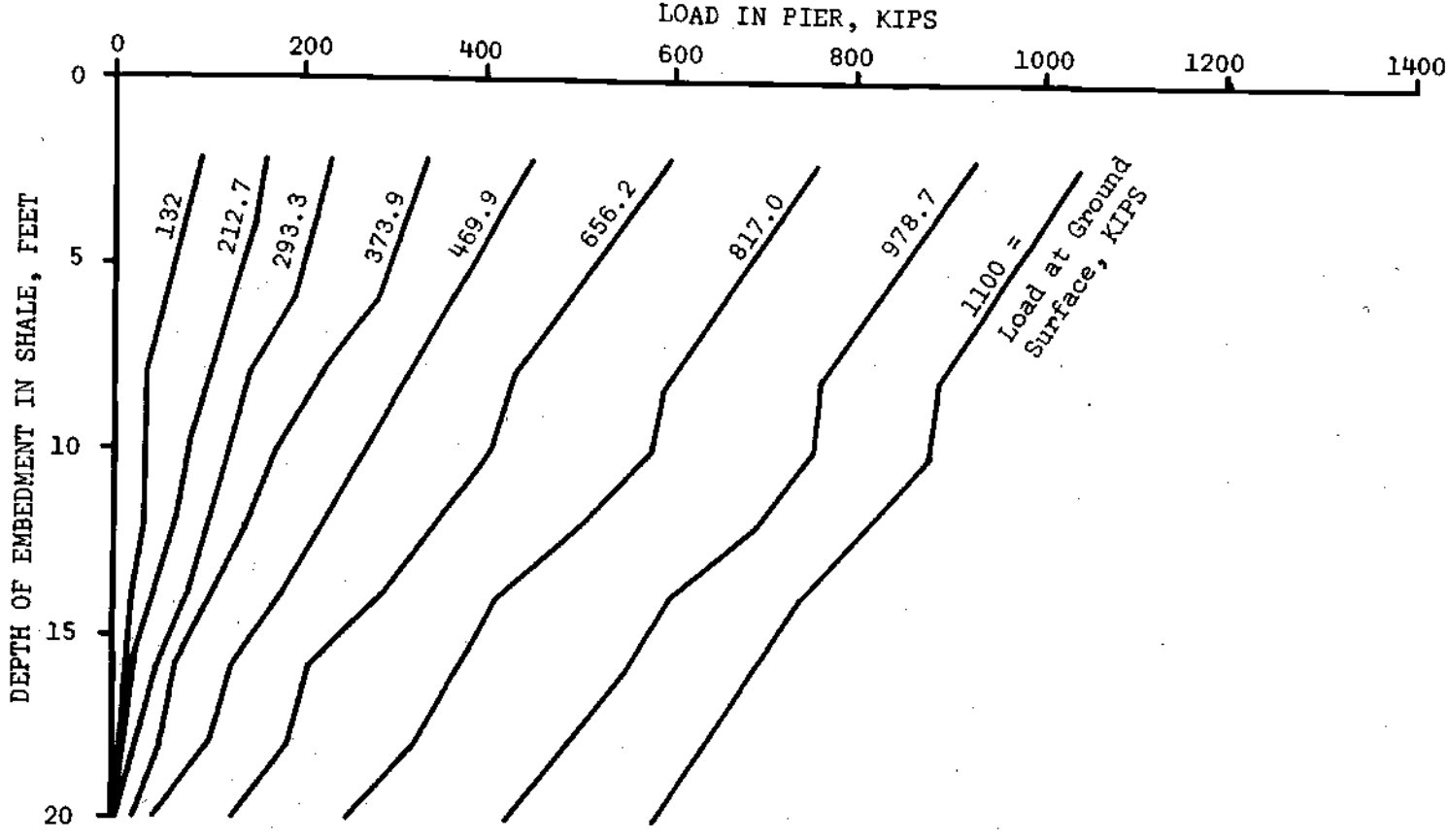

Figure 3. Load Distribution Curve for a Drilled Pier in Weathered Shale (After Henley, 46)

Summary of Literature Review on Drilled Piers

The previous work on drilled piers tends to validate the ultimate capacity predicted by the Terzaghi formula with minor modifications for local soil conditions and past experience. A more complete discussion of the theoretical solutions for the ultimate capacity of deep foundations, including piers and piles, is presented in Chapter III.

There has been considerable work done on determining the ultimate capacity of drilled piers. Most of this work is of an empirical nature due to the complicated mathematics involved in predicting the ultimate capacity of a circular shaft. Little work has been done in residual soils or saprolitic soils similar to those found in the Atlanta area. Since the available results for this type of material are very limited and of little use, the data obtained from the load tests done in conjunction with this thesis will be compared to those results obtained by the above-mentioned investigators, and to investigations performed on driven and buried piles.

The various investigators have found that the determination of the ultimate capacity of a drilled pier is dependent on many factors. Primarily the ultimate capacity is a function of the soil properties immediately adjacent to the shaft, including various corrections for the wetted strength of the soils and corrections for the true overburden pressure. The value of unit skin friction was found to vary greatly from the passive earth pressure value to a value approximately equal to the overburden pressure. The ultimate capacity of a drilled pier and the manner in which the load is transferred to the surrounding soil

is also a function of the depth to diameter ratio and the depth itself.

In all the literature reviewed, the base capacity of a drilled pier is seen to be dependent on various dimensionless bearing capacity factors. The bearing capacity factors vary widely between investigators. Many of the various bearing capacity factors reported in the literature are presented by Vesic (43). The bearing capacity factors for different assumed failure patterns are presented in Chapter III. The results of the theoretical and empirical research presented in this chapter will be discussed considering the field test results, obtained as part of this thesis, in Chapter VII.

CHAPTER III

REVIEW OF GENERAL THEORY OF DEEP FOUNDATIONS

In Chapter II some of the theoretical methods for determining the ultimate capacity of a drilled pier foundation and several empirical studies were discussed which were performed to evaluate the ultimate capacity of pier foundations. This review of literature indicates that there has been very little work done in an effort to evaluate the load carrying behavior and ultimate capacity of a drilled pier. To properly evaluate the tests performed as part of this thesis and to establish a general pattern of behavior for deep, circular drilled pier foundations, it is necessary to compare these results with the theoretical and empirical work of others. The general theories of deep circular foundations are discussed in this chapter as they pertain to both piles and drilled piers. These theories will be used to evaluate the field data presented in Chapter VI.

The load carrying capacity of a deep foundation is composed of end bearing and skin friction. This relationship is shown schematically in Figure 4. In the static analysis of deep foundations the effect of end bearing and skin friction are usually superimposed to give the ultimate carrying capacity as follows:

$$Q = Q_s + Q_b = A_s P_s + A_b P_b \qquad (10)$$

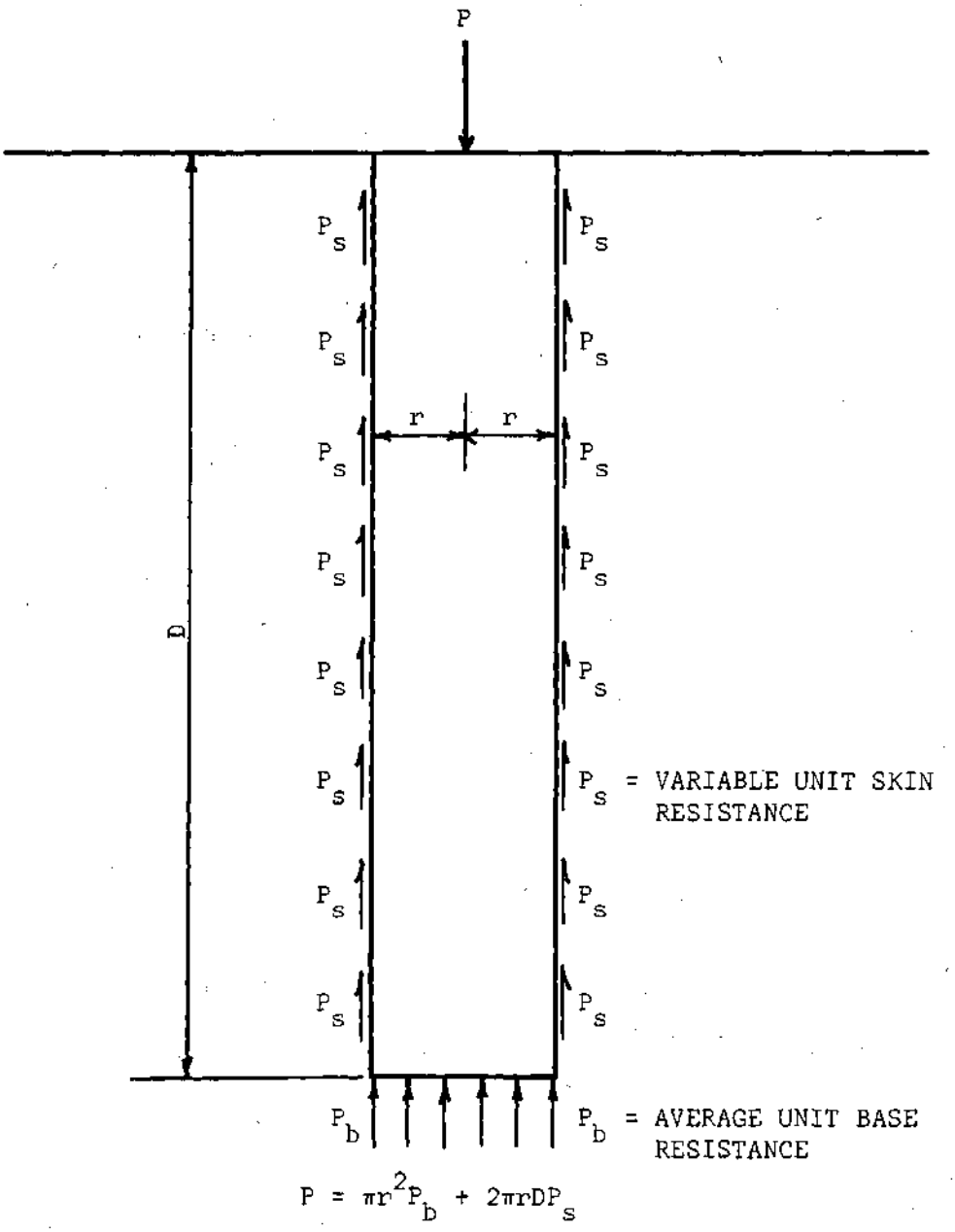

Figure 4. Stresses Acting on a Deep Foundation

where Q = ultimate carrying capacity.

A_b = area of the base.

A_s = effective surface area.

P_b = average unit base resistance.

P_s = variable unit skin resistance.

The unit resistances depend on the strength and deformation characteristics and the initial stress condition of the soil strata being considered. They also depend on the shape, size, and the material properties of the deep foundation as well as the method of placement.

The failure theories for end bearing all make certain assumptions which must be considered in using them. All of the methods presented neglect the effect of skin friction adjacent to the shaft except Meyerhof (35). Terzaghi (26) and Berenzantzev et al. (67) consider the friction force on a vertical plane representing a shear zone some distance from the shaft to evaluate an effective overburden pressure in computing the base capacity. The theories presented all assume some shape of failure zone (Figure 5) in which failure of the soil is assumed to occur simultaneously everywhere in the failure zone. All of the presented theories neglect the effect of soil volume change and rigidity of the foundation. These effects were discussed by Vesic (43) and are summarized in Chapter II. The primary assumption that is made in the development of the theoretical skin friction solution is that the soil behaves as a rigid plastic material (Figure 9). The material is also assumed to be rigid up to a point defined by the Mohr Coulomb failure envelop as the adhesive strength along the soil-conrete interface or

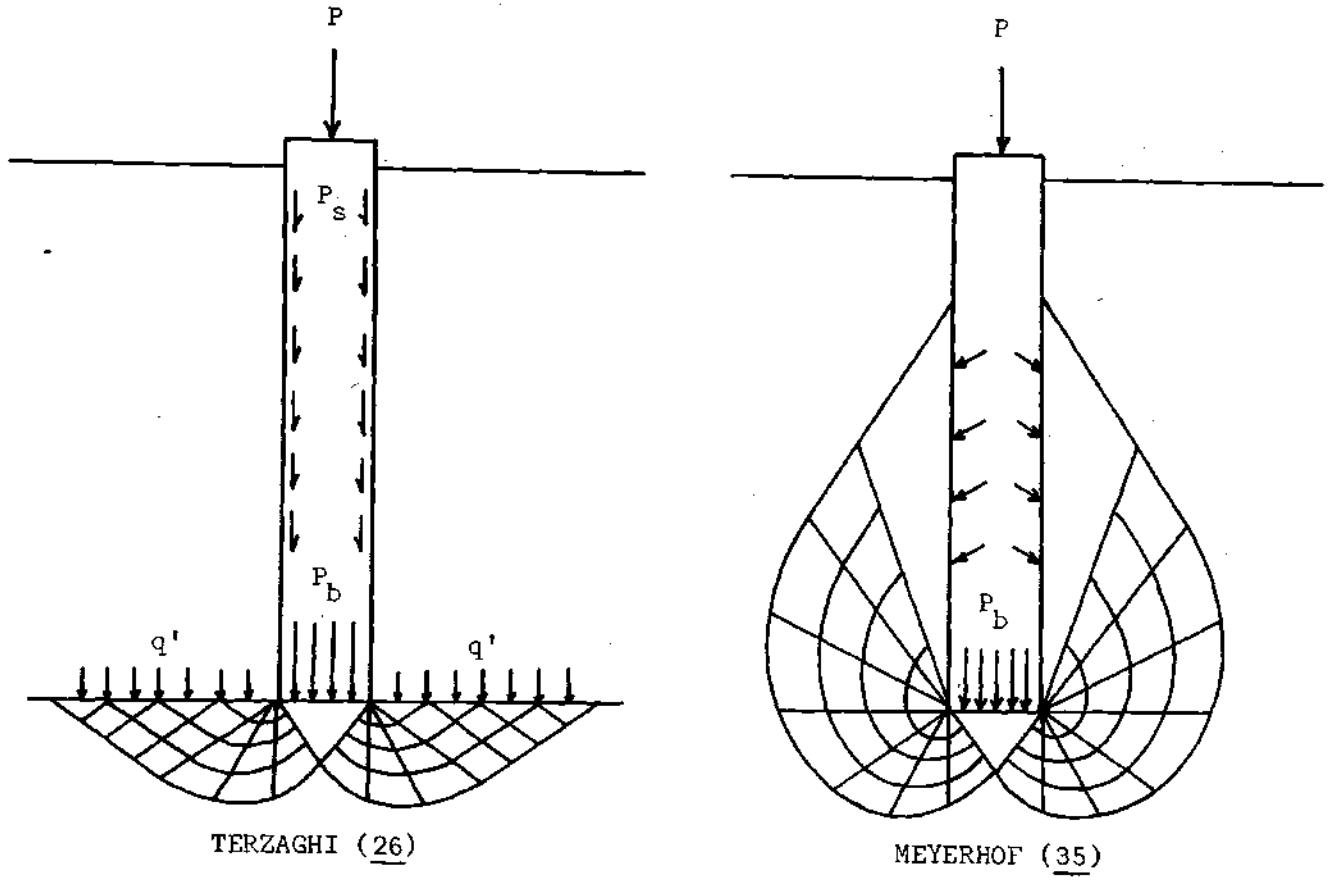

Figure 5. Theoretical Failure Patterns for Deep Foundations

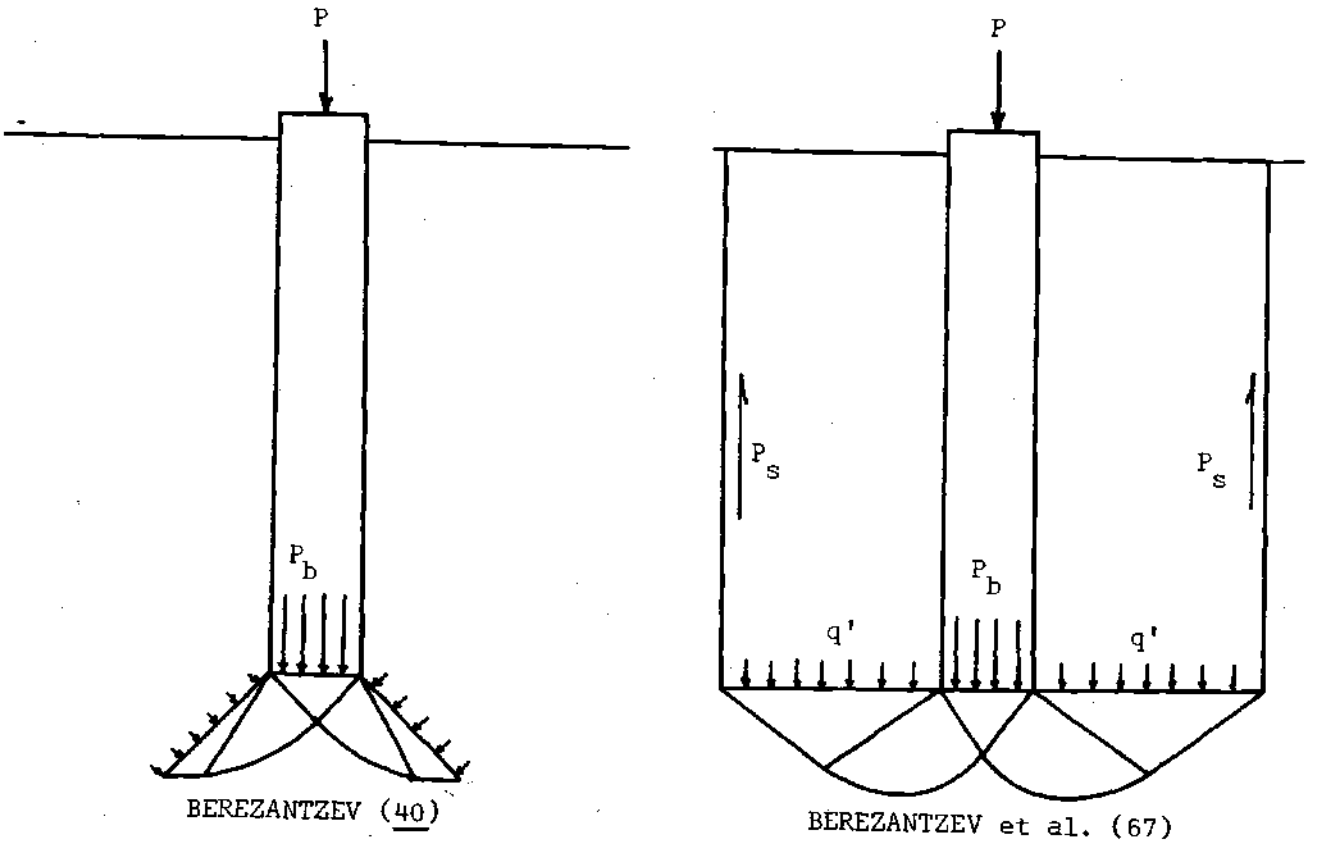

Figure 5. Theoretical Failure Patterns for Deep Foundations (Continued)

the intergranular strength immediately adjacent to this interface. Once the adhesive or intergranular strength of the material is attained, which is dependent on soil adhesion (or cohesion), internal friction and effective lateral pressure, the material is assumed to act plastically.

End bearing and skin friction are assumed to act independently in the available theories but the ultimate capacity in skin friction is assumed to occur simultaneously with the ultimate capacity in end bearing. This will be discussed further in the evaluation of test results presented in Chapter VII.

End Bearing Capacity of a Deep Foundation

A theoretical computation of the end bearing capacity should consider elastic and elastic-plastic movement of the shaft in soil, soil cohesion, angle of internal friction, soil weight, depth of embedment of tip, tip area, shaft shape and dimensions and must approach the problem in three dimensions when the shaft has a finite width-to-length ratio. At present only approximate theoretical methods are available to consider these effects. These effects have been considered to some extent in the choice of a particular failure pattern. Some of the various failure patterns which have been used in determining the theoretical end bearing capacity of a deep foundation are shown in Figure 5. The most widely accepted theories of end bearing have been proposed by Terzaghi (26), Meyerhof (35), and Berezantzev (40, 67).

Terzaghi's Method

The end bearing capacity of a deep foundation as proposed by Terzaghi is equivalent to a general shear failure of a shallow

foundation. In this solution it is assumed that the resisting strength is developed in the material underlying the shaft tip with the material above the base behaving as a surcharge in which a shear zone does not develop (see Figure 5). Terzaghi has developed a theoretical solution for determining the critical base capacity of a long strip footing. He has extended this solution to the axisymmetric case of a circular footing using empirical shape factors obtained from model studies. The resulting ultimate base stress for a circular footing can then be expressed by:

$$q = 1.3cN_c + \bar{\gamma}D_f N_q + 0.6\gamma r N \qquad (11)$$

where q = ultimate unit base resistance.

c = unit cohesion.

r = radius of bearing area.

$\bar{\gamma}D_f$ = effective surcharge weight.

$\bar{\gamma}$ = effective unit weight of soil above tip.

D_f = depth of embedment of foundation.

γ = effective unit weight of soil below tip in failure zone.

N_c, N_q, N_γ = bearing capacity factors which show the influence of cohesion, surcharge and soil unit weight and width, respectively.

Berezantzev's Methods

The critical end bearing stress for a deep foundation in cohesionless soil has been analyzed by Berezantzev (1966) considering a plane strain failure (40). The assumed failure pattern is similar to

that proposed by Terzaghi (27). A schematic diagram of the assumed failure surface is shown in Figure 5. The critical stress determined by this method is:

$$q = 2\eta N_k \bar{\gamma} r \tag{12}$$

where q = critical unit base resistance.

η = reduction factor (0.6 to 0.7) to agree with test results.

N_k = bearing capacity factor depending on the angle of internal friction and the depth-to-width ratio of the foundation.

$\bar{\gamma}$ = effective unit weight of soil.

r = radius of bearing area.

In earlier work Berezantzev, Krestoforov and Golubleov (67) performed a three-dimensional analysis of a punching shear failure having a pattern of failure similar to that proposed by Terzaghi. They stated that the critical unit base resistance of a granular soil can be expressed by:

$$q = \alpha_p N_q + 2\gamma_t r N_\gamma \tag{13}$$

where q = critical unit base resistance.

N_q = surcharge coefficient depending on the depth-to-diameter ratio and the angle of internal friction.

p = surcharge at the foundation base.

γ_t = unit weight of the soil below the tip.

r = radius of the loaded area.

N_q, N_γ = bearing capacity factors as described previously.

Meyerhof's Method

In deference to the methods described above, the theoretical solution proposed by Meyerhof considers the influence of the shaft in determining the bearing capacity of the tip of a deep foundation. The failure pattern proposed by Meyerhof is illustrated in Figure 5 and shows a heart shaped failure zone which intersects the foundation shaft above the base. Meyerhof assumed that the shaft surface is rough and frictional resistance is developed along the shaft and base. The critical base resistance for this failure configuration is approximately:

$$q = cNc + q'Nq + \gamma_t r N_\gamma \qquad (14)$$

where the terms are identical in definition to the previous equation except that q' is the effective lateral pressure against the pile tip which is determined from the material properties of the soil and the depth of embedment.

Summary of End Bearing Capacity Equations

The work of Terzaghi shows most of the variables involved in the determination of the end bearing capacity of deep foundations. The later solutions proposed by Berezantzev are very similar to the original work of Terzaghi. The main difference between these relationships is that Terzaghi did not consider the depth of placement of the foundation base to the extent that Berezantzev did.

Investigators have long realized that the end bearing capacity of a deep foundation is a function of the considerations expressed by Terzaghi and later by Berezantzev. The primary difference in the capacities determined by the various methods is due to the selection of bearing capacity factors which depend on the assumed failure pattern and various simplifying assumptions (such as neglecting the N_γ term for very deep foundations, Meyerhof (35). The bearing capacity factors for the methods expressed here are shown in Figure 6. This figure shows that the bearing capacity factors are quite different from one investigator to another, and depend on many factors including the angle of internal friction and the shape of the failure zone.

Berezantzev's methods also consider factors which indicate the importance of the depth of embedment. These factors (N_k and α) are shown in Figure 7.

In the above methods the effect of side friction on the end bearing capacity has been practically neglected by all but Meyerhof during the original development of the theories. However, Broms (68) has stated that the end bearing capacity of a pile is affected by skin friction resistance. The results of field tests presented in Chapter VI support this statement. Berezantzev's method partially overcomes this shortcoming with the introduction of the depth factors N_k and α. The Terzaghi formula can be adjusted to approximately account for the increase in effective surcharge caused by the side friction forces. This can be considered by defining the effective surcharge ($\bar{\gamma}D_f$) in Equation (11) by:

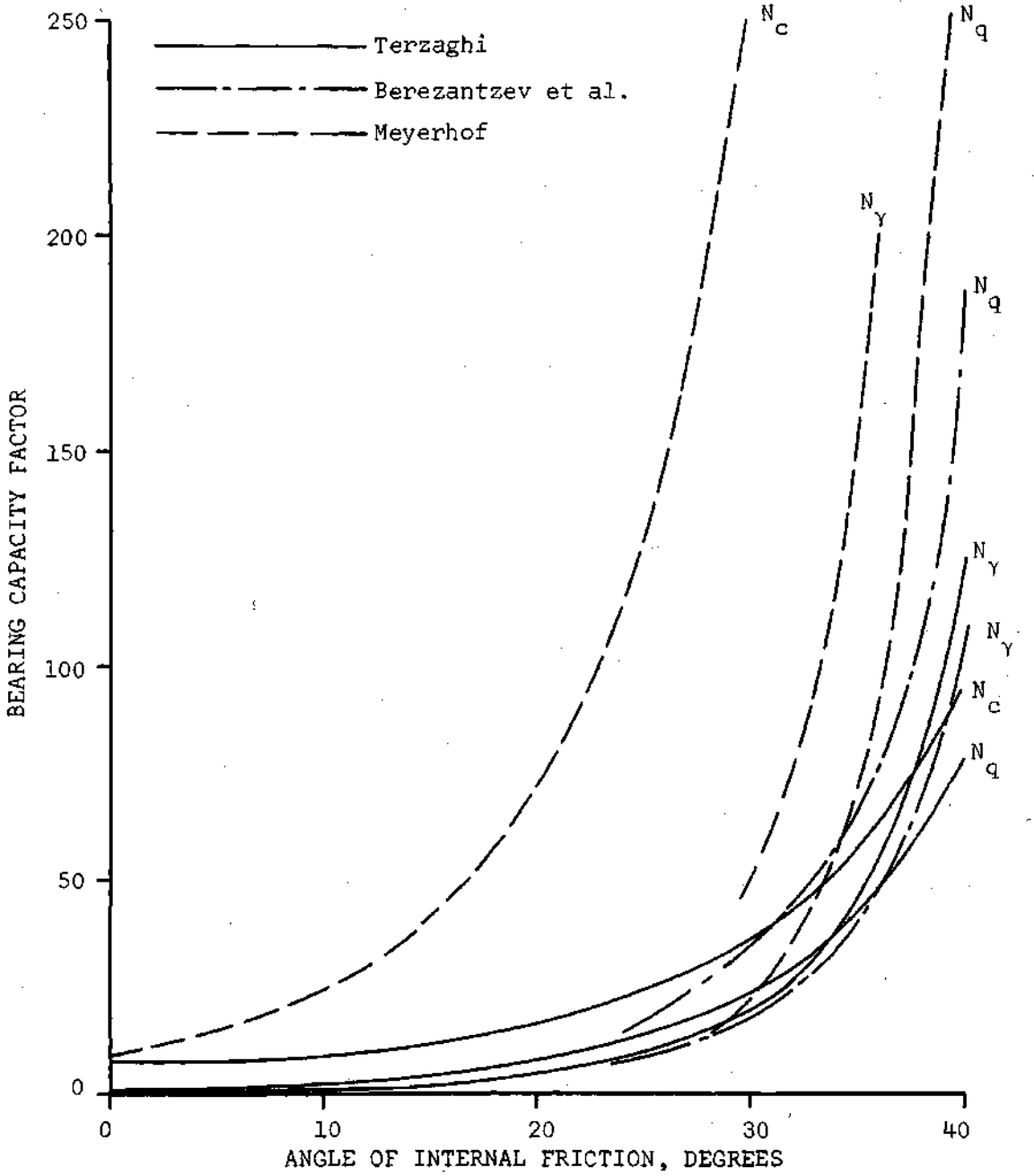

Figure 6. Theoretical Bearing Capacity Factors

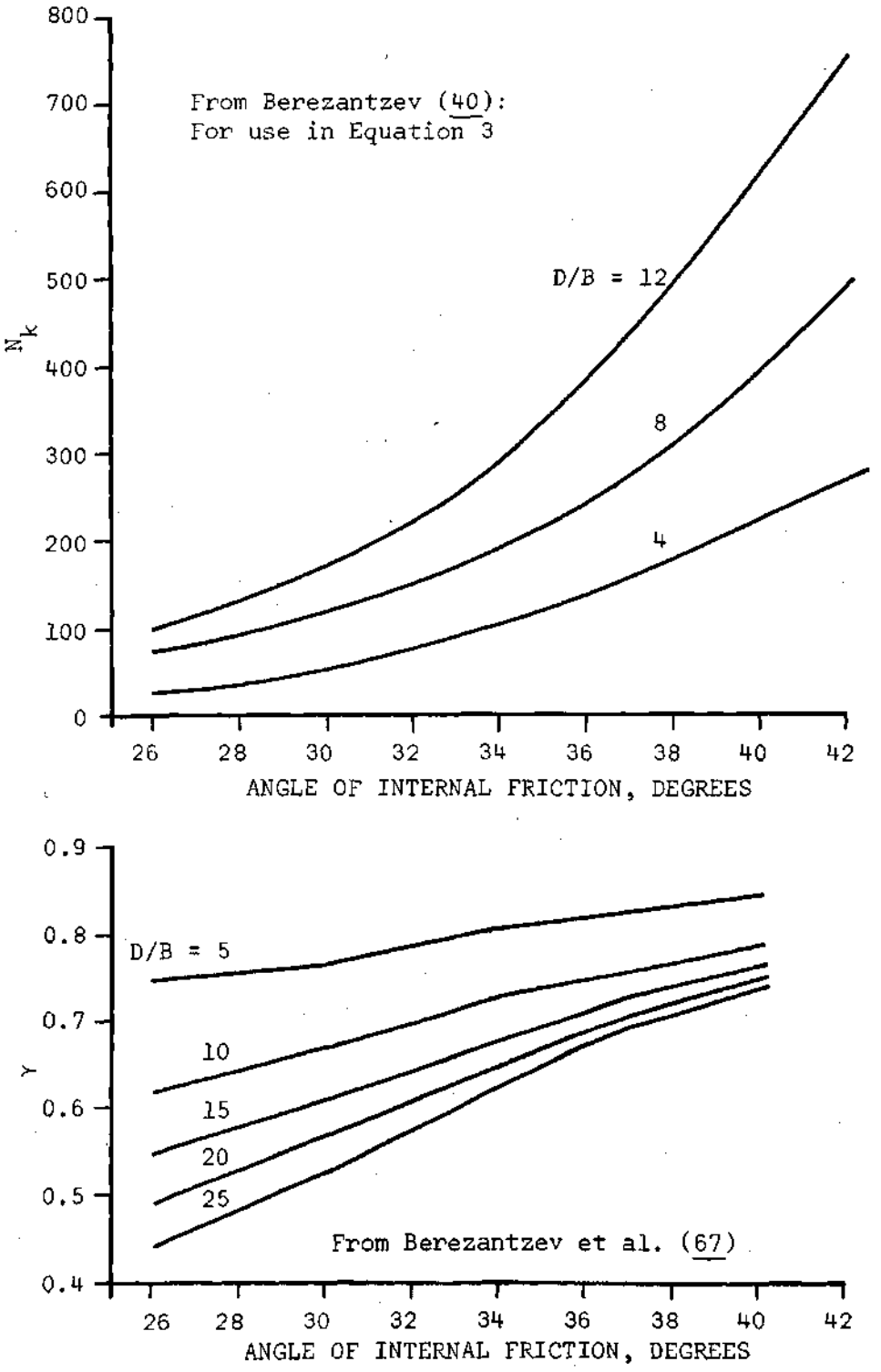

Figure 7. Depth Factors for Berezantzev's Solutions

$$\bar{\gamma}D_f = D\bar{\gamma} + (L-D)\gamma_b + \sigma_r \qquad (15)$$

where $\bar{\gamma}D_f$ = effective surcharge.

D = depth from surface to ground water table.

$\bar{\gamma}$ = unit weight of soil above the water table.

L = depth of embedment.

γ_b = bouyant unit weight of soil.

σ_r = vertical stress caused by the friction forces at a distance equal to the distance to the edge of the base shear zone.

The Terzaghi method of computing the end bearing capacity (with or without considering the side friction effect) has been the method usually used for many years. Recent work indicates that the method proposed by Berezantzev et al. usually yields more accurate results as confirmed by large scale and model tests (43, 63, 69). However this method is relatively new and has not been evaluated under more varied conditions. The Meyerhof solution has been used with limited success primarily because it neglects the actual radius of the bearing area by letting N_γ in Equation (14) be equal to zero in the simplified form for very deep foundations, and the stresses caused by side-friction (which cause a change in soil volume) may help to prevent the failure surface from coming completely back to the surface of the deep foundation.

Skin Friction Capacity of a Deep Foundation

The ability of a pile or pier to develop skin friction is determined using the same parameters considered for end bearing except the deep foundation's surface roughness and the effective force acting

perpendicular to the foundation are now major considerations. A theoretical approach to solving skin friction problems must involve the selection of a strength criteria. For the following discussion the Mohr-Coulomb strength criteria has been used.

The skin friction capacity of a deep foundation can be expressed by:

$$Q_s = 2\pi \int_0^L \int_{p_{s_1}}^{p_{s_2}} \{r(dl)(dp_s)\} \tag{16}$$

where Q_s = total skin friction capacity.

L = depth of embedment in soil.

r = radius of foundation shaft.

p_s = variable unit skin resistance.

The unit skin resistance is further defined, using the Mohr-Coulomb criteria, as follows:

$$P_s = C_a + P_h \tan\delta \tag{17}$$

where P_s = unit skin resistance.

C_a = unit adhesion.

Ph = average effective horizontal stress.

$\tan\delta$ = coefficient of friction along the shear failure surface.

For solution of the frictional resistance of a deep foundation it is necessary to determine the above variables. Probably the most difficult variable to determine is the effective horizontal stress at

some point along the shaft. This stress is influenced by the soil surcharge load at a point and the stress which is placed into the soil by frictional resistance of the soil along the foundation shaft. The effective horizontal stress for a vertical deep foundation can be approximately for a homogeneous elastic soil by:

$$P_h = k\bar{\gamma}D_f - \sigma_h \tag{18}$$

Where σ_h is the horizontal stress caused by removing some of the vertical load in the deep foundation by skin friction, K is a dimensionless number analogous to an earth pressure coefficient relating effective vertical stress to effective horizontal stress, and the other terms are described previously.

Combining the above relationships, the unit skin resistance can be expressed by:

$$P_s = c_a + [K(\bar{\gamma}D_f) - \sigma_h]\tan\delta \tag{19}$$

The horizontal stress caused by a vertical force assumed to act at a point (component of the resultant skin friction force) for a semi-infinite, elastic, homogeneous, isotropic solid has been developed by Mindlen (45) and later adopted by Westergaard (70) for a semi-infinite stratified elastic solid. The radial (horizontal) stresses can be approximated by the following equations:

Mindlen

$$\sigma_h = \frac{P}{8(1-u)}\left[\frac{(1-2u)(z-a)}{R_1^3} - \frac{(1-2u)(z+7a)}{R_2^3} + \right. \tag{20}$$

$$\frac{4(1-u)(1-2u)}{R_2(R_2+z+a)} - \frac{wr^2(z-a)}{R_1^5} + \frac{6a(1-2u)(z+a)^2 - 6a^2(z+a)}{R_2^5} -$$

$$\left.\frac{3(3-4u)r^2(z-a)}{R_2^5} - \frac{30ar^2z(z+a)}{R_2^7}\right]$$

For a layered elastic solid,

Westergaard

$$(R_1^1)^2 = k^2r^2 + (z-a)^2 \tag{21}$$

$$(R_2^1)^2 = k^2r^2 + (z+a)^2$$

$$\sigma_h = \frac{pk^2}{8(1-u)}\left[\frac{z-a}{(R_1^1)^3} - \frac{1-u_o}{R_1^1(\pm R_1^1+z-a)} + \frac{z+a}{(R_1^1)^3} - \frac{1-u_s}{R_2^1(R_2^1+z+a)}\right]$$

where $$k = \frac{1-2u}{2(1-u)}$$

where the upper sign of ± in Westergaard's equation applies when $0<Z<a$ and the lower sign when $Z>a$, and u_s is Poisson's ratio for the strong soil strata. The rest of the notation is illustrated in Figure 8.

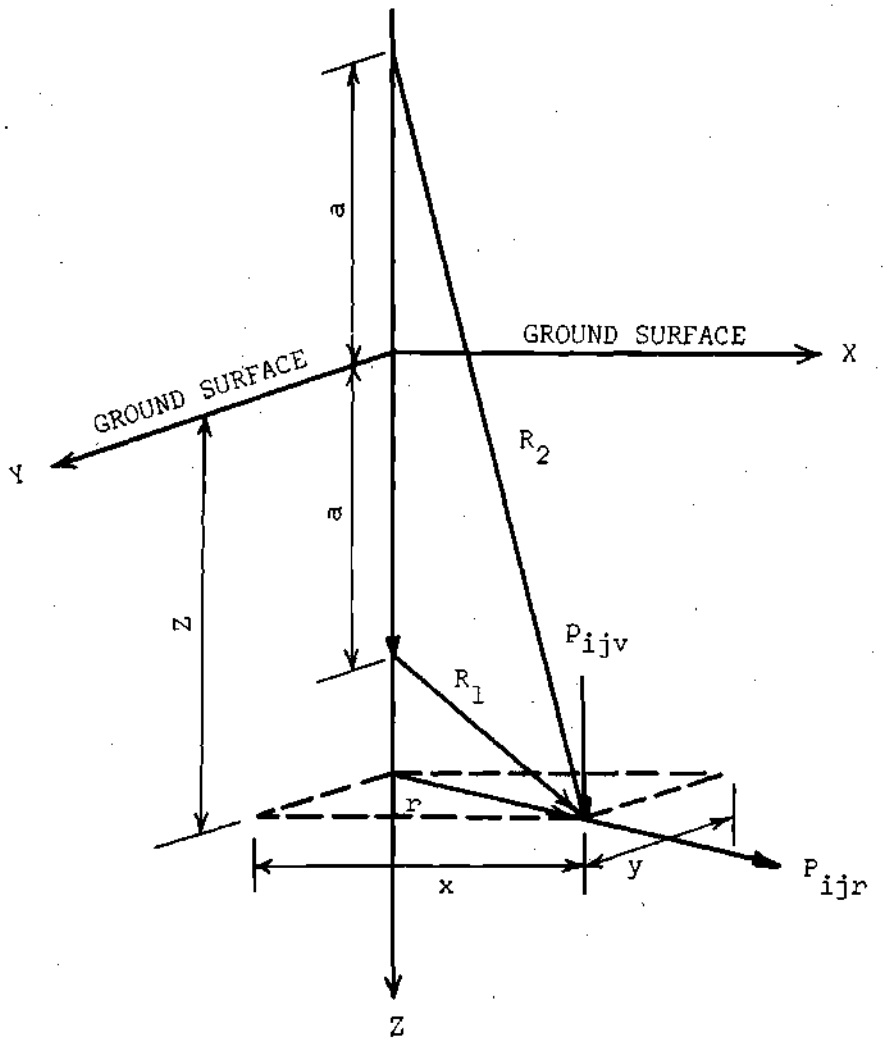

MINDLIN SOLUTION

$$r^2 = x^2 + y^2$$

$$R_1^2 = r^2 + (Z-a)^2$$

$$R_2^2 = r^2 + (Z+a)^2$$

WESTERGAARD SOLUTION

$$(R_1')^2 = k^2r^2 + (Z-a)^2$$

$$(R_2')^2 = k^2r^2 + (Z+a)^2$$

$$k = \left[\frac{1 - 2u}{2(1-u)}\right]^{1/2}$$

Figure 8. Notation for Determining the Change in Radial Stress D_o to a Vertical Load

Using Equation (19) and integrating over the effective length of the deep foundation the total friction support is obtained.

$$Q_s = \int_0^L (2\pi r)\{Ca + [k(\bar{\gamma}D_f) - \sigma_h]\tan\delta\}d\ell \qquad (22)$$

where L = the effective length of the foundation shaft in skin friction and the other terms are as previously described.

Equation (22) has been simplified for a cohesionless soil by several researchers including Noland (69) by neglecting the horizontal stresses caused by the vertical skin friction stresses at a level above the point being considered. This relationship is:

$$Q_s = 2\pi r \int_0^L K(\bar{\gamma}D_f)\tan\delta)d\ell \qquad (23)$$

This is identical to Equation (22) when the adhesion and horizontal forces due to skin friction are neglected and the definitions used in Equation (5) are applied.

Summary of the Theoretical Capacity of a Deep Foundation

The previous sections described the major theoretical aspects of the capacity of deep foundations. The total capacity of a foundation system is the sum of the side friction capacity and the tip or end bearing capacity. The total capacity in skin friction probably occurs before the total capacity in end bearing due to the greater displacement which is probably needed to mobilize the entire base capacity (25).

Since theoretically the soil is considered rigid plastic the ultimate capacity in skin friction and end bearing occur simultaneously even though the skin friction capacity may be developed first. By superimposing the loads in end bearing and skin friction, researchers have assumed that the soil is a rigid-plastic material for computation of skin friction capacity and behavior. Soils do not behave in this manner but have stress strain relationships as are shown in Figure 9. These relationships show that the stress increases to a certain strain and then remains essentially constant or decreases at greater strains. This means that the deep foundation would have varying stresses acting on it depending on the foundation deformation and stress strain characteristics of the soil. To complicate the problem further, various investigators have shown that along the side of a deep foundation the absolute displacement along the soil concrete interface is probably the primary consideration and not the strain of the soil itself (25, 43).

For practical engineering applications of these theories the end bearing capacity for deep foundations is usually determined by either Terzaghi's (26) or Berezantzev's (40, 67) methods. The skin friction capacity is then usually determined from Equation (23) in the case of a cohesionless soil. A major problem is determining the lateral force acting along its sides. Theoretical capacity is dependent on the lateral earth pressure coefficient (k) which has been shown to vary along the foundation depth and also varies with the load on the foundations.

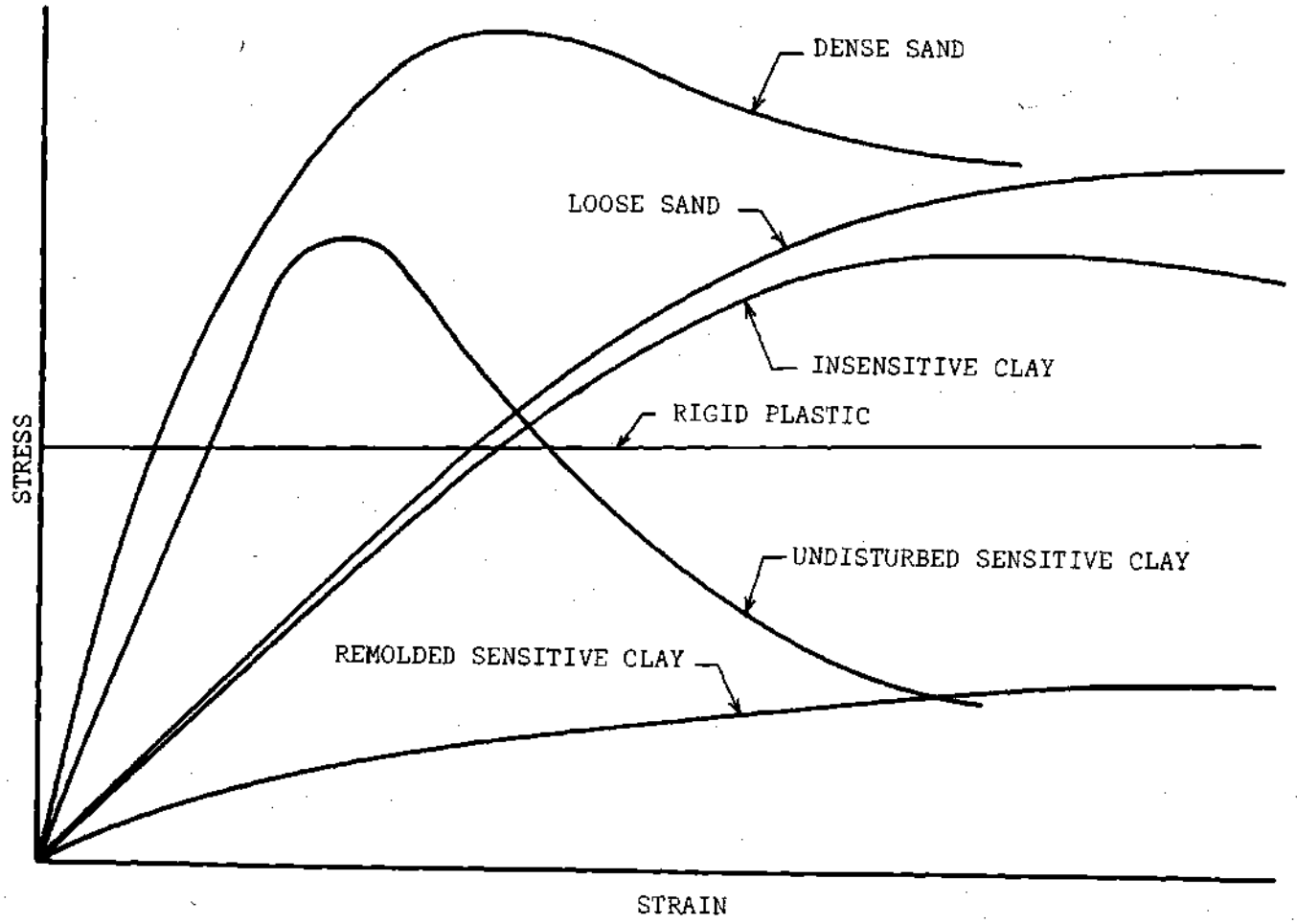

Figure 9. Typical Stress-Strain Relationships for Axially Loaded Cylindrical Soil Samples

CHAPTER IV

SITE EVALUATION

Several problems are involved in finding a feasible site to perform load bearing tests on piers in weathered rock. Primarily it is a problem of locating a site which has the desired geologic and soil conditions. In Chapter I, three different soil types were discussed which overlie the intact continuous rock in the Atlanta area. It was decided that a site should be selected where the lowermost soil zone exists close to the surface to minimize the cost of the test piers and soil test borings. Secondly, the chosen site must be one on which the owners will permit installation of the test piers.

Both considerations were met by the selection of a site located on the Georgia Institute of Technology campus. Permission to use this site for field testing was obtained from the campus architect and planner. The site is located at the corner of State and Fourth Streets as is illustrated in Figure 10.

A visual examination of an exposed cut on the test site showed that the soil profile has rock stringers of various thickness throughout a residual soil. The soil conditions at the site were examined in detail by five soil test borings. The location of these borings is shown in Figure 11. In the test borings, split spoon samples were obtained at five foot intervals with a standard 1.4 inch I.D., 2.0 inch

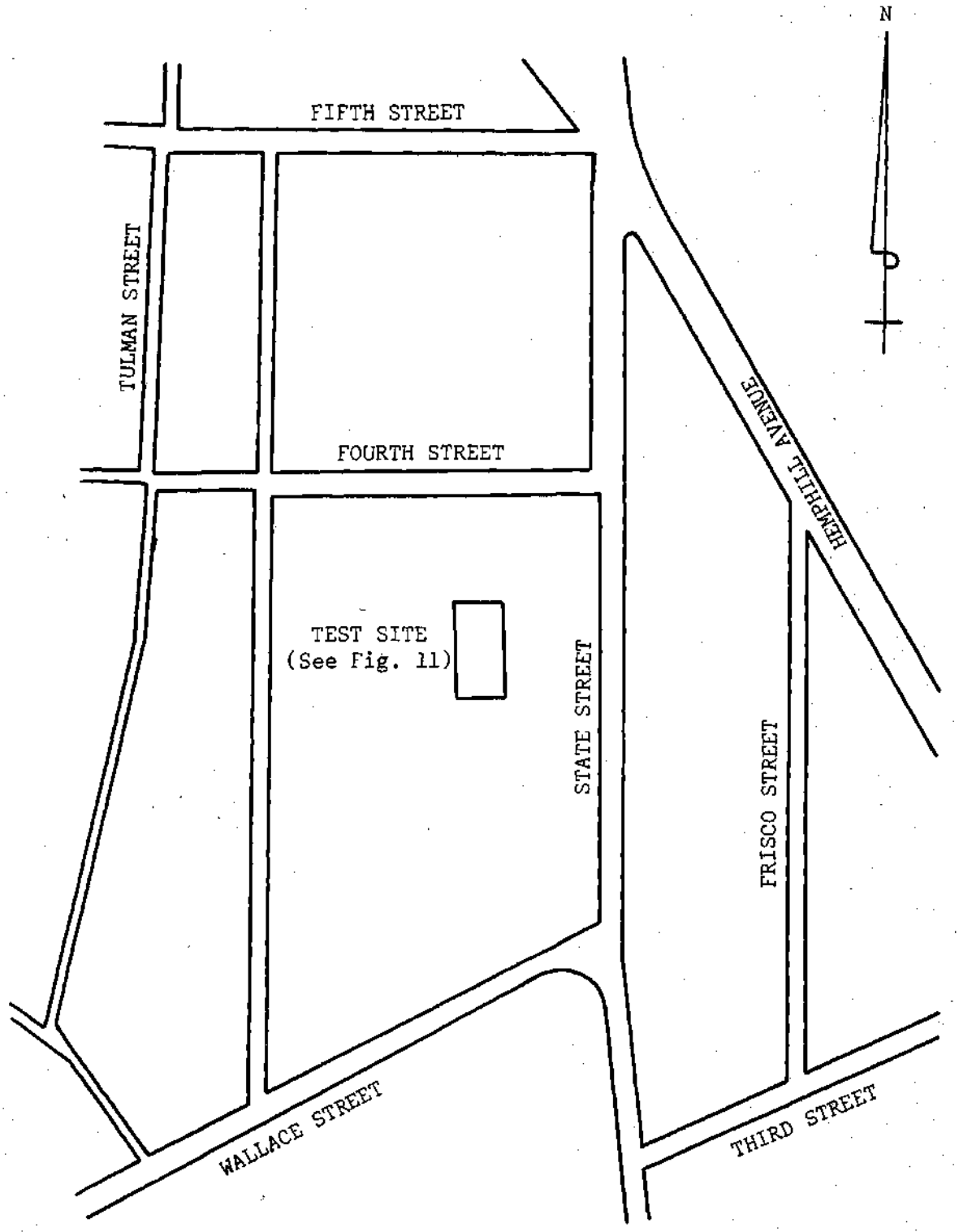

Figure 10. Test Site for Pier Investigation Located on the Campus of Georgia Institute of Technology, Atlanta, Georgia

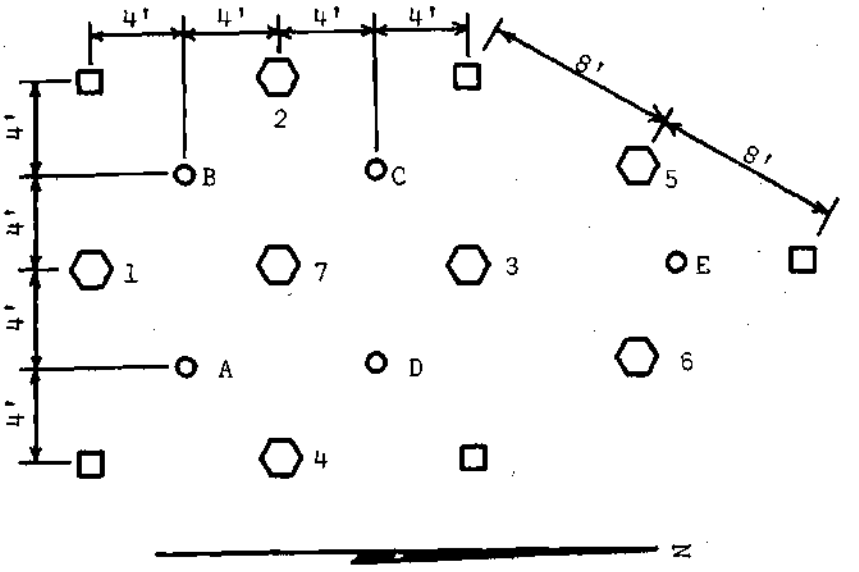

TEST PIER, DIAMETER EQUALS 18 INCHES

REACTION PIER, DIAMETER EQUALS 30 INCHES

SOIL TEST BORING

PIER NUMBER	DEPTH (FEET)	TYPE OF TEST
1	15	SKIN FRICTION AND END BEARING
2	15	SKIN FRICTION AND END BEARING
3	22	SKIN FRICTION AND END BEARING
4	22	SKIN FRICTION AND END BEARING
5	20	SKIN FRICTION (COMPRESSION)
6	20	SKIN FRICTION (COMPRESSION)
7	20	SKIN FRICTION (TENSION)

NOTE: Boring Logs for Soil Test Borings are Given in Appendix A.

Figure 11. Location of Piers and Soil Test Borings on Test Site

O.D., split spoon sampler. The sampler was first seated six inches, to penetrate any loose cuttings, then driven an additional foot with blows of a 140-pound hammer falling 30 inches. The number of blows required to drive the sampler the final 12 inches is called the "standard penetration resistance." Samples obtained in this manner are suitable for visual examination and classification tests, but are too disturbed for quantitative laboratory testing. The standard penetration resistance is an index to the soil strength profile showing standard penetration resistance variation with depth as is shown in Figure 12. This figure shows that the standard penetration resistance, N, varies a great deal in tests taken at the same depth. The standard penetration resistance varied from 11 blows per foot to over 100 blows per foot with most of the values between 15 and 40 blows per foot. The variation in standard penetration resistance indicates the extreme variability of the virgin soil. This variability was also observed in the samples obtained and made evaluation of laboratory and field test results very difficult.

Relatively undisturbed samples were obtained by forcing sections of 3 inch O.D., 16 guage, steel tubing into the ground at the desired sampling levels. This was accomplished by driving the tubing with a 140-pound hammer falling 30 inches or by pushing down on the sampler with the hydraulic loading equipment on the drill rig. Each tube together with the encased soil, was carefully removed from the ground, made airtight by sealing with wax, and transported to the laboratory. Undisturbed samples were also obtained by means of a Dames and Moore Sampler (Figure 13) during the actual installations of the piers.

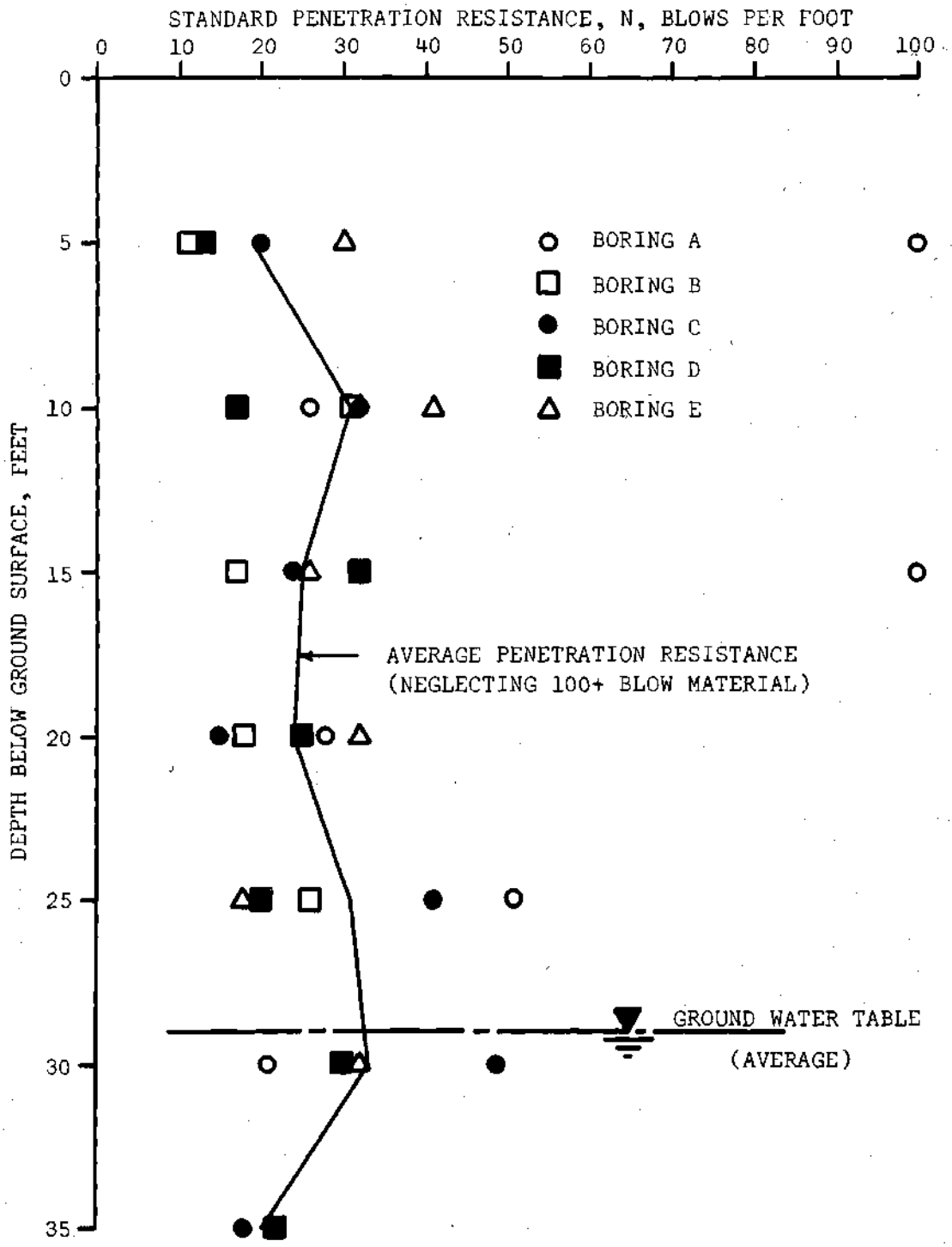

Figure 12. Variation of Standard Penetration Test Results as a Function of Depth

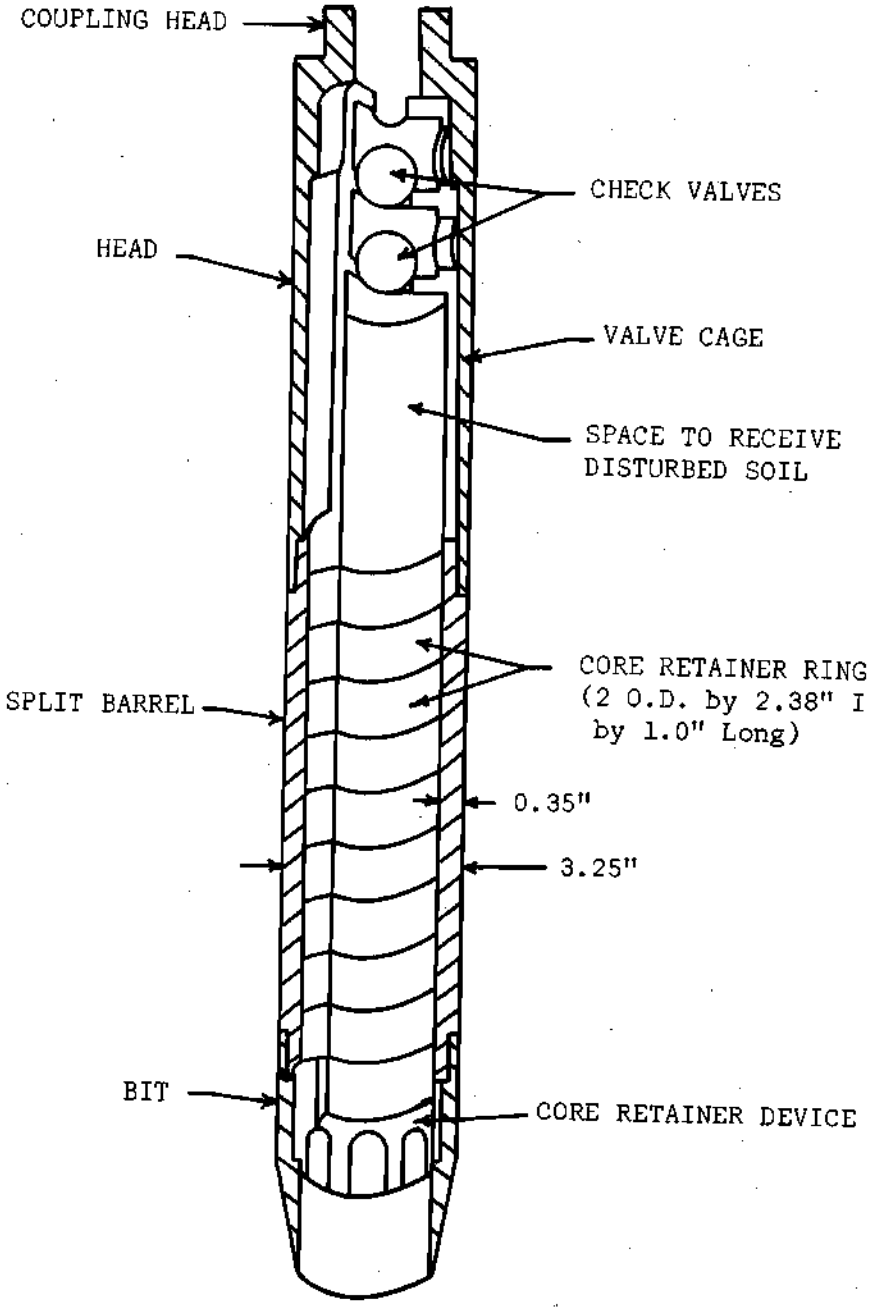

Figure 13. Isometric Section View of Dames and Moore Soil Sampler, Type U

Samples obtained in this manner were tested in the Dames and Moore soil laboratory in Atlanta, Georgia. Locations and depths of undisturbed samples are shown on the test boring records given in Appendix A.

The test borings indicated that the ground water table was approximately 28 feet below the surface at completion of drilling in February 1968. During the construction of a reaction pier on May 23, 1968, the water level was not apparent after 8 hours in a hole drilled 26 feet below the ground surface. Visual examination of this hole showed that the water table was at a depth greater than 26 feet on this date. This indicates that the water table is probably at least several diameters below the bottom of the deepest test pier.

Materials Testing Program

The jar samples were examined and visually classified in the laboratory. The soil samples were quite heterogeneous in mineral composition, color and grain size. In general the soil materials can be classified as fine to course sandy silts and silty sands with varying mica content.

Jar samples, obtained from a split spoon sampler were tested to determine the grain size, specific gravity and moisture content of the soil. Portions of the undisturbed samples were subjected to the following tests:

1. Triaxial Shear.
2. Consolidation.
3. At Rest Earth Pressure.
4. Density and Specific Gravity Determination.

5. Double Ring Shear.

The above tests will be discussed separately for clarification. These laboratory tests were used to establish the soil properties, including strength parameters for the site being investigated.

Triaxial Shear Tests

Representative portions of the undisturbed samples were extruded by a hydraulic jack from the sampling tube for triaxial shear testing. The samples were manually trimmed to a diameter of approximately 2.80 inches and a height of approximately 5.60 inches. The samples were difficult to trim in some places because of the inclusion of quartz seams and zones of weak soil. The extruding and trimming process is believed to have disturbed the soil to some extent. In the trimming process some large particles had to be removed to avoid puncturing the rubber membrane. After the samples were extruded their natural tendency was to expand, due to the stress release, causing some of the cemented contacts to break. Both of these effects and the effect of driving the sampling tube disturb the samples to an unknown extent and give strength values which are probably below the strength of a similar sample of virgin soil.

After trimming, the samples were weighed and measured prior to encasement in a rubber membrane and placement in the triaxial test cell. Once in the triaxial cell, the samples were subjected to an unconsolidated-undrained test. In this test no drainage was permitted and the pore water pressure was measured. Since the samples were not saturated, an effective stress envelope could not be determined. Since

the duration of the pier load tests were rather small, the use of the undrained shear strength is justified in evaluating the field test results.

In some cases the samples were tested in a progressive or multiple-stage triaxial test (49, 50). This test procedure makes possible the multiple testing of the same soil sample, reducing the time and number of samples needed for triaxial testing. After initial confinement, the axial load is increased to a point of imminent failure. At that time the loading is stopped and the confining pressure is increased to the next desired confining condition. After a period of consolidation the axial load is again increased to a point of imminent failure. This may be repeated indefinitely if the soil sample has not deformed excessively or if the soil is not sensitive to this type of loading sequence.

Single and multiple stage undrained triaxial tests were performed on relatively undisturbed samples. No noticeable difference in strength values can be observed in the test results.

The samples were all tested at a deformation rate of 0.05 in/min or a strain rate of about 1 per cent per minute. This strain rate is in the middle of strain rates usually used in testing sands and on the high end of the testing rate for clays (51).

Besides load rate, the mechanical operation of the triaxial test is influenced by piston friction, end restraint of the sample, and confinement by a rubber membrane. The piston friction was minimized by coating the piston with silicone grease and is not thought to affect the

measured strength of soil significantly. End restraint is generally not a consideration in causing strength reduction when the length to diameter ratio is greater than two (72). The confining effect of a rubber membrane effects the slope of the stress strain curve, but has little influence on the maximum measured stress. The effects of the rubber membrane, end restraint and piston friction are believed to be less than 1 per cent based on typical values given by Bishop and Henkel (72). Corrections were not made to the strength test results to consider these effects.

A general Mohr failure envelope obtained from the triaxial test results is illustrated in Figure 14. The results of the individual triaxial tests are given in Appendix A.

The results of the individual triaxial tests also show the stress-strain relationships for the soil samples tested. From the stress-strain relationships, the tangent modulus of elasticity of the soil was found to vary from 27.4 kips per square foot to 304.3 kips per square foot with the higher values being obtained from the less weathered rock.

The triaxial shear test results show that the average value of the angle of internal friction is 31 degrees with a cohesion of 300 pounds per square foot. The maximum value for the angle of internal friction is 32 degrees and the minimum value was 30 degrees when all the samples tested were considered together.

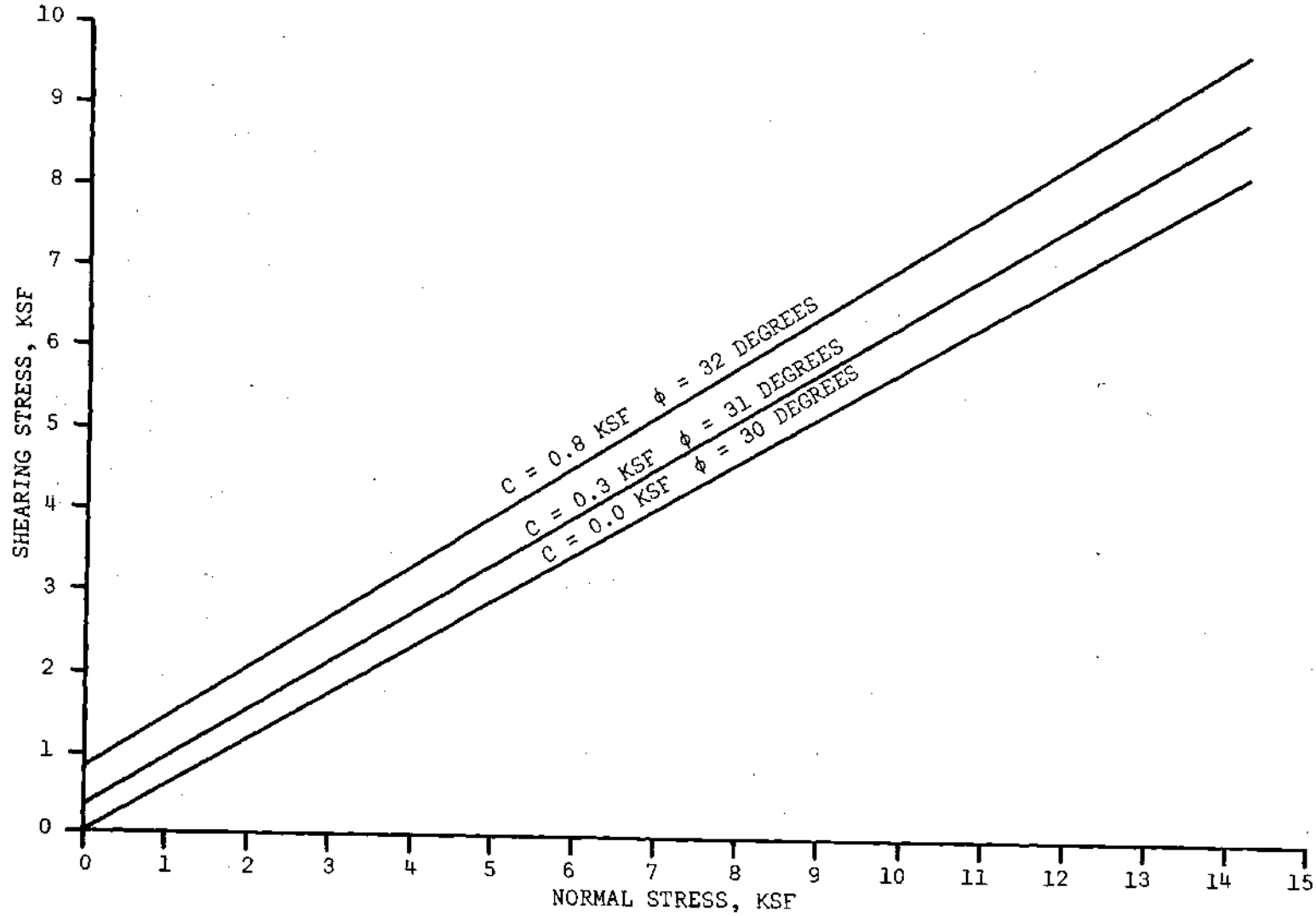

Figure 14. Limiting Mohr Failure Envelopes Determined from Triaxial Shear Testing of Weathered Rock

Consolidation Tests

Several undisturbed samples were extruded from their Shelby tubes, for use in the consolidation test, in the same manner as for the triaxial test. The samples were trimmed to a 2.40 inch diameter having a height of 1.0 inch. The samples were then confined in a steel ring and subjected to the standard (ASTM D 2435-65T) one dimensional consolidation test. The results of these tests indicated that the settlement and rebound was a function of applied load only and practically independent of time for each sample. This type of relationship was expected since the samples were not saturated and the soil was predominately sand. On two of the tests the indicated preconsolidation load is nearly identical to the existing overburden pressure. The coefficient of consolidation of the three samples tested was 0.267, 0.220, 0.275 for samples from Boring E at 19.2 feet, Boring B at 14.85 feet and Boring D at 25.6 feet, respectively. The consolidation test results are presented in Figure 15 in the form of a curve of void ratio vs. the logarithm of the vertical pressure.

At Rest Earth Pressure Coefficient

The at rest earth pressure coefficient was determined from samples obtained and trimmed in the same manner as for the triaxial test. A lateral deformeter sensed the lateral deflection at three points in a horizontal plane. By maintaining the lateral deformeter reading at its zero strain value (obtained prior to loading the sample) during the loading sequence the lateral deformation was maintained at zero in one horizontal plane at approximately the 1/3 point of the sample.

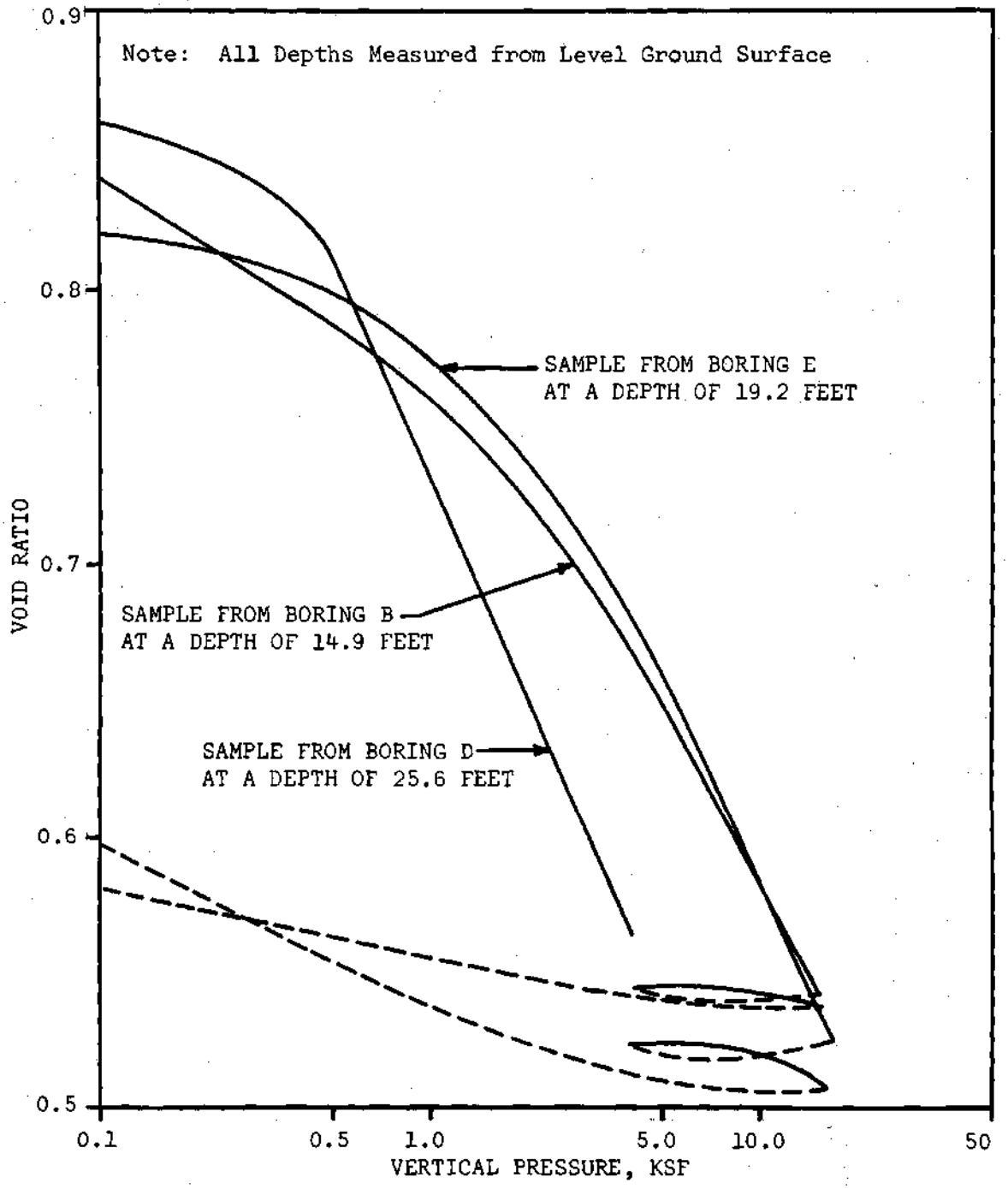

Figure 15. Results of Consolidation Testing of Weathered Rock

The assumption was made that if the lateral strain remained zero in one horizontal plane, it remained zero in the other horizontal planes.

An initial load was placed on the sample and the cell pressure was increased to maintain the original diameter of the sample. The axial load was increased in five and ten pound increments with corresponding incrementally increasing confining pressures to maintain a constant diameter in the measuring plane. In this manner, values were obtained of the axial stress and the confining stress at zero lateral deformation on the measuring plane. The slope of the curve of axial stress vs. confining stress is the coefficient of at rest earth pressure, Figure 16.

In Figure 16 the lines do not pass through the origin. This was believed due to the fact that the soil is not completely elastic. Some axial deformation also occurred without a corresponding lateral deformation during the initial load increments due primarily to sample disturbance. This may also be due to consolidation of the sample as the loading sequence progresses.

Double Ring Shear Test

Samples to be used in the double-ring shear test were obtained using the Dames and Moore sampler illustrated in Figure 13.

The samples were obtained while drilling test piers two, three and four by pushing the samples into the bottom of the pier utilizing the drilling rig. Samples obtained in this manner are less disturbed than samples obtained by driving the sampler with a drop hammer. The samples were not completely undisturbed, however, since the sampler

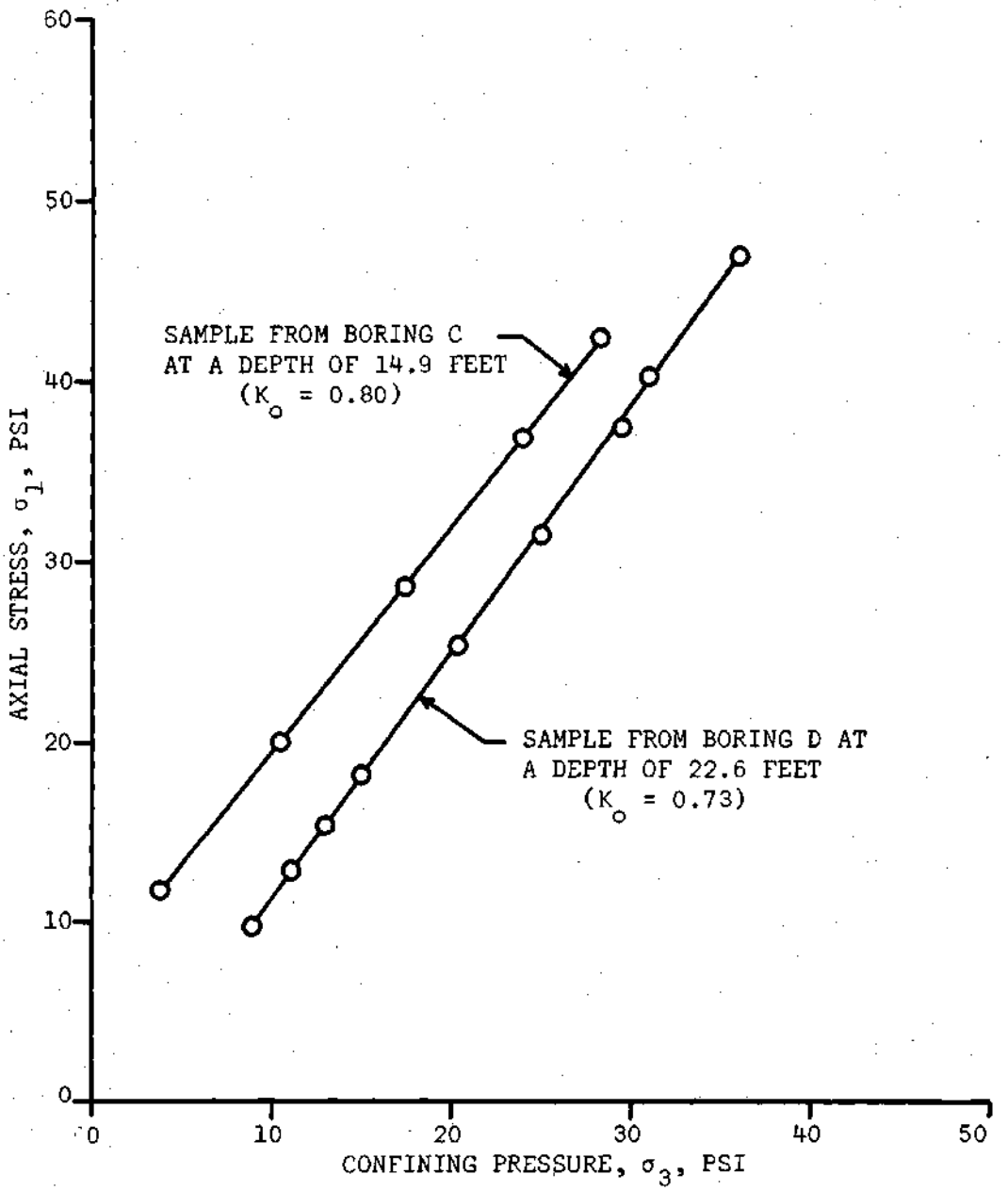

Figure 16. Results of At Rest Earth Pressure Coefficient Testing

used was a thick wall sampler. Samples obtained in this manner were believed to be slightly less disturbed than samples obtained by driving the sampler during the field boring program.

In the double ring shear test a center disk of soil is pushed from a ring of soil resting on either side. A normal stress can be applied to the soil in the outside rings so that a stress envelope can be obtained in the same manner as for the direct shear test. The results of these tests are shown in Figure 17 and the equipment is illustrated in Figure 18. The tests performed gave scattered results as seen in Figure 17. The results obtained indicate an average initial angle of internal friction of 44 degrees with a cohesion of 450 pounds per square foot. At normal loads in excess of about 1200 pounds per square foot the average angle of internal friction is 16 degrees for samples obtained at a depth of 22 feet. These tests were all drained double ring shear tests. The test results indicate, however, that the samples were tested too rapidly to permit drainage. This is shown by the lower angles of internal friction when the normal load was in excess of 1200 pounds per square foot, which is indicative of a more completely saturated soil at greater normal pressures. These test results are more indicative of an undrained test than a drained test.

Grain Size Analysis

The grain size distribution of several samples of soil were obtained to verify the visual classification. The results of these tests are shown in Figure 19. They confirm the classification of the soil as a fine to medium silty sand or sandy silt, according to the

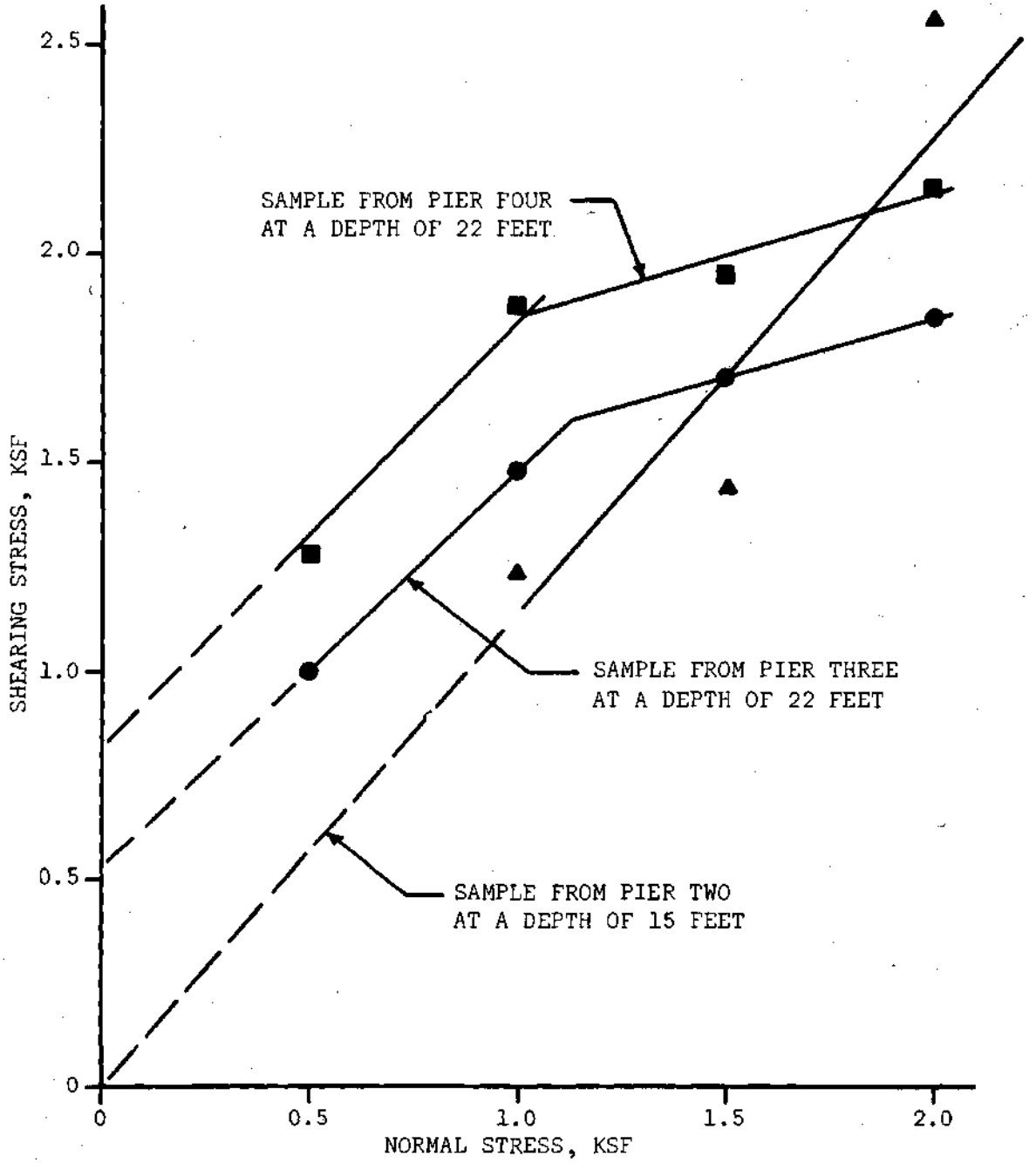

Figure 17. Mohr Failure Envelopes Determined from Double Ring Shear Test

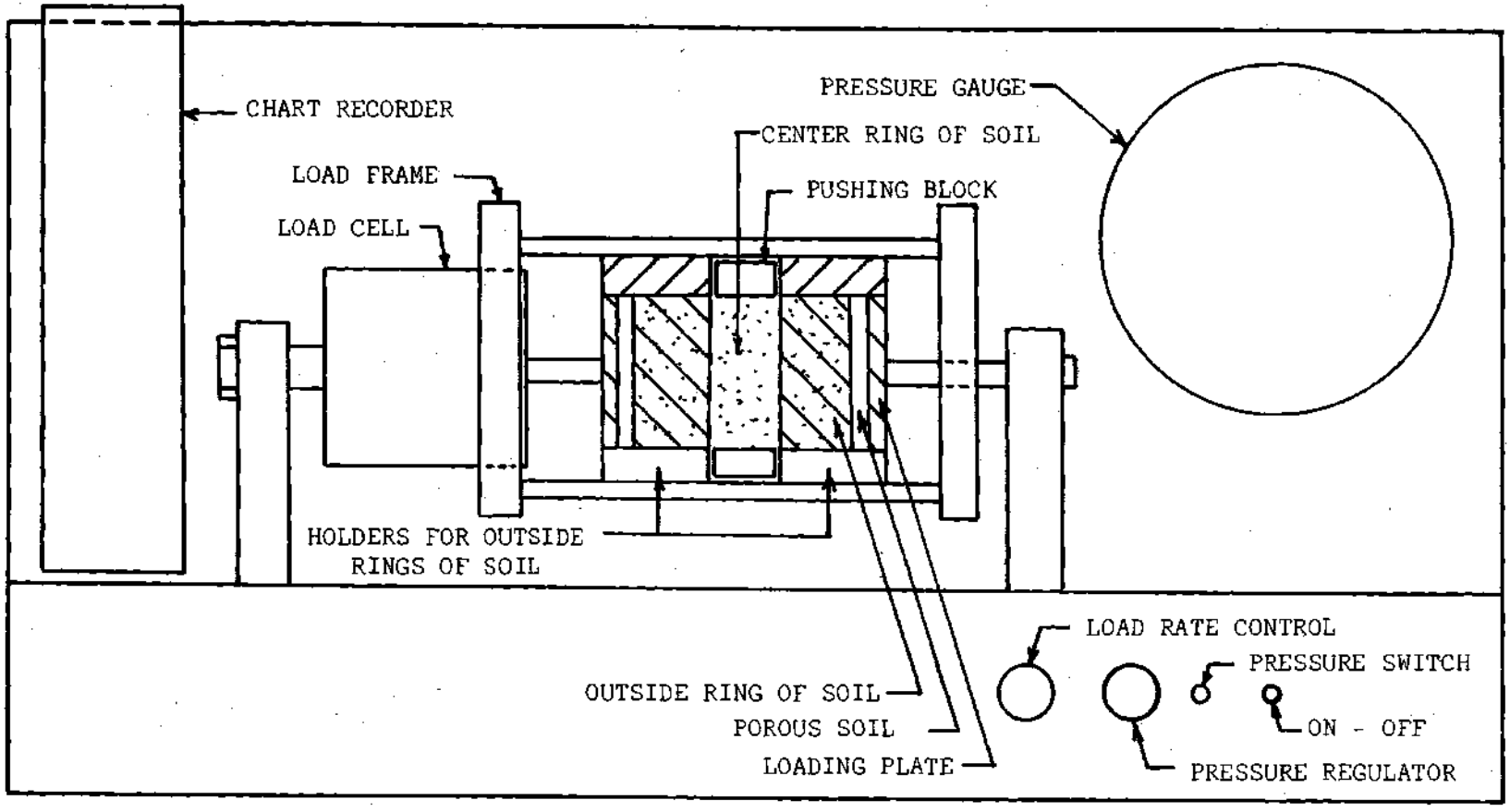

Figure 18. Schematic Drawing of Dames and Moore Double Ring Shear Apparatus

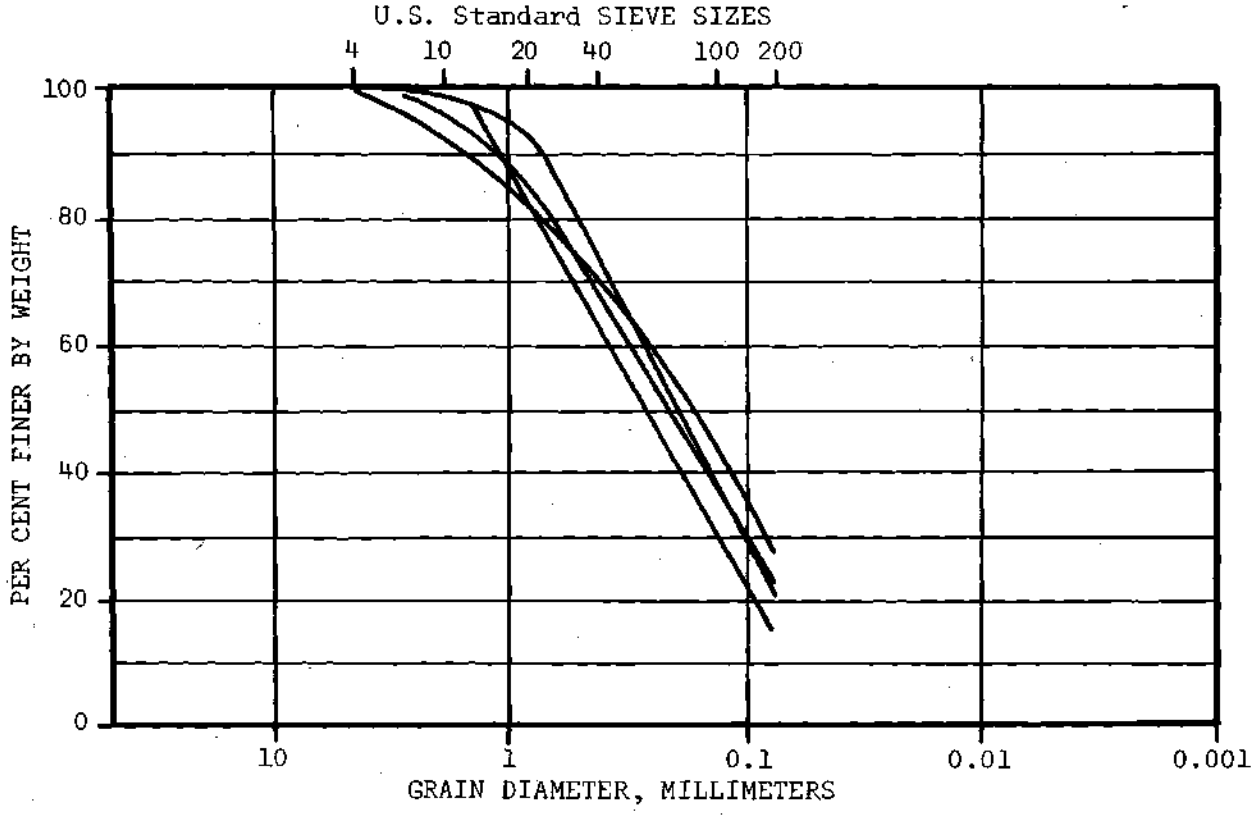

Figure 19. Results of Grain Size Tests on Weathered Rock

unified classification system. The grain size tests were performed by mechanical separation of individual grains over a set of nested sieves, as described in ASTM D422.

In addition to the tests mentioned above, the density of the soil was determined for each undisturbed sample. Diagrams showing average moisture content vs. depth, wet density vs. depth and dry density vs. depth are shown in Appendix A. The curves show a generally increasing moisture content with depth and a great deal of variation (up to 22 per cent) in the moisture contents at any particular depth. The average dry density is quite variable ranging from 83 to 116 pounds per cubic foot.

Discussion of Classification Test Results

The test results indicated that there was a great amount of variability in the properties being tested. This variability is due mainly to the nature of the soil itself and also to the random errors which occur in sampling and testing. Since the results are so variable, a maximum, average and minimum value of the soil strength tests are reported.

Although the test piers are all located within a small area as shown in Figure 11, the borings and supplementary investigation show that the soil is extremely variable, even within this confined space. To minimize the effect of soil variations the results of the tests on undisturbed samples have been grouped together to obtain a most likely value for the soil at the site because the sample closest to the pier in question may not actually represent the existing condition.

This variability has made the description of soil samples extremely difficult and the interpretation of the test results has been severely hampered by this effect. During the field exploration program and in subsequent laboratory tests, the soil was shown to be quite variable and in all cases the laboratory test samples were composed of several materials which were in banded layers. Probably the best description of the soil would be a firm-to-dense weathered rock consisting of alternating layers of firm micaceous silty sand, dense to very dense partially cemented feldspar and quartz layers, with less weathered lenses of partially decomposed gneiss. Individual material layers are approximately between 1/2 inch and 8 inches thick with an undetermined lateral extent. During triaxial testing, the samples sheared along and across the interface of these materials, and in several cases failure was determined on the basis of excessive deformation.

The difference in the direct shear and triaxial shear test results, as shown in Figures 17 and 14, respectively, is probably due entirely to the method of testing and sampling since the materials tested were similar. In the triaxial test the soil can fail along its weakest plane under the imposed stress conditions. The double ring shear test imposes a failure plane on the sample which may not be the weakest possible plane. If the samples were oriented perpendicular to the failure planes in the soil-pier structure, the results of the double ring shear test would probably give the most accurate results. For this study, however, the samples were obtained for double direct shear

testing in a vertical direction and forced to shear in a horizontal plane. This is probably not the manner in which the soil failed in the field. Failure along a predetermined plane adjoining the soil concrete interface resembles the mechanism of failure in the direst shear test.

In all cases the thin wall tube samples used in triaxial testing had to be driven into the ground since they could not be pushed with the available equipment without crushing the tube. This process disturbed the sample to an unknown extent and probably reduced the strength and modulus of elasticity of the soil.

The angle of internal friction determined from triaxial tests is believed to be a little low because of sample disturbance. The samples were first disturbed by driving the sampler and were further disturbed while extruding from the thin wall sampler and during the trimming process. Some disturbance was noted during the trimming in the form of surface hairline cracks. The samples used for double ring shear testing were considerably less disturbed for three reasons: (1) The sampler was pushed into the ground, (2) the samples did not have to be extruded, and (3) the samples did not have to be trimmed to fit the testing machine. Disturbance of samples for the double ring shear test can be attributed only to the sampling operation which utilized a thick wall tube. The sampler is shaped to minimize the disturbance of the thick wall (see Figure 13).

Since both the triaxial test and the double ring shear test have their inherent faults with this material, the triaxial results will be used to represent a lower boundary of the shear strength. The double

ring shear test parameters will be used to represent the upper boundary of shear strength. These bounds were selected since the direct shear test generally gives higher values for the angle of internal friction in sands than the triaxial shear test. For design purposes the soil has been assumed to have an average angle of internal friction of 37 degrees and a cohesion of 500 pounds per square foot.

The average coefficient of at rest earth pressure was determined to be 0.76. This coefficient can be used to estimate the lateral pressure acting on the side of the pier if initial strain is neglected. The pressure on the side of the pier before loading is approximately the effective vertical pressure multiplied by the at rest earth pressure coefficient. This relation is true only if the concrete is poured rapidly enough to prevent deformation of the soil toward the center of the drilled shaft and does not apply at loads other than the initial stress state in the virgin soil assuming the effect of arching can be neglected. This pressure varies during the test as the concrete expands laterally against the soil due to the applied load. The lateral pressure will then approach the passive pressure at the top of the pier as the pier expands laterally and begins to settle.

The results of the load tests on drilled piers in weathered rock are presented in Chapter VI. The materials evaluation program will be discussed again in Chapter VII, where the load test results are analyzed using the strength parameters determined in this chapter.

The complete results of the materials testing program are presented in Appendix A. These results indicate the material variability

in composition, density, water content, strength and modulus of elasticity.

CHAPTER V

INSTRUMENTATION FOR DRILLED PIERS

Introduction

In order to evaluate the stress distribution along the sides of drilled piers, the piers used in testing were instrumented by using electric strain gauge and mechanical load cells. By knowing the load distribution along the drilled pier it is possible to develop a stress distribution pattern. If actual numerical values of load are known at a number of depths in the pier, an approximate quantitative evaluation can be obtained of the stress distribution. These values can then be compared with theoretical results. A design procedure for determining the capacity of drilled piers in weathered rock can then be developed.

To date there have been few published reports (36, 37, 38, 39, 46), of actual interior instrumentation to determine the pattern of skin friction along the sides of a drilled pier. Driven piles have been instrumented in a number of studies (14, 52, 53, 54, 55, 56, 57, 58, 59) to determine the distribution of skin friction. None of the previous instrumentation has been performed on deep foundations in saprolitic soils similar to that found in the Piedmont Region of the United States. Because of the lack of work done on drilled pier instrumentation there have been only a few instruments developed which are able to evaluate the distribution of stress or strain in the drilled piers.

For the study of drilled piers it is mandatory that the instruments (1) perform satisfactorily in concrete, (2) be durable, (3) can be effectively waterproofed, (4) are accurate, and (5) are reasonably inexpensive. A commercial instrument to satisfy all of these is not available at the present time. This necessitated the modification of available instruments and the development of new ones.

A mechanical type of gauge was first thought to be a practical solution to the problem. Since the mechanical gauges had to be installed in concrete, the modulus of elasticity of the gauges had to be similar to that of the concrete and at the same time satisfy the other requirements. It was decided that this would not be satisfactory except at the bottom or along the sides of the piers. The use of a mechanical gauge is further limited since they are not commercially available, they would require an excessive amount of time to manufacture in the necessary quantities, they are expensive to build, and they are not very durable.

Electric strain gauges were then considered. An electric strain gauge was found which was commercially available and had been used in other installations inside a concrete member. After several gauges were obtained for evaluation, it was found that they could be made durable and satisfy the other requirements. The preliminary evaluation of the gauge consisted of molding it in a 6-inch diameter by 12-inch high concrete cylinder. The concrete cylinder with the AS-9 gauge embedded in it having a common long axis was then subjected to axial compression tests under various confining pressures to determine the modulus of elasticity indicated by the electric strain gauge and by mechanical

means (ASTM-C-469). This study showed that the electrical strain gauge readings were nearly identical with the mechanical strain indicator, and that the modulus of elasticity was essentially independent of the confining pressure. The gauges were tested to axial stresses up to 1200 psi and confining pressures up to 25 psi. The type of gauge finally selected was an AS-9 valour concrete embedment gauge manufactured by Baldwin-Lima-Hamilton Electronics. These gauges were placed in different locations and orientations throughout the drilled piers. However, since these gauges are fairly expensive it was prohibitive to use them exclusively to measure all the desired strains.

A type 80, Universal strain gauge manufactured by University Precision Instrument Company was selected for supplementary strain gauge instrumentation. It was found that they could be effectively waterproofed and made sufficiently durable by attaching them to a reinforcing bar or to the pipe frame used to hold the AS-9 gauges in the proper position and orientation. The gauges were also used in groups of three to form two rectangular rosettes for placement in the first test pier.

Because of the difficulty involved in the adaptation of available instruments and the problems involved in the installation of these gauges, it was decided that a trial pier would be installed to evaluate the performance of the instrumentation. This pier would also be part of the test series.

During the testing of pier one it was determined that the difficulty with the mechanical gauge originated in the connections and the pressure tubing. The connections were not durable enough to withstand

the force imposed by the falling concrete. The gauge and connections were modified for the use in pier number six by use of a more durable copper tubing and sweated connections. The gauges were placed at a shallow depth and were not positioned in the drilled pier until the concrete was up to the desired gauge location. This limited the quantity of concrete striking the gauges. During the test these gauges failed to operate property. The cause of failure is not known.

Test pier number one illustrated that the electric strain gauges were performing satisfactorily. The type of electric gauges or installation was not modified for the remaining tests.

Description of Test Gauges

1. *Mechanical Pressure Gauge.* The mechanical gauge selected operated on a hydraulic principle. It consisted of a piston moving inside a confining chamber on one pair of rubber "O" rings. Figure 20 illustrates a cross section of this gauge. These gauges were fabricated in the machine shop at the Georgia Institute of Technology. The various components had to fit together so that the piston could be free to move with respect to the casing and at the same time be sufficiently tight to be able to maintain the cell pressure with the assistance of the "O" rings.

The gauges were milled out of aluminum rods to the desired size and shape. Since the gauges have essentially the same modulus of elasticity as the confined fluid, which is considerably more than that of the concrete, it was decided that these gauges could be used effectively only at, or along, a soil concrete interface. The fluid used to fill

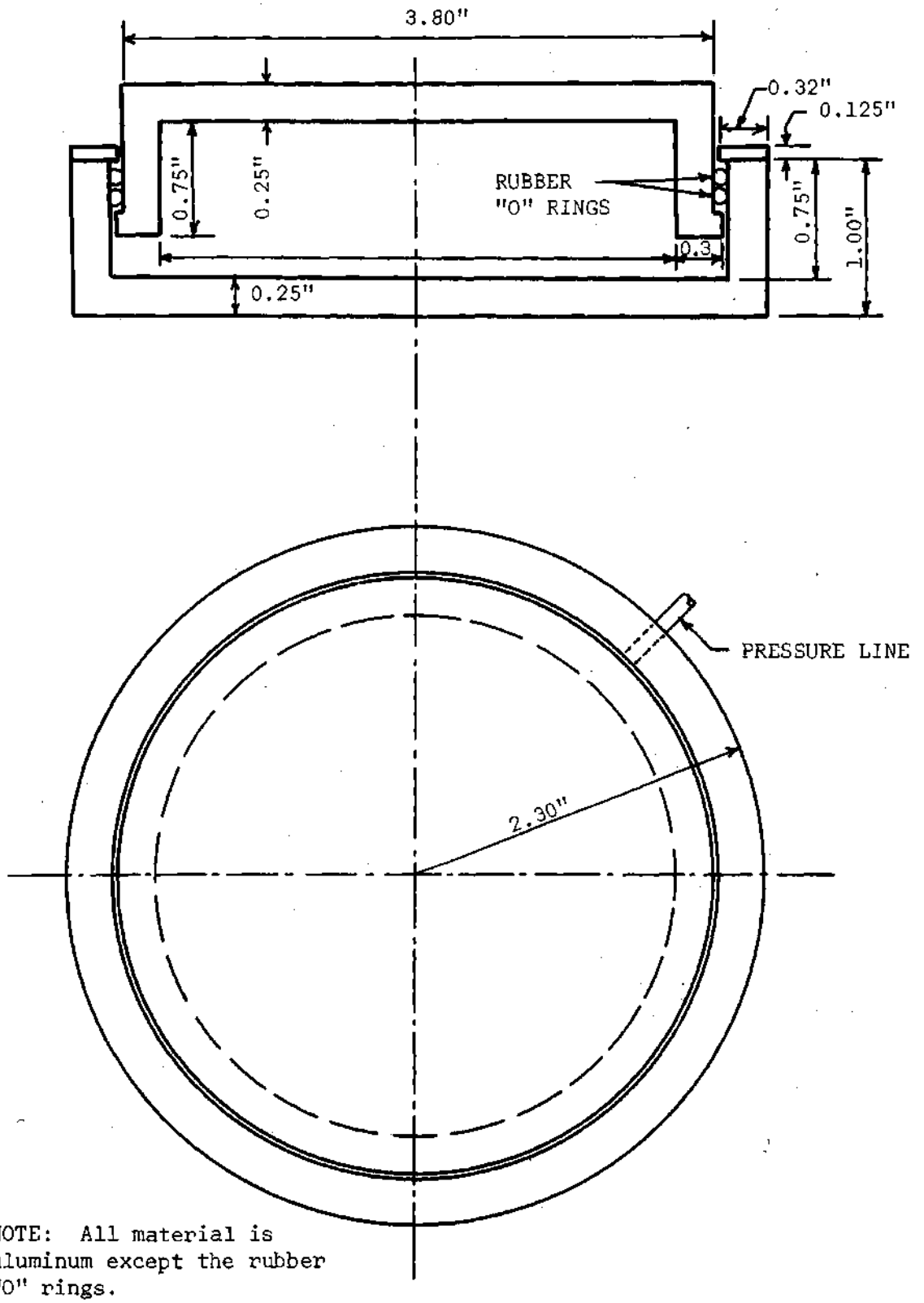

NOTE: All material is aluminum except the rubber "O" rings.

Figure 20. Schematic Drawing of Mechanical Pressure Gauge

the cells at first was a light lubricating oil but was later changed to water. Water was selected since it was easy to work with and it could be de-aired readily. In filling the gauges and tubing it was necessary to eliminate all air from the system, so that the fluid would be practically incompressible and the load would register with only a very small movement. This was accomplished by assembling the gauges in a water tank.

Upon filling the gauges with water, all connections were made tight. The cell was then ready for calibration. Several loading and unloading cycles were required in order to obtain reproducible pressure readings. During the initial loading the "O" rings were probably just rolling into an equilibrium position aided by the pressure and the slight movement of the piston. After calibration the cells were fitted with a 1/4-inch piece of foam rubber covering the "non-moving" piston base to prevent the concrete from intruding into the "moving" parts of the cell.

Approximately 0.06 inches of movement were required to build the pressure up to 1000 pounds per square inch. This is a considerable amount of deflection for the concrete alone to take over the thickness of the cell. It was felt that this movement was due to trapped and dissolved air in the cell and indicating gauge and was not considered too excessive to give estimates of lateral pressure excessive if the cell was placed at the soil-concrete interface.

2. *Electric Strain Gauges.* The primary type of gauge used for this study was an AS-9 concrete embedment gauge. This gauge has an

effective gauge length of six inches which should be sufficient to avoid any local irregularities in stress within the concrete mass. These gauges were initially developed by Worley and Meyer (60).

The gauges consist of several turns of fine wire glued to a thin brass foil. Extra foil is folded over the wires and soldered into place. The leads are made waterproof by means of a heavy wax coating surrounding the area where the leads are connected to the gauge itself. In this manner, a strain gauge is obtained which has essentially the same modulus of elasticity as concrete (obtaining by volume ratios of the constituent materials) and which is completely waterproof.

The strain gauges could not be used without protection since they would break when struck by the falling concrete. The AS-9 gauges were adapted for use in this study by embedding them in mortar prisms measuring 2' x 2" x 10". These gauges were then secured in a holder which was attached to a pipe frame as shown in Figure 21. The gauge was oriented so that its long axis would be either perpendicular or parallel to the vertical axis of the pier.

The other type of electrical gauge used for this study was the type 80, Universal strain gauge with a paper back. These gauges were secured to either a reinforcing bar or to the pipe frame. The procedure used to attach the strain gauges to the reinforcing bars is described in references 61 and 62. The gauges were attached to the pipe frame after cleaning the surface, by gluing with Duco cement. After the gauges were attached the leads were soldered, and the gauge and leads waterproofed in a six-step operation:

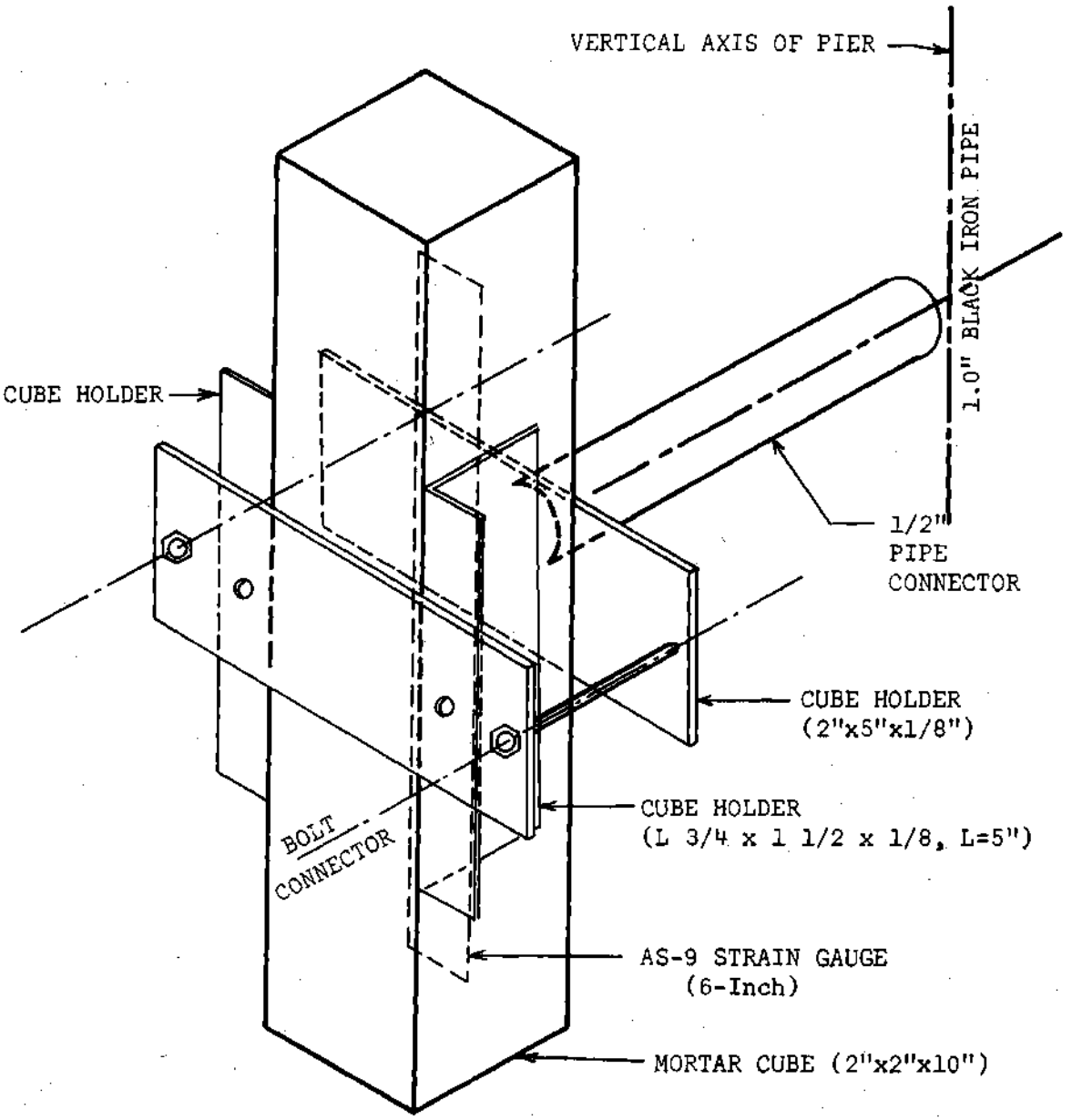

NOTES:
1. All Gauges Alligned in a Plane Parallel or Perpendicular to the Vertical Axis of the Pier.
2. Cube Holder is Made of Aluminum.
3. Pipe Connectors are Made of Black Iron Pipe.
4. Bolts are Brass.

Figure 21. Schematic Drawing of Electric Strain Gauge Embedded in Mortar

1. Scotchgard heat shrink plastic was placed over the wires.

2. The wires were soldered together.

3. The Scotchgard heat shrink plastic was placed over the bare wire and heated to form a tight bond over the exposed section of the wires to maintain continuity and to avoid grounding the wires through the mortar and concrete.

4. The leads were then taped with Scotch electrical tape.

5. The lead wires were bent back over the gauge and fastened to the pipe or reinforcing bar with electrical tape.

6. The gauge and wire were given a liberal coating of Barrier D waterproofing compound manufactured by BLH Electronics. The connecting and waterproofing of the leads for the AS-9 gauges was accomplished in the same manner except the gauges themselves were not coated.

The strain readings obtained using the Type 80 strain gauges had to be corrected for the modulus of elasticity of the reinforcing bars or steel pipe in order to evaluate the stress in the concrete. Since the modulus for the AS-9 gauges were essentially the same as the concrete, a correction did not have to be made. In several cases the gauges were placed where the stress was known. This alleviated the problem of computing the modulus of elasticity of the concrete as placed in the drilled pier if it is assumed that the stress is directly proportional to the strain by the same proportionality constant throughout the pier length. In this manner the stress at various points and in various directions within the concrete pier could be ascertained.

The type 80 strain gauges were also used to make two rectangular rosettes which were installed in test pier number one. These gauges were installed so that one axis was in the vertical direction, one in the radial direction and the other located at an angle of 45 degrees from the other two in the same vertical direction. In this manner the direction of the principal stress could be determined for the vertical plane. The type 80 strain gauges were mounted on the 1/16-inch brass plate as illustrated in Figure 22.

With the exception of test pier seven, all of the instruments were attached to a pipe frame. This frame consisted of a vertical one-inch diameter pipe with elbows and "T's" to connect the strain gauges. The frame was used to hold the gauges securely in place while the concrete was being poured. The vertical pipe was placed along the outside of the drilled pier, at the concrete. In test pier seven a number six reinforcing bar was used instead of the steel pipe. The arms to hold the instruments were welded in place.

Diagrams giving the location of the strain gauges are shown in Figures 23 and 24.

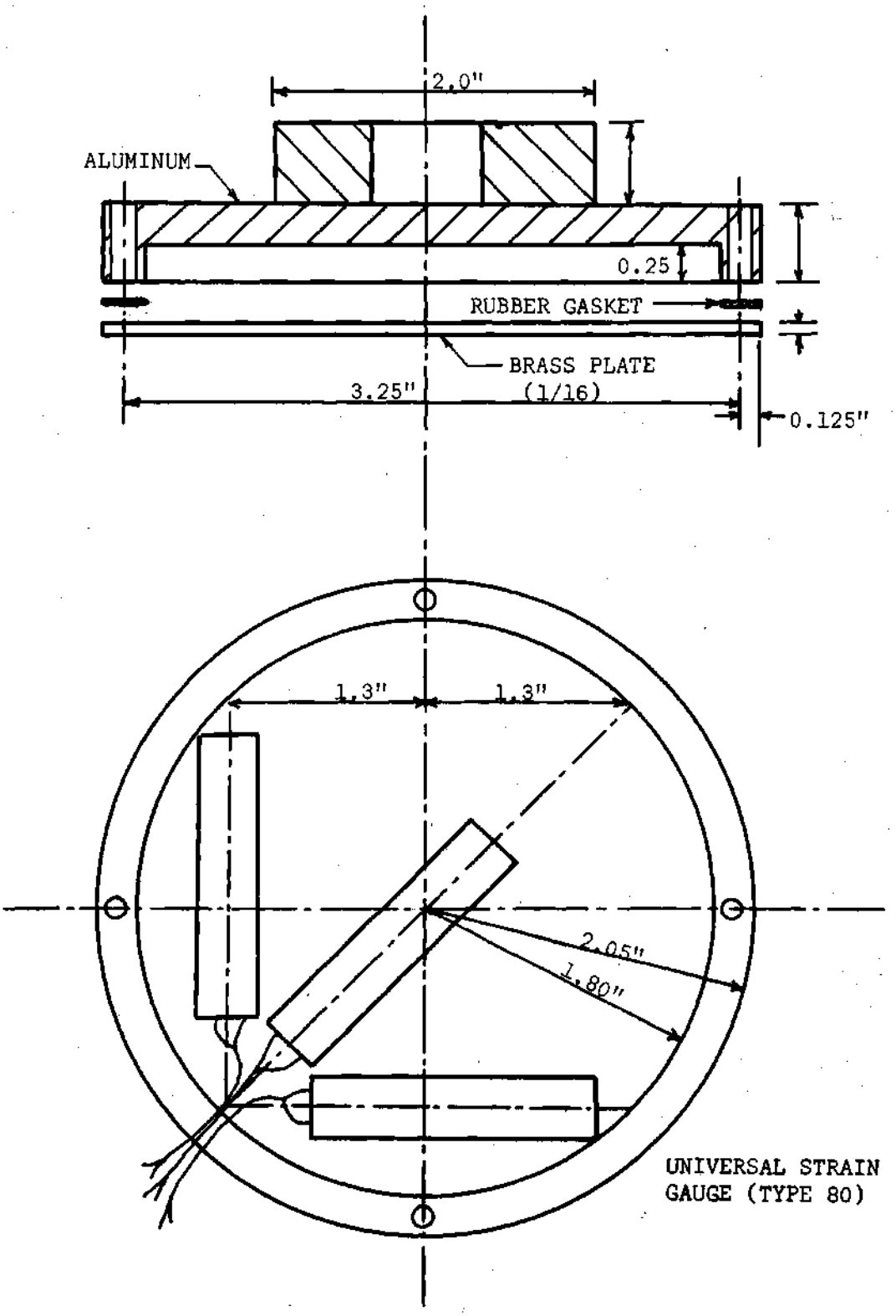

Figure 22. Schematic Drawing of Strain Gauge Rosette

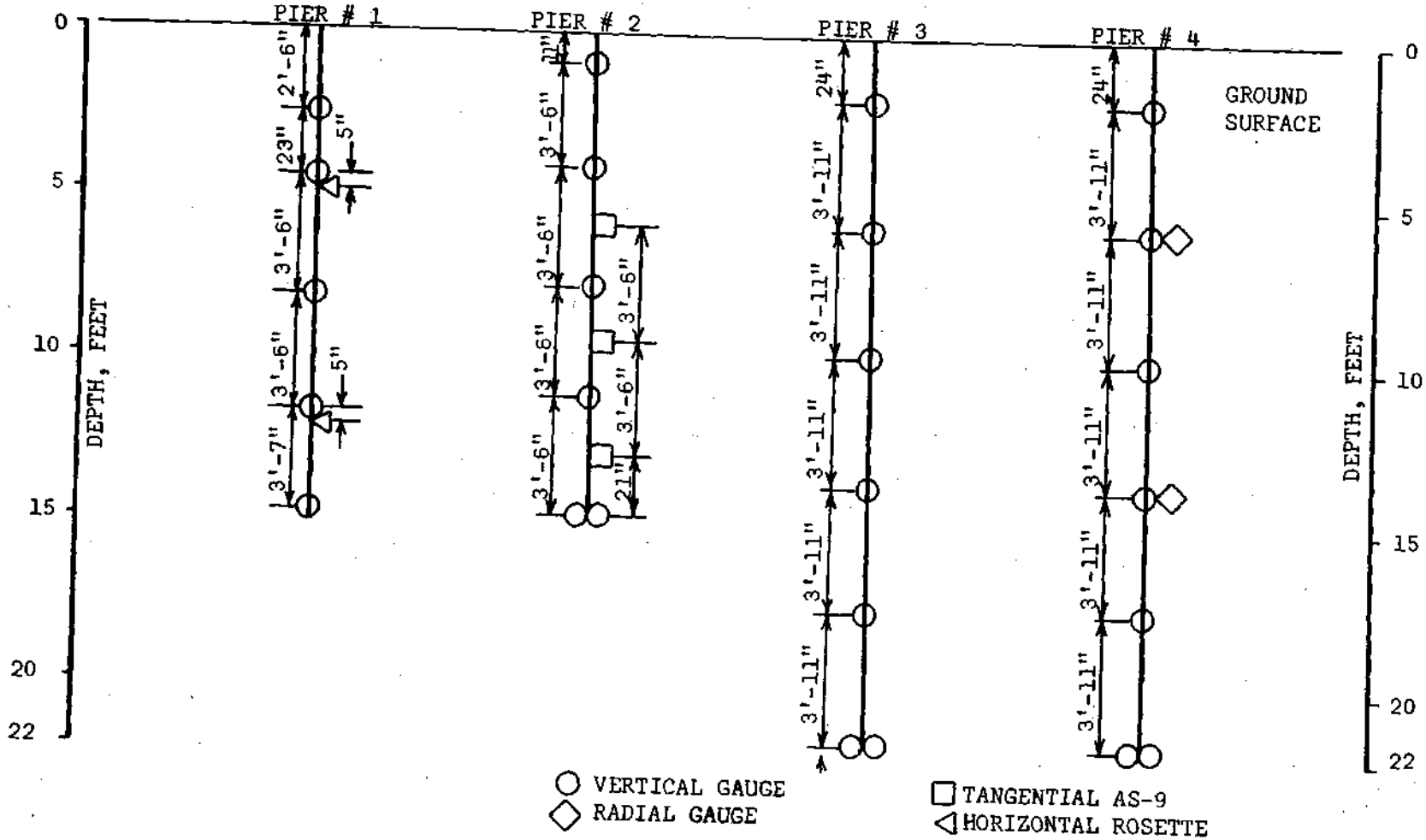

Figure 23. Location and Orientation of Electric Strain Gauges in Test Piers One through Four

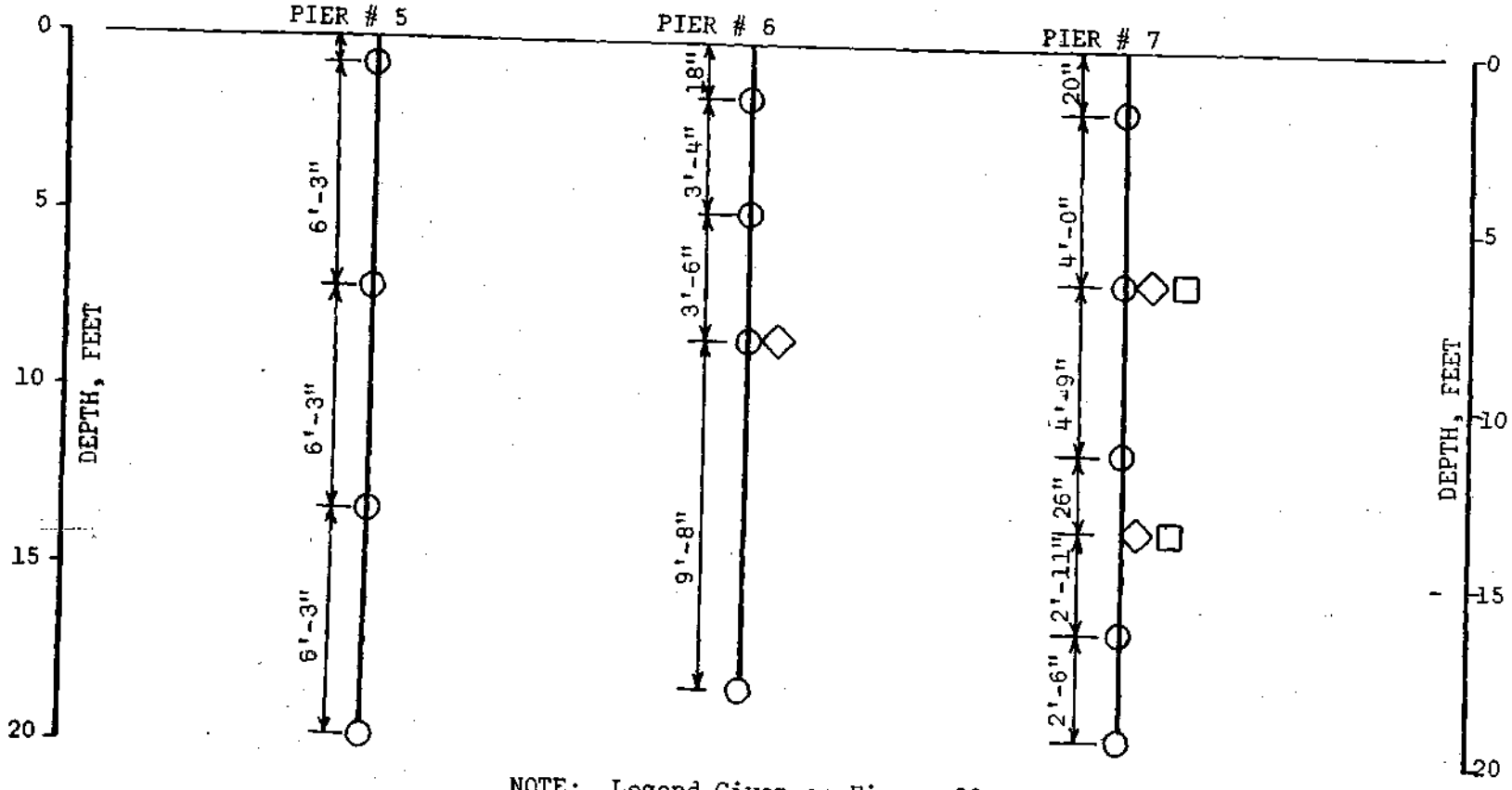

NOTE: Legend Given on Figure 23.

Figure 24. Location and Orientation of Electric Strain Gauges in Test Piers Five, Six and Seven

CHAPTER VI

FIELD TESTING PROGRAM

Introduction

In recent years there has been a large increase in the theoretical and empirical knowledge of the load-carrying capacity of drilled piers. This research has been concerned primarily with the evaluation of various constants which may be used in the standard bearing capacity formulas proposed by Terzaghi (26). Theoretical research has been done for purely cohesive materials and purely cohesionless materials, but to date the theoretical approach has proven to be too cumbersome for a material which exhibits both internal friction and cohesion.

Load bearing tests were performed in this study to evaluate the existing bearing capacity formulas and methods of predicting behavior of drilled piers in weathered rock. The tests were also conducted to determine the distribution of the applied load as a function of depth in the pier. This is an indirect method of determining skin friction forces. Data obtained from the load bearing tests will be presented and discussed briefly in this chapter. Evaluation and further discussion of the test data is given in Chapter VII.

Testing Program

Seven load tests were performed on drilled piers in weathered rock to determine their load-carrying characteristics with regard to

load capacity, skin friction distribution, and load-settlement characteristics. All of the piers tested were nominally 18 inches in diameter. They were drilled utilizing the procedure described in Chapter I. After drilling with a power auger, an attempt was made to clean the bottom with an industrial vacuum prior to filling with concrete having a specified 28-day strength of 3000 psi and a slump of 4 inches. The concrete was not vibrated. Four of the piers tested were designed and constructed to develop their ultimate capacity in a combination of skin friction and end bearing. The remaining three piers were designed to carry their entire load by skin friction. Two of the friction piers were tested in compression while the remaining one was tested in tension. Ice was placed in the bottom of the friction piers to be tested in compression before pouring the concrete to assure that the piers obtained their support from skin friction alone.

The seven test piers were labeled in consecutive order, one through seven. Figure 11 shows the location of the test piers, with respect to the reaction piers and soil test borings, and illustrates the type of loading conditions and depth for the test piers.

Different depths of pier embedment were used to study the effect of depth on the ultimate load-carrying capacity and short term settlement characteristics of a drilled pier.

Test piers one through six were tested using the set-up illustrated in Figure 25. This apparatus was modified for testing pier seven. The modified load test equipment is illustrated in Figure 34. The load test procedure was similar to that described in ASTM D 1143.

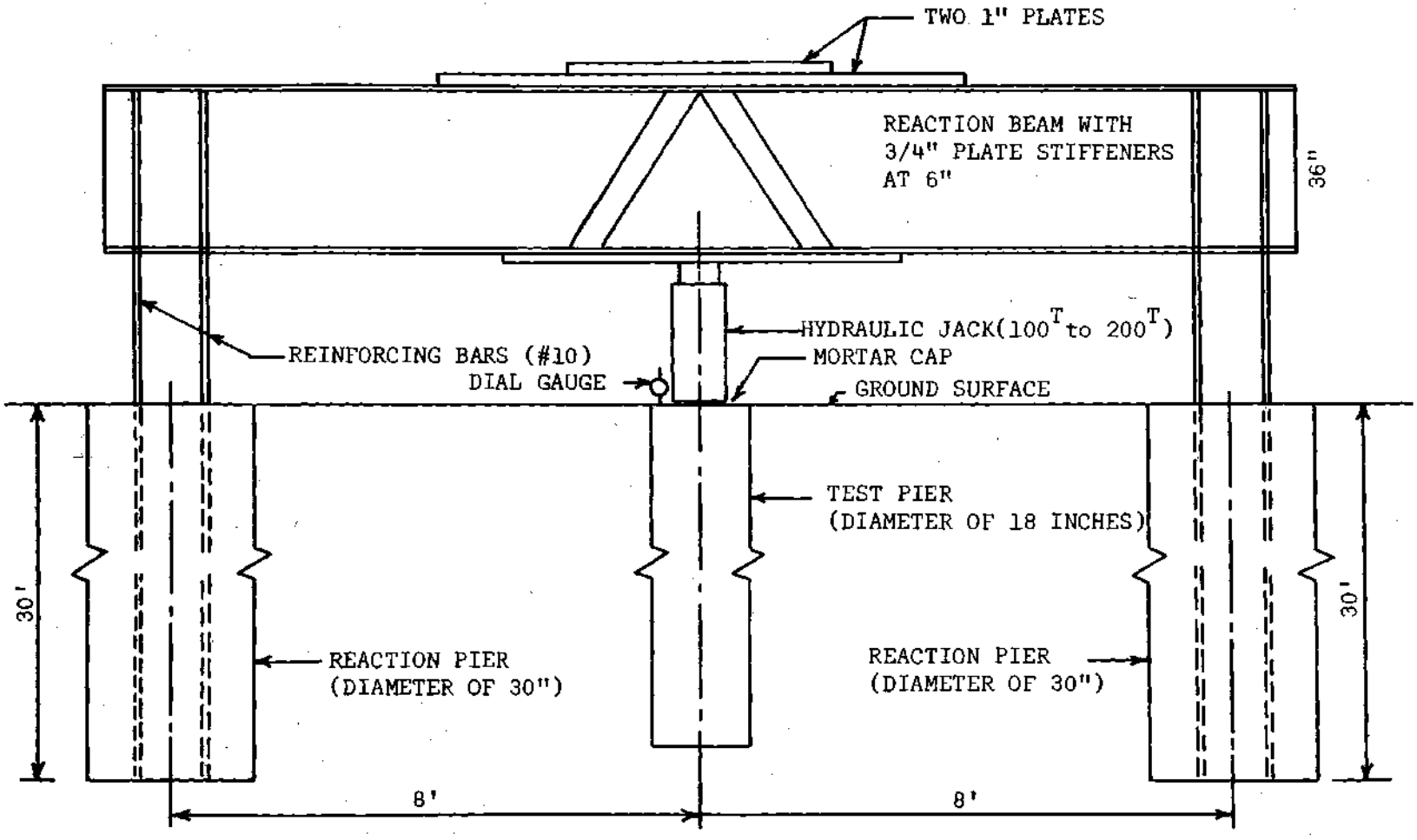

Figure 25. Load Frame and Test Apparatus for Test Piers One through Six

The loads were applied incrementally in such a manner that the deformation rate was less than 0.01 per hour prior to applying the next load increment. The load duration period for each load increment is shown in Table 1 for all test piers.

Presentation of Field Test Data

During the loading of the test piers, the vertical movement of the top was carefully measured by means of a Starret dial gauge with divisions of 0.001 inch. The data obtained were plotted as a load-settlement curve for each pier. Figures 26 through 32 illustrate the load settlement characteristics of the test piers.

Figures 26 and 27 show the load-settlement relationships for test piers one and two, respectively. Each pier is embedded 15 feet into the soil and derives its load-carrying capacity from both skin friction and end bearing. These figures show a curve having an initial linear portion which progresses into a curve having an increasing slope at greater loads.

The ultimate load may be defined as the load at which settlement will continue indefinitely without any increase in load (43, 63, 64, 65). The hypothetical failure load, which is always less than or equal to the ultimate load may be defined as the load at which the tangent from the initial section of the load settlement curve intersects the tangent drawn to the final portion of the load settlement curve. There are several other methods of defining failure load, but they all usually give approximately the same values (65). The definitions

Table 1. Summary of Load Deflection Data

Test Pier	Estimated Ultimate Load, P_u, in Tons	Loading Cycle Number	Total Applied Load at Surface, P, in Tons	P/P_u	Deflection at Top of Pier, Inches (Total/Per Cycle)	Net Deformation at Top of Pier, Inches	Load Duration, Minutes	Total Load at Bottom of Pier, P_B, in Tons	Percentage of Total Applied Load at Bottom
1	108	1	7.5	0.069	0.0037		60	1.8	24
			15.0	0.138	0.0041		57	5.6	37.4
			22.5	0.207	0.0078		60	8.9	39.5
			30.0	0.276	0.0166		90	8.6	28.6
L=15'			37.5	0.345	0.0252		127	10.5	28.0
D=18"			45.0	0.414	0.0346		60	6.2	13.8
			52.5	0.483	0.0469		60	5.3	10.1
			60.0	0.552	0.0670		173	3.9	6.5
			67.5	0.621	0.0863		155	12.0	17.8
			75.0	0.690	0.1132		159	17.3	23.1
			82.5	0.759	0.1428		419	22.0	26.7
			90.0	0.828	0.1730		120	34.4	38.2
			100.0	0.926	0.2606	0.213	610	31.2	31.2
2	110	1	7.5	0.068	0.0000		60	-0.3	-4.0
			15.0	0.136	0.0068		60	-2.7	-18.0
			22.5	0.204	0.0149		60	-5.1	-22.6
			30.0	0.272	0.0251		60	-7.9	-26.3
L=15'			37.5	0.340	0.0365		60	-5.5	-14.7
D=18"			45.0	0.408	0.0514		60	-4.5	-10.0
			52.5	0.476	0.0710		60	-2.2	-4.2
			60.0	0.544	0.0960		60	0	0
			67.5	0.612	0.1200		60	-0.8	-1.9
			75.0	0.680	0.1623		86	0.3	0.4
			82.5	0.748	0.2150		360	4.1	4.1
			90.0	0.816	0.2510		74	3.1	3.1
			97.5	0.884	0.3303		180	7.1	7.1
			105.0	0.952	0.4452	0.389	1290	10.1	10.1
3	120	1	10	0.083	0.0031		15	1.2	12.0
			20	0.167	0.0068		15	2.2	11.0
			30	0.250	0.0100		15	3.6	12.0
			40	0.338	0.0159	0.0038	15	6.0	15.0
		2	20	0.167	0.0116/0.0078		15	1.2	6.0
L=22'			40	0.333	0.0179/0.0141		15	4.5	11.2
D=18"			50	0.417	0.0269/0.0231	0.0100	15	10.2	20.4
		3	20	0.167	0.0171/0.0071		15	0	0
			40	0.333	0.0248/0.0148		15	1.33	3.3
			60	0.417	0.0422/0.0322	0.0046	505	3.33	5.6
		4	20	0.167	0.0099/0.0053		15	-10.5	52.5
			40	0.333	0.0189/0.0143		15	-18.4	-46.0
			60	0.500	0.0291/0.0245		30		
			70	0.583	0.0399/0.0353		30	-14.5	-20.7
			80	0.667	0.0640/0.0594		30	12.1	15.1
			90	0.750	0.1010/0.0964		60	5.9	6.6
			100	0.833	0.1158/0.1512	(1)	2		

(1) Net settlement not measured.

Table 1. Summary of Load Deflection Data (Continued)

Test Pier	Estimated Ultimate Load, P_u, in Tons	Loading Cycle Number	Total Applied Load at Surface, P, in Tons	P/P_u	Deflection at Top of Pier, Inches (Total/Per Cycle)	Net Deformation at Top of Pier, Inches	Load Duration, Minutes	Total Load at Bottom of Pier, P_B, in Tons	Percentage of Total Applied Load at Bottom
4	135	1	10	0.074	0.0025		30	4.8	48
			20	0.148	0.0065		30	3.7	18.5
			30	0.222	0.0128		30	-1.6	-1.6
L=22'			40	0.296	0.0187		30	-4.7	-4.7
D=18"			50	0.370	0.0259		30	-5.0	-5.0
			60	0.444	0.0337	(1)	30	-10.2	-10.2
		2	30	0.222	0.0272/0.0112		15	6.1	20.4
			60	0.444	0.0413/0.0253		15	8.8	14.7
			70	0.518	0.0490/0.0330		30	3.3	4.7
			80	0.592	0.0660/0.0550	0.0230	60	-1.7	-2.1
		3	20	0.148	0.0481/0.0091		15	0.7	3.5
			40	0.296	0.0586/0.0196		15	0.6	1.5
			60	0.444	0.0676/0.0286		15	-0.6	-1.0
			80	0.592	0.0792/0.0402		30	0	0
			90	0.666	0.0940/0.0550		30	-5.0	-0.5
			100	0.740	0.1298/0.0908		105		
			110	0.814	0.1793/0.1403		75	21.2	19.3
			120	0.888	0.2430/0.2040		75	25.1	20.9
			130	0.962	0.3710/0.3320	0.2840	705	31.4	24.2
5	85	1	7.5	0.088	0.0021		62		
	(2)		15.0	0.176	0.0061		60		
			22.5	0.264	0.0132		60		
			30.0	0.353	0.0254		60		
			37.5	0.441	0.0412	0.0258	15		
		2	15.0	0.176	0.0339/0.0079		15		
			30.0	0.353	0.0432/0.0172		15		
			45.0	0.529	0.0972/0.0712		60		
			52.5	0.617	0.1985/0.1727	0.1405	60		
		3	15	0.176	0.1500/0.0095		15		
			30	0.353	0.1633/0.0228		18		
			45	0.529	0.1803/0.0398	0.0110	8		
6	85	1	10	0.117	0.0091		30		
			20	0.234	0.0248		30		
			30	0.351	0.0492		30		
			40	0.468	0.0864		30		
			50	0.585	0.1737		65		
			60	0.702	0.3295		60		
			65	0.760	0.4085		60		
			70	0.819	0.5190		60		
			75	0.877	0.6344		60		
			80	0.936	0.8040	0.7374	1530		
7	40	1	10	0.250	0.0040		15		
			20	0.500	0.0115		30		
			30	0.750	0.0488		64		
			35	0.875	0.0834	(1)	60		

(1) Net settlement not measured.
(2) Based on results from Test Pier 6.

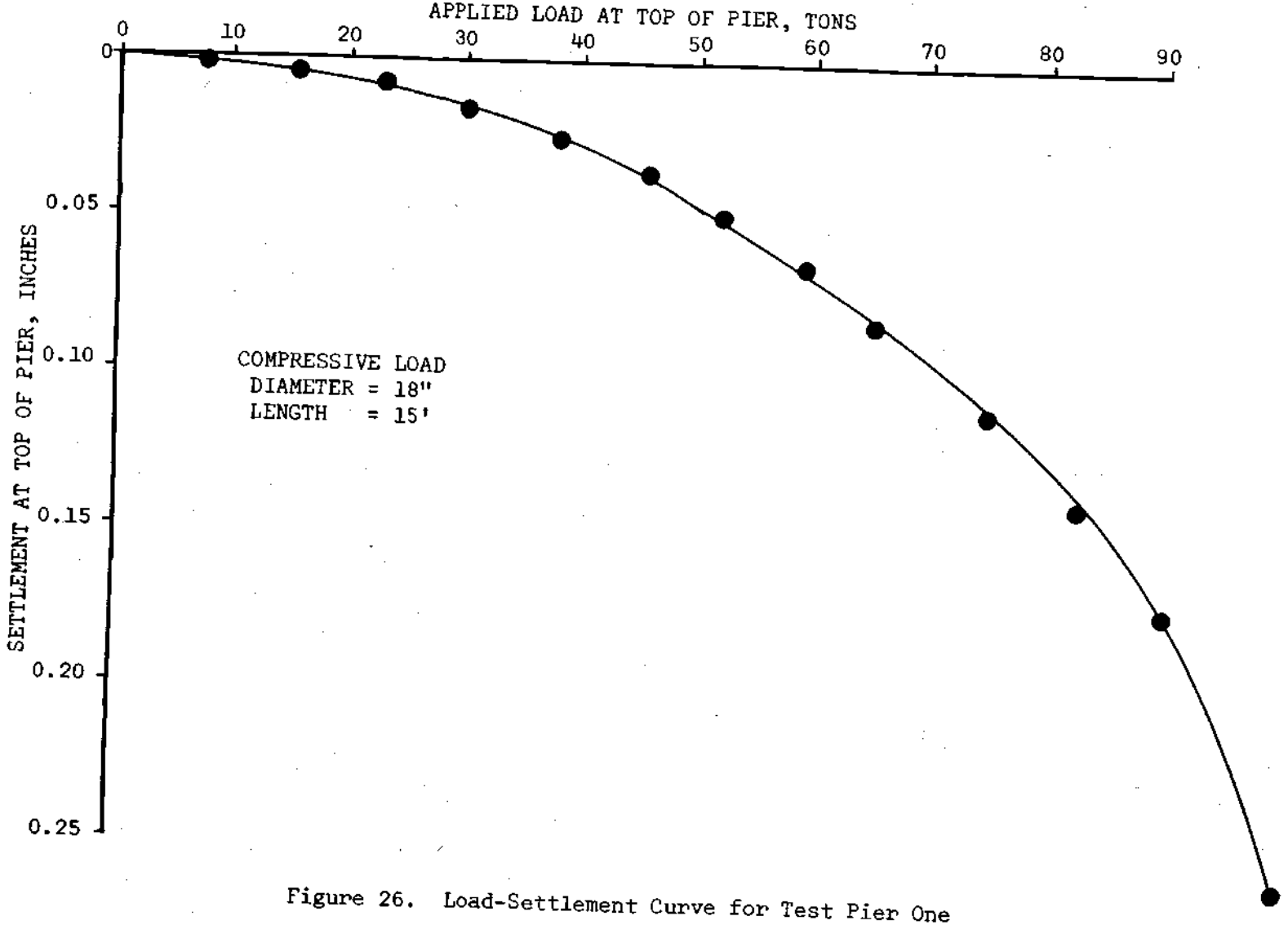

Figure 26. Load-Settlement Curve for Test Pier One

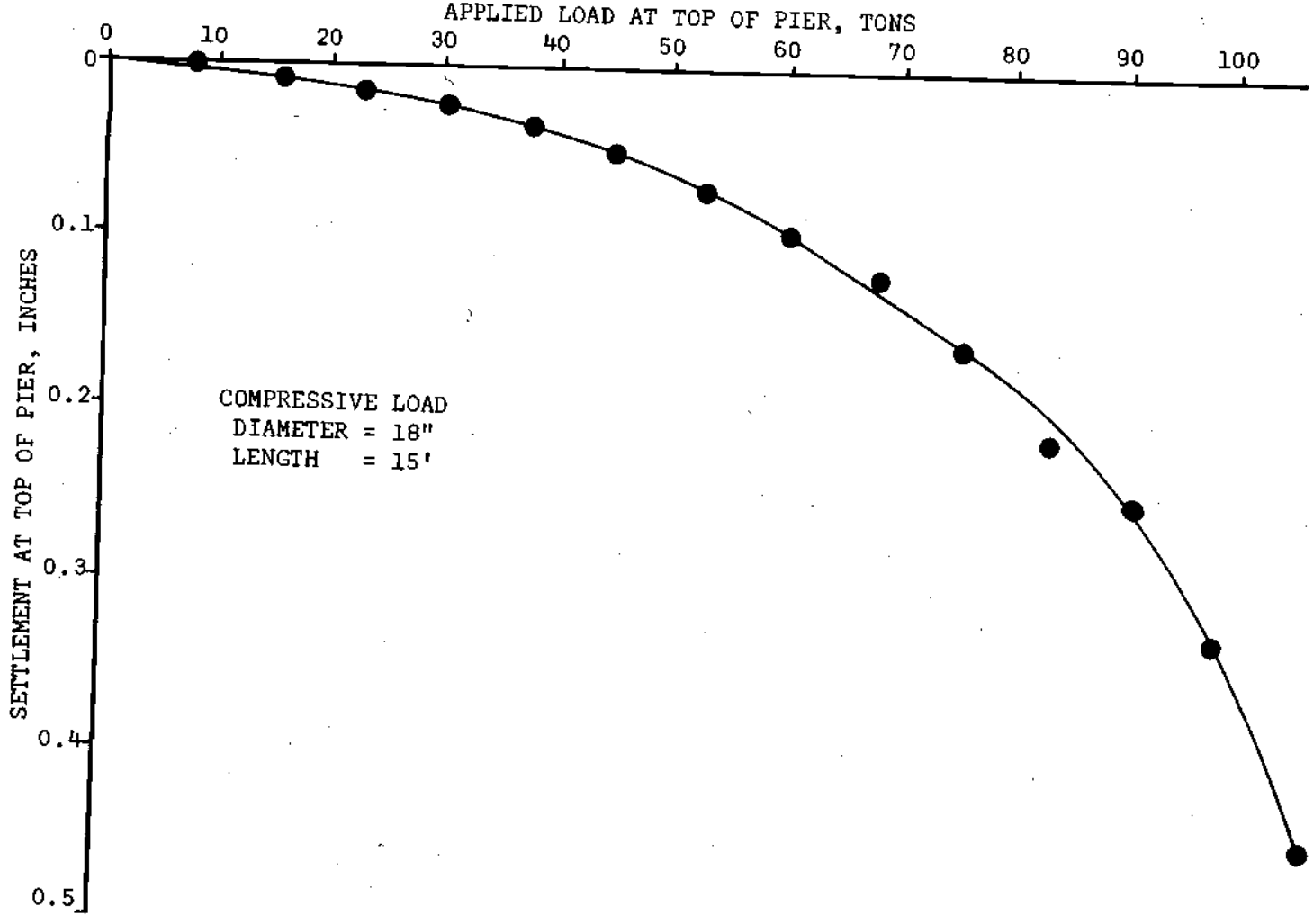

Figure 27. Load-Settlement Curve for Test Pier Two

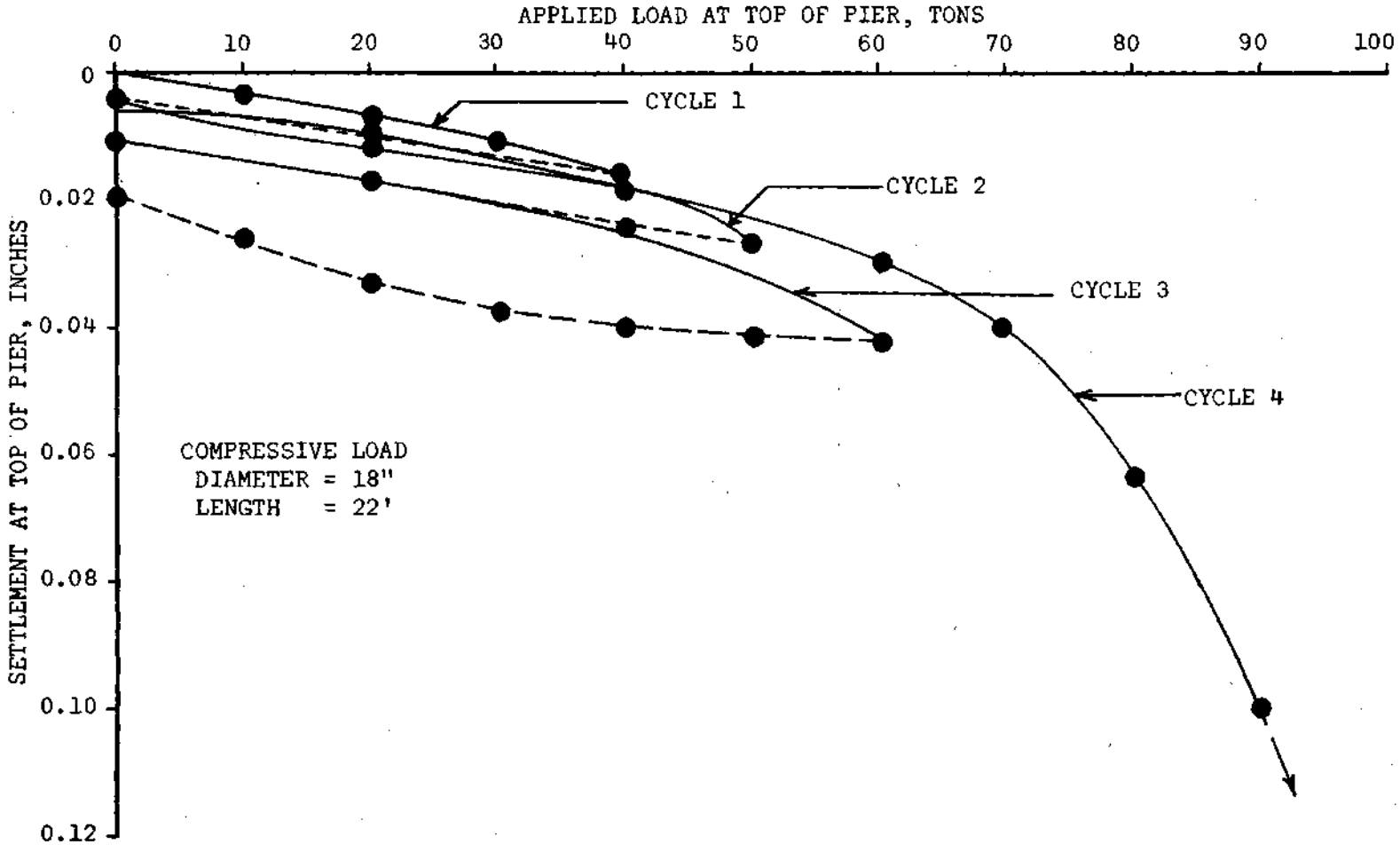

Figure 28. Load-Settlement Curve for Test Pier Three

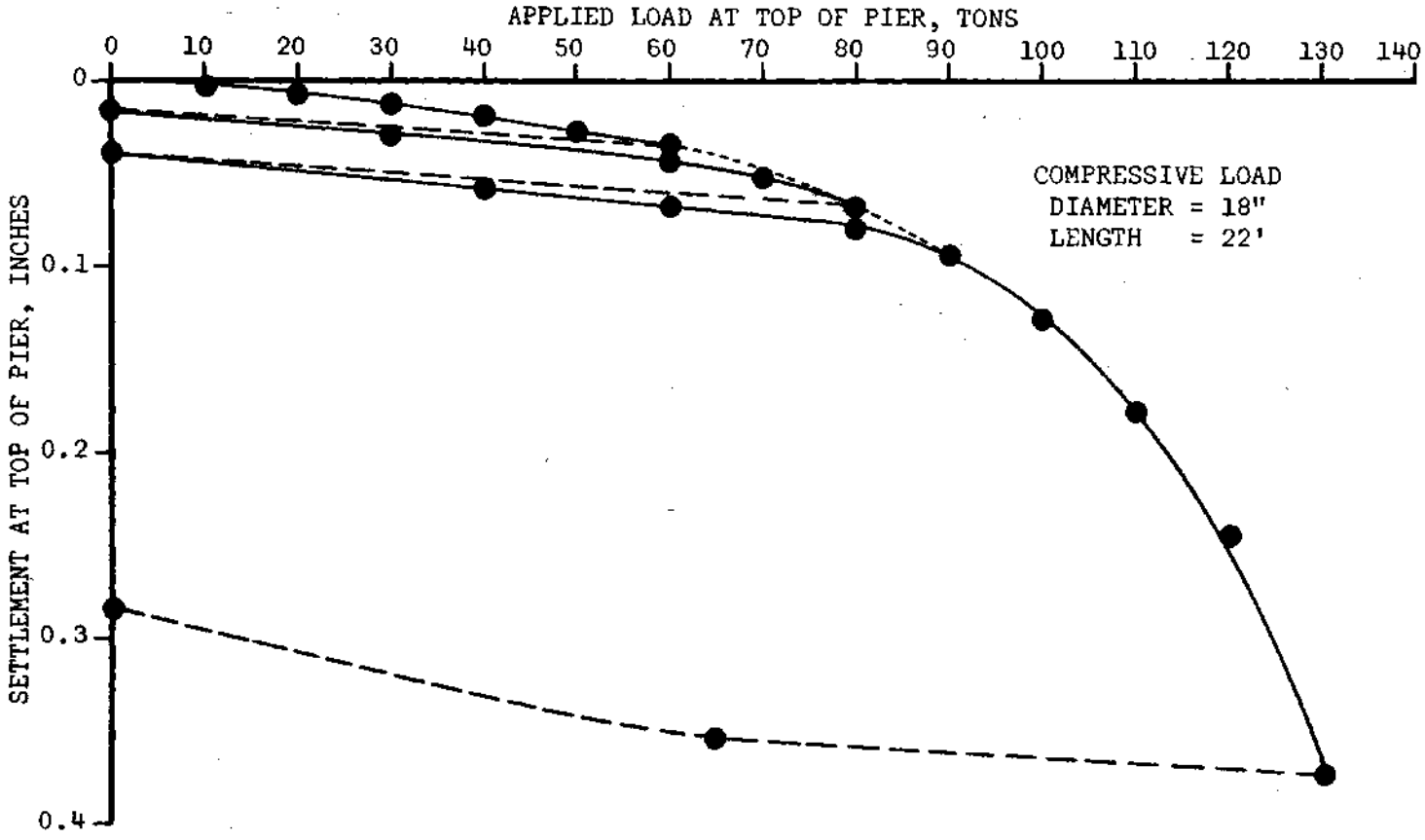

Figure 29. Load-Settlement Curve for Test Pier Four

presented above for ultimate load and failure load will be used throughout this paper.

The ultimate load for test piers one and two could not be measured because of the limitations of the loading equipment, but it was in excess of 100 tons in both cases. The failure load for test pier one was 75 tons and test pier two failed at 84 tons. The total settlement for test pier two is greater than for test pier one. The settlement at the indicated failure load is 0.106 inches for test pier one and 0.215 inches for test pier two. The failure loads of all test piers and the settlements at the indicated failure load are shown in Table 2.

Table 2. Failure Loads and the Settlement at the Indicated Failure Load

Pier Number	Failure Load (Tons)	Deflection at Failure (Inches)
1	75	0.106
2	84	0.215
3	76	0.028
4	115	0.210
5	59	0.285
6	58	0.311

Test piers three and four were tested so that various cyclic loads could be applied and removed several times before loading the pier to its ultimate value. Test pier three was loaded four times and test pier four was loaded three times. Table 1 illustrates the load

deflection data for each cycle of loading for each test pier. The loading sequences are illustrated in Figures 28 and 29 for test pier three and four. The approximate failure load for test pier three was 76 tons at a settlement of 0.028 inches. The failure load for test pier four was 115 tons at a settlement of 0.21 inches. The failure load and displacement for each test pier are tabulated in Table 2. The loading of test pier three could not be carried any further. Several welds on the reaction beam failed at an applied load of 90 tons, causing an eccentric load to be applied to the pier, which subsequently caused the concrete at the top of the pier to split. The load-deflection curve was not extended enough to permit an accurate prediction of the failure load for test pier three. From the shape of the other load-settlement curves it appears that test pier three had not yet been loaded to a point of impending failure or to a point which would indicate that the slope of the load settlement curve was increasing at a sufficient rate to indicate failure would occur within the next few load increments. The small deflections at the applied loads also indicate that the pier had not failed. The tangent drawn to the final linear portion of the load settlement curve to determine an estimate failure load in Figure 28 is probably only the gradual curvature portion of the curve before the load-displacement relationship starts showing a continually greater slope with increasing loads.

It is of interest to note the different effects of repeated loadings shown by load tests three and four as illustrated in Figures 28 and 29, respectively. In test pier three the initial three load

cycles were applied within a five-hour period. The load was then maintained for seven and a half hours (Table 1). At this time the pier was unloaded and allowed to remain unloaded for approximately eight hours. The load was then increased until the concrete failed while trying to increase the applied load to 100 tons (Figure 30). After the extended unload period, test pier three showed a net settlement of 0.0046 inches from the original position which indicates that the drilled-pier soil system behaved almost entirely in an elastic manner.

The settlement of test pier three as a function of time for each load increment is illustrated in Figure 30 for all four load cycles. At small loads the settlement occurs almost instantaneously upon application of load. This is illustrated for the first three loading cycles and for the initial portion of the fourth loading cycle. At greater applied loads, during the fourth loading cycle, the settlement continues with increasing time, and at the ultimate load the settlement will continue for an extended period under the same applied load.

The time periods between the load cycles for test pier four were greater than for test pier three. A five-day period elapsed between the first and second load cycles and a one-day period between the second and third load cycles. Displacements were not monitored during these periods. The slope of the load-settlement curves for subsequent cycles of loading are practically identical for test pier three while the slopes of the load-settlement curves in test-pier four become flatter on subsequent load repetitions. The relative settlements incurred for each load increment are illustrated in Table 1. The slopes of the curves

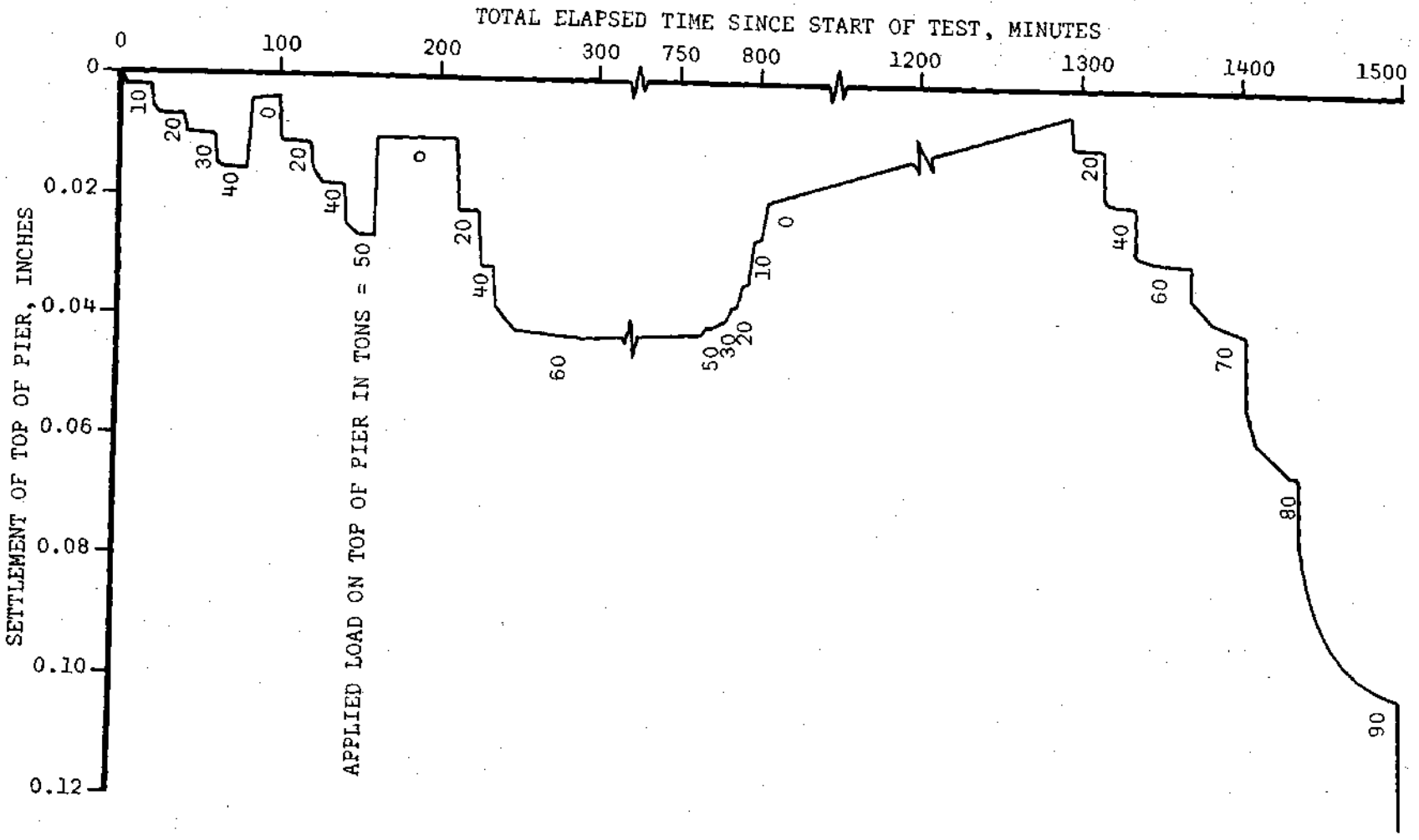

Figure 30. Time-Settlement Curve for Test Pier Three

indicate that the soil-pier system behaved nearly elastically for the loading cycles of test pier three up to about 50 tons. The gradually increasing slope of the load deformation curve for test pier four upon subsequent load repetitions indicates that the behavior of the soil-pier system is not completely elastic. Table 1 illustrates the load settlement relationships for all test piers.

For all three cycles of loads in test pier four and for the first three cycles in test pier three, the additional cycles did not affect the shape of the cumulative load settlement curve. This is illustrated by the dotted lines in Figures 29 and 31. This means that for these tests, few cycles of slow load repetition has little, if any, effect on the shape of the load settlement curve, and that approximately the same deflection is obtained under the same loading during each subsequent loading cycle for the number of cycles tested while the load was still in the elastic range. Table 1 illustrates the load level obtained and the settlement for each cycle of loading. This same type of relationship is also shown in Figure 32 for test pier five. The curve for pier five could not be extended any further due to a failure of the load testing apparatus during the third loading cycle.

Test piers five, six and seven were tested to evaluate the frictional load-carrying capacity of drilled piers. End bearing was prevented, as described previously in tests five and six, and test pier seven was tested in tension. The load-deflection curves for test piers five, six and seven are presented in Figures 32, 33, and 34, respectively. The shape of the load displacement curves for the friction

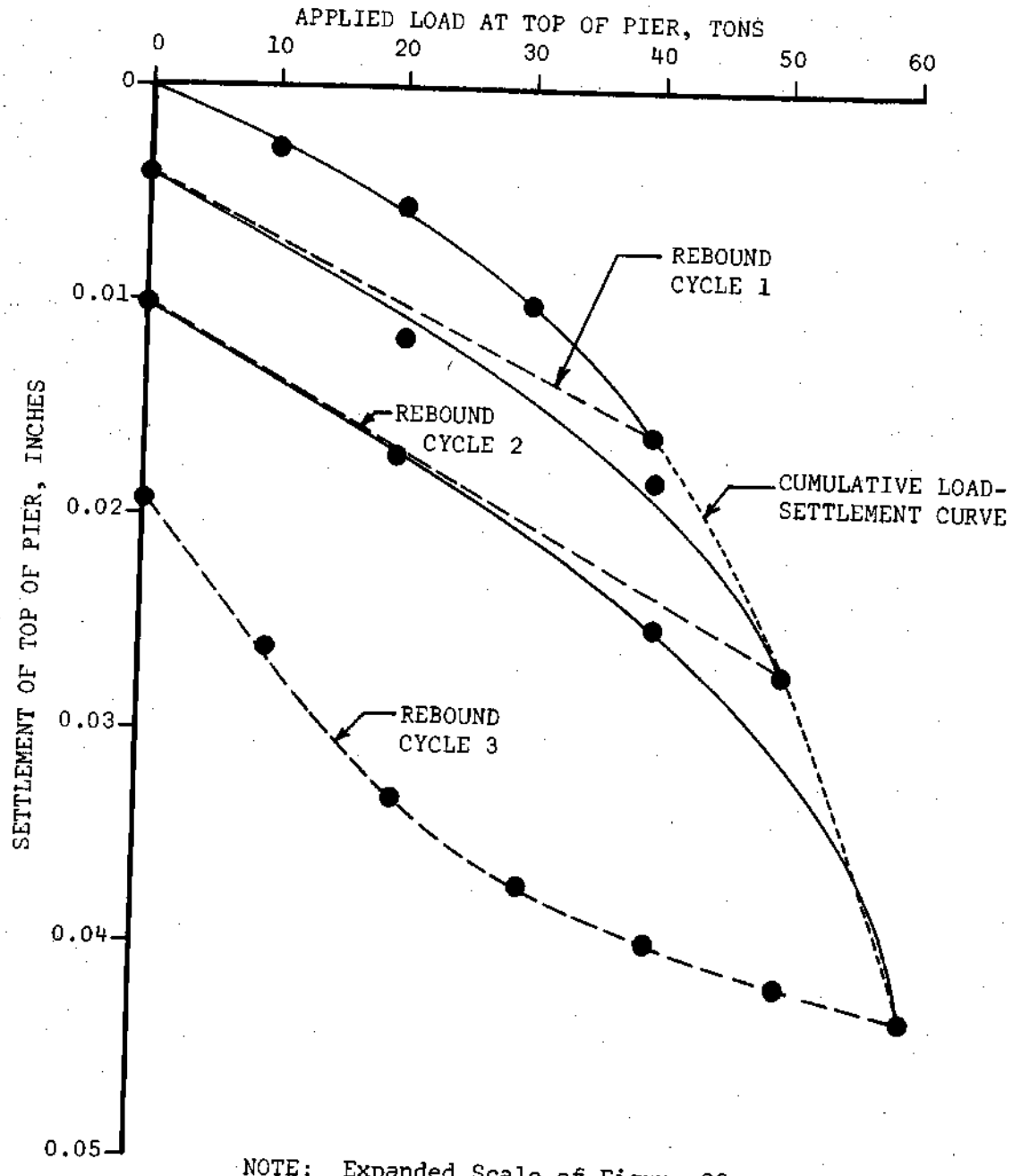

NOTE: Expanded Scale of Figure 28.

Figure 31. Load-Settlement Curve for Test Pier Three

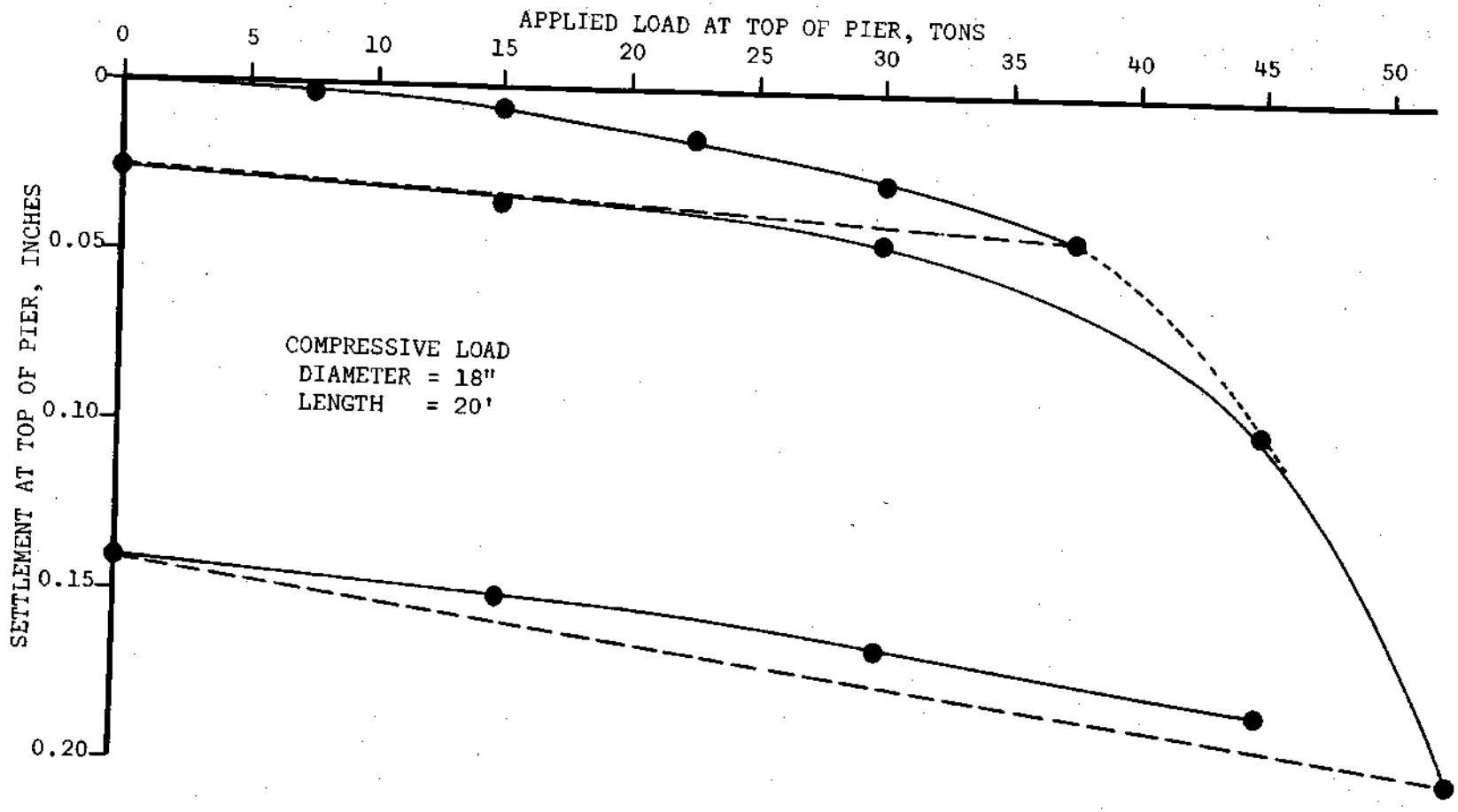

Figure 32. Load-Settlement Curve for Test Pier Five

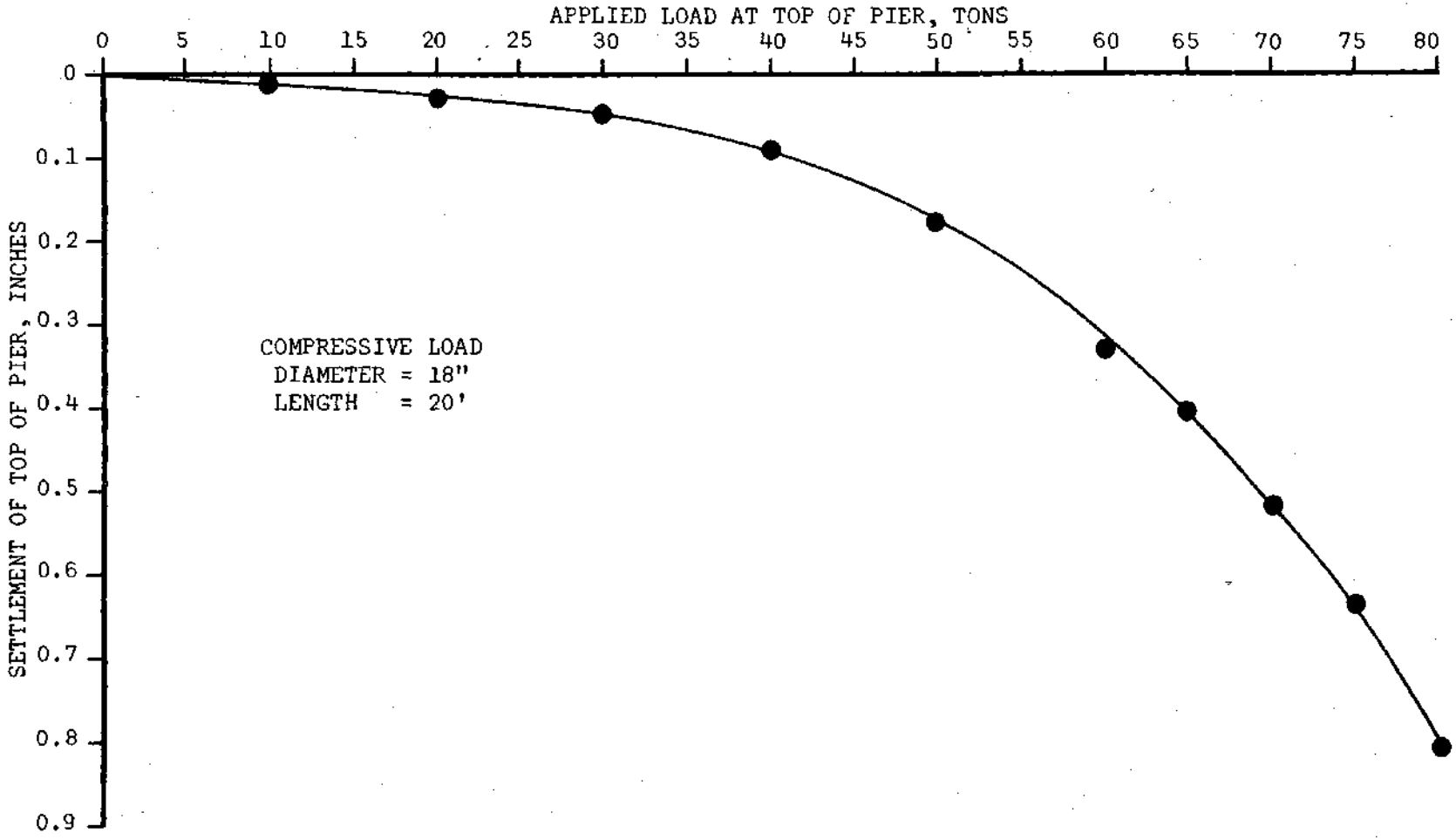

Figure 33. Load-Settlement Curve for Test Pier Six

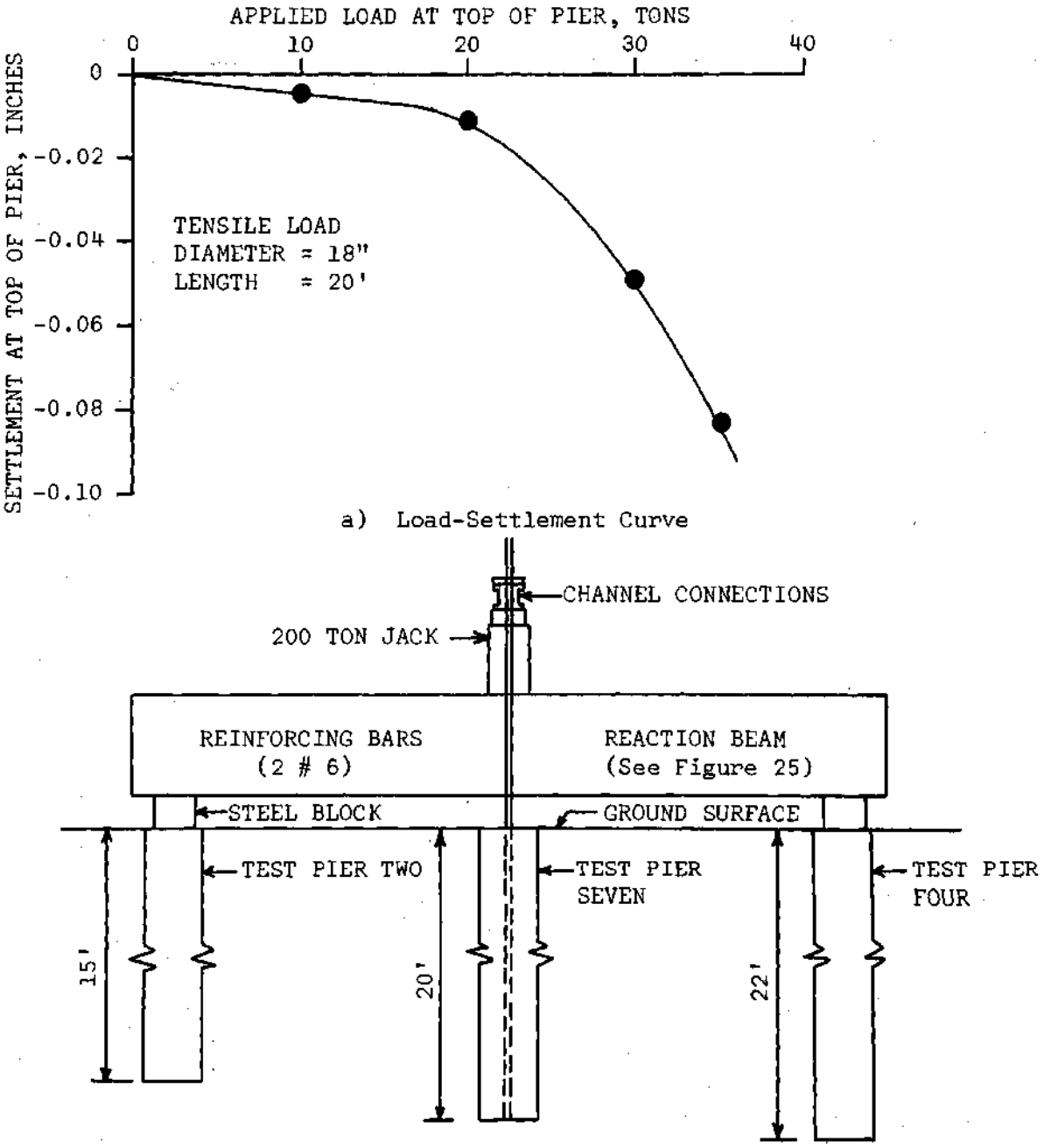

Figure 34. Load-Settlement Curve and Load Test Apparatus for Test Pier Seven

piers is similar to piers which derive their support from end bearing and skin friction, the only difference being the shorter length of the initial approximately linear portion and greater slope of the curved portion of the load deflection curve for friction piers.

From the load deflection curves for friction piers the failure load could be determined for test pier six only. This pier failed at a load of 57 1/2 tons and a deflection of 0.311 inches. The load-displacement curve for test pier five permitted evaluation of an approximate failure load which is estimated to be 41 tons at a deflection of 0.06 inches. The approximate failure load for test pier five is seen to be considerably less than for test pier six which is also 20 feet long and 18 inches in diameter. The settlement at the approximate failure load for test pier five is also considerably less than for test pier six. The difference in failure load and deflection at failure are probably because of the variation in soil conditions from one test pier to another. If the loading could have been continued for test pier five, a different failure load may have been determined.

The tests on piers deriving their support from skin friction alone indicate that the load at failure is considerably less and occurs at a greater settlement than for piers which derive their support from a combination of skin friction and end bearing. This aspect of the load-deflection relationships is discussed in greater detail in Chapter VII.

The approximate failure loads and deflection at the failure loads are given in Table 2.

The second purpose of the field testing program was to determine the distribution of the load in the pier as a function of depth. The load distribution was measured for all seven test piers. Unfortunately, meaningful results could not be obtained from horizontally oriented gages and from the piers which derived their load-carrying ability from skin friction alone due to failure in the instruments. Correlatable data was available at a sufficient number of locations to evaluate the load distribution along the length of test piers one, two, three and four. The load in the test pier is presented as a function of depth for test piers one, two, three and four in Figures 35 through 38.

The load at various depths was computed utilizing the strain measurements obtained using the instrumentation described in Chapter V. Since the load was not measured directly, the strain readings had to be transformed to the corresponding stress. This was accomplished by assuming:

(1) that the strain indicated by the strain gage nearest the point of load appliation at the top of the pier, was directly proportional to the applied load. A load factor was thus obtained for each load increment in each test pier and may be described as follows:

$$LF = \frac{P}{e}$$

where LF = Load Factor; P = Applied Load (Tons); e = Strain Measured in Uppermost Strain Gage (in/in x 10^{-6}).

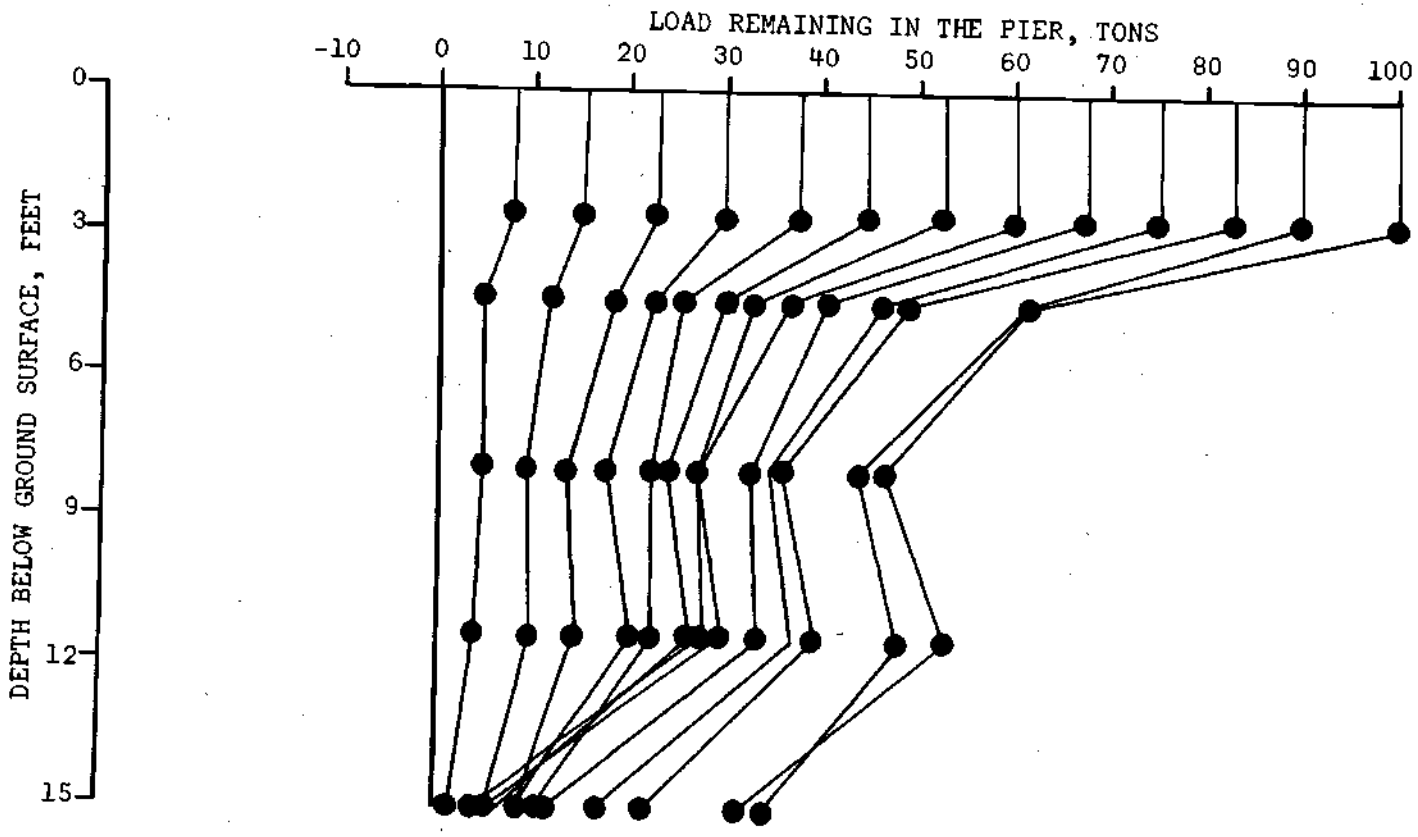

Figure 35. Load Remaining in Test Pier One as a Function of Depth and Applied Load

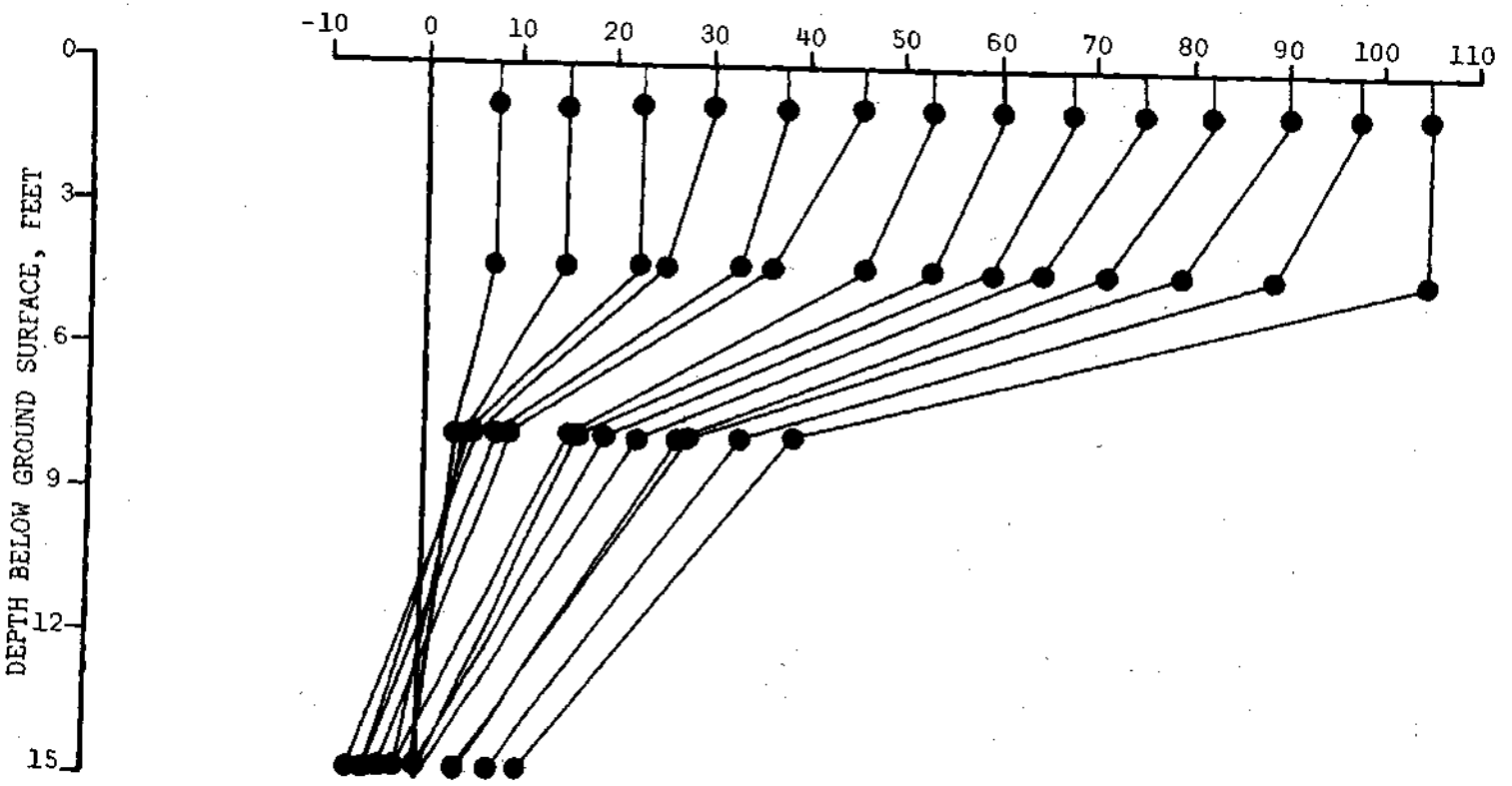

Figure 36. Load Remaining in Test Pier Two as a Function of Depth and Applied Load

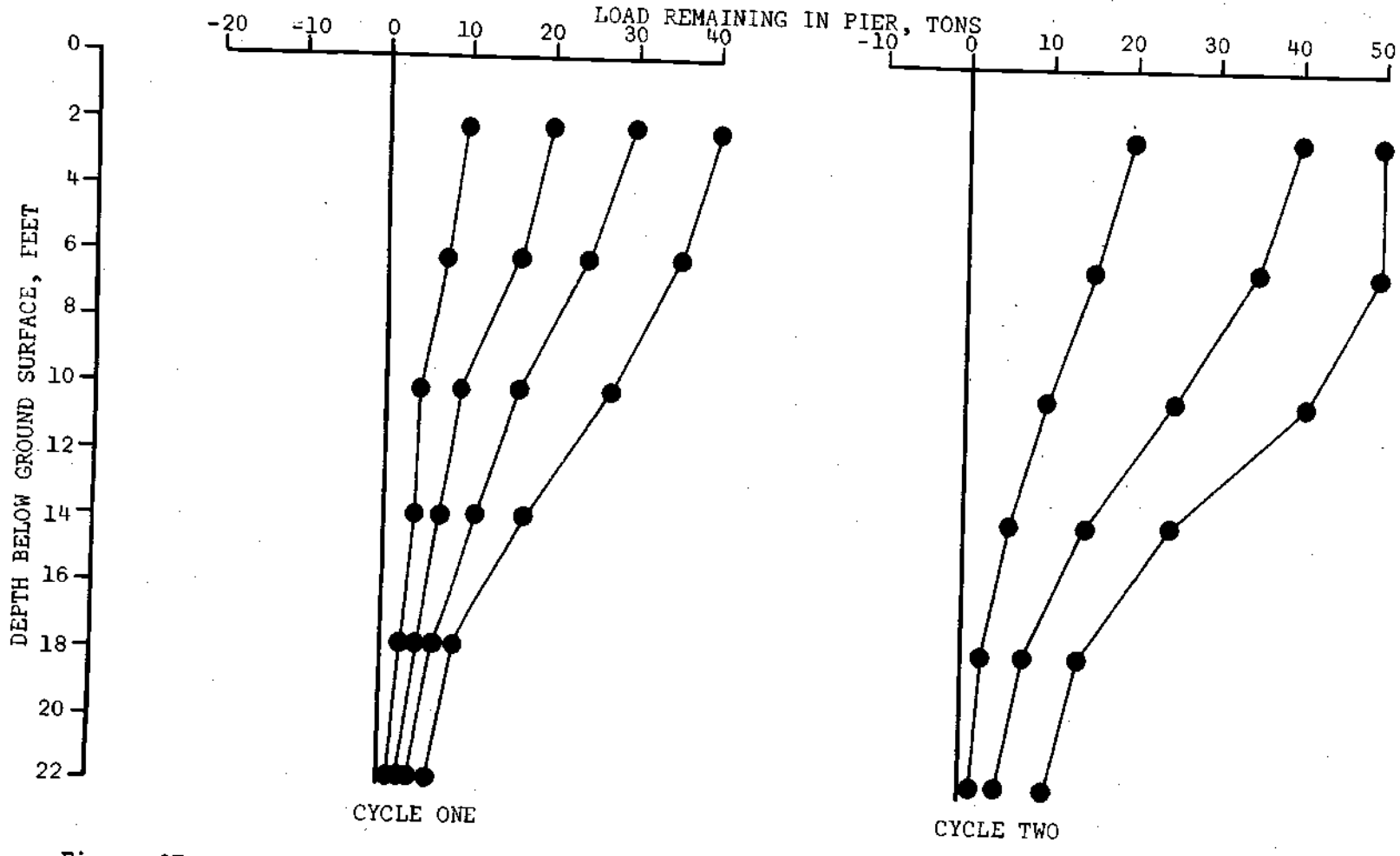

Figure 37. Load Remaining in Test Pier Three as a Function of Depth and Applied Load

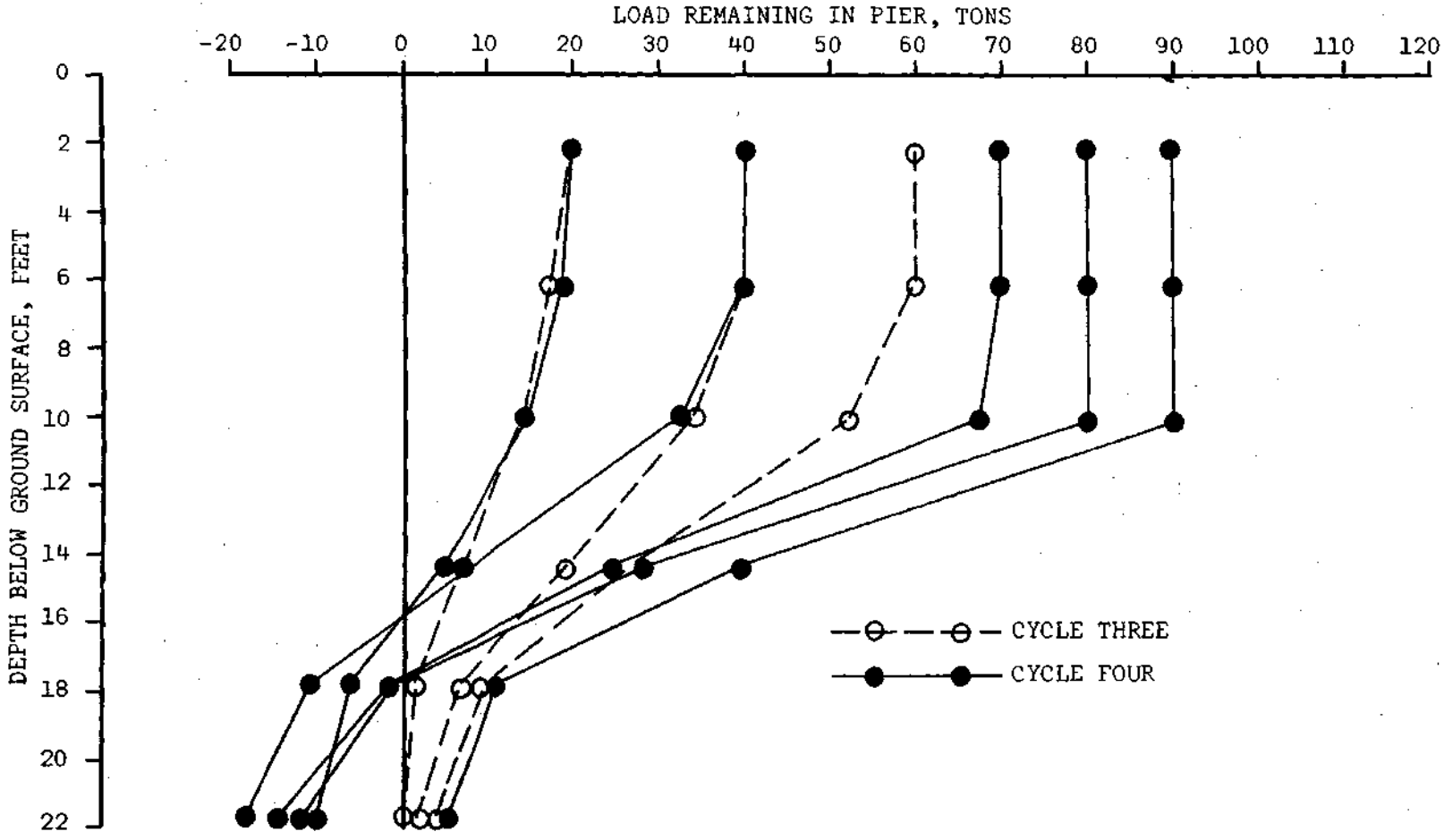

Figure 37. Load Remaining in Test Pier Three as a Function of Depth and Applied Load (Continued)

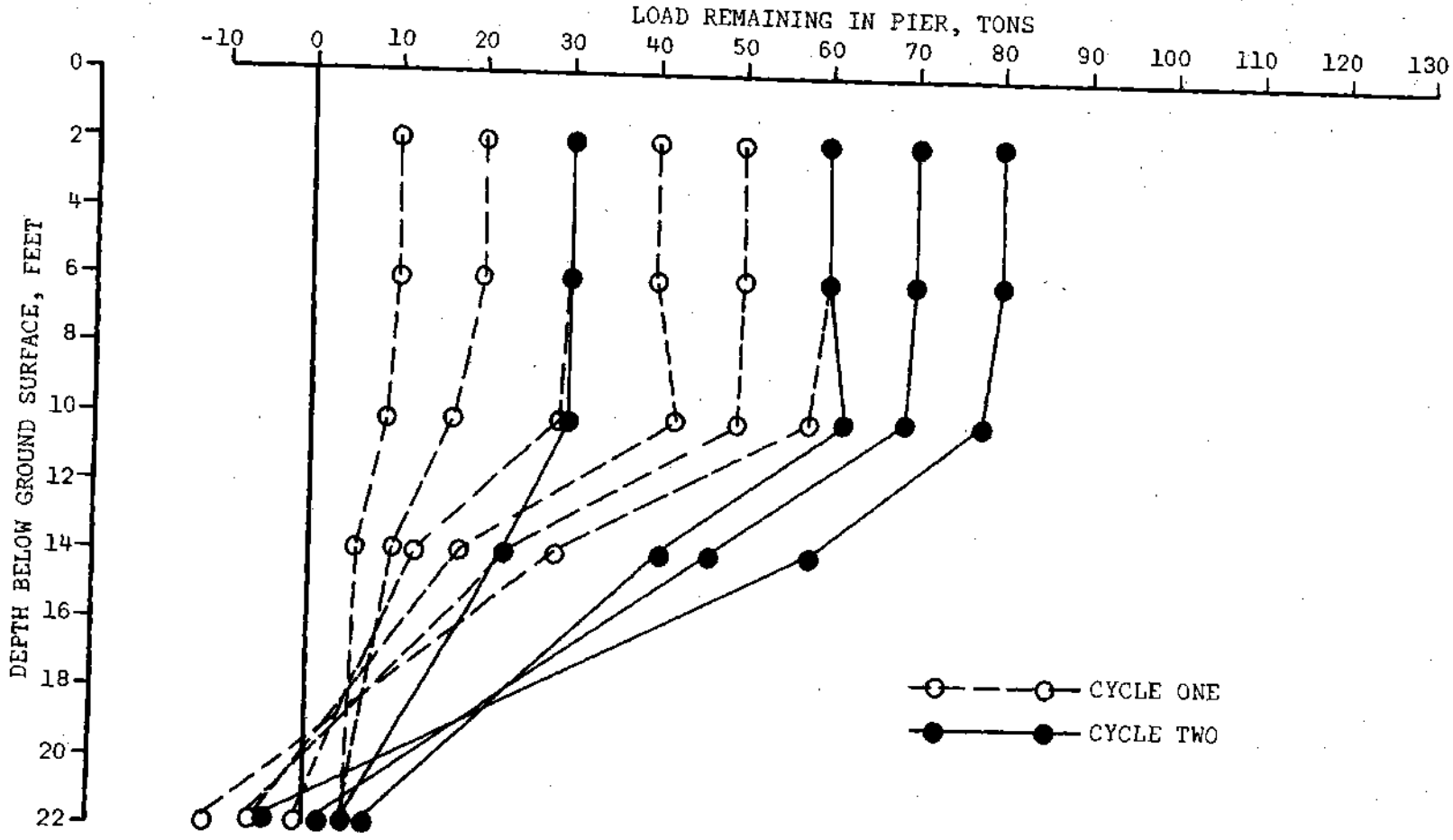

Figure 38. Load Remaining in Test Pier Four as a Function of Depth and Applied Load

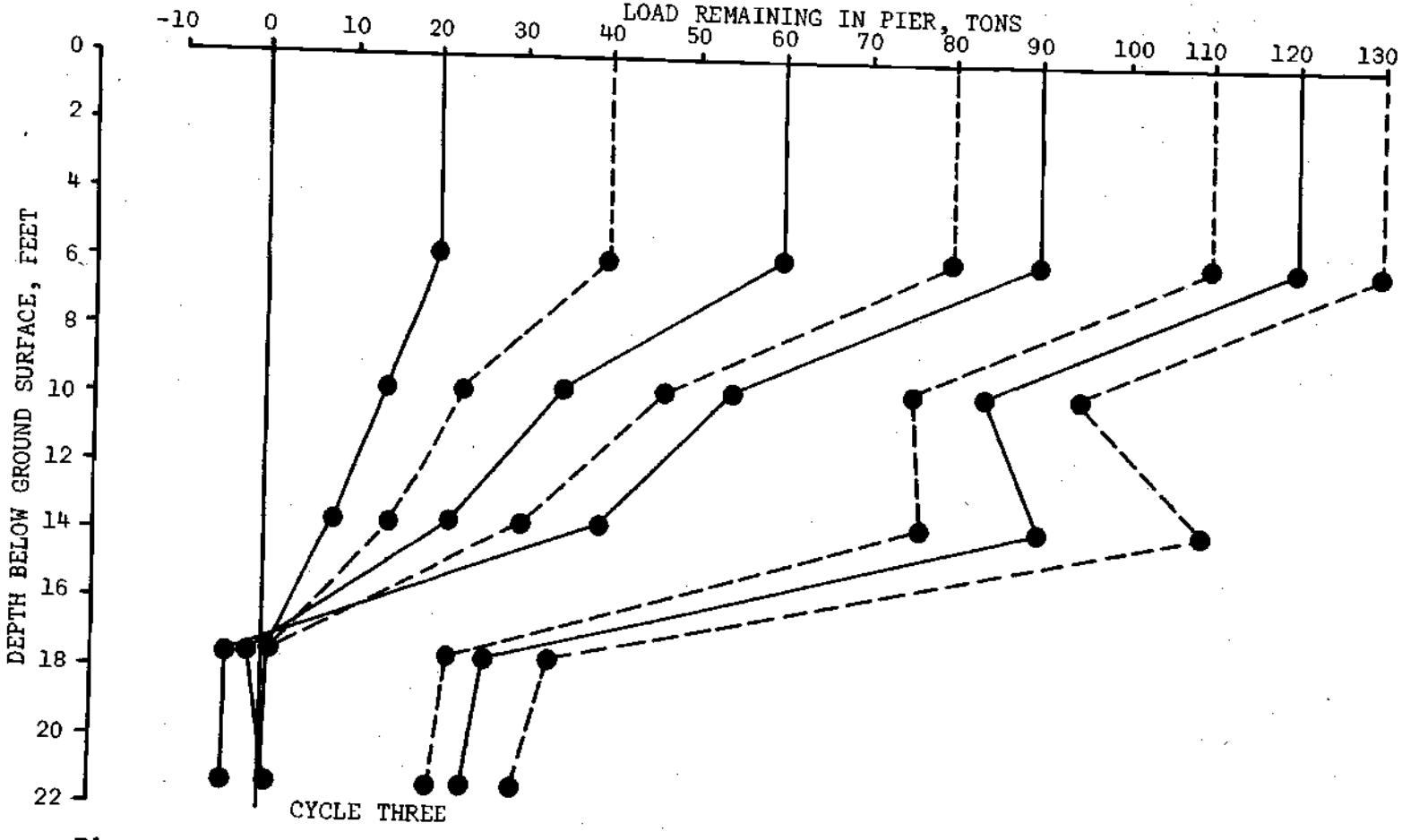

Figure 38. Load Remaining in Test Pier Four as a Function of Depth and Applied Load (Continued)

(2) that for a given load increment at the surface, the load at any strain indicator at some depth in the pier could be computed by multiplying the load factor by the strain in micro-inches.

The use of this load factor is limited because it must be assumed for each load increment that the initial strain gauge reading is correct and the modulus of elasticity of the concrete is a constant at all stress levels for the entire length of the pier. Laboratory tests on concrete cylinders molded during the pouring of the pier indicated that the modulus of elasticity is approximately a constant at an axial stress of above 200 psi and is not affected by confining pressure. Thus for the piers tested this assumption is valid for applied loads on the piers above 25 tons. Some indication of the validity of these assumptions is obtained by comparing the load factors for each cycle of loading. Such a comparison shows that the extreme in the load factor for a given cycle of loading are generally within 13 per cent of the average value. Other investigators have used this method to determine a load at a point in a deep foundation (54, 58, 66).

Figure 35 shows the load in the pier as a function of depth for test pier one. This figure shows that under an initial loading, 24 per cent of the load is transferred to the base of the pier (see Table 1). For all load levels a greater percentage of the load was taken in skin friction than in end bearing. The curves illustrate that the load in the pier decreases approximately lineally with depth up to a load of about 25 tons, but after that there is an irregular decrease in load

with depth, with little or no load being removed between 8 and 12 feet. This somewhat erratic behavior between 8 and 12 feet may be caused by the location of a hard, less weathered seam at 11 feet which required a great deal of effort to break through while drilling the pier. This extra effort may have softened up the sides of the drilled hole to such an extent that only a negligible skin friction force could be developed in that area. Loose soil and rock dust may also have coated the sides of the shaft in this area during excessively difficult drilling, causing an area of reduced adhesive strength.

A similar load-depth profile is shown in Figure 36 for test pier two. The load distribution pattern is similar to that obtained from test pier one with two distinct differences:

(1) The load-depth profile indicates that the entire length of the pier was contributing to the skin friction resistance which may be due to the fact that no exceptionally hard layer was encountered during drilling.

(2) The strain gauges at the bottom of the pier indicated that the base of the pier was in tension when the applied load at the surface was between 15 tons and 75 tons.

This tensile load reached a maximum of 8 tons at an applied load of 30 tons and then decreased upon subsequent loadings and went back into compression at an applied load of 75 tons. The occurrence and significance of tensile forces in the base of the piers during loading will be discussed in Chapter VII.

The load in the pier as a function of depth for test piers three and four are presented in Figures 37 and 38, respectively. A different load-depth relationship is obtained for each repetition of loading. This change may be related to the reorientation of the soil particles caused by the first and subsequent loading cycles and also to the stress history of the pier. The load as a function of depth is plotted for each loading cycle. These figures illustrate that the load in the pier is less at greater depths. Some of the cycles indicate that the base of the pier is in tension as with test pier two.

Figures 37 and 38 show the same relationships as discussed for test piers one and two except that a lesser percentage of the load was carried to the bottom for the deeper 22-foot piers than for the shallower 15-foot piers.

The rosette of strain gauges placed in pier one indicated that after approximately 20 per cent of the ultimate load was applied, the major principal stresses were oriented almost vertically and horizontally.

The load testing program illustrates the small amounts of deflection needed to cause failure of a drilled pier. The results also indicate that small diameter (18 inch), shallow, drilled piers are capable of supporting great loads with little short term settlement. Time-settlement curves, like that shown in Figure 30 illustrate that the settlement takes place rapidly in the weathered rock and any further settlement beyond the values indicated should be insignificant.

In all cases the majority of the applied load was transferred to the soil through skin friction.

The results of these tests performed indicate the variability in the load-carrying capacity, settlement, and load distribution patterns of drilled piers within the limited area at the test site. The data obtained will be compared to theoretical and empirical data obtained by others in the evaluation of test results section of Chapter VII. The evaluation of the test data will also consider the variability of the soil conditions at the site as determined in Chapter IV.

CHAPTER VII

EVALUATION OF TEST RESULTS AND RECOMMENDED DESIGN PROCEDURE

Introduction

In this chapter the data obtained from field testing of drilled piers will be discussed considering available theoretical solutions, empirical test results and an elastic analysis using a finite element computer solution developed by Barksdale (75). The data presented in Chapter VI for seven test piers in weathered rock is used to develop a general design criteria for drilled piers.

End bearing, skin friction and settlement are compared to other solutions separately, and the combined results are used to develop a general design procedure. The influence of different material properties and different size piers (length and diameter), are discussed in order to extend the data obtained from field tests on drilled piers in weathered rock into a general behavior pattern.

Data Evaluation

The results of seven load tests on drilled piers in weathered rock are presented in Chapter VI. These piers were tested to determine their load-carrying behavior and failure loads. The load distribution along the length of a pier, and the load-settlement relationships were obtained for each test pier, using the instrumentation described in Chapter V. This data permits evaluation of the load carried by skin

friction and the load carried by end bearing. The distribution of the load throughout the length of the pier illustrates that length, diameter, modulus of elasticity, shaft adhesion and construction technique influences the ability of a drilled pier in weathered rock to support load through skin friction. The load distribution curves also illustrate the significance and interrelationships of the two support mechanisms of skin friction and end bearing.

The data evaluation section is subdivided into two categories: (1) load-settlement relationships and (2) load-distribution relationships. The data obtained from the seven field tests are compared to theoretical results, other field results, and the computer solutions.

Extensive use is made of a finite element computer program to assist in evaluation of the data obtained from the seven test piers and to extend the data to different size piers in different soils. This program permits the input of the variables which affect the pier's behavior. A range of values for the variables (Young's Modulus, Poisson's Ratio, applied load, pier diameter and pier length) were studied to determine their effect on the load-carrying characteristics of the pier. Since the program assumes an elastic medium, its use is limited to the linear portion of the load-settlement curve. This, however, is not too serious a shortcoming, since the design load is generally in the linear portion of the load-settlement curve. In order to determine the ultimate load of a pier, it is necessary to consider the soil failure mechanisms which are not elastic but behave in a non-linear manner which varies with the type of soil (see Figure 9).

The finite element computer solution used in this thesis considers a semi-finite, axisymmetric elastic solid. A dimensionless grid system, containing 330 elements, was selected so that the diameter and length of the pier could be varied by changing the properties of the materials in several of the elements. The grid system used is shown in Figure 39.

Prior to proceeding with the solution of the problem of an axisymmetric deep foundation, the problem of a shallow foundation was used to evaluate the accuracy of the program. A comparison was made between the finite element solution and a Boussinesq solution of a circular footing resting on the surface of a semi-infinite elastic solid. The stresses and settlements calculated using the two methods were nearly identical. The small differences were probably due to the use of rigid vertical and horizontal boundaries at a finite distance from the center of the circular load in the finite element solution.

The results of the finite element computer solution are presented throughout the data evaluation section of this chapter. The comparisons made between the field results, theoretical results and empirical relationships are then summarized to show the general behavior pattern of drilled piers.

Load-Settlement Relationships

Seven piers were tested to evaluate the field performance of drilled piers in weathered rock. Load-settlement curves for all test piers and load in the pier as a function of depth are presented in Chapter VI. Measured profiles of the load remaining in the pier as a

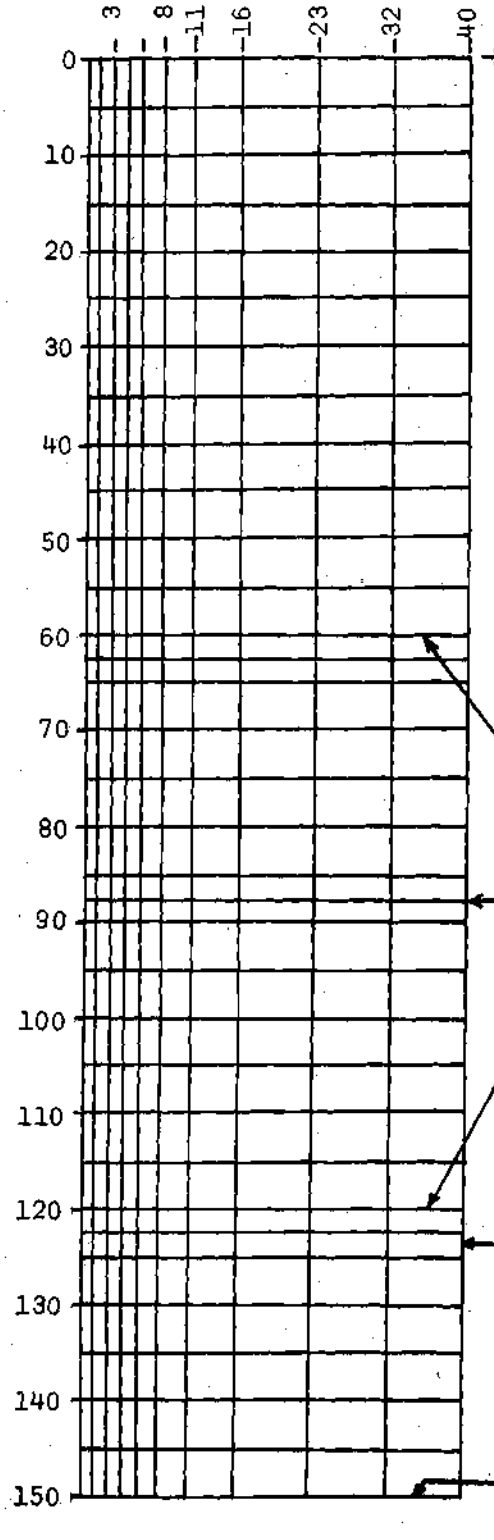

NOTES:

1. Dimensions have no units.
2. Elements are connected at nodal points.
3. Elastic properties of adjoining elements may be different.
4. Dimensions of pier for study:

ACTUAL		GRID	
Length	Dia.	Length	Dia.
15	18	60	3.0
	27		4.5
	36		6.0
22	18	88	3.0
	27		4.5
	36		6.0
30	18	120	3.0
	27		4.5
	36		6.0
60	18	120	1.5
	36		3.0

BOTTOM OF 15 FOOT PIER

BOTTOM OF 22 FOOT PIER

BOTTOM OF 30 FOOT PIER

Vertical loads cannot be transmitted past here.

Horizontal loads cannot be transmitted past here.

Figure 39. Grid System Used for the Finite Element Solution of an Elastic Axisymmetric Solid

function of depth have been utilized to estimate the settlement of the bottom by elastic theory. This approximate method of computing the bottom settlement has been used by others (39, 54, 58, 59, 66). The procedure for computing the settlement of the bottom of a friction bound shaft in soil is illustrated in Figure 40.

This procedure consists of taking known loads at various depths in the pier and utilizing elastic theory to determine the settlement between any two points where the load is known.

The procedure has been shown to converge rapidly with increasing number of elements. The major shortcoming is not, however, in the number of elements used but in the number of locations where the load is measured. Thus the selected elements should have their boundaries as close to the measured values as possible.

Utilizing the procedure outlined in Figure 40, the settlement of the bottom of the pier was computed for each load increment. The results are superimposed on the load-deflection curves for the top of the piers in Figures 41 through 44, and are presented in Table 3.

Figures 41 and 42 show that the curves for the settlement of the bottom have approximately the same shape as the curve for the settlement of the top for test piers one and two. The difference in settlement between the two curves is equal to the computed elastic compression of the pier shaft tabulated in Table 3.

The settlement of the top and bottom of test piers three and four is presented as a function of load in Figures 43 and 44, respectively. These curves indicate that there is a negative tip deformation for some loading conditions for piers 3 and 4.

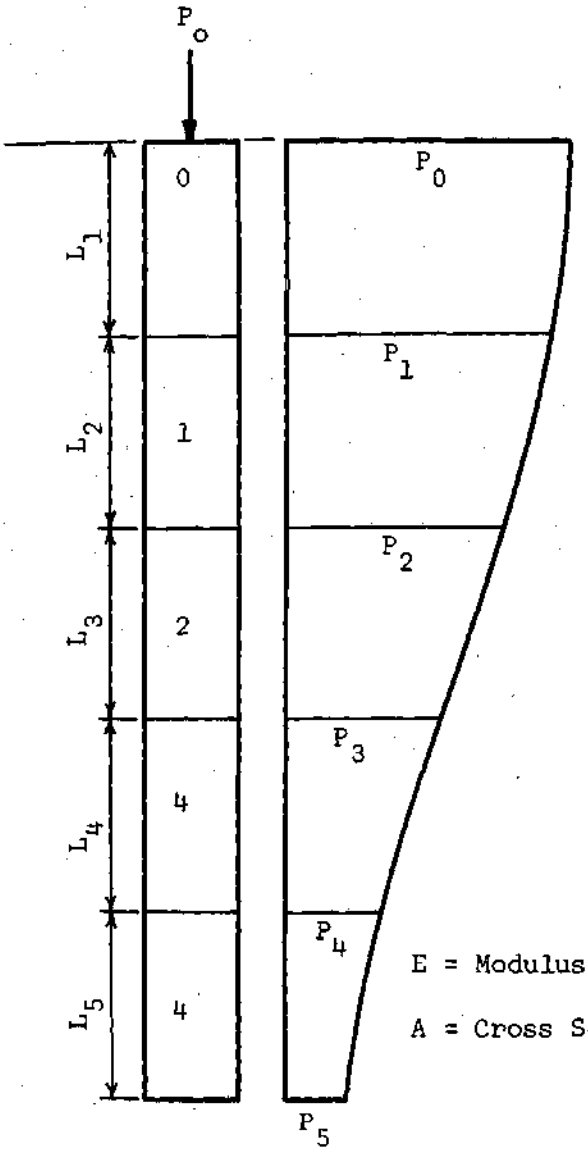

P_0 through P_5 Known.

$L_1=L_2=L_3=L_4=L_5$

ϕ = Deflection.

$$\phi_0 = \phi_1 + \left(\frac{P_1+P_0}{2}\right)\frac{L_1}{AE}$$

$$\phi_1 = \phi_2 + \left(\frac{P_1+P_2}{2}\right)\frac{L_2}{AE}$$

$$\phi_2 = \phi_3 + \left(\frac{P_2+P_2}{2}\right)\frac{L_3}{AE}$$

$$\phi_3 = \phi_4 + \left(\frac{P_3+P_4}{2}\right)\frac{L_4}{AE}$$

$$\phi_4 = \phi_5 + \left(\frac{P_4+P_5}{2}\right)\frac{L_5}{AE}$$

ϕ_5 = Tip Deformation.

E = Modulus of Elasticity for Concrete.

A = Cross Sectional Area of Pier.

COMBINING THE ABOVE EQUATIONS:

$$\Delta H_{BOTTOM} = \phi_3 = \phi_0 - \left[\frac{P_0 + 2(P_1+P_2+P_3+P_4) + P_5}{2}\right]\frac{L}{AE}$$

where $\left[\frac{P_0 + 2(P_1+P_2+P_3+P_4) + P_5}{2}\right]\frac{L}{AE}$ = Shaft Deformation.

Figure 40. Computational Procedure for Determining Tip Deformation

Table 3. Load-Settlement and Load-Duration Data for Test Piers One Through Four

Test Pier	Loading Cycle	Applied Load at Surface P, Tons	Load Duration Minutes	Estimated Ultimate Load, P_u, Tons	Settlement at Top, Inches per Cycle	Shaft Compression Inches	Deflection at Bottom, Inches (1)	$\frac{P}{P_u} \times 100$
1	1	15	57	108	0.0041	0.0056	-0.0015	13.8
L=15'		30	90		0.0166	0.0110	.0056	27.6
D=18"		45	60		.0340	.0152	.0194	41.4
		60	173		.0670	.0180	.0486	55.2
		75	154		.1132	.0237	.0895	69.0
		90	120		.1730	.0303	.1427	82.8
		100	610		.2606	.0324	.2282	92.6
2	1	15	60	110	.0068	.0032	.0036	13.6
L=15'		30	60		.0251	.0054	.0197	27.2
D=18"		45	60		.0514	.0086	.0428	40.8
		60	60		.0980	.0144	.0816	54.4
		75	86		.1623	.0182	.1441	68.0
		90	74		.2510	.0227	.2283	81.6
		105	1290		.4452	.0302	.4150	95.2
3	1	10	15	120	.0031	.0040	-.0009	8.3
L=22'		20	15		.0068	.0080	-.0012	16.7
D=18"		30	15		.0100	.0124	-.0024	25.0
		40	15		.0159	.0182	-.0023	33.0
	2	20	15		.0078	.0075	.0003	16.7
		40	15		.0141	.0172	-.0031	33.3
		50	15		.0231	.0255	-.0024	41.7
	3	20	15		.0071	.0081	-.0010	16.7
		40	15		.0148	.0194	-.0046	33.3
		60	505		.0322	.0288	.0032	50.0
	4	20	15		.0053	.0065	-.0012	16.7
		40	15		.0143	.0139	.0004	33.3
		70	30		.0353	.0307	.0046	58.3
		80	30		.0594	.0360	.0234	66.7
		90	60		.0964	.0445	.0519	75.0
		100	2		.1512	-	-	83.3
4	1	10	30	135	.0025	.0058	-.0033	7.4
L=22'		20	30		.0065	.0101	-.0036	14.8
D=18"		30	30		.0128	.0140	-.0012	22.2
		40	30		.0187	.0184	.0103	29.6
		50	30		.0259	.0229	.0030	37.0
		60	30		.0337	.0264	.0073	44.4
	2	30	15		.0112	.0164	-.0052	22.2
		60	15		.0253	.0321	-.0068	44.4
		70	30		.0330	.0353	-.0025	51.8
		80	60		.0500	.0400	.0100	59.2
	3	20	15		.0091	.0087	.0004	14.8
		40	15		.0196	.0175	.0021	29.6
		60	15		.0286	.0256	.0030	44.4
		80	30		.0402	.0346	.0056	59.2
		90	30		.0550	.0386	.0164	66.6
		110	75		.1403	.0577	.0836	81.4
		120	75		.2040	.0646	.1394	88.8
		130	705		.3320	.0727	.2593	96.2

NOTE: The deflection at the bottom is the algebraic difference between the settlement at the top of the pier and the shaft compression.

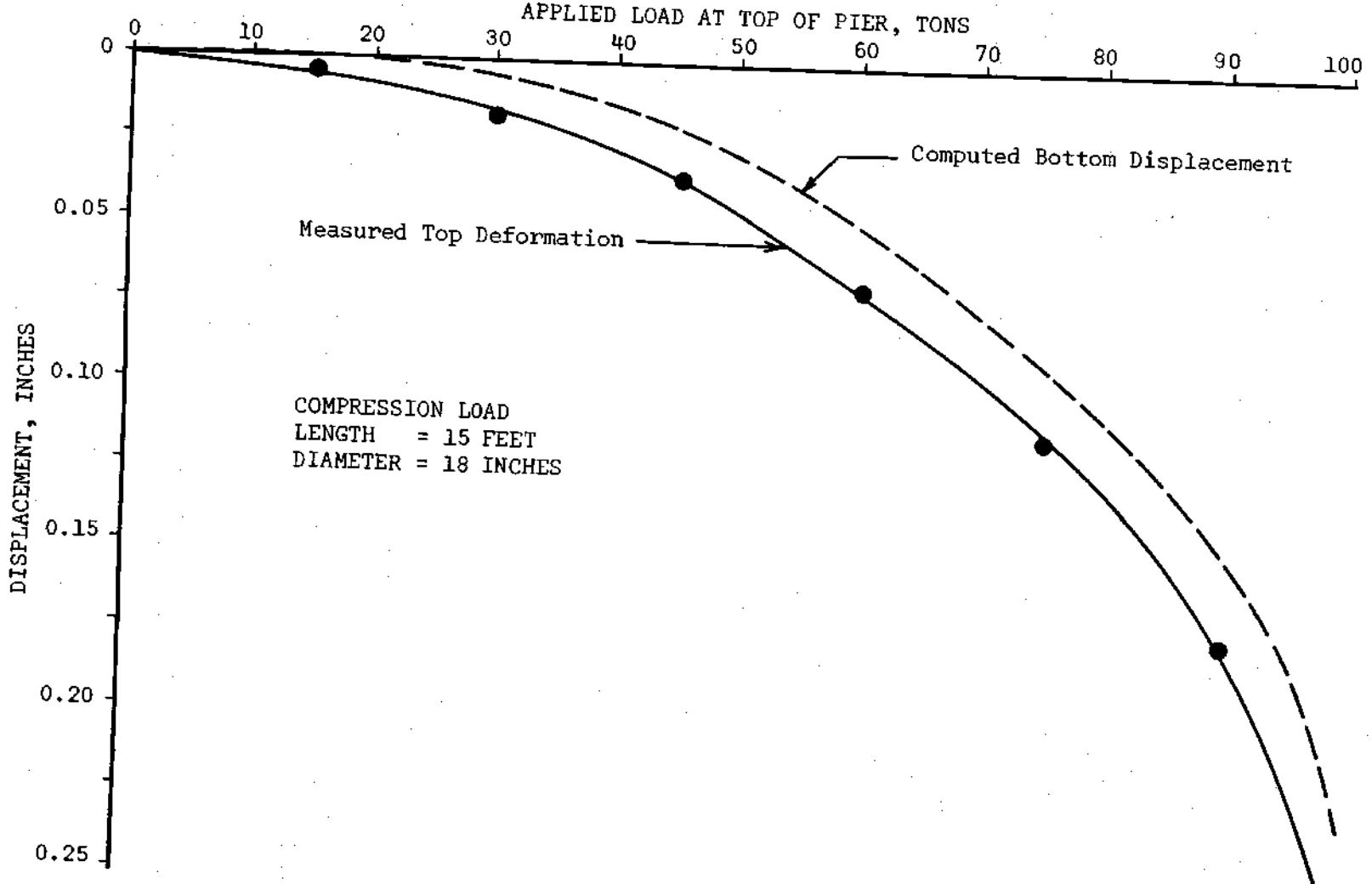

Figure 41. Load Displacement Curve for Test Pier One

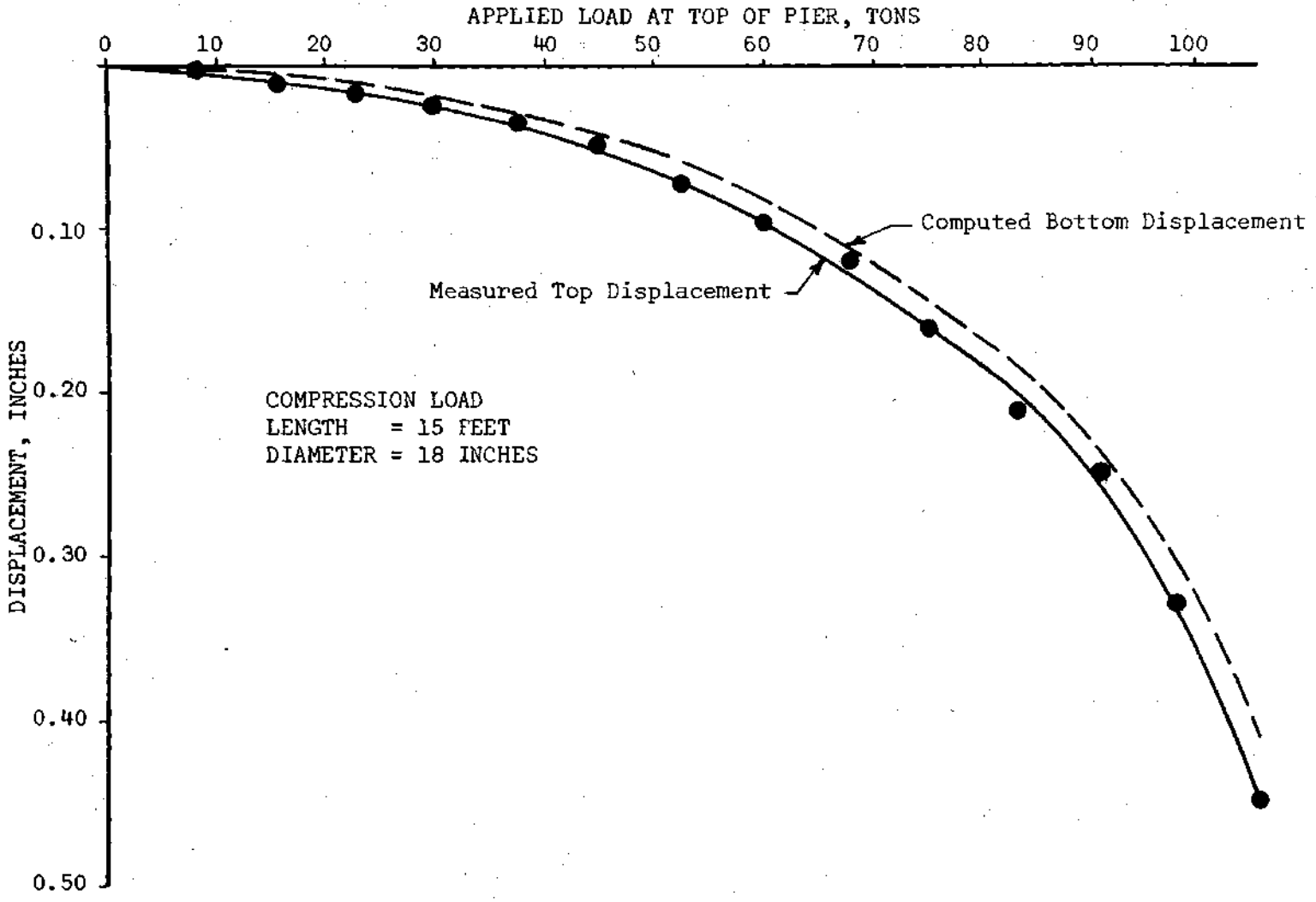

Figure 42. Load Displacement Curve for Test Pier Two

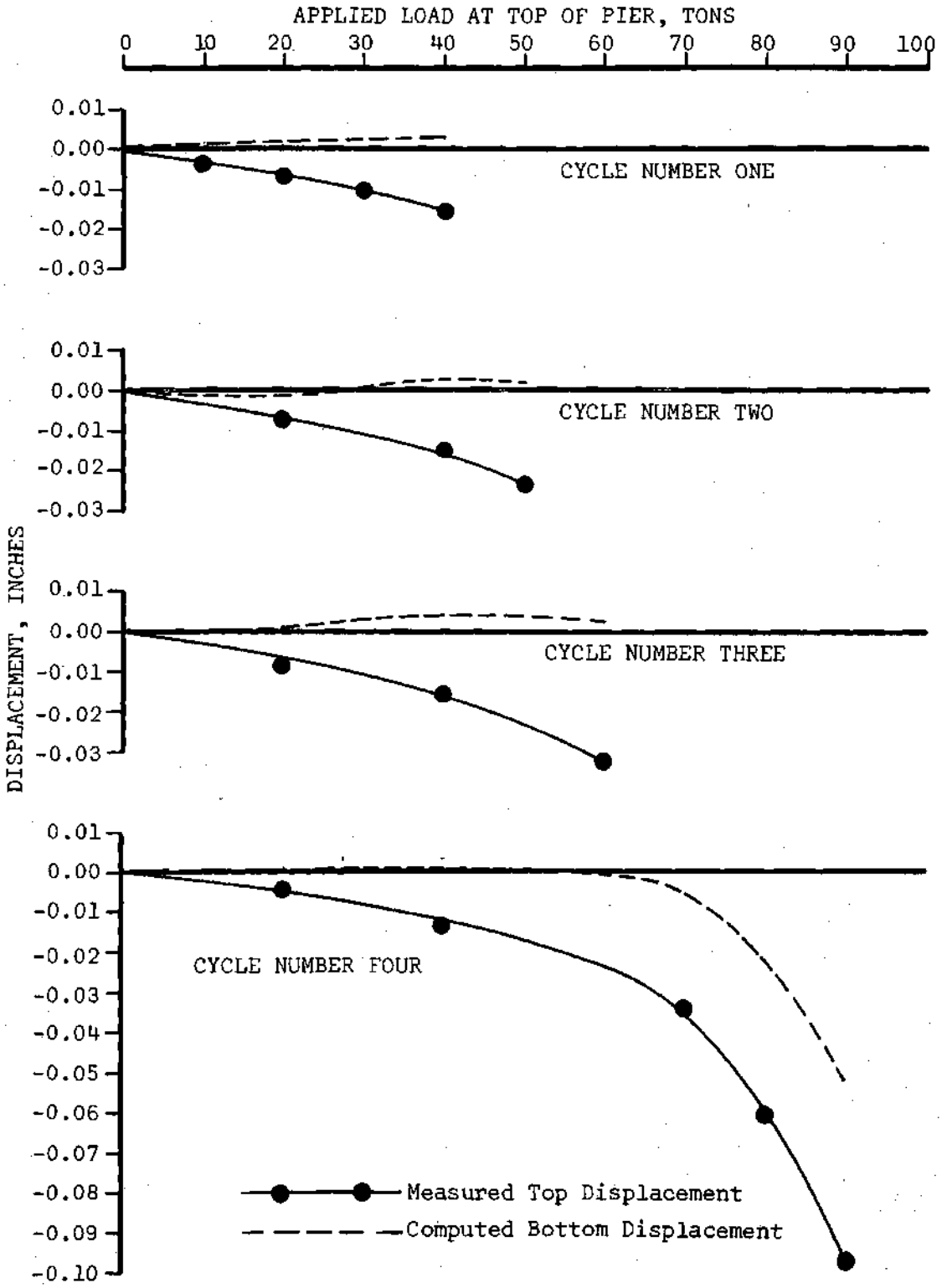

Figure 43. Load Displacement Curves for Test Pier Three

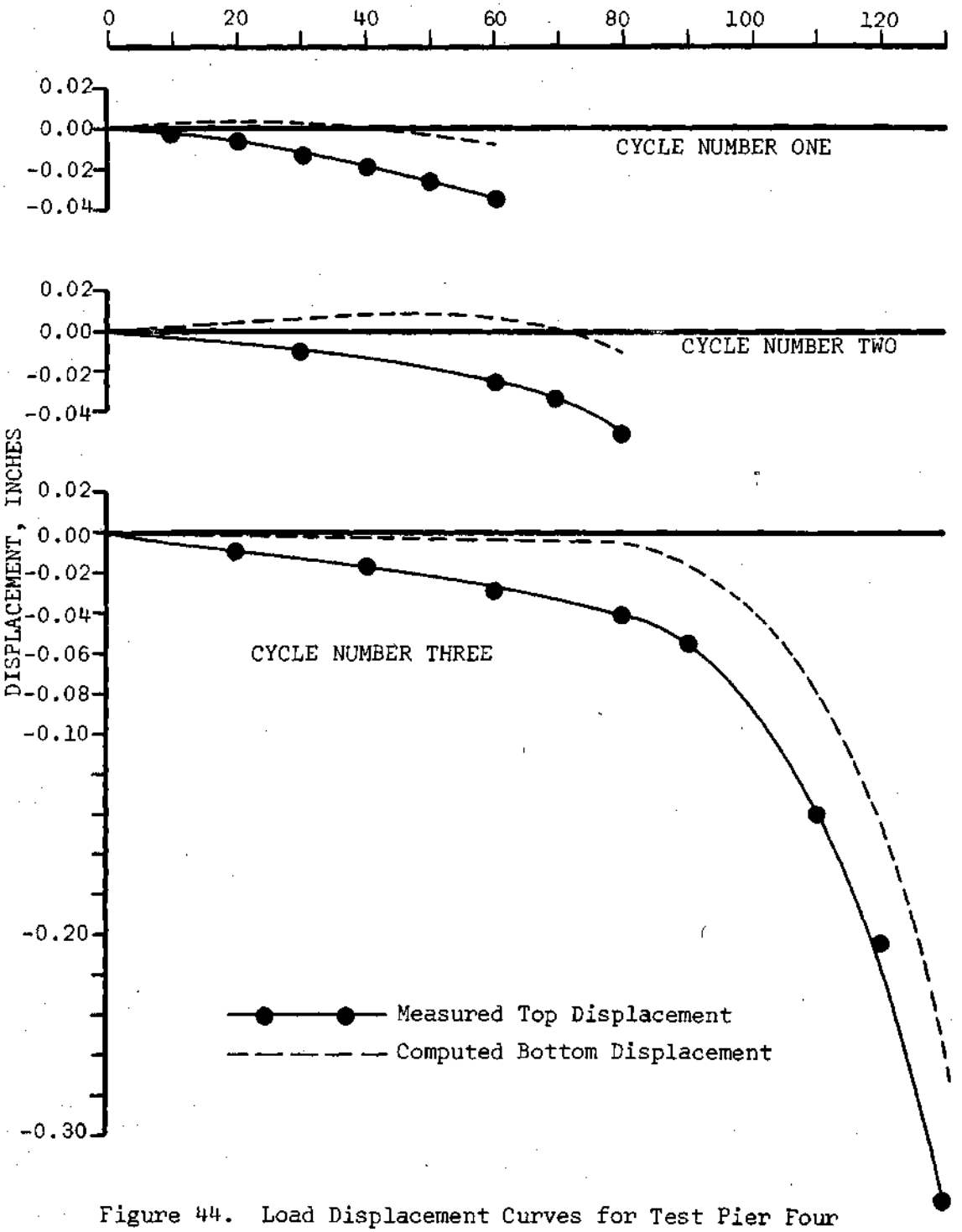

Figure 44. Load Displacement Curves for Test Pier Four

Figures 41, 43, and 44 show that there is a tendency for the bottom to apparently have a deflection towards the surface for all cycles of loading except cycle three of test pier four. This happened even in test pier one when the bottom load, as determined using headings from the bottom strain gauges, did not decrease upon applying load. This irregularity could be due to the selection of the modulus of elasticity of concrete. The modulus used in these calculations was obtained from laboratory tests on concrete cylinders molded during placement of the concrete piers. Since the change in axial length is computed from the load remaining in the pier, it is possible to get a compression greater than the settlement at the top of the pier if the load in the shaft at some point below the surface is greater than a point closer to the surface as illustrated in Figure 35 for test pier one or is tensile as illustrated in Figures 36 through 38. This increase in vertical load at some depth is discussed in the load distribution section of this chapter. The decrease in axial length at the bottom is also indicated by the tensile strain readings obtained in the pier. This may be due to the shrinkage of concrete, the lateral deformation behavior of the pier, or an error in the gauges. Other researchers have found a tensile condition or a reduction of compressive forces in the bottom of piers and piles (39, 55, 68). This condition may also be caused by the horizontal stress developed from the reduction in load due to skin friction. The finite element computer solution shows that there is a zone of horizontal tensile stress immediately above the bottom of the pier (Figure 60). The reduction in compressive force

may also be caused by bending moments in the pier, due to hard seams or eccentric loadings. Any or all of these factors could account for the expansion of the concrete or the development of tensile forces and the apparent negative deformation at the base of the pier. The load distribution patterns obtained from the field tests are discussed in greater detail in the next section of this chapter.

A study has also been made of the comparison in load displacement performance for the seven test piers. Figures 45 and 46 show these relationships.

The load-settlement curves in Figure 45 are plotted for the final loading cycle of test piers one through four. This figure indicates a great similarity in shape of the load-settlement curves and magnitude of settlement for each depth of pier tested. Thus the curves for test piers one and two (each 15 feet deep) are nearly the same, and the curves for test piers three and four (each 22 feet deep) are nearly identical. Any difference in the relationship for the same length piers could probably be attributed to the variations in the soil itself. The displacements of the top of the piers at a given applied load are less for the 22-foot piers than for the shallower 15-foot piers. The curves for the deep piers also illustrate a greater load-carrying ability. It may be concluded from Figure 45 that at greater depths of embedment, the settlement under an applied load is less.

A similar relationship is shown in Figure 46 for 20-foot long piers deriving their load-carrying ability from skin friction only. This figure shows that the initial portion of the curves for the piers

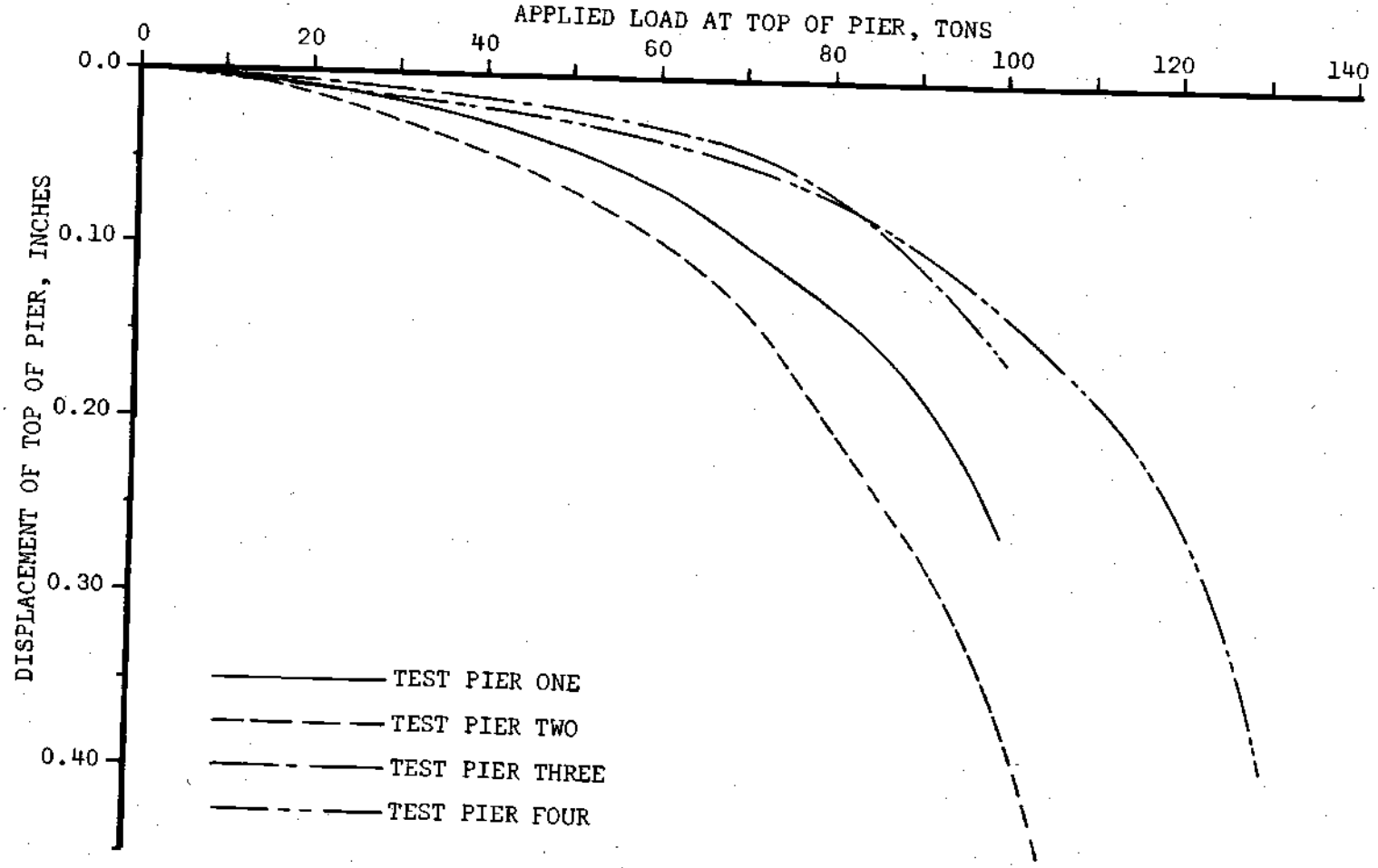

Figure 45. Load Displacement Curves for Piers Deriving Their Load-Carrying Capacity from Skin Friction and End Bearing

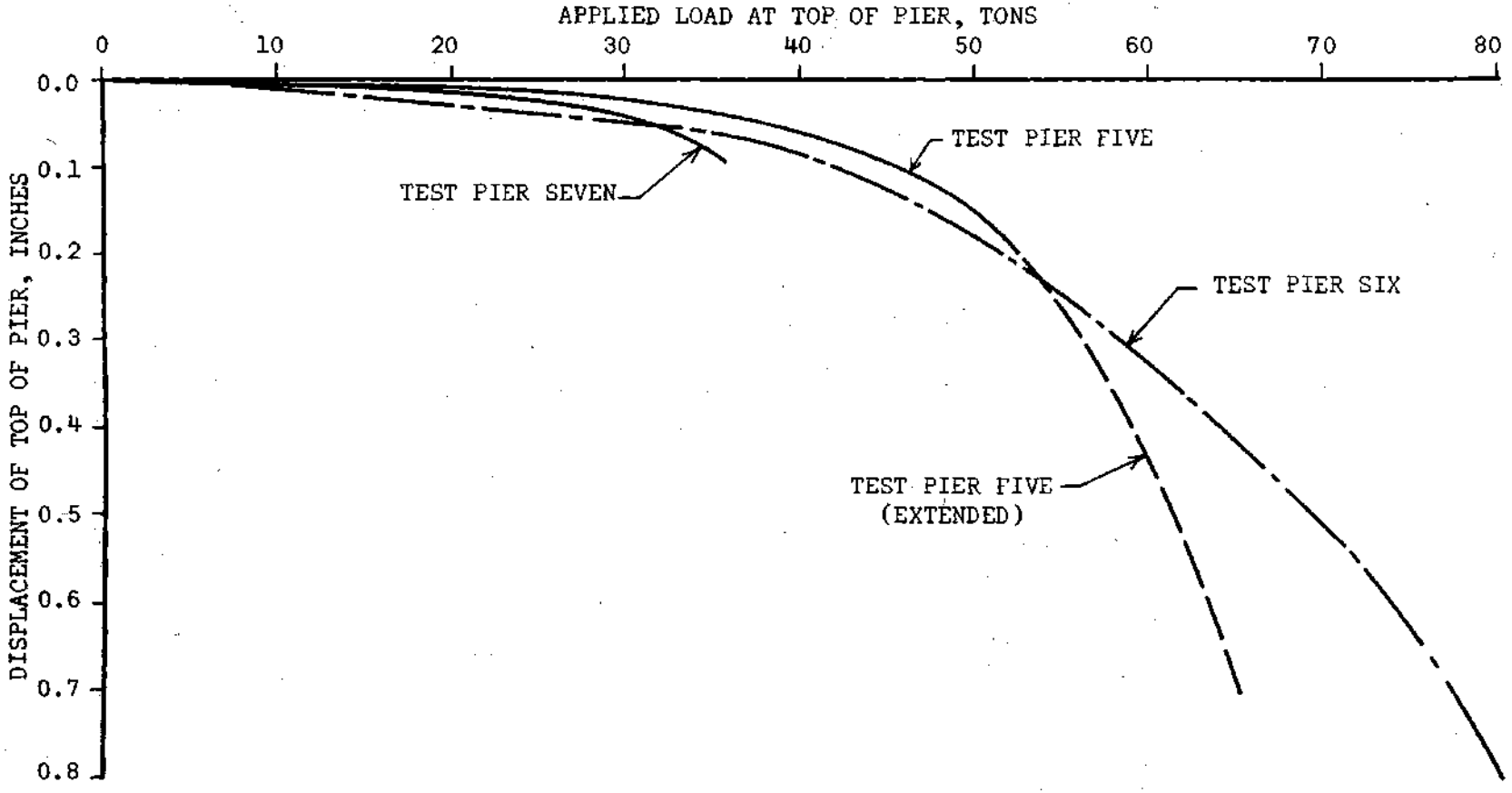

Figure 46. Load Displacement Curves for Piers Deriving Their Load-Carrying Capacity from Skin Friction

tested in compression (tests five and six) have nearly identical shapes up to a load of 50 tons. Test pier five has less settlement at the applied loads than test pier six. The difference in settlement at applied loads between approximately 15 and 50 tons is 0.03 inches which is probably due to material variation and cyclic load characteristics. Since the test could not be extended past 52 1/2 tons, a dashed line representing expected performance was superimposed on the graph for test pier five. This was done so that the settlement at failure and the failure load could be estimated for test pier five. Test pier seven, tested in tension, shows similar values to piers five and six for displacement up to an applied load of 20 tons. At loads greater than this, the deformation increases rapidly. The load could not be applied beyond 35 tons due to a failure in the reinforcing bars which were used in the pull-out test. Figure 46 shows that the ultimate carrying capacity for a tensile pier is considerably less than that for a compression pier support by friction forces alone.

A comparison of the load settlement curves presented in Figures 45 and 46 shows that piers deriving their support from skin friction alone settle more under an applied load than those deriving their support from skin friction and end bearing. This was further substantiated by the computer solution which indicated that the lower the modulus of elasticity of the soil directly below the bottom of the pier, the greater was the settlement, irregardless of the modulus of elasticity of the soil surrounding the pier. For piers having the same length and method of support, the difference in the curves presented is most

probably due to material variation from one test pier to another.

If the settlement is plotted versus the percentage of the estimated ultimate load, a relationship is developed which may be used to predict the load-settlement nature of a pier. Such a relationship is presented in Figure 47 for the seven piers tested in this study. This figure shows a wide scatter in results for piers five, six and seven, deriving their support from skin friction only. The curve for test pier five should begin showing an increasing rate of settlement as the percentage of ultimate load is increased and should be parallel to the curve for test pier six. Test pier seven shows very little settlement up to about 80 per cent of the ultimate load. Beyond 80 per cent of the ultimate load, the settlement per unit load increases rapidly upon application of additional load, indicating that a pier in tension does not show a yielding behavior but is instead more "brittle" in nature. This may indicate a tensile failure in the lightly (two number six bars) reinforced concrete. A computation of the stress in the steel bars indicated that they were loaded considerably past their yield stress.

Curves of the settlement as a function of applied load for test piers one through four show similar behavior patterns. In fact, the curves for test piers three and four are practically identical from 65 to at least 85 per cent of the ultimate load. An average curve of per cent of ultimate load vs. settlement may be used to determine the approximate settlement characteristics of a pier in weathered rock.

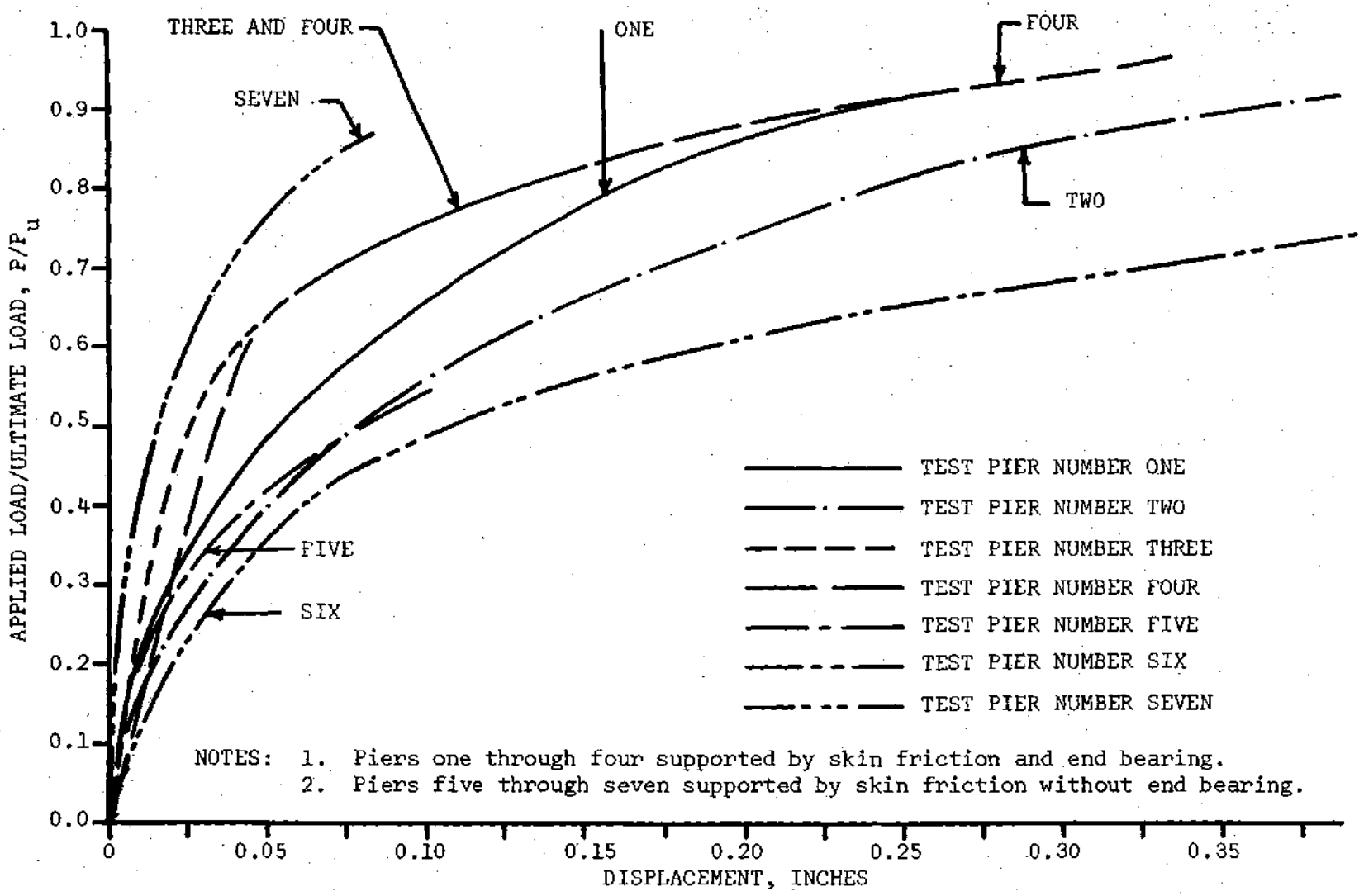

Figure 47. Portion of the Estimated Ultimate Load as a Function of Displacement

This is discussed in the design recommendation section of this thesis.

The results of several other load tests on drilled piers are presented in Appendix B in the form of per cent of estimated ultimate load vs. settlement. These curves all show a similar trend but the curves themselves are different. The settlement of a pier in soil depends on the length of the shaft, the diameter of the shaft, the modulus of elasticity of the soil and concrete, the quantity of applied load and the time the load is maintained. At working loads the modulus of elasticity of the soil in an elastic soil media is, theoretically, the most important variable in determining the settlement of a pier. The difference in the curves presented as part of this thesis and those presented in Appendix B is probably due primarily to the difference in modulus of elasticity of the soil, which is affected by the method of construction, climatic conditions and position of the water table. Some of the difference is probably due also to the various length and diameters of other piers tested. With the exception of one of the curves presented in Appendix B for piers in the Atlanta area (Figure 85) the curves of percentage of ultimate load vs. settlement presented in Appendix B are nearly identical to the curves obtained for the seven test piers. The major difference is that at low percentages of ultimate load the settlement from the seven test piers is less. This is partially because the piers tested were all concreted the same day they were drilled and the weather and construction conditions were ideal.

The theoretical settlement of a pier in a uniform homogeneous soil decreases as the modulus of elasticity of the soil increases. The settlement of a pier in soil is also less at the same applied load for piers of greater length than for shorter piers having the same diameter. A relationship has been developed by Poulos and Davis (74) to show the effect of pile or pier length on the load-settlement behavior to failure. This relationship was obtained by integrating the Mindlin Formula with consideration of the soil strength characteristics and by applying these strength characteristics when the stress is greater than an elastic stress condition will permit. This relationship is illustrated in Figure 48 and shows that as the length is increased or the diameter is decreased the settlement of a pier or pile increases for the same percentage of ultimate load. This relationship must be used with caution since the ultimate load capacity of a pier also increases with increasing length in approximately a linear manner (Vesic, 41).

Increasing the diameter will also cause a reduction in settlement for the same applied load on the same length pile. Skempton (30) has pointed out that increasing the diameter causes settlement to be the major consideration and not bearing capacity for large diameter piers in clay where the ultimate end bearing capacity increases in direct proportion to the square of the diameter of the pier if the length remains constant. Figure 48 can also be used to predict the change in settlement due to changing diameter if the change in ultimate capacity is also considered.

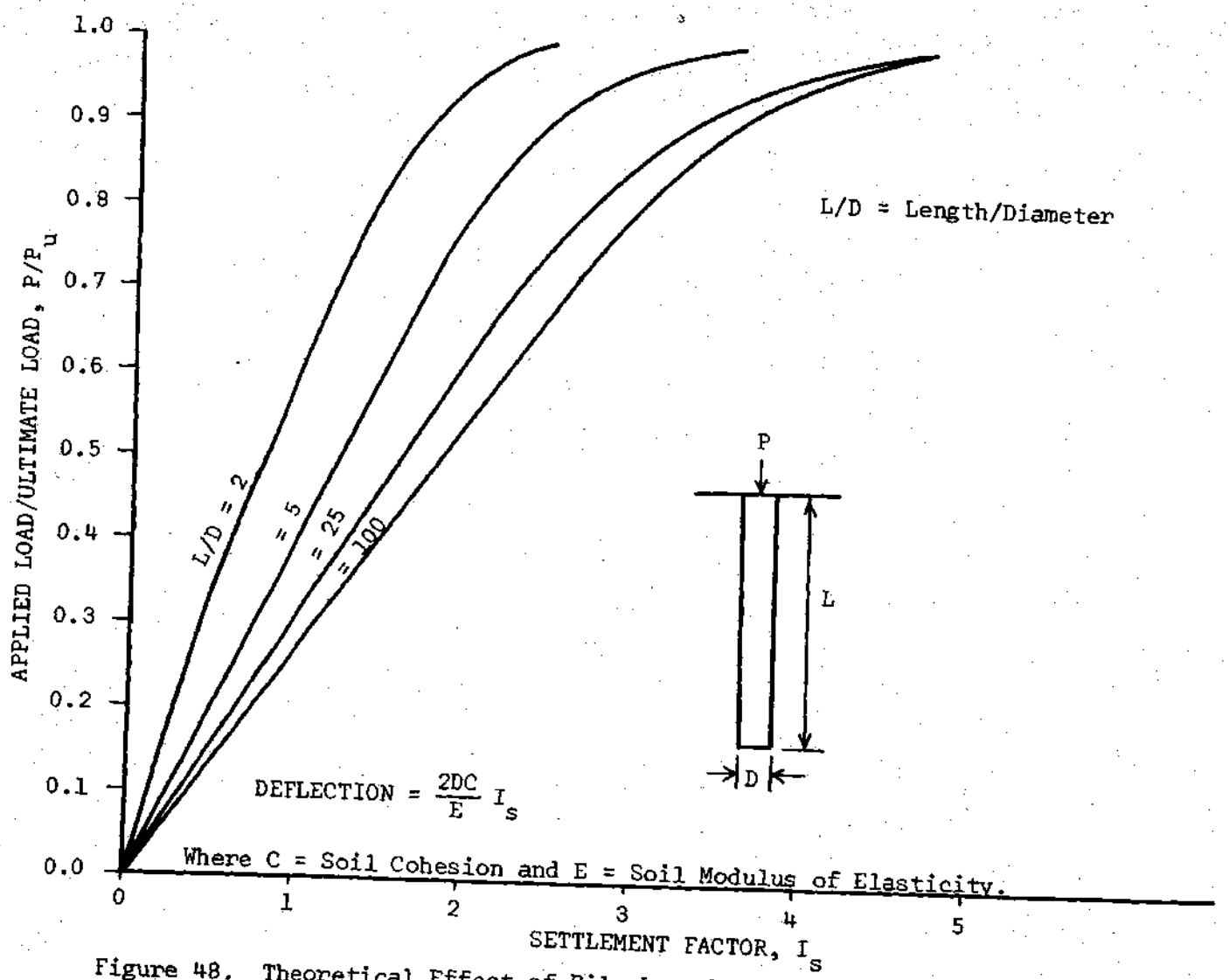

Figure 48. Theoretical Effect of Pile Length on Load-Settlement Behavior to Failure (After Poulos and Davis, 74)

The results of the tests on piers obtained from the field testing program part of this investigation do not agree with the curves given by Poulos and Davis (74). Test piers three and four, which were 22 feet in length (L/D=14.7) showed approximately the same settlement at the same percentage of ultimate load as test piers one and two, which were 15 feet in length (L/D=10). This discrepancy may be caused by the inability to develop complete bottom support in the test piers. DuBose has performed several load tests to determine the effect of length and diameter on the load-settlement relationship of drilled piers in clay (36, 37). The results of some of these tests are presented in Figure 49 and show that as the length is increased the settlement under the same applied load is the same or less, and as the diameter is increased, the larger diameter piles will generally settle less under the same applied load. These curves also illustrate the increase in pier capacity obtained by either increasing the diameter or length. The results from the two lengths of piers tested in weathered rock as part of this investigation agree with the general behavior trend obtained by DuBose for piles in medium stiff clay.

An elastic analysis of piers in a homogeneous soil using the finite element solution shows that the settlement at some applied load decreases proportionally with an increase in length. The relationship is shown in Figure 50 for piers having lengths from 15 to 60 feet and diameters of 18, 27 and 36 inches and embedded in a soil having the average elastic properties determined from soil samples obtained at the test site. The indicated ratio of settlement to load is 10 to 15 times

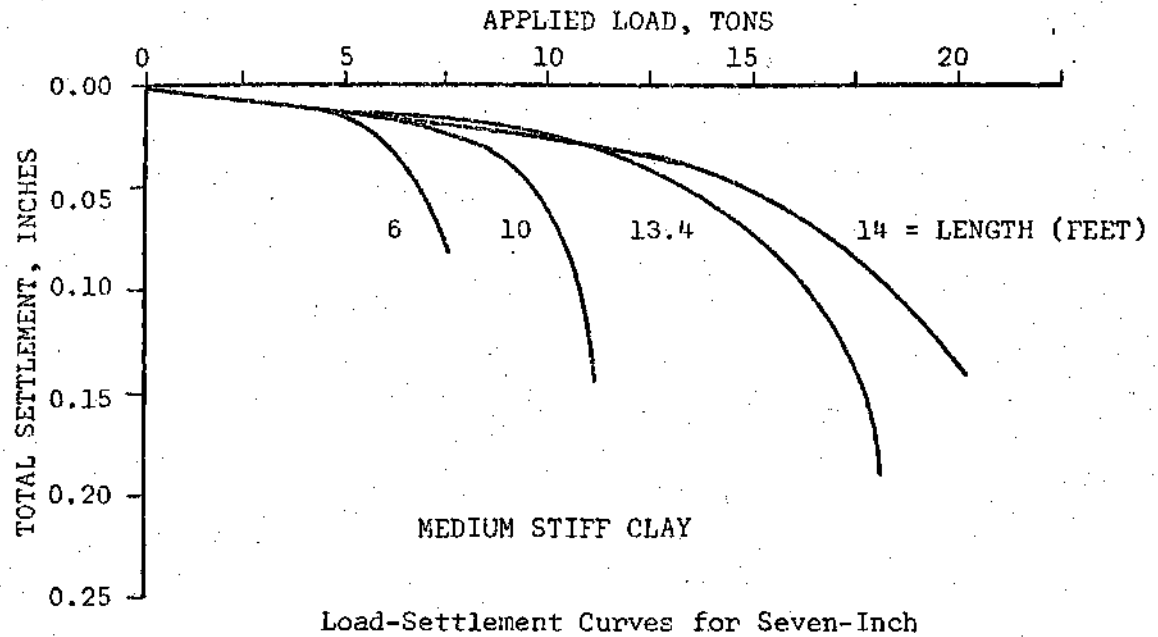

Load-Settlement Curves for Seven-Inch Diameter Drilled Shafts (After DuBose, 36)

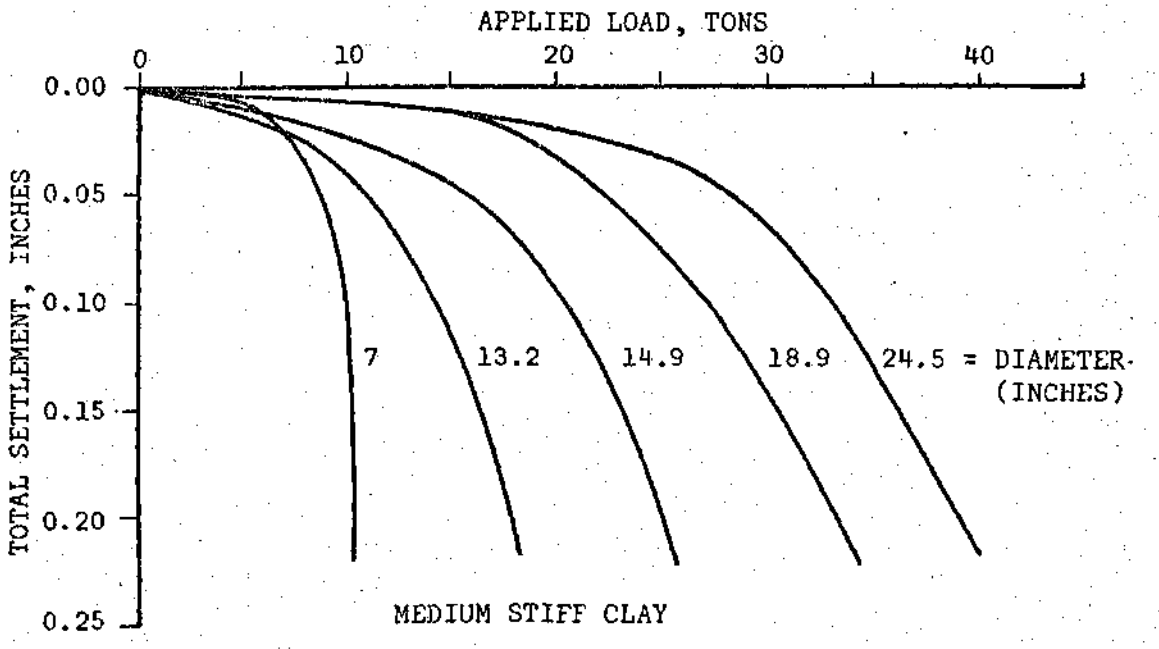

Load Settlement Curves for Piers Having an Effective Length of Ten Feet (After DuBose, 37)

Figure 49. Observed Load-Settlement Relationships for Different Diameter and Different Length Piers (After DuBose, 36,37)

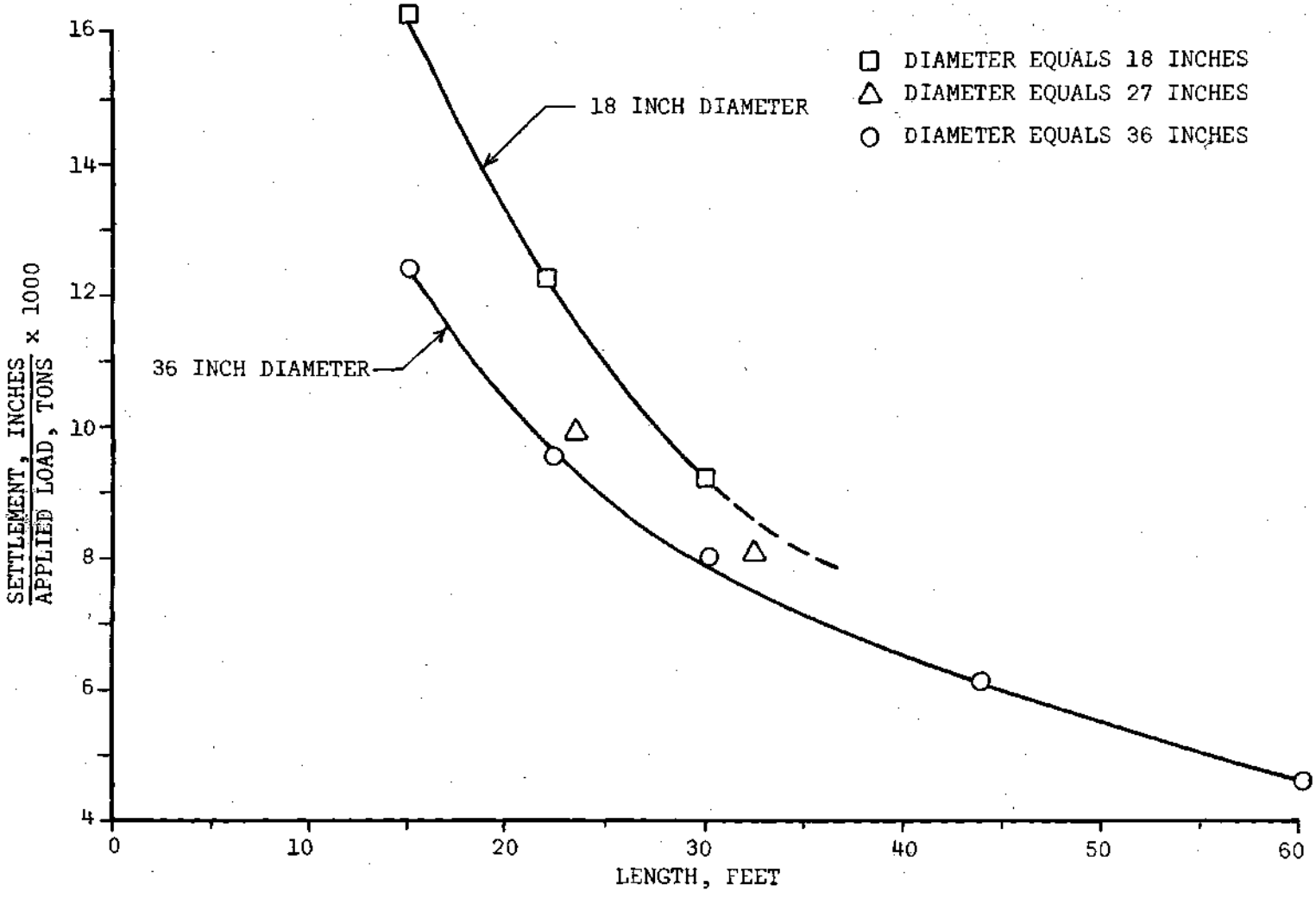

Figure 50. Theoretical Effect of Length and Diameter on the Settlement of a Drilled Pier Embedded in an Elastic Media

that encountered in field tests. These curves also show that for the same applied load the elastic settlement is less for a larger diameter pier than for a smaller diameter pier of the same length. This was also shown to a limited degree, by DuBose (37) for piers in medium stiff clay, but the effect of the diameter was far less than for the elastic solution. The theoretical effect of modulus of elasticity of the soil on settlement is illustrated in Figure 51. Figure 51 shows that for a given load as the modulus of elasticity of the soil is increased, the settlement decreases in direct proportion to the inverse of the modulus of elasticity for geometrically identical piers embedded in the same elastic medium. The percentage error incurred by assuming the settlement is almost directly proportional to the soil's modulus of elasticity as illustrated in Table 4.

Table 4. Per Cent Error Incurred by Assuming that the Settlement is Inversely Proportional to the Modulus of Elasticity of a Homogeneous Soil

E (psf)		67,000	134,000	268,000	400,000	1,206,000
LENGTH (Feet)	DIAMETER (Inches)	ERROR %	ERROR %	ERROR %	ERROR %	ERROR %
22	18	+1	0	-2	-7.5	-4.5
15	18	+2.5	0			-10.3
60	36		0	-4		
15	36				0	-3

NOTES:
1. + indicates overestimates.
2. - indicates underestimates.
3. Data obtained from elastic finite element computer solution.

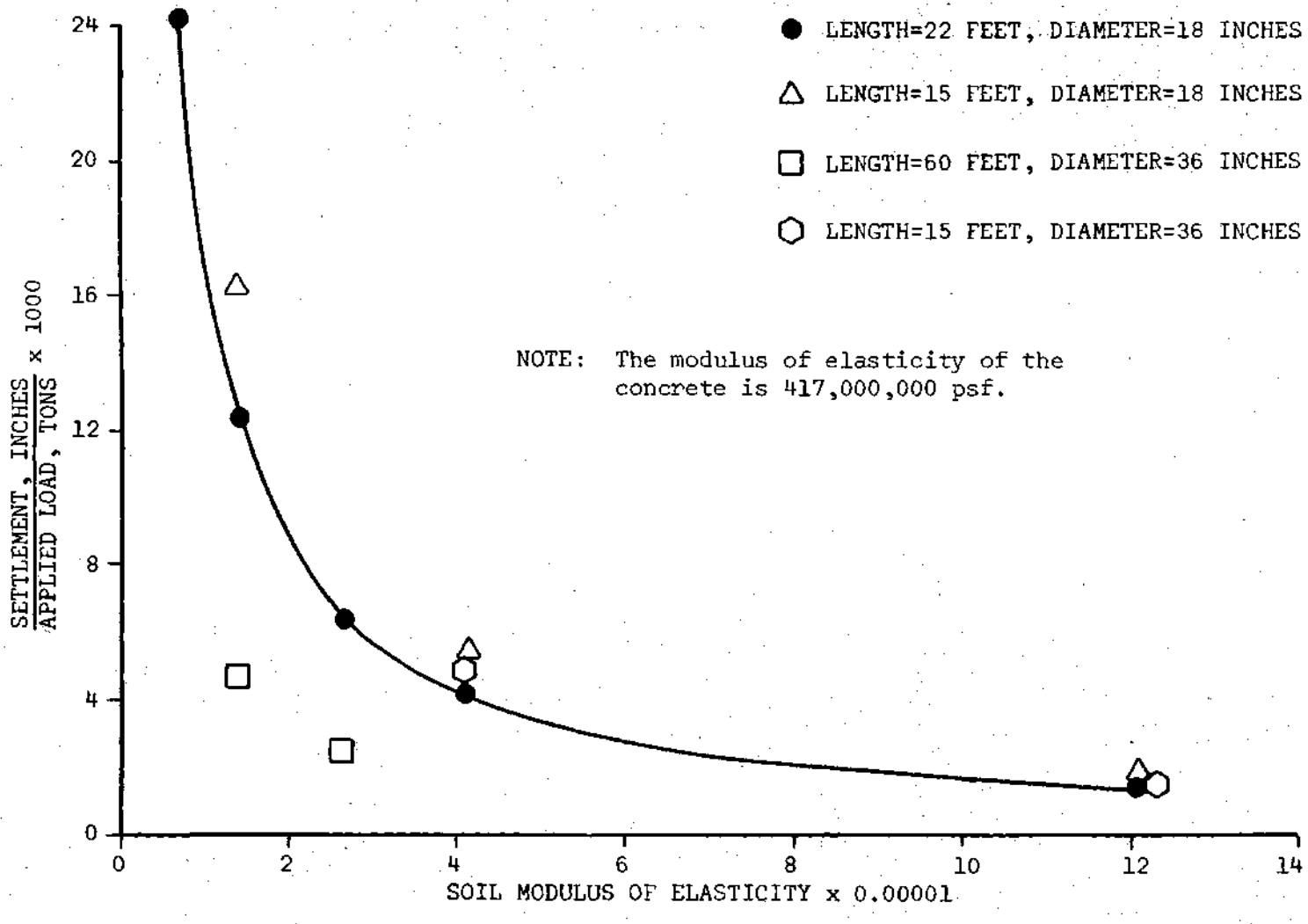

Figure 51. Effect of Modulus of Elasticity of the Soil on the Settlement of a Pier in an Elastic Homogeneous Soil

The elastic finite element computer solution for drilled piers in weathered rock has also been used to investigate the effect of hard seams on the side of a shaft and soft zones beneath the shaft. The results of these solutions indicate (1) the softer the material directly underneath the pier, the greater the settlement of the pier will be, regardless of the modulus of elasticity of the surrounding soil, and (2) the presence of a hard layer on the side of the pier gives less settlement than for a homogeneous soil. Examples of this are presented in Figure 52 and described in Table 5 for the cases studied. The presence of the hard layer on the side of test pier one would tend to make it settle less than test pier two, which did not have a hard zone on the side. This difference in settlement between piers one and two is illustrated in Figure 45.

The load-settlement relationships obtained from elastic procedures using laboratory determined values for the modulus of elasticity greatly overestimate the actual settlement of drilled piers in soil, although at low load levels the settlements should be nearly equal. This may be attributed to the fact that the settlement is a function of the absolute displacement of the soil and not the strain as determined by previous researchers (29). Another source of error may also be due to sample disturbance in the laboratory or field. Some error is also introduced into the field measurement of the settlement of a drilled pier by placing the supports for a settlement gauge too close to the pier being tested. Figure 53 shows theoretical elastic ground displacements at various loads for a pier 15 feet long and 18 inches in diameter

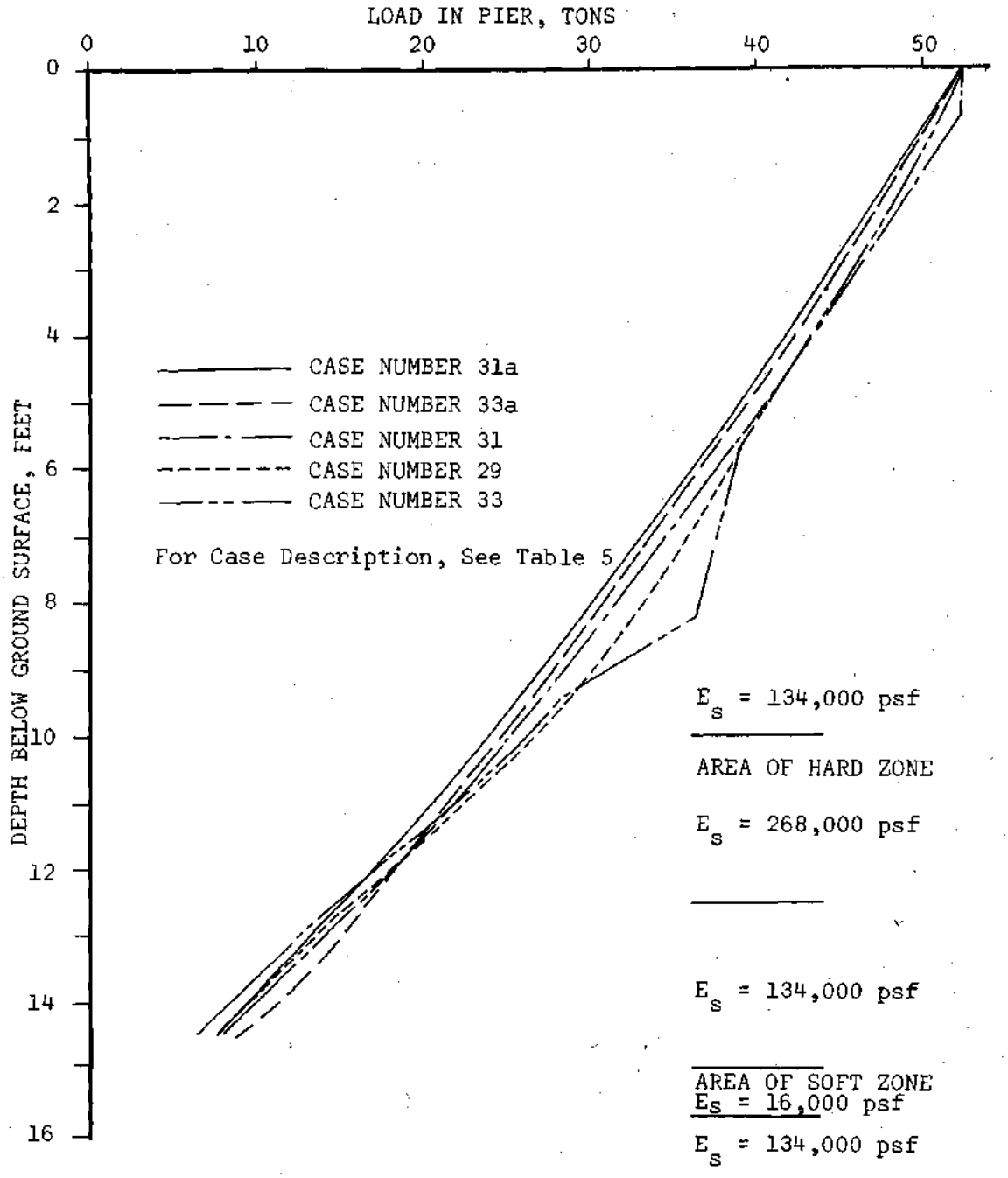

Figure 52. Theoretical Effect of Different Moduli Materials on the Load Distribution Pattern of a Pier 18 Inches in Diameter and 15 Feet Long at an Applied Load of 52.5 Tons

Table 5. Description of Cases Studied in Figure 52 for the Variation of Soil Properties in an Elastic Media

Case	Load in Bottom Tons	Average Shear Stress psf	k tanδ Average	Bottom Load / Applied Load	Settlement Inches
29	8.01	1260	0.86	0.152	0.783
31	8.13	1220	0.85	0.155	0.855
31a	7.40	1276	0.87	0.141	0.861
33	6.92	1290	0.89	0.131	0.792
33a	9.00	1230	0.83	0.172	0.843

Case	Description
29	Uniform Soil (E = 134,000psf) with a hard (E = 268,000psf) zone between 10 and 12.5 feet below the ground surface.
31	Uniform soil (E = 134,000psf) with a soft (E = 16,000psf) zone between 15 and 15.75 feet below the ground surface.
31a	Same as case 31 except the bottom zone has a modulus of elasticity of 1600psf.
33	Uniform soil (E = 134,000psf) with a hard (E = 268,000psf) zone between 10 and 12.5 feet below the ground surface and a soft (E = 16,000psf) zone between 15 and 15.75 feet below the ground surface.
33a	Uniform soil (E = 134,000psf) with no vertical load transfer for the first 2 1/2 feet below the ground surface.

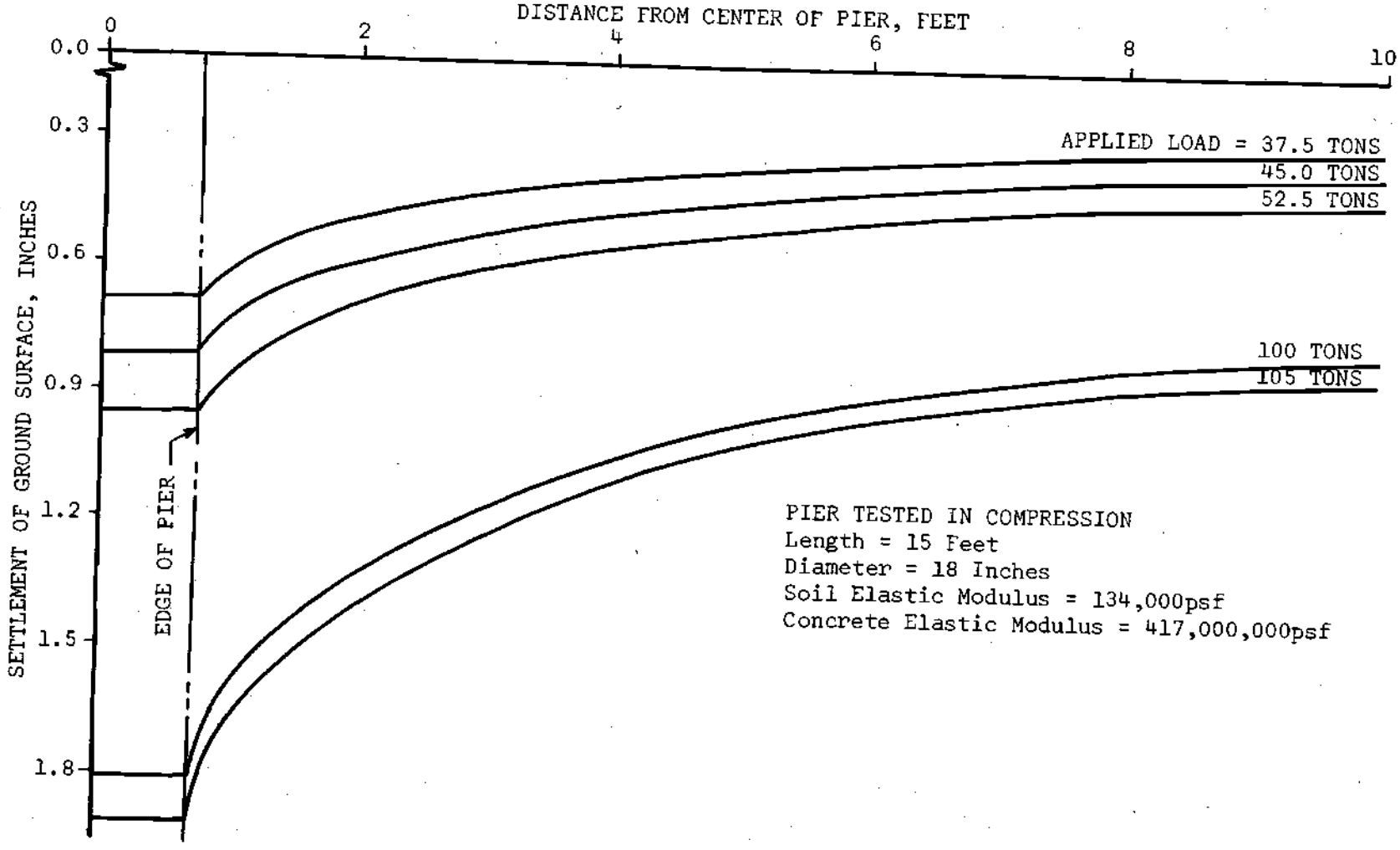

Figure 53. Theoretical Settlement of the Ground Surface Adjacent to a 15-Foot Long Pier 18 Inches in Diameter Embedded in an Elastic Media

computed by the finite element method. These curves indicate that the supports for the settlement gauges should be placed at a distance greater than four diameters from the pier. In testing piers whose settlement at failure is extremely small (like those tested for this thesis) an error of about 30 per cent on the unsafe side may be incurred by placing the settlement gauges closer than four diameters to the edge of the pier. The effect of ground surface settlement, which was not investigated, may be partially offset by the soil uplift around the reaction piers.

The curves presented in this section obtained from various field tests and theoretical solutions show the influence of length, diameter, and soil modulus of elasticity on the settlement of a drilled pier in soil. The theoretical curves do not accurately predict the settlement of a drilled pier in soil due to the large modulus of elasticity needed to match field results, the elastic theory limitations and the fact that settlement of a pier is not directly related to soil modulus of elasticity. Their purpose is to show the effect of the variables and the relative effects due to changes in the elastic modulus, diameter, and length.

To predict the theoretical work load settlement of a pier in weathered rock, it would be necessary to have a modulus of elasticity approximately ten times the values determined from the laboratory tests (Appendix A).

Proposed methods of predicting settlement will be discussed in the recommended design procedure section of this chapter.

Load Distribution Patterns and Load Carrying Capacity

The field testing part of this investigation gave load distribution patterns for the four test piers which derived their load carrying ability from a combination of skin friction and end bearing. These load distribution patterns will be discussed in this section to illustrate the support mechanisms which are involved and the effect of material properties. The elastic finite element computer solution has been used to extend the results to include the effect of variation of elastic material properties and pier dimensions. The measured load-carrying capacity of the drilled piers will also be discussed in this section since it is directly related to the load distribution patterns and is also related to the load-settlement patterns discussed in the previous section.

The instrumentation discussed in Chapter V was used to obtain the load distribution patterns presented in Figures 34 through 37. These curves show that the load is removed in a non-uniform manner. Figures 34 through 37 also show that there are zones where no load is removed from the pier, zones where load is apparently added to the pier and zones where the load is apparently negative or tensile. The elastic model was used to evaluate some of the factors which affect the shape of the load distribution curves.

In piers two, three and four there are apparently zones where there is no load being removed from the pier near the surface. There are several possible reasons for this phenomena:

1. If the soil surrounding the pier near the surface settles due to the imposed pier load there will be less load removed from the pier (Kerisel, 73). This occurs because the soil is moving with the pier and is not offering any support. This phenomena may also cause an increase in load, at depths below the no-load transfer zone.

2. The elastic finite element solution indicated that there is a zone of tangential and radial tensile stress adjoining the pier surface for approximately the uppermost third of the length of the pier. In zones having these tensile stresses little effective support can be realized. In a true soil system this effect may be partially counteracted by the settlement of the soil.

3. Upon completion of the testing program a seven-foot deep pit was excavated between test piers four and seven. Observations made in the pit indicated that there is very little contact between the pier and the soil at shallow depths up to about four feet as shown in Table 6.

Table 6. Efficiency of Soil-Concrete Interface for Drilled Piers in Weathered Rock

Depth		SURFACE AREA OF CONCRETE IN CONTACT / TOTAL SURFACE AREA OF CONCRETE
From	To	
0	1'-8"	0.2
1'-8"	3'-0"	0.7
3'-0"	7'-0"	0.9

NOTE: Data obtained from a test pit located between test piers four and seven.

Because the area of contact is small there is less opportunity for the load to be removed from the pier. The small areas which are in contact will be taking a large load and can more easily be overstressed and support capacity will be reduced for the first several feet below the ground surface. The area of contact is considered to be a function of the construction technique alone. The contact area may be increased by vibrating the concrete, using a higher slump concrete mix, using non-shrinking (expanding) cement or all three.

4. The support capacity of the upper feet of the pier could also be disturbed excessively by the drilling operation which required insertion and removal of the auger. The areas near the top of the pier shaft will be more disturbed than the lower sections by this operation since the auger passes through these zones more often.

The inability of the uppermost few feet to carry some of the applied load is significant. Table 6, showing data obtained from the exploratory test pit, indicates the effective contact areas observed and may serve as a guideline in estimating the support capabilities of the upper few feet of a drilled shaft. The percentage of area of concrete in contact with the surrounding soil might be greatly increased by changing the construction procedure as mentioned above. The effective support capability of the upper few feet is influenced the most by climatic conditions. The climate, or anticipated climate should also be considered as an environmental effect, since it will influence the ability of the pier to support the imposed load. The climatic effect has been shown to decrease with time (36, 37, 54, 66).

5. Inaccurate or misleading readings from the strain gauges could also affect the measured loads. However, the results of Vesic's (76) work on driven piles in sand indicate that the upper few feet of a pile contribute little or nothing to the pile capacity.

The load distribution curve for test pier one (Figure 35) shows that there is an increase in the load in the pier between depths of 9 and 12 feet. This increase in load could be caused partially by the settlement of the soil above this level or by the removal of vertical stress above this level accompanied by a zone of no load removal between 9 and 12 feet. This load increase may be caused by an irregularity in the gauge readings or more likely by the presence of a hard zone. In Chapter VI it was mentioned that there was a hard zone at about 11 feet below the ground surface which was encountered while drilling the pier.

The effect of a hard zone was investigated using the finite element computer solution. The results of the computer solution for an applied load of 52.5 tons and a hard zone extending from 10 to 12.5 feet are shown in Figure 52. This figure shows that there will be a decrease in load in the pier through a hard zone, represented by a material having twice the modulus of elasticity than the surrounding soil. With a higher ratio of the modulii of elasticity it is expected that the load decrease will be more prominent. The figure also shows the effect of a hard side zone and a soft bottom. In the latter case there is a tendency for the load in the pier to be decreased at a lower rate than in the former case. Either of these effects when

coupled with the settlement of the soil above the hard zone might cause an increase in the load remaining in the pier.

The indicated increase in the load remaining in the pier could also be caused by bending in the pier. Bending or moments in the pier may occur by applying the load eccentrically or by having one side of the pier embedded in a more resistant material than the other side. Since the gages were located on only one side of the pier they would show an increased load if they were on the side of the pier where the hard zone was absent.

Any of the above explanations could account for the increased load in pier one as shown in Figure 35. These events are all plausible in the material at the test site because of the extreme variability of the soil.

In test piers two, three, and four there is a tendency for the load in the bottom of the pier to be tensile. The tension force in the bottom was measured from the initial no load condition on the pier, just prior to applying the first load increment. The tensile force generally occurred after the initial applied load and then returned to a compressive force when about 70 per cent of the estimated ultimate load (as determined from the load-settlement curves) was applied. Several possible reasons for the tensile condition were presented in Chapter VI. In addition to these reasons given previously another explanation can be obtained from the elastic finite element computer solution which shows that the radial stress immediately above the bottom is tensile. This tensile stress in the soil would reduce the lateral support

capability and could cause an axial tensile stress in the bottom of the pier until sufficient deformation occurred to cause a compressive stress. This tensile stress may not be obvious for the first few load increments because of the weight of the concrete alone and the increase in load which could be caused by any or all of the reasons given previously. The tensile condition can also be caused by a zone of no load transfer followed by a compressible zone which would tend to pull the pier down with it as the soil settles. The tensile condition at the bottom may also be associated with soft bottom which would tend to make the end of the pier "hang" from the upper portions of the pier when the radial stress becomes large enough to prevent lateral support. The possibility of a bending stress at the bottom of the pier was investigated in piers two, three and four by multiple strain gauge installations. These readings were essentially identical. This indicated a lack of moment at the bottom of the pier.

The shapes of the load-distribution curves have several things in common. In all cases there was an initial increase in load at the bottom and then the bottom load decreased before beginning to increase again. In some cases the bottom load decreased enough to apparently place the bottom in tension for the reasons given above. After the bottom load reached its minimum value, the load distribution curves are practically parallel for all subsequent load increments.

As the pier loses its load carrying ability in a certain zone the load distribution curve becomes vertical, indicating that no load is being removed. One way that the soil will not take any of the load is

if it is separated from the pier. The zone of no load transfer was encountered in three of the test piers, and occurred generally just below the ground surface for reasons discussed previously. It is also possible to have an apparent no load transfer zone at other locations due to hard or soft sides, bending or a combination of these conditions.

The load-distribution curves obtained from the elastic computer solution have uniformly increasing slopes with the greatest slope occurring at the bottom of the pier. The slope of the load distribution curve is directly related to the shear stress as is indicated in Figure 54 for a pier embedded in a banded elastic soil. The curves are practically identical to curves obtained for a uniform soil having a modulus of elasticity equal to the average value of the two banded materials with the exception that the banded soil results in a curve which does not have smooth transition of loads at different depths. In fact, the finite element computer solution shows that for reasonable bounds the modulus of elasticity of a homogeneous, isotropic material has little effect on the load distribution pattern.

There has been very little other work done in actual measurement of the load distribution in a pier, due primarily to the instrumentation and test cost involved. The load distribution curves which are available, however, are interesting and are unique for each pier tested. Figure 2 shows the results of two load tests performed by Mohan et al. (39). These curves show the same general pattern as those discussed above, but more clearly illustrate the relationships predicted by the computer solution with the exception that less load is transferred near

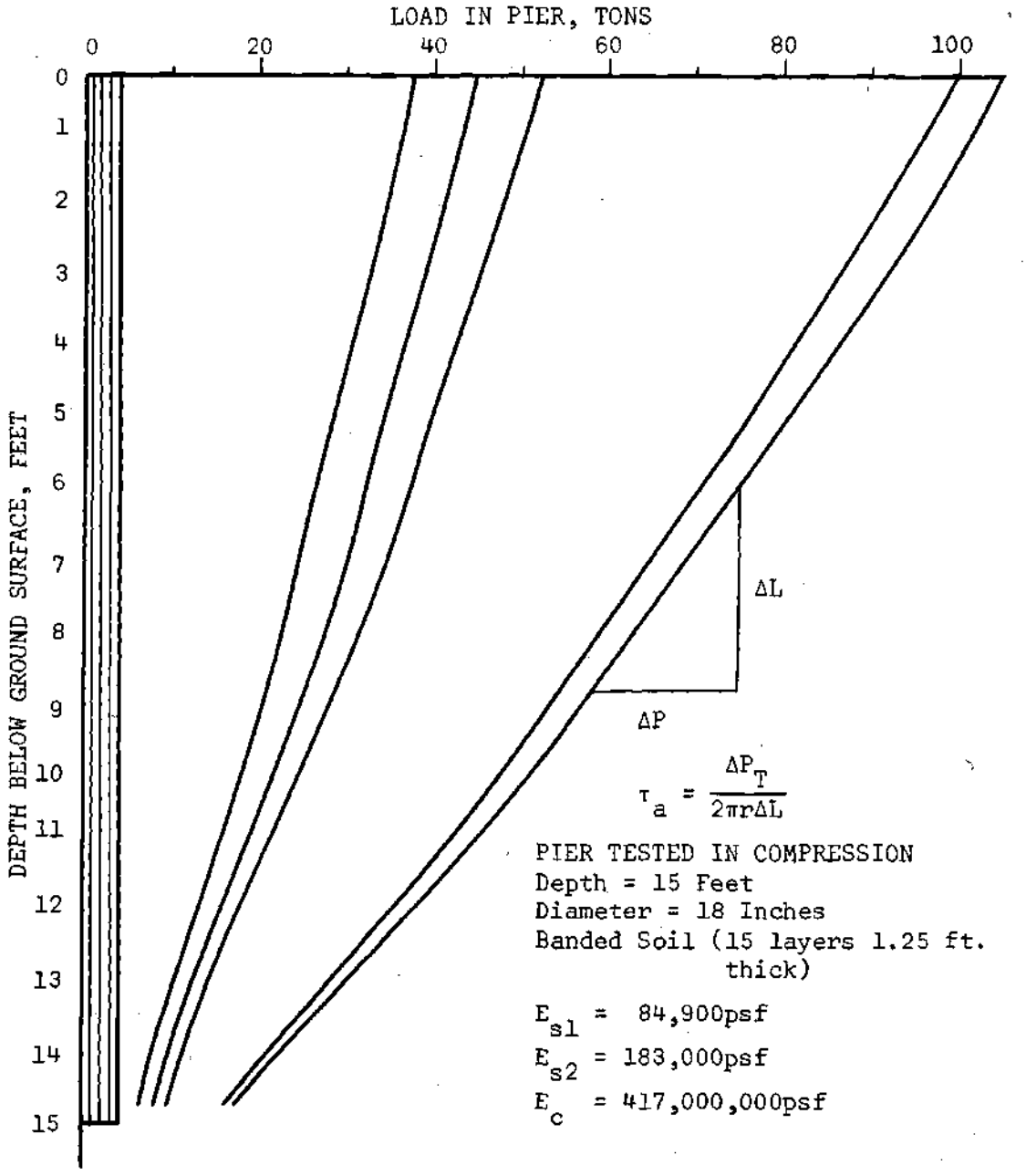

Figure 54. Theoretical Amount of Load Remaining in the Pier as a Function of Depth of Embedment in an Elastic Material

the bottom in the Mohan et al. tests. This is probably the true case since the developed radial tensile stress may limit load transfer in a real soil. The load distribution patterns obtained by Henley (46), and shown in Figure 3 are a combination of the curves that would be predicted by the computer solution and those curves obtained from this study of drilled piers in weathered rock. The initial portion of the curves at low applied loads closely resemble those curves obtained from the computer solution considering minor deviations from a smooth line. As the applied load increased, past about 25 per cent of the tested load, the curves obtained by Henley are seen to move outward in approximately a parallel manner. The parallel nature of the curves indicate that the increase in load is taken almost entirely by the bottom.

The parallel nature of the load distribution patterns obtained by Henley, and to a certain extent by Mohan et al., is similar to the relationship obtained from the field work performed as part of this thesis. In order for this phenomena to occur, one of two things must be happening:

1. The soil surrounding the entire length of the pier must be behaving in a plastic manner.

2. The loss in support over a small area of the pier-soil interface must be counteracted by an identical gain in support by an adjacent small area of pier soil contact.

The first of these is more plausible especially if one considers that the relative displacement along the soil pier interface is practically identical throughout the entire length of the shaft once the

load is past the initial linear portion of the load displacement curve, since the shaft compression is very small compared to the surface displacement of the pier. The magnitude of the shaft compression was computed on an elastic basis for the piers tested as part of this thesis and is shown in Figures 41 through 44. From these figures it is seen that the shaft compression is generally a substantial part of the total top displacement initially but becomes proportionally less as the load is increased past the elastic range of soil behavior. Once the entire pier length is acting to support the pier load the movement is such that at least part of the soil surrounding the pier will be stressed beyond the elastic limit. As further loading occurs more and more of the soil will be stressed beyond its elastic limit until the entire soil system is behaving in a non-elastic manner.

The elastic finite element solution indicates that the shaft compression is small compared to displacement because the modulus of elasticity of the shaft is several orders of magnitude greater than the modulus of elasticity of the surrounding soil. In order for the soil to behave in a completely plastic manner, as in the first statement, it would have to be rigid-plastic or an elastic-plastic material (see Figure 9). It is not likely that the soil behaves in this way but instead behaves in a non-linear manner as is indicated by changes in the load distribution curves. The gradual rotation of the load distribution curves indicates that the shear stress is increasing, but not as rapidly as for lower load levels.

If both of the above phenomena occurred simultaneously, the lines indicating the load remaining in the pier would progress in approximately a parallel manner and the material would not have to be elastic-plastic or rigid-plastic. It would, in fact, tend to substantiate the failure mechanism discussed earlier which is caused by the entire surface of the pier not being in contact with the soil.

Another aspect of the load distribution curves which is very important is the evaluation of the amount of load taken in skin friction and the quantity of load taken by end bearing. These two load support mechanisms determine the design procedure to be utilized as explained in Chapter III. The amount of load taken in end bearing and skin friction for each of the test piers is presented in Table 1. This table shows that at least 70 per cent of the applied load is transferred to the soil through skin friction for the loads investigated. As the load-distribution curves for each successive load increment become parallel it is apparent that an increasing percentage of the applied load is being transferred to the soil through end bearing. When both the load distribution curves and the load-settlement curves are considered together it is apparent a significant amount of the load is not carried by end bearing until the applied load is past the elastic range of the soil pier system. Even at the estimated ultimate load for the piers tested only about 30 per cent of the applied load ever reaches the bottom of the pier. This indicates that over two-thirds of the applied load will be carried by skin friction forces at the ultimate load and a greater percentage will be carried by skin friction forces at loads less than ultimate.

The percentage of load which reaches the bottom of a pier embedded in an elastic media was investigated by use of the finite element program and was also investigated by Poulus and Davis (74) by integrating the Mindlin (45) solution. The percentage of load which reaches the bottom of a pier in an elastic media is presented as a function of the depth-to-diameter ratio in Figure 55. Figure 55 shows that as the depth-to-diameter ratio is increased the percentage of the applied load which reaches the base of the pier decreases. The curves in Figure 55 show that the banded materials have a different effect than the homogeneous materials and also that the values obtained by Poulos and Davis give a lesser amount of load reaching the base of the pier than that obtained from the finite element solution. The difference between the finite element solution and the integrated Mindlin solution is probably due to differences in the modulus of elasticity and also to several simplifying assumptions made by Poulos and Davis (74) in the integration of the Mindlin Solution. The finite element solution is more realistic and should have values which more closely represent those obtained from field tests in the elastic range of loading.

The amount of load reaching the bottom of a drilled pier in a uniform, elastic homogeneous soil is also a function of the modulus of elasticity of the soil. The effect of various modulus of elasticities of soil were investigated for a 22-foot long pier 18 inches in diameter and are presented in Figure 56. This curve shows that as the modulus of elasticity of the soil is increased, the amount of load which reaches the bottom of the pier decreases slightly and for practical purposes this effect can be neglected.

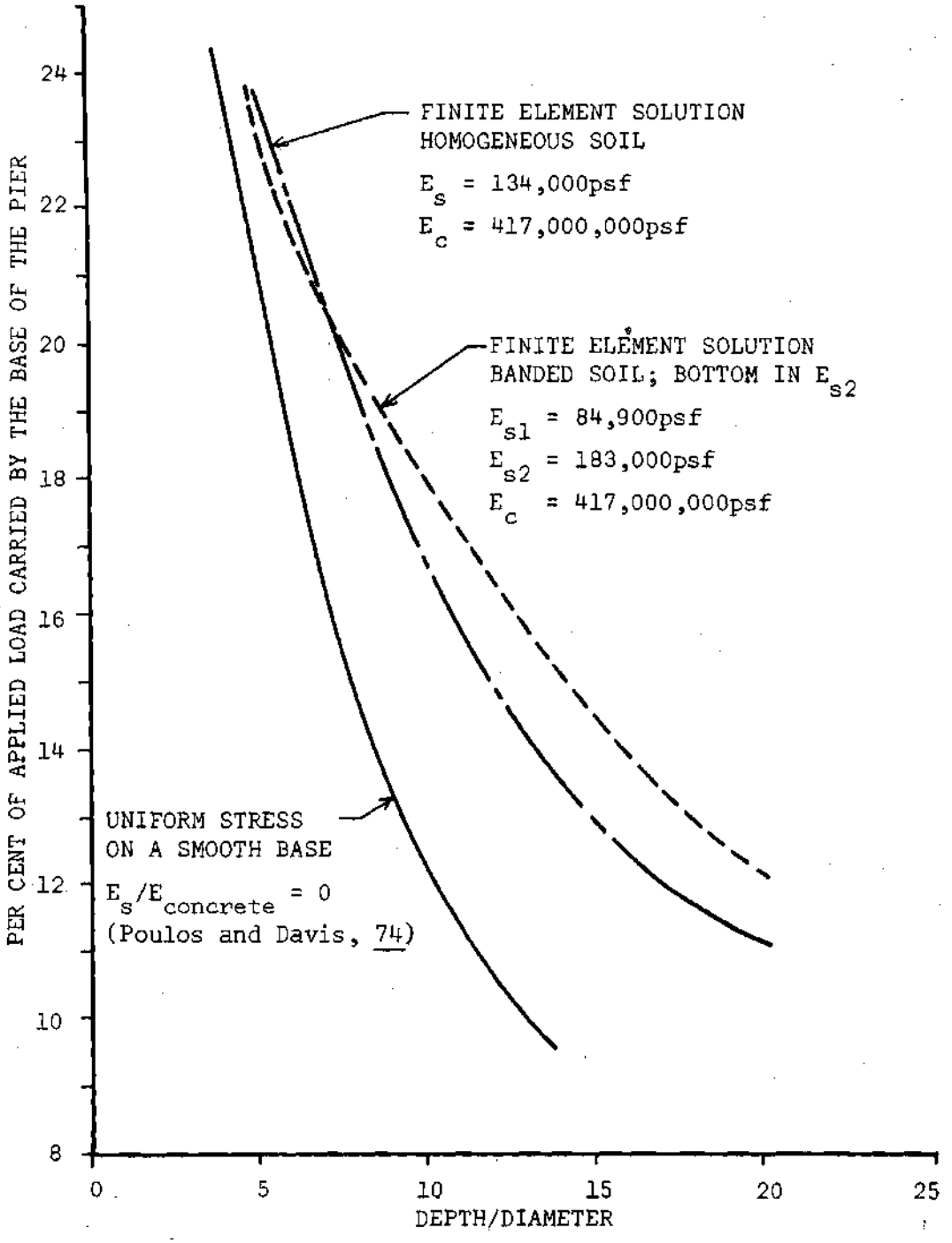

Figure 55. Per Cent of Applied Load Carried by the Base of the Pier as a Function of the Ratio of Depth to Diameter

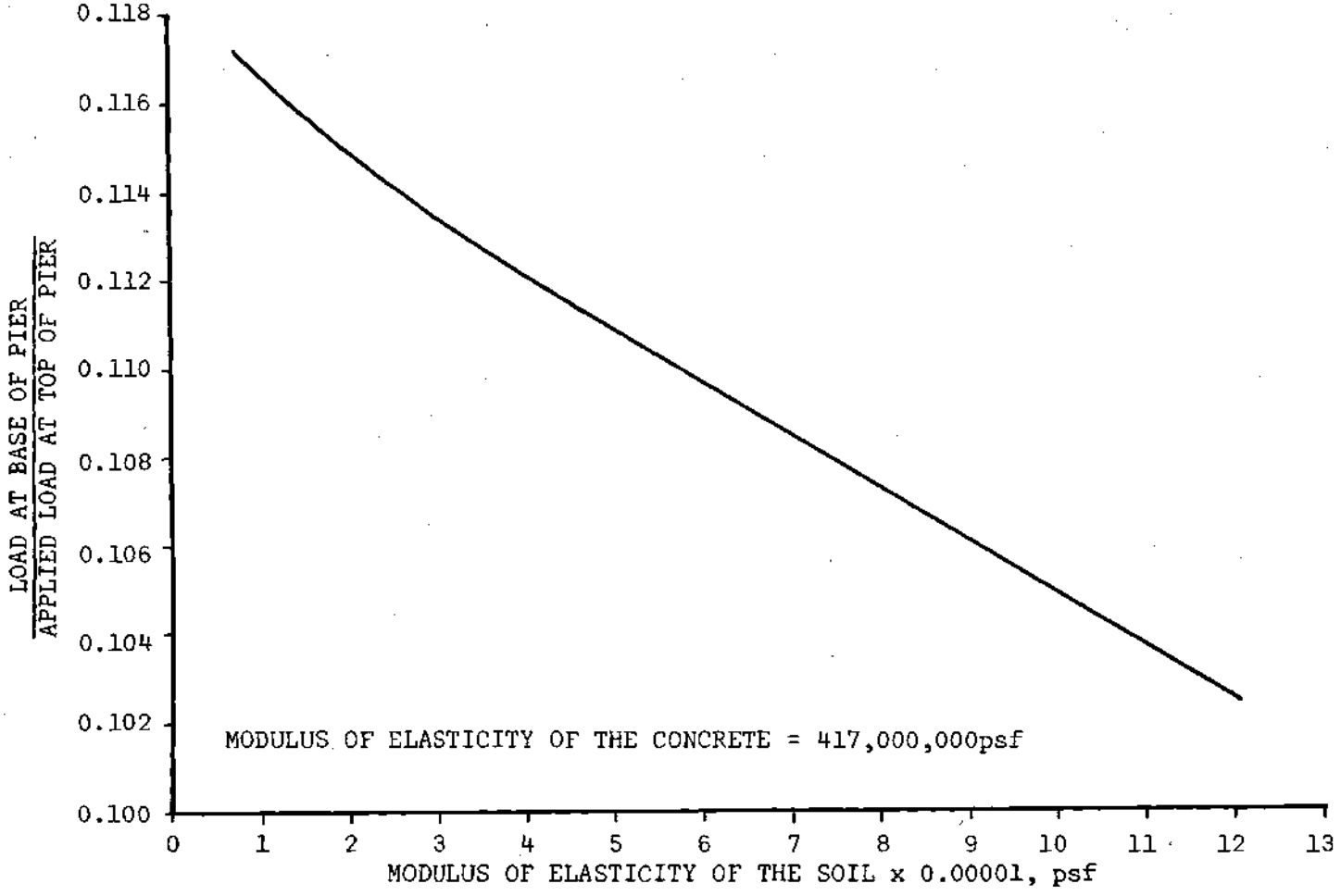

Figure 56. Effect of Modulus of Elasticity of the Soil on the Percentage of Applied Load Reaching the Base of a 22-Foot Long Pier 18 Inches in Diameter Computed Using the Finite Element Solution

The amount of applied load reaching the bottom of a deep circular foundation has been plotted for several field results including those obtained as part of this study. The results are presented in Figure 57 along with the results of the finite element study. Figure 57 shows that at the ultimate load the percentage of load carried by the base of the pier decreases as the depth-to-diameter ratio increases. The data obtained by all investigators indicate that the relationship between applied load and depth to diameter is almost identical to the trend predicted by the finite element method. The only difference between the elastic solution and the field solution is that the majority of the field data indicates a higher percentage of the load is carried by the base at the ultimate load. This is readily explainable since the field solution extends past the elastic range and into the range where the load-distribution curves are "parallel." In this range practically all additional load applied at the surface is carried by the base as previously explained. The percentage of load carried by the base for tests performed by the other investigators presented in Figure 57 would probably be very close to the values predicted by the finite element curve for values of load still in the elastic range of the soil system. It is of interest to note that the values obtained from the field tests performed as part of this thesis are close to the values predicted by elastic theory. This may be because the ultimate load may not have been reached or because of the lack of adequate bottom support. It is likely that the bottom support was not adequate. A loose bottom will cause more load to be transferred by skin friction and

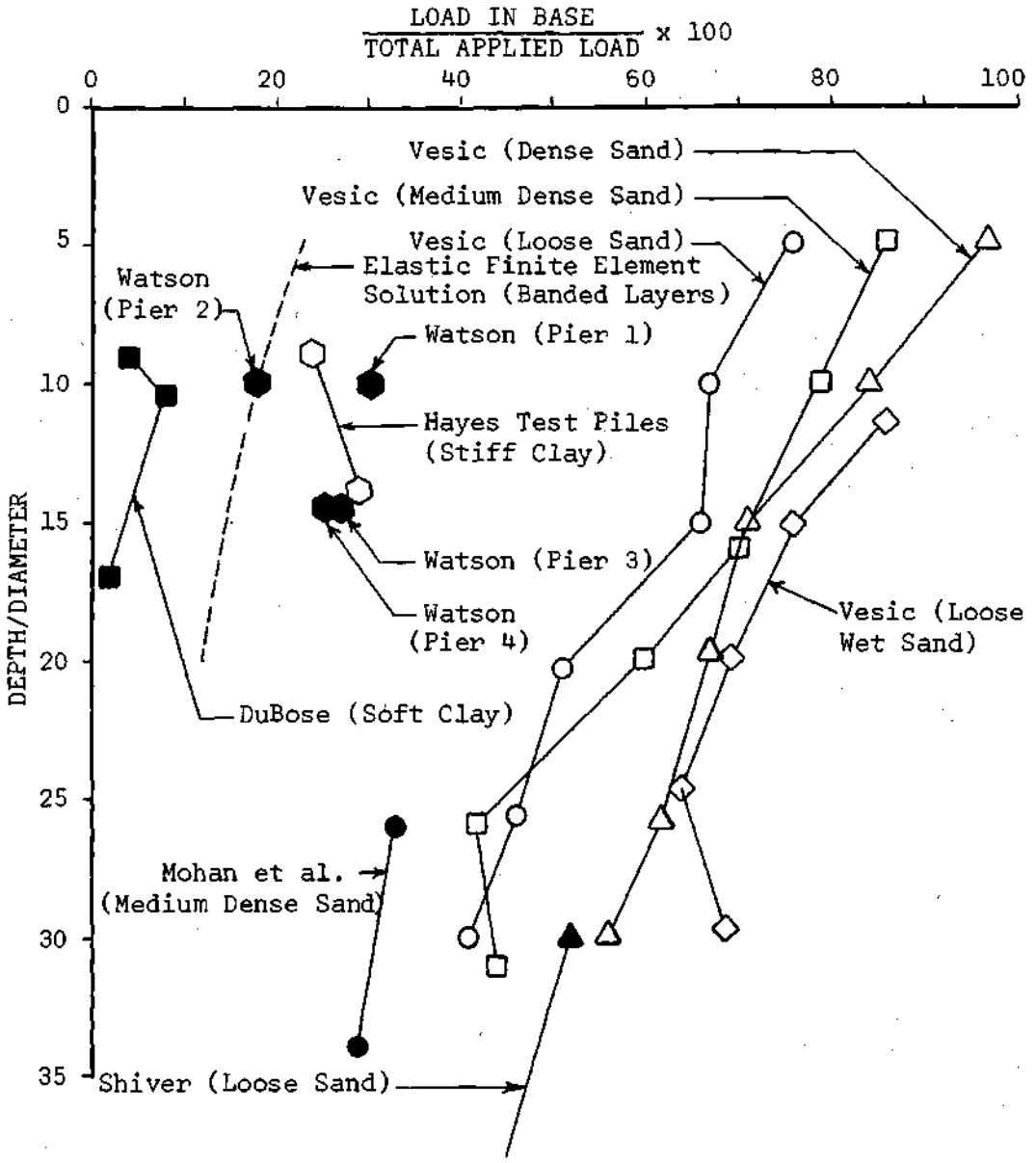

NOTE: Watson Piers are in Weathered Rock

Figure 57. Percentage of Applied Load Reaching the Bottom of an Embedded Circular Foundation at Ultimate Load Determined from Field Test Results

will not permit the ultimate load to be achieved without greater settlements. The effect of a soft base in a drilled pier will be discussed later in this chapter.

Before analyzing the different mechanisms of end bearing and skin friction it is useful to review the load distribution patterns briefly. The pattern of load transfer is seen to be a function of the soil properties, pier geometry, applied load, and construction technique. The amount of load transferred by skin friction has been shown to be a function of the properties of the surrounding soil and is greatly influenced by the bottom material properties (loose bases cause more load to be transferred by skin friction and hard bases cause more load to be transferred by end bearing) and the applied load. As the applied load in the test piers increases, the amount of load reaching the bottom decreases and in most cases a tensile force exists in the bottom until about 70 per cent of the ultimate load is applied at the top. After about 70 per cent of the ultimate load is reached, almost all additional load is carried by the bottom, and the load distribution curves remain essentially parallel for subsequent loads. Since the load distribution curves remain essentially parallel there is no reduction in skin friction forces. This indicates that skin friction acts almost independently of end bearing in contributing to the support of a pier in a "uniform" soil. Since these forces act almost completely independently, the discussion of the different mechanisms will be considered separately in the remainder of this section and also in the section on the recommended design procedure.

Skin Friction Studies

The theoretical aspects of the skin friction capacity of a deep circular foundation were discussed in Chapter III. The results of the derivation show that the skin friction capacity can be approximately expressed by

$$Q = 2\pi\eta \int_0^L \left(Ca + k(\gamma L+\sigma_h)k \tan\delta\right) d\ell \qquad (24)$$

where all of the terms have been discussed previously.

For practical considerations the influence of the horizontal stresses caused by the vertical component of the skin friction forces (σ_h) can be neglected except near the tip of the pier where the value is tensile and is of significant magnitude compared to the vertical compressive stress. If the influence of the vertical component of skin friction forces for a constant shaft diameter is neglected the above formula is simplified to

$$Q = C_a A_s' + \frac{L\gamma}{2} A_s' k \tan\delta \qquad (25)$$

where A_s' is the effective area of contact between the concrete and the soil.

The average unit skin friction stress (τ_a) can be computed by using

$$Ca + \left(\frac{L}{2}\right)\gamma k \tan\delta = \tau_a \qquad (26)$$

The average skin friction stress (τ) for a pier is equal to the load removed from the pier by skin friction divided by the surface area of the pier; utilizing this relationship Equation (26) becomes

$$\frac{P_T - P_B}{2\pi rL} = Ca + \frac{L}{2}\gamma k \tan \delta \qquad (27)$$

Equation (27) has the effect of smoothing out the load distribution curve to a straight line between P_T and P_B and this formula is the one commonly used to compute the skin friction capacity of a deep foundation. Figure 58 shows the theoretical elastic load distribution curve for an applied load of 130 tons on a pier 30 feet long and 18 inches in diameter supported in a homogeneous, elastic, isotropic soil media. At loads less than 130 tons the average shear stress curve agrees more closely with the true theoretical load distribution curve than indicated in Figure 58.

The value of the average shear stress (τ_a) can be obtained from the elastic finite element computer solution for loads which are still in the elastic range for the soil pier system. Values of τ_a obtained from the finite element solution at loads greater than this are not valid. In the remaining discussion the attention will be focused on the values of the average shear stress and the coefficient of horizontal earth pressure (k) since they are the parameters which assess the importance of the skin friction support mechanism. The other parameters in Equations (25) and (27) can be obtained from laboratory testing and from geometric properties of the pier.

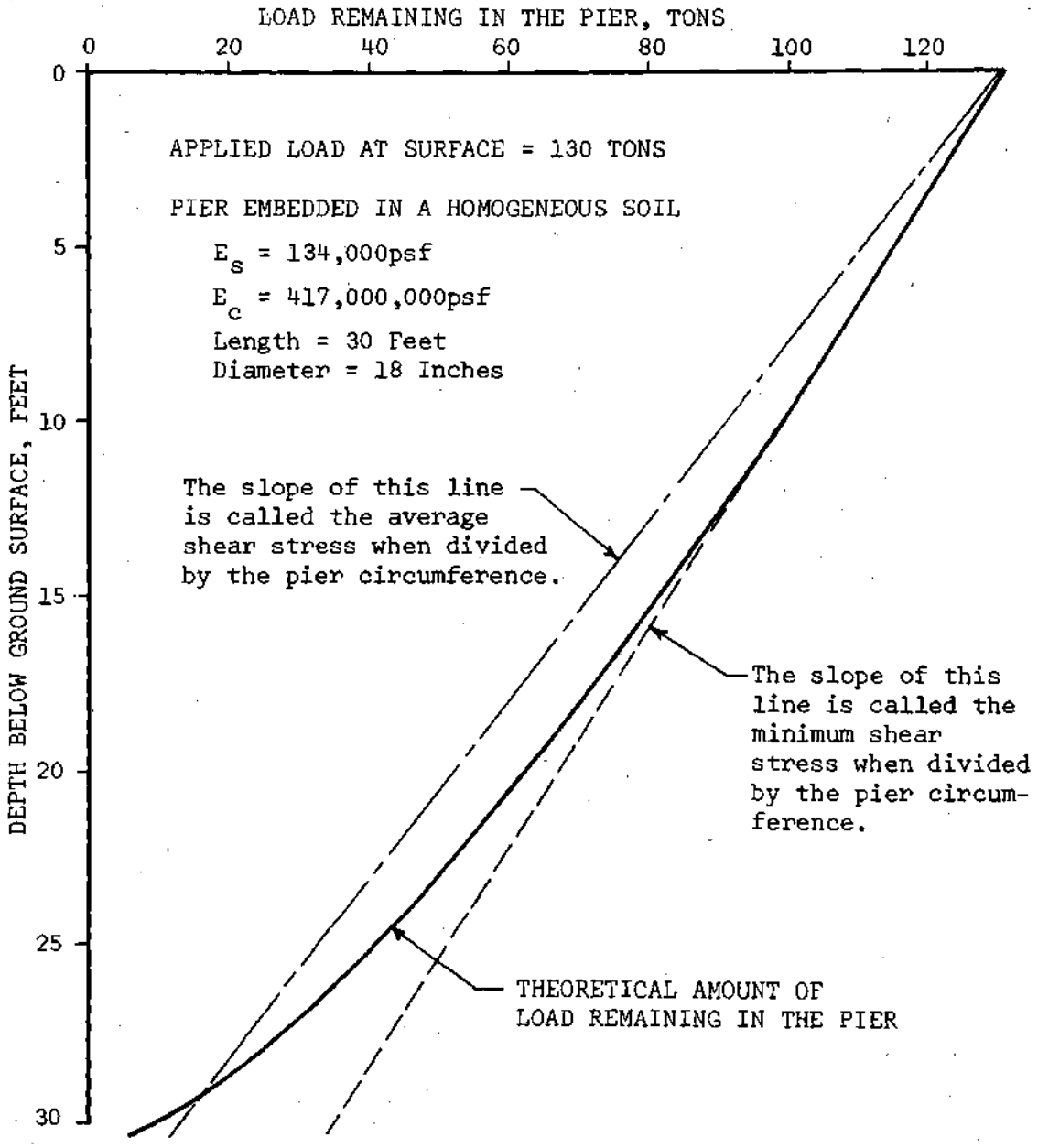

Figure 58. Theoretical Amount of Load Remaining in a 30-Foot Long Pier 18 Inches in Diameter Embedded in an Elastic, Homogeneous Material at an Applied Load of 130 Tons

Since the finite element computer solution will be used to describe some of these parameters it is desirable that it be further compared to the actual field results obtained from the test piers. This can be done on the basis of the average shear stresses over the length of the pier. Such a relationship is shown in Figure 59 for the two lengths of piers tested. Figure 59 shows that the average shear stress is directly proportional to the applied load for the elastic solution. This is to be expected since the actual percentage of the applied load reaching the base of the pier is a constant for all applied loads at a given depth to diameter ratio. The field results, also presented in Figure 59, are seen to be linear up to a certain point and then the value of the average shear stress begins increasing at a decreasing rate. The average shear stress from the field tests has a limiting value which depends on the geometry of the pier. The initial departure from a straight line for the field results generally occurs when the load in the bottom of the pier has reached its minimum value and then starts increasing (see Figures 35 through 38). At this point the load distribution curves also become essentially parallel, denoting the end of the elastic range of the soil-pier system at about 70 per cent of the ultimate load. Figure 59 shows that the computer results agree very well with the field results as long as the load remains in the elastic range. At loads above the elastic range for the soil pier system the curves indicate a limiting value for the average shear stress. This limiting value for the average shear stress can be used to compute an approximate average value of the coefficient of

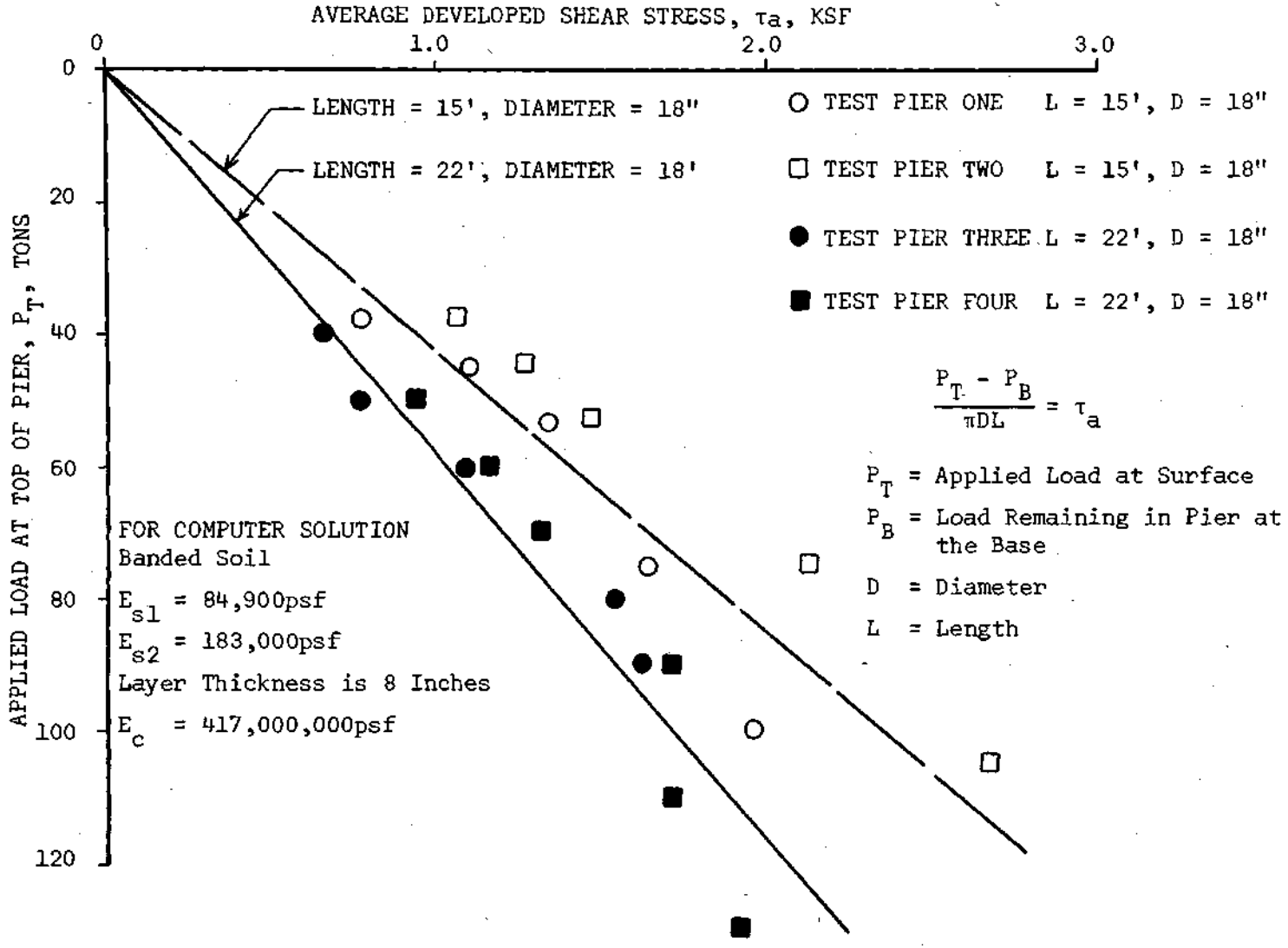

Figure 59. Comparison of the Average Shear Stress Obtained with the Elastic Finite Element Solution and Those Obtained from Field Tests in Weathered Rock

horizontal earth pressure using Equation (27). Figure 59 also indicates that the horizontal earth pressure coefficient can be computed accurately using the finite element computer solution while the loading on the pier is in the elastic range. The value for the coefficient of earth pressure in the elastic range is quite different than the limiting value and is a function of the length, diameter and applied load. Since there is a difference between the two coefficients of horizontal earth pressure, the coefficient in the elastic range will be called the elastic coefficient of horizontal earth pressure.

The elastic coefficient of horizontal earth pressure at various depths was investigated extensively by use of the elastic model. This coefficient is defined as the ratio of the horizontal stress to the vertical stress while the applied load is in the elastic range for the soil-pier system. The variation of the elastic coefficient of earth pressure is presented in Figure 60 for a 22-foot long pier 18 inches in diameter. This figure shows curves for both a weightless soil and one having weight. The values for the weightless soil are due only to the applied load on the pier. These two curves have similar shapes and serve to point out that even in the elastic range the coefficient of earth pressure is not a constant over the length of the pier.

For a soil media having weight it shows that the radial stresses are tensile at the top and bottom of the pier and that there is almost a constant value of the elastic coefficient of horizontal earth pressure of approximately 1.2. This value is approximately equal to the reciprocal of the at rest earth pressure coefficient determined from laboratory tests.

Figure 60 also shows that the values of the elastic coefficient of horizontal earth pressure (k') for a weightless soil are lower than for a soil having weight. With a weightless media the change in vertical and horizontal stresses at the surface are both tensile. Since this is a tensile force, the actual coefficient should be zero since large tensile stresses probably cannot be taken by most soils and should not be counted on, even in soils which have some cohesive strength.

The data for a weightless media presented in Figure 60 may be used in conjunction with Figure 61 to compute the actual stresses resulting from applied load at the top of the pier embedded in an elastic media. The curves presented in Figures 60 and 61 are not greatly affected by the modulus of elasticity of the soil but depend primarily on the geometry of the pier. The main purpose of Figures 60 and 61 is to show that the coefficient of earth pressure is not a constant over the length of the pier.

From the computer results it is apparent that the average shear stress is a linear function of the surface area of the pier. The coefficient of earth pressure is, however, a complicated polynomial function of the length of the pier or the effective length of the pier. In Figure 62 the values of k tanδ calculated from the field test data have been normalized to a common length of 15 feet considering both the effective length (the length actually contributing to the load support determined from the load-distribution curves) and the total lengths. The curves were normalized by multiplying the values of k tanδ by the

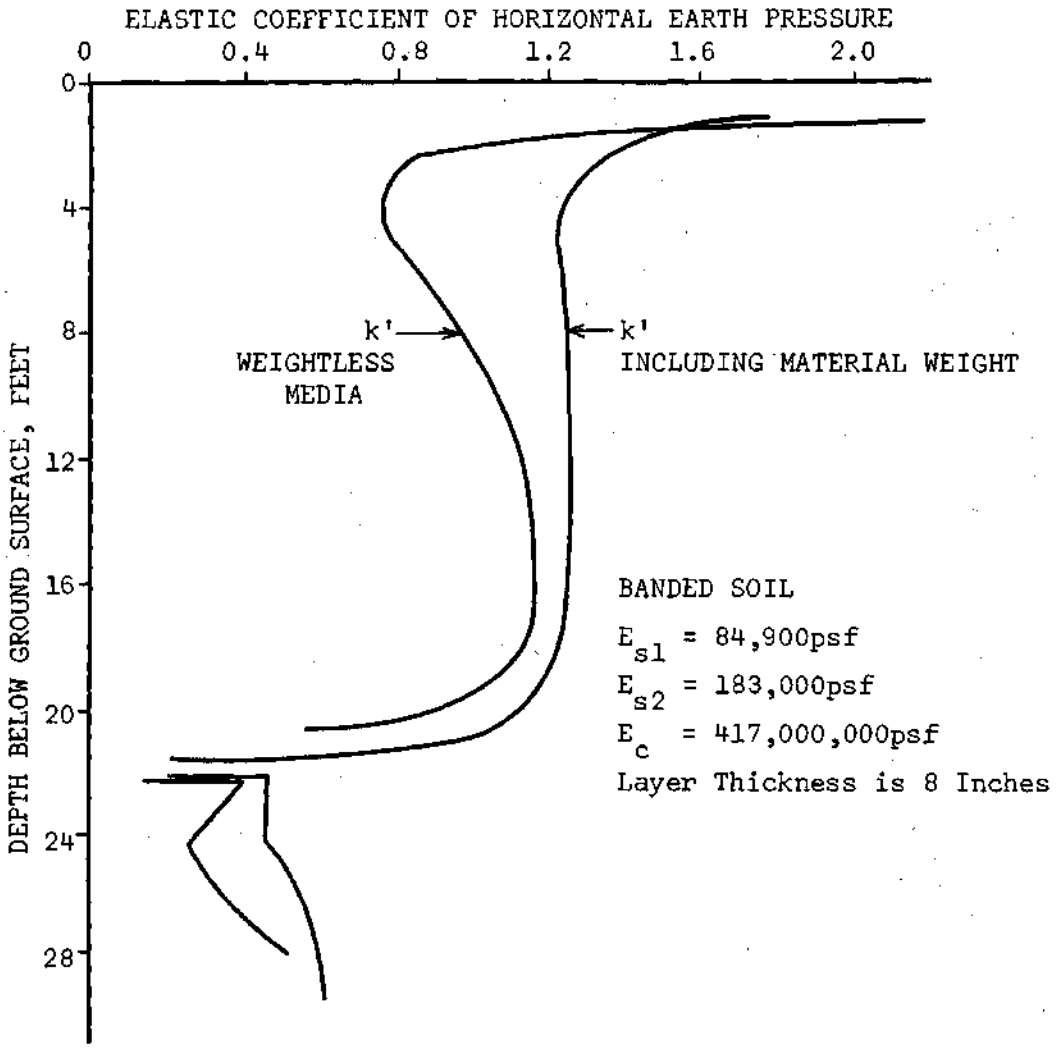

Figure 60. Variation of the Elastic Coefficient of Horizontal Earth Pressure with Depth for a 22-Foot Long Pier 18 Inches in Diameter Embedded in a Layered Elastic Soil

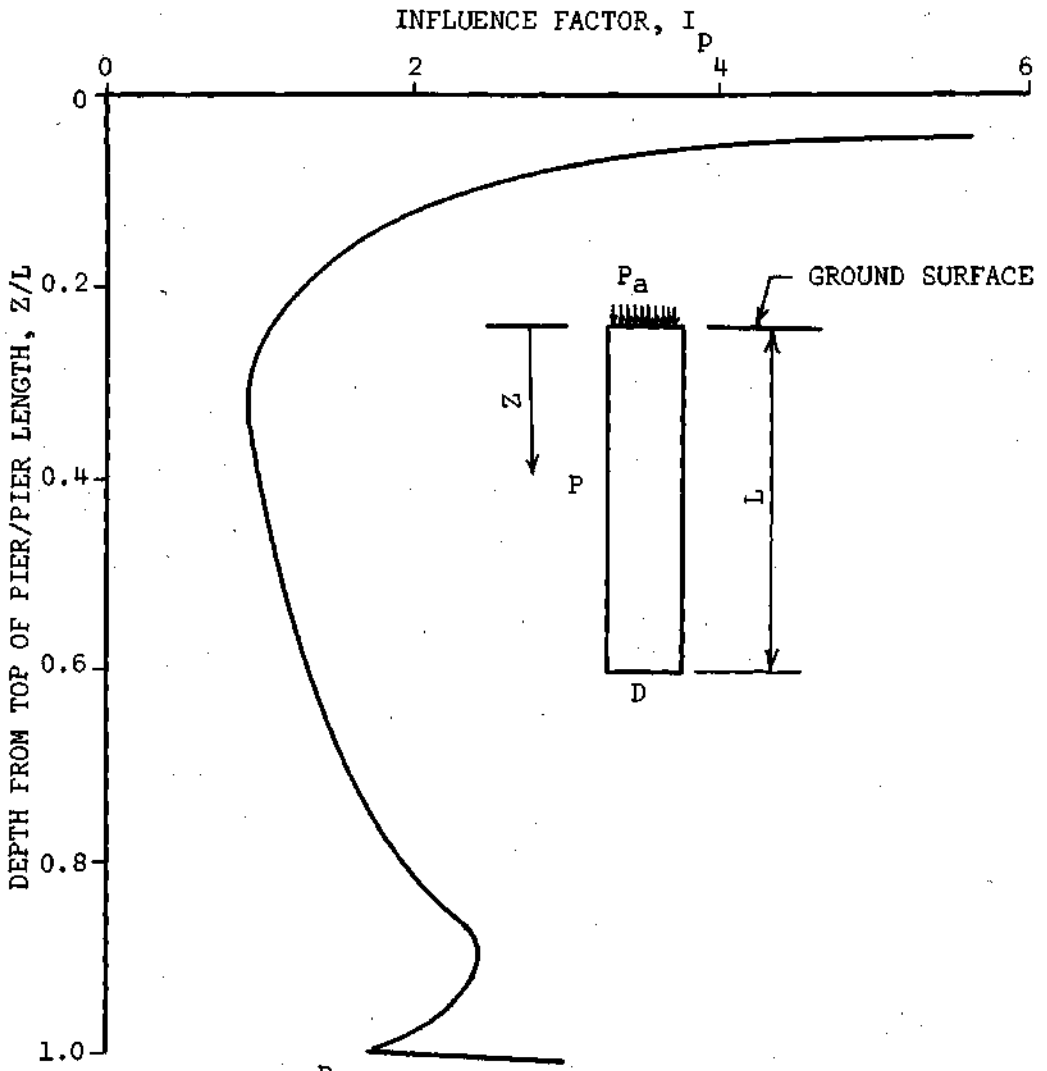

$$I_p = 1000 \frac{P}{P_a}$$

P = Increase in vertical stress immediately adjacent to the pier due to the applied vertical stress at the top of the pier.

P_a = Applied vertical stress.

Figure 61. Change in Vertical Stress in the Soil Adjacent to a Deep Foundation Due to an Applied Vertical Load at the Surface

square of the ratio of the actual length to 15 feet and by the ratio of load carried by skin friction to applied load. The square of a common length of 15 feet was used because the total horizontal stress is approximately a quadratic function of the depth due to the increase in surface area with depth for the same diameter pier and also to the increase in the average horizontal stress which is a direct function of the depth of embedment. The equation is developed in the recommended design procedure section of this chapter. Both of the curves presented in Figure 62 show good agreement with the field data which were limited to 15 feet and 22 feet long piers. A small degree of scattering does occur which can be attributed to variations in material properties, testing errors and approximate scaling law. Thus it is seen that the value of k tanδ is an approximate quadratic function of the length of the pier since the normalized curves for both length piers is almost colinear.

This relationship is presented in Figure 63 which may be used for any length pier once data is corrected for average stresses which will consider various diameters. Figure 63 shows a completely normalized curve which permits a value of k tanδ to be obtained for any length pier. Since the elastic model solutions presented in Appendix C agree with the curve in the linear range, the values can be used for any length pier (the diameter does not affect the value of k tanδ directly but serves to increase or decrease the average shear stress and affects the percentage of load at the bottom of the pier).

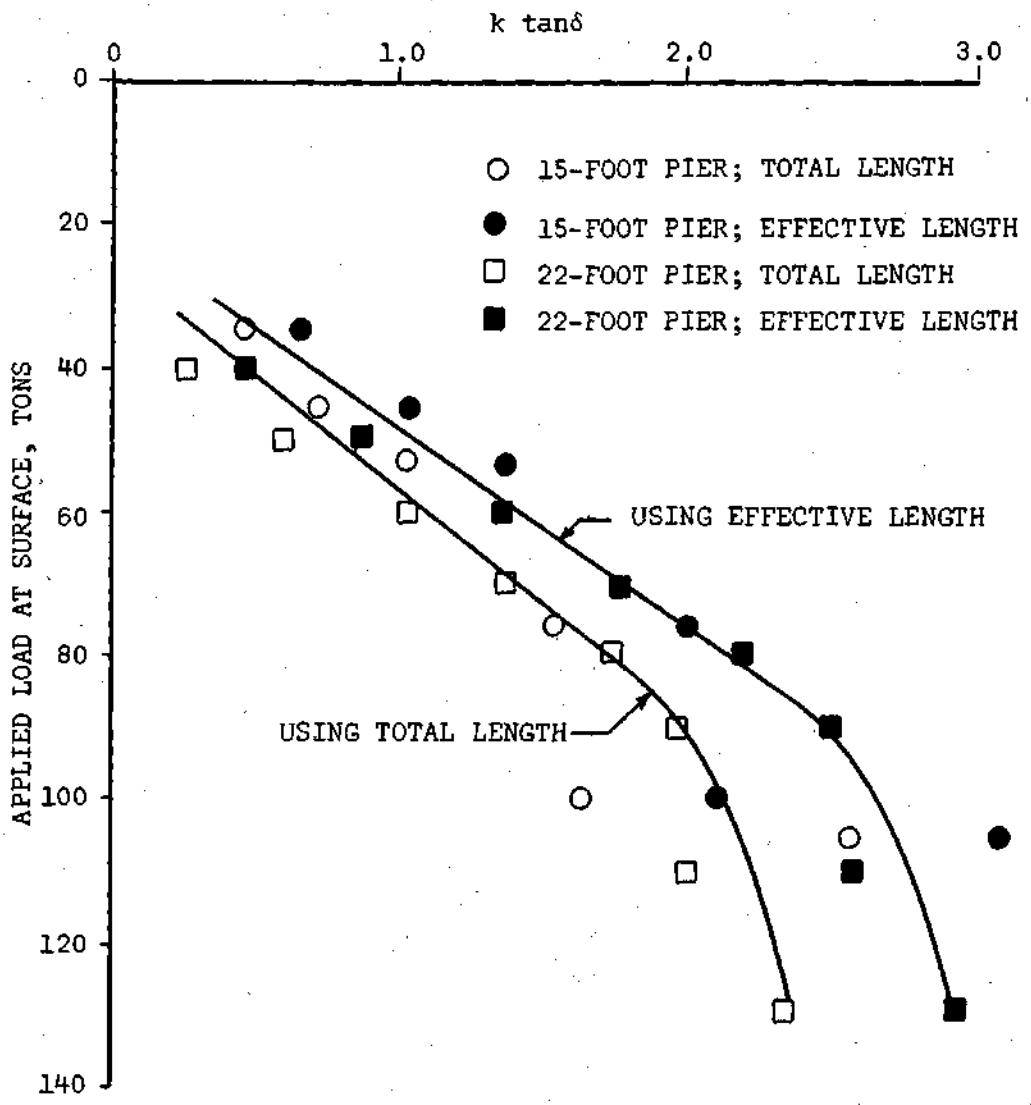

NOTES:
1. The data presented are the average value for the two piers of each length tested.
2. Data from the 22-foot long piers were normalized to a 15-foot long pier by multiplying the measured values by

$$\left(\frac{22}{15}\right)^{2}\frac{(1-P_B/P_T)15}{(1-P_B/P_T)22}.$$

3. Data obtained from using Equation (26) with C_a = 500psf as determined from the lab tests.
4. Base value of length is 15 feet.

Figure 62. Normalized Field Test Data for k tanδ as a Function of Applied Load

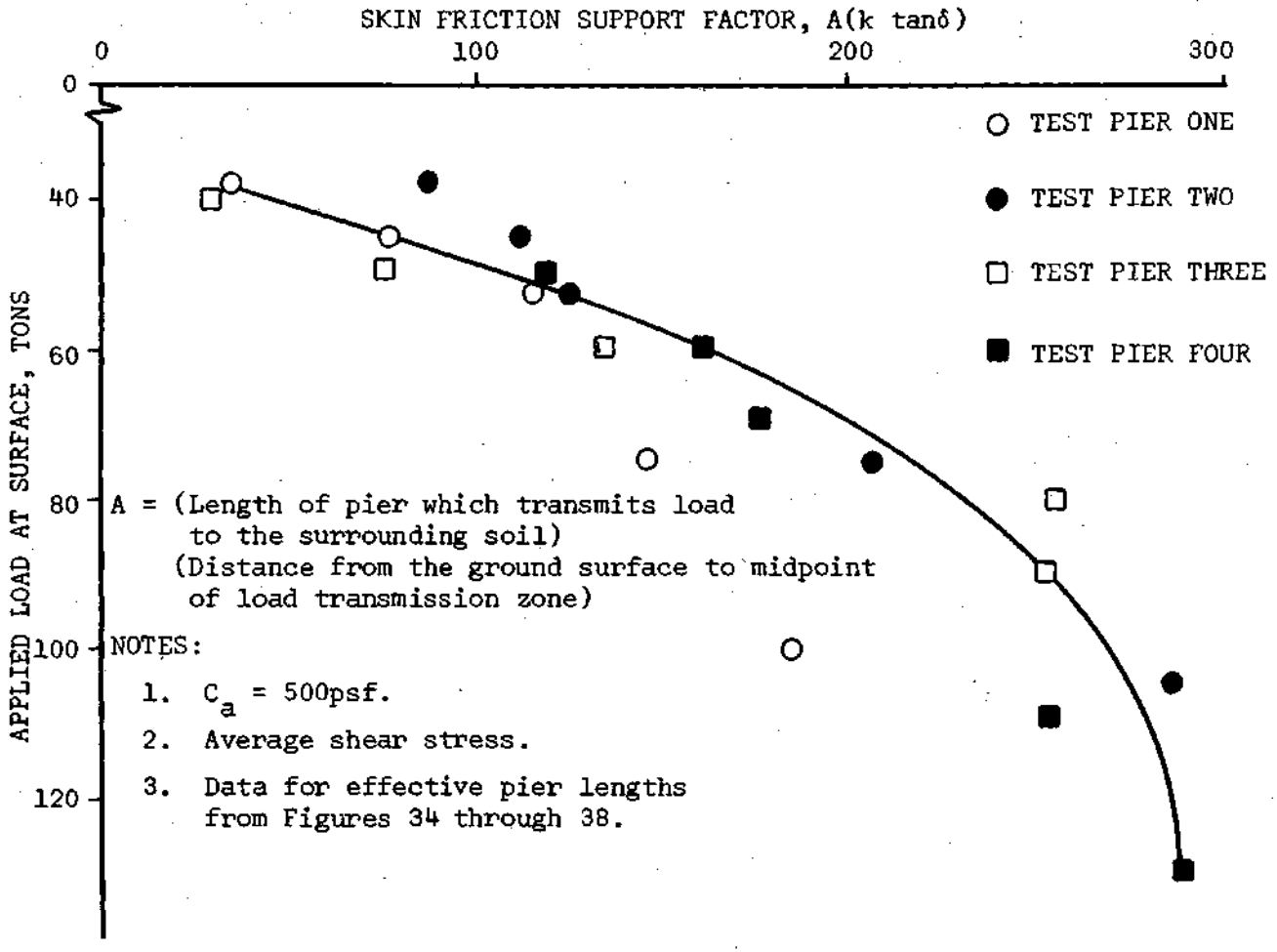

Figure 63. Variation of k tanδ as a Function of the Effective Working Length of Test Piers One through Four

Since the data presented in Figure 63 is approximately a quadratic function, the values of k tanδ are small for long piers. This tends to support the theory proposed by Vesic (43) that the value of the shear stress becomes a constant after a certain depth with deep piers. Vesic explained this on the basis of arching in sands. It is not possible to hypothesize any other cause for this from the results of this study.

Little research has been done in determining the average values or the limiting values of shear stress for deep foundations. The foremost researcher in this field has been Vesic. From buried and driven piles in sand he determined the value of the horizontal earth pressure coefficient at the limiting (failure) stress condition. This permitted him to use the soil strength defined by the Mohr-Coulomb criteria. The values he determined from buried four-inch diameter steel piles in sand of various lengths are shown in Table 7.

Table 7. Values of Horizontal Earth Pressure Coefficient for Buried Piles in Sand (After Vesic, 43)

Soil Consistency	k
Loose Sand	1.6
Medium Dense Sand	2.2
Dense Sand	3.3
$\delta = 32^\circ$	$\tan\delta = 0.625$

NOTE: k determined from initial portion of load distribution curve.

The limiting values of the coefficient of earth pressure determined from tests on drilled piers in weathered rock are presented in Table 8.

Table 8. Values of the Coefficient of Horizontal Earth Pressure Obtained from the Limiting Average Shear Stress for 18-Inch Diameter Piers in Weathered Rock

Pier No.	Skin Friction Load, Kips	Length (Feet)	Average Total Shear Stress(1)	$-C = L/2\ k \tan\delta$	$\frac{\gamma L}{2}$	$k \tan\delta$	k
1	137.6	15	1.95	1.45	.885	1.64	2.18
2	176.0	15	2.48	1.98	.885	2.24	2.98
3	168.2	22	1.62	1.12	1.3	.86	1.14
4	197.2	22	1.90	1.40	1.3	1.02	1.43

NOTE: 1. All diameters are 18".
2. The average value of $\phi = 37°$ ($\tan\phi = \tan\delta = 0.754$).
3. C = 0.5 ksf from lab test.

A comparison of Tables 7 and 8 show dissimilar values for the limiting value of the horizontal earth pressure coefficient. The values obtained from the field tests on drilled piers in weathered rock cover almost the entire range of values given by Vesic for sands. Much of the differences between the investigation performed by Vesic and this thesis are:

1. The values reported by Vesic were determined from controlled laboratory tests on a homogeneous sand. The values obtained from this

study are from piers constructed in a very heterogeneous granular cohesive soil derived from the inplace weathering of rock.

2. Model studies on four-inch diameter steel piles were used by Vesic. The presented field results are on prototype (18-inch diameter) concrete piers.

3. In Vesic's study the piles were buried during placement of the homogeneous sand deposit. The piers for this study were drilled into the soil.

4. The values of the horizontal earth pressure coefficient determined by Vesic were computed from the initial portion of the skin friction vs. depth curve. The results presented in Table 8 are average values for the entire length of embedment. If only the initial portion of the curve is used, the effect of length is neglected. The results of this investigation show that the length must be considered.

Recent field testing by Vesic (76) of 18-inch diameter piles driven into medium dense to dense sand near Savannah, Georgia, illustrate that the average value of k tanδ varies with the length of the pile in an approximately quadratic manner. These results are presented in Table 9.

The values obtained as part of this study, which are presented in Table 8, are compatible with the values presented in Table 9. Any differences that are present are probably due primarily to the different soils involved and the different construction techniques which were used.

Table 9. Average Values of k tanδ Determined from 18-Inch Diameter Steel Pipe Piles Drive in Medium Sand (After Vesic, 76)

Length (Feet)	k tanδ (Average)
9.9	1.04
20.1	1.15
29.1	0.93
39.3	0.87
49.3	0.72

End bearing also contributes to the support capacity of a drilled pier in weathered rock. Figures 54, 55, and 56 show the relative significance of the end bearing support and indicate that the load reaching the tip depends on the pier length and diameter as well as the properties of the soil. In the elastic range the percentage of load reaching the bottom of the pier is almost independent of applied load. When the applied load exceeds the elastic range the percentage of load reaching the bottom increases as discussed earlier.

The instrumentation used in this thesis permitted the load in the base of the pier to be measured. These measurements are shown in Figures 35 through 38 and indicate that the load reaching the bottom is very small. The maximum measured load reaching the bottom of the pier is shown in Table 10.

Table 10. Measured Load in the Bottom of the Pier for the Final Load Increment

Caisson Number	Estimated Ultimate Load (Tons)	Applied Load at Surface (Tons)	Load on Bottom (Tons)	Stress on Bottom TSF
1	108	100	31.2	17.7
2	110	105	17	8.7
3	120	90	5.9	3.3
4	135	130	31.4	17.8

Table 10 shows values of end bearing stress which are considerably less than those computed using the methods discussed in Chapter III for determining the critical base stress. The computed values of critical base stress for a wide range of angles of internal friction has been computed using the following methods:

1. Berezantzev (40).
2. Berezantzev, et al. (67).
3. Terzaghi (26).
4. Meyerhof (35).

The values of critical base stress determined by these methods, neglecting the cohesion component, is shown in Figure 64 for various values of the angle of internal friction. These values may be adjusted to include the cohesion component of strength by multiplying the measured cohesion (500 pounds per square foot) by the bearing capacity factor Nc (assumed equal to 9) and adding the product to the values shown in Figure 64.

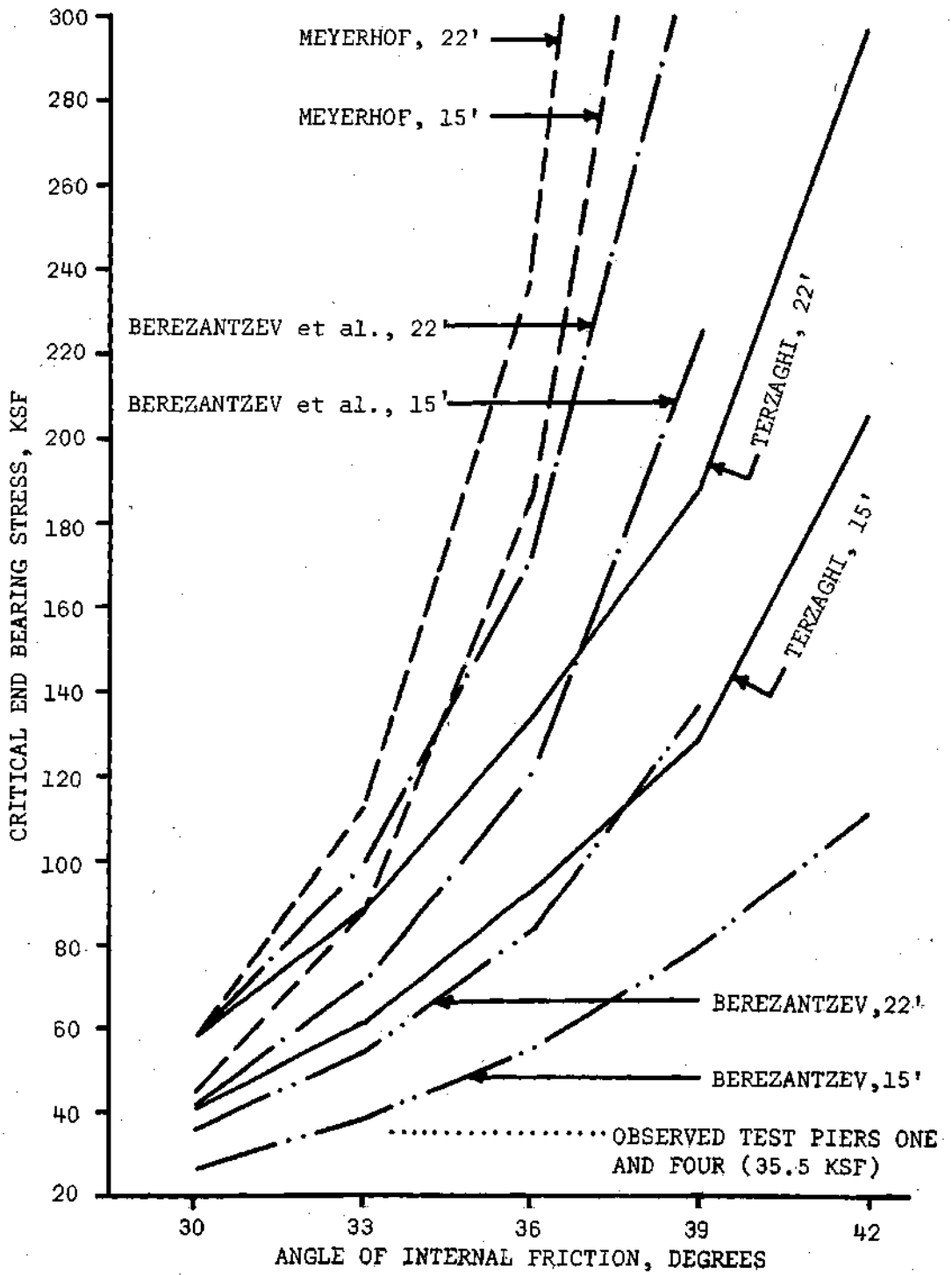

Figure 64. Computed Critical End Bearing Stress Computed from Theoretical Methods and Compared to Observed Test Values

This figure shows that the maximum values of base stress determined from this study where the soil had an average angle of internal friction of 37 degrees are considerably less than those which may be predicted using available theoretical solutions and their associated bearing capacity factors. This variation may be due to several reasons:

1. The material at the bottom of the piers was not as strong as that tested in the laboratory.

2. The load reaching the bottom was greater than that indicated on the instruments.

3. The theoretical methods overestimate the tip capacity.

4. The displacement of the bottom was not great enough to permit the ultimate load to be reached.

The material in the bottom was probably weaker than that tested in the laboratory since all the loose material could not be removed prior to concreting. A comparison based on the angle of internal friction of the loose soil would make the field results agree more closely with the theoretical results since the angle of internal friction of the loose material is less than that tested in the laboratory.

The deformation of the bottom of the pier was computed using the procedure outlined previously. The computed deformation at the bottom is plotted as a function of the measured load in Figure 65. This figure shows an initial increase in load and then a decrease in load with increased deformation for test piers one and four. Then after reaching a minimum value the load in the bottom increased rapidly with

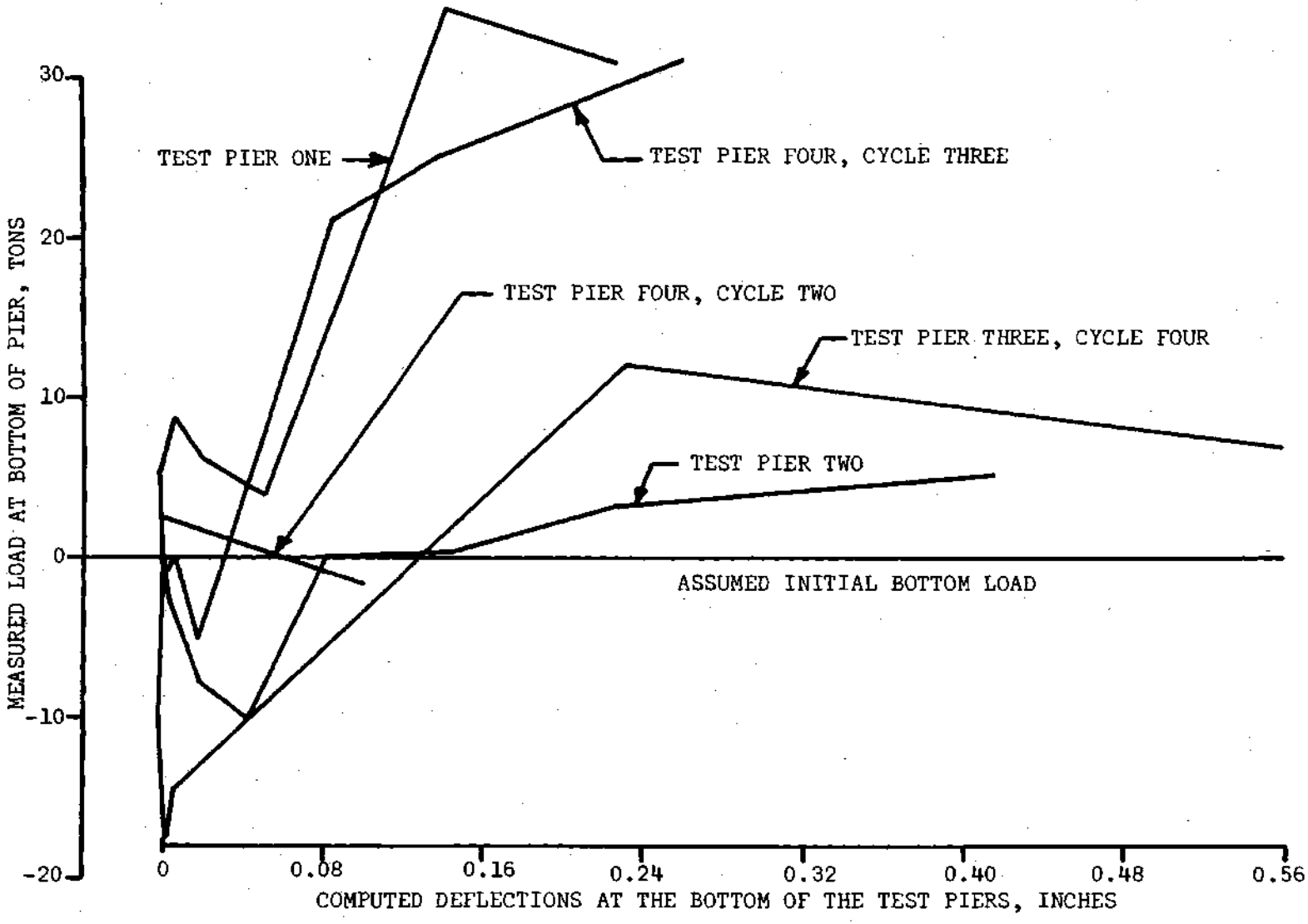

Figure 65. Load-Deformation Curves for the Bottoms of Test Piers

additional bottom deformation. The curve for test pier one then decreased after reaching the maximum value indicating that the base may have failed. The load deflection curve for test pier four shows that the bottom resistance is still increasing at a gradually decreasing rate indicating that the soil is yielding.

The curves for piers two and three show that the load at the bottom is considerably less than for piers one and four. The deflections for the loads in tests two and three are also greater than for tests one and four. These erratic results can be explained on the basis of the bottom bearing conditions. During the drilling operation it was impossible to remove all of the loose soil from the bottom of the piers once the desired depth was obtained. Every effort was made to clean out the bottom by vacuuming, since manual cleaning was impossible for an 18-inch diameter shaft.

The curves in Figure 65 can be interpreted to show the degree of removal of loose material from the base. The comparison indicates that there was a considerable quantity of loose material in the bottoms of test piers two and three. Test piers one and four have less settlement and greater load transfer than test piers two and three. Thus it may be concluded that the bottoms of piers one and four may have had less loose soil in the bottom than piers two and three. The loose soil in the bottom also appears to cause an indication of a greater tensile load. This indicates that a clean bottom will probably produce greater end bearing capacity at less settlement than piers which have not been adequately cleaned.

Recommended Design Procedure

In the preceding sections the results of this investigation have been discussed and compared with results from other studies. This section will describe a method which can be used to design drilled piers. Both load-carrying capacity and settlement are considered. While the method presented is primarily for drilled piers in weathered rock, the general concepts can be used for piers in other materials.

The two mechanisms of support for drilled piers and other deep foundations are skin friction and end bearing. A method of evaluating the load which may be carried by each of these mechanisms will be discussed below.

End Bearing

The test results indicate that the actual load carried by end bearing at failure is considerably less than that which may be predicted by available theories. One reason for this may be that the bottom of the small diameter piers could not be cleaned out properly.

From the results of tests performed on 18-inch diameter drilled piers in weathered rock, it is not possible to establish a design procedure for end bearing capacity. For small diameter piers (which cannot be cleaned out properly and cannot be inspected by lowering a man into the drilled hole) it is recommended that the end bearing capacity be neglected in computing the ultimate load. Any end bearing capacity which is achieved will reduce the settlements and also add to the computed capacity resulting in a conservative design. In larger diameter piers, which may be properly cleaned and inspected, it is recommended

that the base capacity be included in computing the design capacity. The exact value of base capacity is difficult to predict. Other researchers (43, 63, 69) have found that Berezantzev's (67) method of predicting the critical base stress fits the results of experimental test data better than any other available method. The best available method to use could not be determined from this study due to the complications discussed above. For this reason it is recommended that Berezantzev's method be employed to compute the ultimate critical base stress for drilled piers in weathered rock when conditions are favorable for its inclusion. In order to use any of the end bearing formulas the strength parameters of the soil must be known. For end bearing it is recommended that the lowest quartile of available strength results for the material beneath the pier tip be used, and the effective overburden pressure should be adjusted to consider arching of the soil (67).

Even though test data indicates that the theoretical end bearing capacity was not attained, the field test results and finite element computer solution indicate that the rigidity of the bottom affects the immediate settlement characteristics. This is indicated by comparing the settlements of the piers deriving their load-carrying ability from skin friction alone to the piers which derive their load-carrying ability from a combination of skin friction and end bearing. Piers supported by skin friction alone settle more than those supported by a combination of skin friction and end bearing and have less load-carrying ability. The test results indicate that the benefit of bottom support is far more important for settlement considerations than for

ultimate capacity considerations. The results show that a small amount of bottom support helps a great deal for settlement considerations but does not greatly affect the load-carrying capacity. This shows that both end bearing and skin friction act together from a settlement viewpoint but act independently from a load-carrying capacity viewpoint.

The previous discussion shows that the immediate settlement of a pier depends on the rigidity of the soil below the base, the rigidity of the surrounding soil, and the effect of heterogeneous soil conditions. In general, for a homogeneous soil, the softer the soil the more the settlement. The inclusion of a hard zone along the side of the pier will distribute the load into the surrounding soil and reduce the settlement. The settlement which a pier will undergo due to an applied load is difficult to predict. At present the most feasible way to predict settlement is from previous load test data as presented in Appendix B, or by testing a small scale pier and extrapolating these results using elastic theory as long as the load remains in the elastic range.

Design Procedure for Skin Friction

The test results indicate that a large majority of the load-carrying capacity of a drilled pier in weathered soil is developed in skin friction. The skin friction capacity has been shown to be affected by the soil weight, soil modulus of elasticity, and geometry of the pier. In addition, the skin friction capacity is affected by the moisture content of the soil and ground water level which can be

taken into account in the shear strength and the effective overburden pressure. The curves presented in the beginning of this chapter can be used to determine the ultimate skin friction capacity of a drilled pier in weathered rock. Figure 63, obtained from field tests in weathered rock, can be used for determining a value of k tanδ for use in computing the average ultimate value of skin friction according to:

$$(\tilde{\tau}_a)_{ult} = C_a + \frac{\gamma L}{2} k \tan\delta \tag{28}$$

Equation (28) can also be used to determine k tanδ for loads which are in the elastic range of the load-settlement curve. In the elastic range Equation (28) becomes

$$\bar{\tau}_a = C_a + \frac{\gamma \cdot L}{2} k \tan\delta \tag{29}$$

where k is now the elastic coefficient of horizontal earth pressure. Using Equation (29), equations will be developed for cohesionless soils and cohesive soils. For cohesionless soils the following equations can be derived.

$$\tau_a = \frac{\gamma \cdot L}{2} k \tan\delta = \frac{P_T - P_B}{2\pi r L} \tag{30}$$

Then

$$\frac{P_T - P_B}{\pi r L} = \gamma \cdot L \cdot k \tan\delta \tag{31}$$

$$\frac{(1 - P_B/P_B)P_T}{\gamma \pi r L^2} = k \tan\delta \tag{32}$$

Several curves for different diameter and different length piers indicating values of the average shear stress computed from the elastic finite element solution are presented in Figures 88 through 93 in Appendix C for a banded elastic soil. These curves are colinear with the curves obtained by using Equation (32) and can be used to predict the average shear stress in the soil while the pier soil system is still in the elastic range.

These curves have been used to develop a relationship between piers having different geometric properties. This can be accomplished by equating Equation (32) for one size pier to another size pier. This results in an algebraic identity as follows:

$$\frac{\left[(1 - P_B/P_T)P_T\right]_m}{\left[(1 - P_B/P_T)\right]_n} \left\{\frac{r_n L_n^2 \gamma_n}{r_m L_m^2 \gamma_m}\right\} = \frac{(k \tan\delta)_m}{(k \tan\delta)_n} \qquad (33)$$

In Equation (33) the soil properties and the method of placement are considered by the ratio of the base load to the applied load (P_B/P_T). This ratio is also dependent on the length and diameter of the pier as shown in Figure 54.

Equations (30) through (33) can be adjusted to consider the cohesive strength of the soil. This is done by reducing the load taken by skin friction (P_T-P_B) by an amount equal to the cohesive strength multiplied by the effected surface area of the pier. When this is done the resulting equation becomes

$$\frac{\gamma_m L_m \left[\left(\frac{P_r - P_B}{rL}\right)_n - 2\pi c_n\right]}{\gamma_n L_n \left[\left(\frac{P_T - P_B}{rL}\right)_m - 2\pi c_m\right]} = \frac{(k \tan\delta)_n}{(k \tan\delta)_m} \qquad (34)$$

Equation (34) can be used for soils having cohesive strength and an angle of internal friction. For purely cohesive soils the k tanδ term is not applicable and the skin friction capacity should be computed on the basis of adhesion between the shaft and the cohesive soil. This method of analysis is described extensively in the review of literature presented previously.

Equations (33) and (34) can be used to develop data for each site and construction technique similar to that presented in Figure 63. Curves like this may be developed from a test pier at a particular site by knowing the applied load, load at the bottom, ground water level, the density of the soil, and the load distribution in the pier shaft. Since instrumentation for the load distribution in the shaft is very expensive, it is recommended that the total length concept, as presented in Figure 62, be utilized.

The curve in Figure 62, which is computed on the basis of a 15-foot long pier can be reconstructed for any length pier by utilizing Equation (33) or Equation (34). The resulting curve will show the value of k tanδ for a particular applied load on a pier having support conditions similar to those tested as part of this investigation.

This procedure should not be used for piers having a ratio of length to diameter less than ten. This is because of the inability of the upper few feet of a deep foundation shaft to develop load transfer conditions which are as effective as they are at greater depths. This condition is illustrated in Figures 34 through 37 and in Table 5 for the site and construction conditions utilized in this investigation.

The method of determining the skin friction capacity of a straight foundation shaft in soil will be illustrated in an example problem at the end of this chapter.

Design Procedure for Settlement

In many instances the settlement of piers is a more critical consideration than its load-carrying capacity. The selection of a deep foundation is generally made when excessive settlement cannot be tolerated and/or high foundation loads are anticipated. Thus, the design of a deep foundation must include both settlement and load-carrying ability. The tests performed on drilled piers in weathered rock made it possible to establish a method for predicting the settlement which a pier will undergo. The procedure presented below considers the short term settlement of drilled piers in partially saturated weathered rock.

Consolidation tests performed on the weathered rock show that the soil does not have significant long term settlement characteristics. Thus the method presented below is justified for partially saturated weathered rock if it is assumed that the load will not shift from skin friction to end bearing with time. This load shift did not occur

during the time increments (up to one day) tested (Table 1) for loads in the range of the design loads.

Before the settlement can be computed the given loading conditions must be known. Once the design load is known it should be multiplied by a factor of safety to determine a desired ultimate load. Knowing the ultimate load required and the design load, the dimensions of the pier can be determined from the procedure discussed previously. Once the desired ultimate load is known it must be decided if this load is to be transmitted to the soil entirely by skin friction or by a combination of skin friction and end bearing. Knowing the load support mechanism and the desired ultimate load, the settlement under a given loading condition can be determined from Figure 66.

The two curves presented in Figure 66 have been obtained from data discussed earlier in this chapter and presented in Figure 46. The curve for piers deriving their support ability from end bearing and skin friction is the average of the data for test piers one through four. Using the results from test piers five and six, a curve is presented in Figure 66 to represent the deformation of an axially loaded, straight shaft, drilled pier deriving its entire support from skin friction alone.

The settlement of a pier can be estimated from Figure 66 by entering the ordinate with the inverse of the factor of safety under ultimate loading conditions. Then proceed in a direction parallel to the deformation axis until the curve for the desired support mechanism is intersected. From this intersection point the settlement is deter-

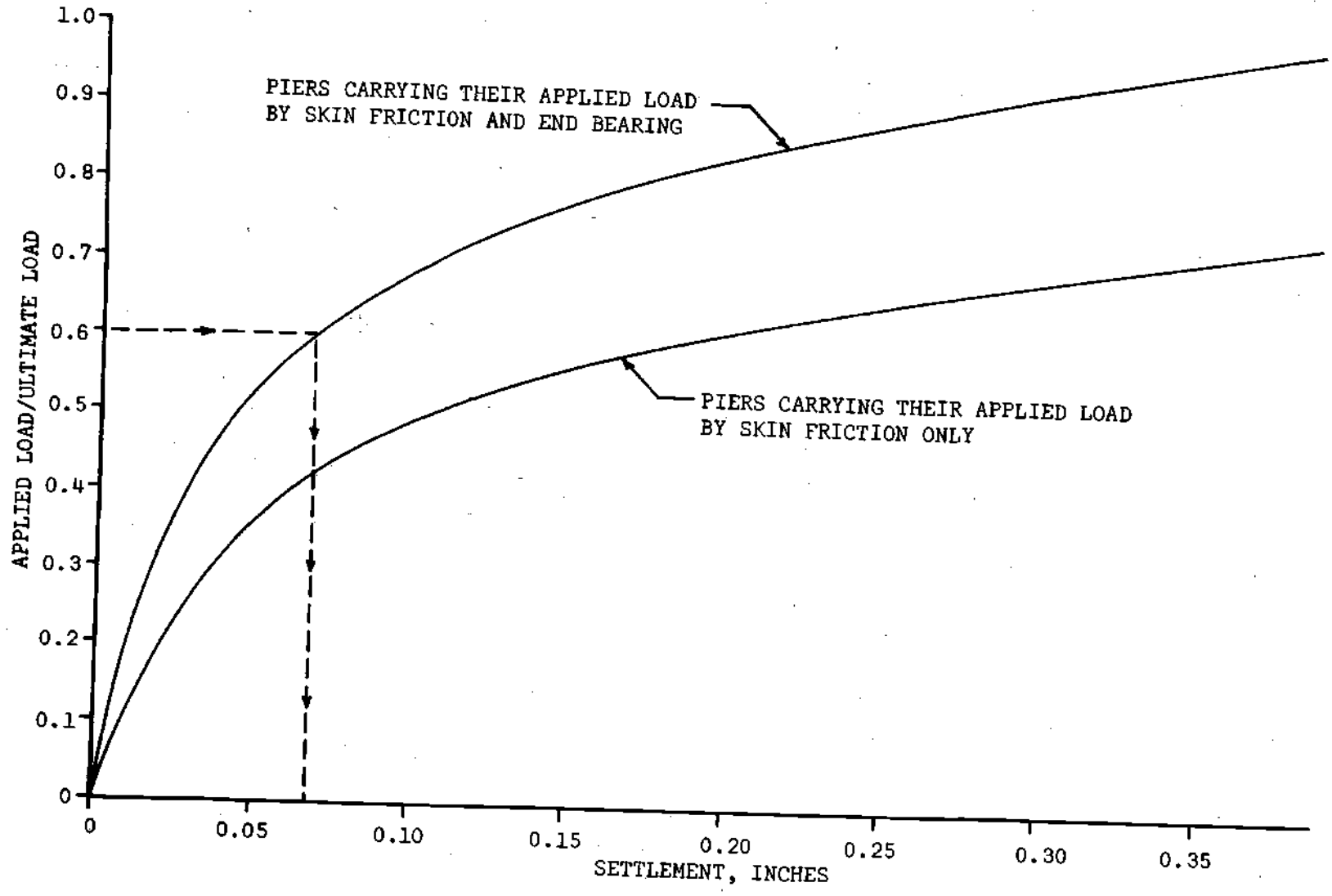

Figure 66. Approximate Procedure for Determining the Settlement of a Drilled Pier in Weathered Rock Under an Imposed Axial Compressive Load

mined by proceeding in a direction parallel to the ordinate until the deformation axis is intersected. The procedure for determining the settlement is illustrated by the dashed lines in Figure 66.

Whitaker and Cooke (29) have shown that for London clay the relationship presented in Figure 66 is independent of length or diameter for a straight shaft pier. These parameters are considered in determining the load-carrying capacity only.

A number of other curves for pier tests performed by others are shown in Appendix B for various soil conditions. These curves all show the same general trend of the deformation as a function of the per cent of ultimate load, but there is a wide variation in the actual numerical values. The variation is probably due entirely to variations in soil and construction techniques as well as testing techniques. A comparison of these curves with the data obtained from this study indicates that it may be prudent to design for settlement considering the entire load to be carried by skin friction.

The results of tests by Vesic (76) and Dubois (36, 37) indicate that the settlement is independent of the pier dimensions and is only a function of the applied load in the initial or elastic portions of the load settlement curves. This is also indicative of the results obtained from test piers one through four as shown in Figure 45. These results show that the settlement of the pier in the elastic portion of the load-settlement curves can be predicted based on the load settlement curve for another pier in the same soil if identical construction techniques are used and if there is a well-defined initial linear portion of the load settlement curve.

Summary of Design Procedures and Example Problem

Since this investigation has shown that skin friction is the primary controlling influence in determining the capacity of a drilled pier in weathered rock, the ultimate capacity should be based on its consideration alone when the bottom conditions cannot be assured. The design procedure can then be broken down into several distinct steps:

1. Determine the soil properties of the site in question.

2. Determine the desired design and/or ultimate load capacity.

3. Using curves similar to Figure 62, determine the value of k tanδ for some normalized length, diameter and percentage of load taken by the base. (Additional values of k tanδ for an elastic banded soil can be obtained by using the average shear stress values in Appendix C in conjunction with Equation (32).)

4. Select a trial length and diameter.

5. Determine the amount of load to be carried by skin friction using data presented in Figure 56.

6. If the soil at the site has some cohesive strength, use Equation (34) to determine the k tanδ for the particular length, diameter and percentage of load taken by the base. Previous investigators have shown that if you are designing for ultimate conditions, only about 45 per cent of the laboratory cohesive strength is effective at ultimate load. Thus the C_a indicated in Equation (34) should be equal to 45 per cent of the laboratory cohesive strength. If the soil at the site is cohesionless, use Equation (33) to determine the value of k tanδ for the particular length, and diameter selected.

7. Compare the value of k tanδ obtained in step six with available data on the limiting values of k tanδ similar to those presented in Tables 7, 8 and 9. If the value of k tanδ obtained in step six is greater than the limiting values for the particular construction technique, new trial dimensions will have to be selected and steps four through seven repeated.

The above procedure should be tested in the field to determine the true values of P_B/P_T and k tanδ for some test pier under actual construction conditions if data are not available for the desired conditions. If a field testing program is not conducted a factor of safety of at least 2.5 should be utilized when end bearing is neglected. If reliable field data is available, a factor of safety of two can be utilized if the end bearing is not computed. This factor of safety is based on the total applied load and not on the load taken in skin friction.

After the desired dimensions and loading conditions are known, the settlement of the pier under a certain loading condition can be determined. Figure 66 or the figures in Appendix B can be used to determine the settlement if the site conditions permit. If a load test has been performed at the site under the same conditions of construction the settlement can be computed from the initial linear segment of the load settlement curve. The following example will illustrate the design procedure outlined above.

Illustrative Examples

Example One

On the site where field testing was performed as part of this thesis, it is desired to support a structure on a deep foundation. A structural engineer has indicated that there are 50-ton column loads. Assume that drilled piers have been selected because previous experience in the area has indicated they are the most economical solution to the problem.

1. Soil exploration has shown the ground water table to be at 26 feet below finished grade and the soil has a cohesion of 500 pounds per square foot.

2. Since field test data are available, a factor of safety of two will be utilized. Therefore design the pier for an ultimate load of 100 tons.

3. Figure 62 shows that a value of $k \tan\delta = 2.1$ can be used for a 15-foot long pier 18 inches in diameter having a $P_B/P_T = 0.25$.

4. Try a pier having a length of 20 feet and a diameter of 18 inches.

5. L/D = 20/1,5 = 13.3.

Figure 56 indicates that P_B/P_T for this L/D is approximately 0.25.

6. From Equation (34),

$$\frac{L_m\left[\left(\frac{P_T-P_B}{rL}\right)_n - 2\pi c\right]}{L_n\left[\left(\frac{P_T-P_B}{rL}\right)_m - 2\pi c\right]} = \frac{(k\ \tan\delta)_n}{(k\ \tan\delta)_m}$$

$$(k\ \tan\delta)_n = 2.1\left\{\frac{15\left[\frac{2000(100-25)}{(1.5)(20)} - 2\pi(0.45\times500)\right]}{20\left[\frac{2000(100-25)}{(1.5)(15)} - 2\pi(0.45\times500)\right]}\right\} = 1.075$$

7. By comparison of the computed value of k tanδ = 1.075 with the data in Table 8, it is seen that this value is safe. Examination of Table 9 shows that a value of k tanδ = 1.075 is also safe for a 20-foot pile in sand but the total capacity will be greater than 100 tons because the driven piles have a greater amount of load taken in end bearing than the 25 per cent indicated by the test piers at the site in question.

8. The settlement is determined to be 0.05 inches from Figure 66 for a $P_T/P_U = 0.5$.

Example Two

Assume that a structure is to be founded on a site where the soil has a combination of properties which is between the soil on the site of this investigation and the soil on the site used for Vesic's (76) investigation. It was determined that the maximum cohesion that can

be developed is 200 psf and the ground water is 45 feet below the ground surface. Using an 18-inch diameter drilled pier determine what the allowable total pier load can be. It is required to determine the settlement of the top of the pier under this load.

1. For ease in construction the pier length should be limited to 40 feet to avoid the ground water and highly saturated soil.

2. The pier will then be 40 feet long, 18 inches in diameter (L/D = 26.7) and will be embedded in a soil having a cohesion of 200 psf.

3. From Vesic's (76) work a value of k tanδ = 0.86 is determined for a 40-foot shaft.

4. From the elastic solution and from field experience we can only expect that 10 per cent of the load will reach the base of the pier (P_B/P_T=0.10).

5. Using the following data from test pier four,

$$P_B/P_T = 0.25$$

$$P_T = 135 \text{ Tons} = 270{,}000 \text{ lbs.}$$

$$k \tan\delta = 1.02$$

$$L = 22 \text{ Feet} \qquad D = 1.5 \text{ Feet}$$

6. Assume that the full 500 psf cohesion was developed at the test site due to the caution that was exercised during construction and the low level of saturation.

7. Utilizing Equation (34):

$$\frac{\gamma_n L_m \left\{ \left[\frac{P_T(1 - P_B/P_T)}{DL} \right]_m - \pi C_m \right\}}{\gamma_m L_m \left\{ \left[\frac{P_T(1 - P_B/P_T)}{DL} \right]_n - \pi C_n \right\}} = \frac{(k \tan\delta)_m}{(k \tan\delta)_n}$$

Assume the soil at each site has the same unit weight

$$\frac{40 \left\{ \frac{270{,}000(1-0.25)}{1.5 \times 22} - \pi(500) \right\}}{22 \left\{ \frac{P_T(1-0.10)}{1.5 \times 40} - \pi(200) \right\} =} = \frac{1.02}{0.86}$$

$$P_T = 504{,}000 \text{ lbs} = 252 \text{ Tons}$$

8. Since there have not been any load tests performed at the site, use a factor of safety of 3.0.

9. The allowable load is 252/3.0 - 84 Tons.

10. The settlement at a ratio of applied load to ultimate load of 0.33 is 0.02 inches from Figure 66.

CHAPTER VIII

CONCLUSIONS

The following conclusions apply to the behavior of drilled piers in weathered rock:

1. The total capacity of a small diameter drilled pier can be conservatively estimated on the basis of skin friction considerations only. The ability of a small diameter pier to sustain load in end bearing is limited by the ability to remove the loose soil after drilling.

2. The elastic finite element computer program and the field tests indicate that as the depth-to-diameter ratio increases, the percentage of applied load reaching the base of the pier decreases.

3. The elastic finite element computer program indicates that the load distribution pattern along the sides of a drilled pier depends upon the soil properties and the geometry of the pier itself. Both of these aspects have been shown by others to be functions of construction techniques and duration of load. Therefore the load distribution pattern as well as the ability of a pier to support a load depends not only on the virgin stiffness and strength of the soil system but also upon the construction technique employed.

4. Excavation of a pier after load testing has shown that for a depth of about one diameter beneath the surface only 20 per cent of the concrete surface is in contact with the soil. This increases to

90 per cent at a depth of two diameters. This factor must be considered when determining the capacity of a drilled pier.

5. If, after several loading cycles, the load is removed, the net settlement for the last cycle may be less than at the beginning of the loading cycle because of the time-dependent nature of the load settlement relationship and because of the load level attained during the particular loading cycle.

6. Several relationships were determined or confirmed for the settlement of drilled piers:

a. For the same load, or percentage of ultimate load, piers which derive their support capability from skin friction alone settle more than piers which derive their support from a combination of skin friction and end bearing if the geometric properties are identical. This was determined to be the case even though the amount of load reaching the bottom of a bottom-supported pier was less than about 20 per cent of the applied load.

b. The amount of settlement necessary to mobilize the maximum amount of skin friction is practically constant for piers of different lengths. This, to a certain extent, confirms other's conclusions that skin friction is a function of absolute displacement and not a function of length or diameter.

c. The elastic finite element computer solution did not accurately predict the settlement of a drilled pier using values of the modulus of elasticity determined from laboratory tests on

undisturbed samples. The settlements predicted by the computer solution were eight to ten times greater than those experienced in the field. This was probably caused by the effect of sample disturbance and test conditions as well as the previously-mentioned conclusion that settlement cannot be expressed as a percentage of some pier dimension.

d. The results of this study have shown that piers embedded in a common material with similar load support mechanisms exhibit a similar relationship between percentage of ultimate load and absolute displacement. Thus if the ultimate load were known, the settlement of a pier could be predicted from load test data from another pier in similar soil.

7. The horizontal earth pressure coefficient was investigated utilizing the field test data and the elastic finite element computer solution. The following conclusions apply to this study:

a. For residual soils similar to those in the Atlanta area the use of an average value of skin friction and thus horizontal earth pressure coefficient is more significant than utilizing individual values which may vary for each layer of material in the saprolitic injection complex.

b. The average working and limiting values of the horizontal earth pressure coefficient decrease with an increase in pier depth in approximately a direct proportion to the square of the pier length and are also dependent to a lesser degree on the pier diameter and modulus of elasticity of the soil. Thus if

the average horizontal earth pressure is known for one pier length, it can be estimated for any other pier length if the entire lengths of the piers are in similar soils.

c. The value of the horizontal earth pressure coefficient varies along the length of the pier because of the different displacements throughout its length and because of the variations of effective contact area in addition to the variance of materials. The displacements vary because of the amount of load removed by skin friction and the effective area of contact is dependent primarily on depth below ground surface and construction technique.

8. The computer study indicated that as the modulus of elasticity of the material in the bottom of the pier increases, there is a corresponding increase in the amount of load which can be effectively transmitted to the bottom of the pier. For this reason it may be concluded that for small diameter piers which cannot be adequately cleaned, there will be less load reaching the bottom than for a similar size driven pile which compacts the soil instead of loosening it during placement.

9. Theoretical considerations indicate that the modulus of elasticity of the pier itself has little effect on the behavior of the pier since it is several orders of magnitude greater than the surrounding soil.

10. The field determined load distribution patterns indicate that the support mechanisms of skin friction and end bearing act

practically independently. This was illustrated by the parallel nature of the load distribution diagrams.

APPENDIX A

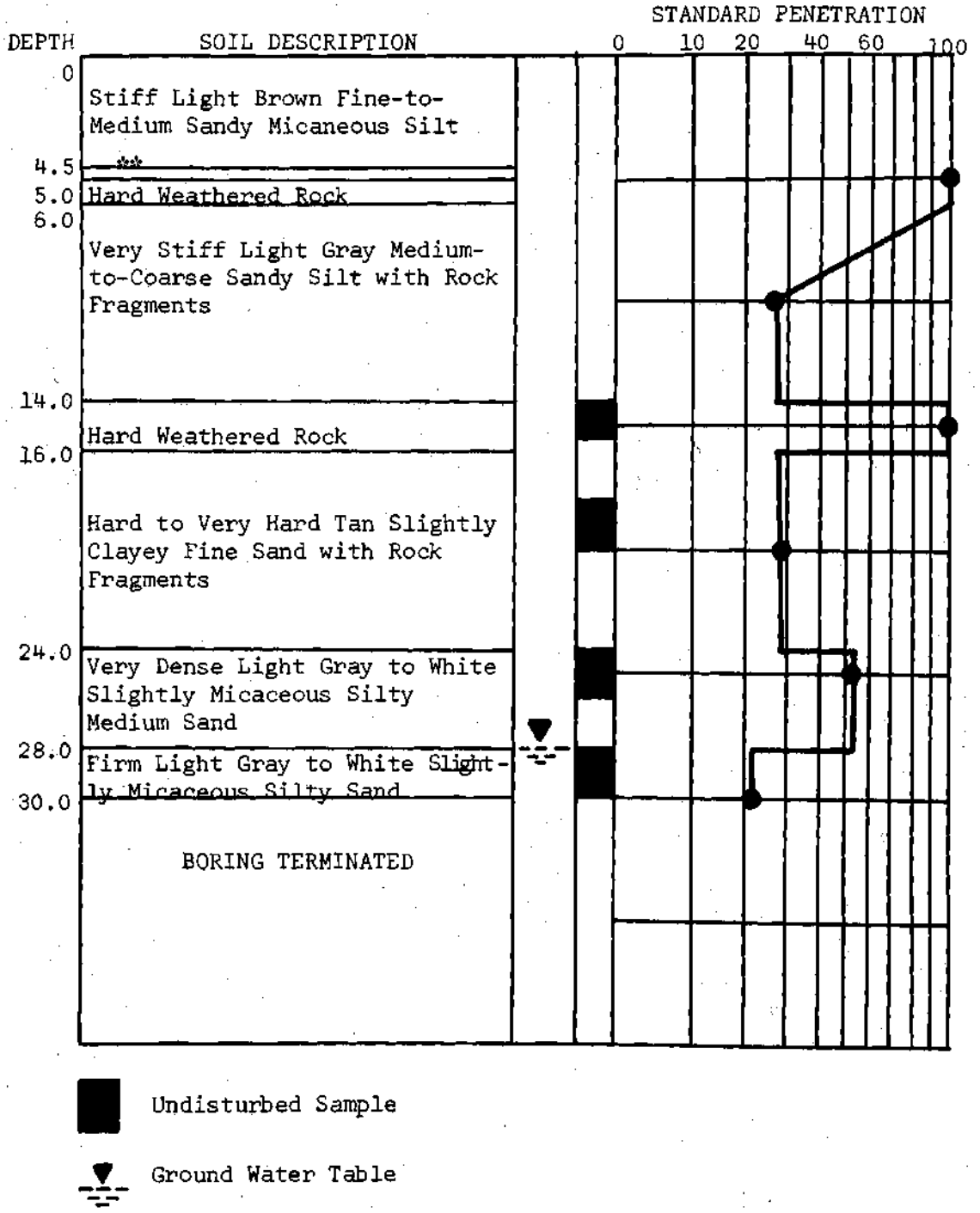

Figure 67. Soil Test Boring A

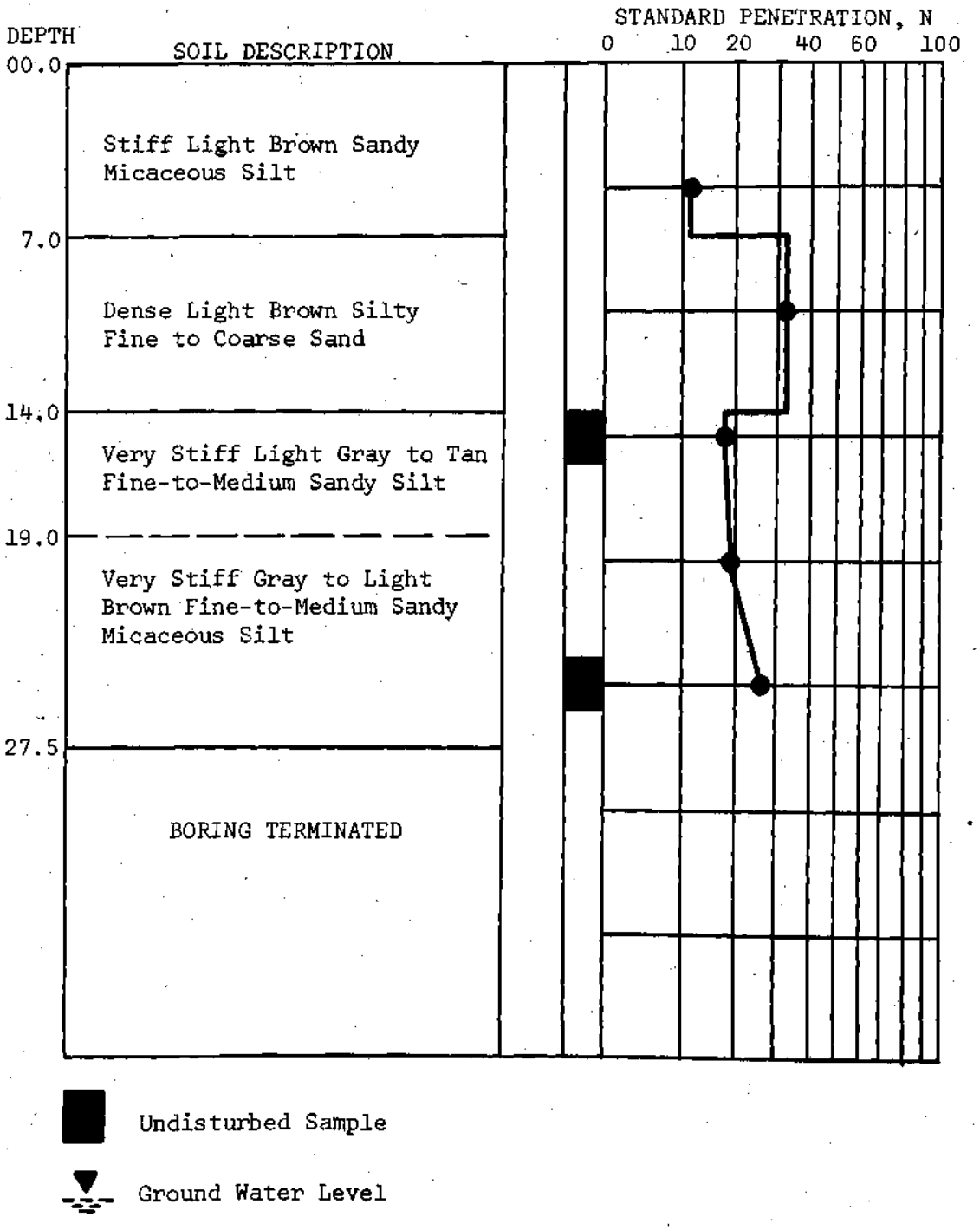

Figure 68. Soil Test Boring B

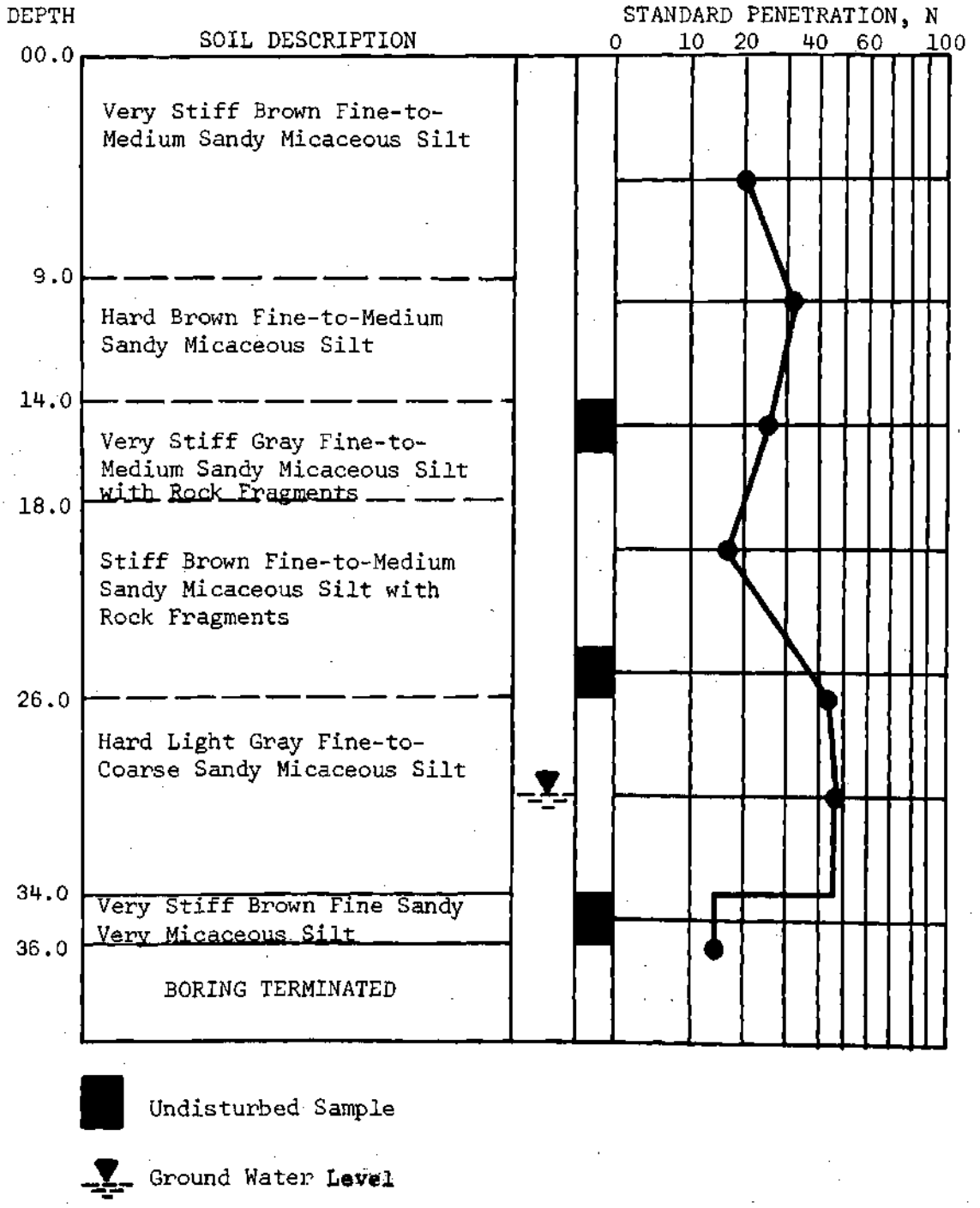

Figure 69. Soil Test Boring C

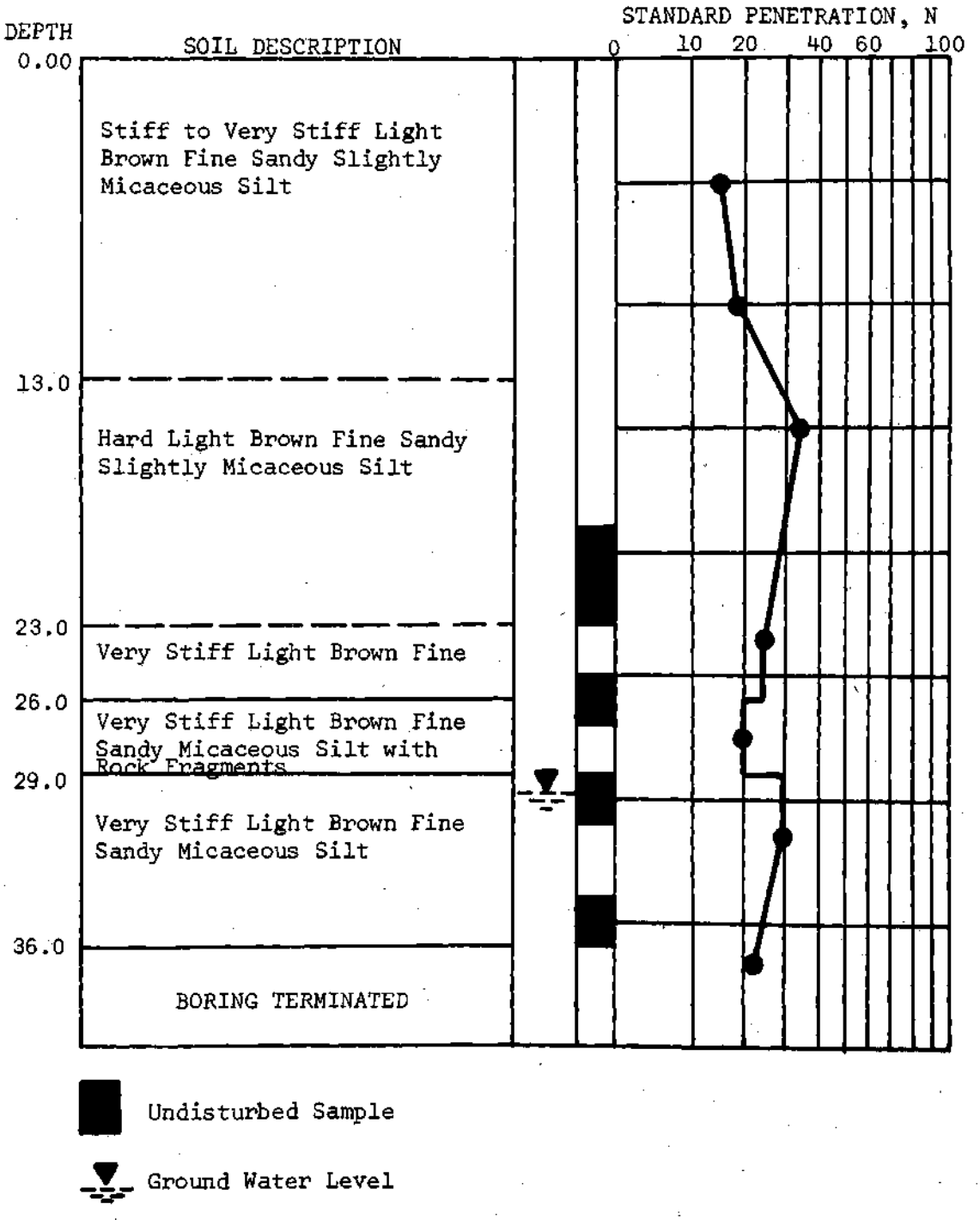

Figure 70. Soil Test Boring D

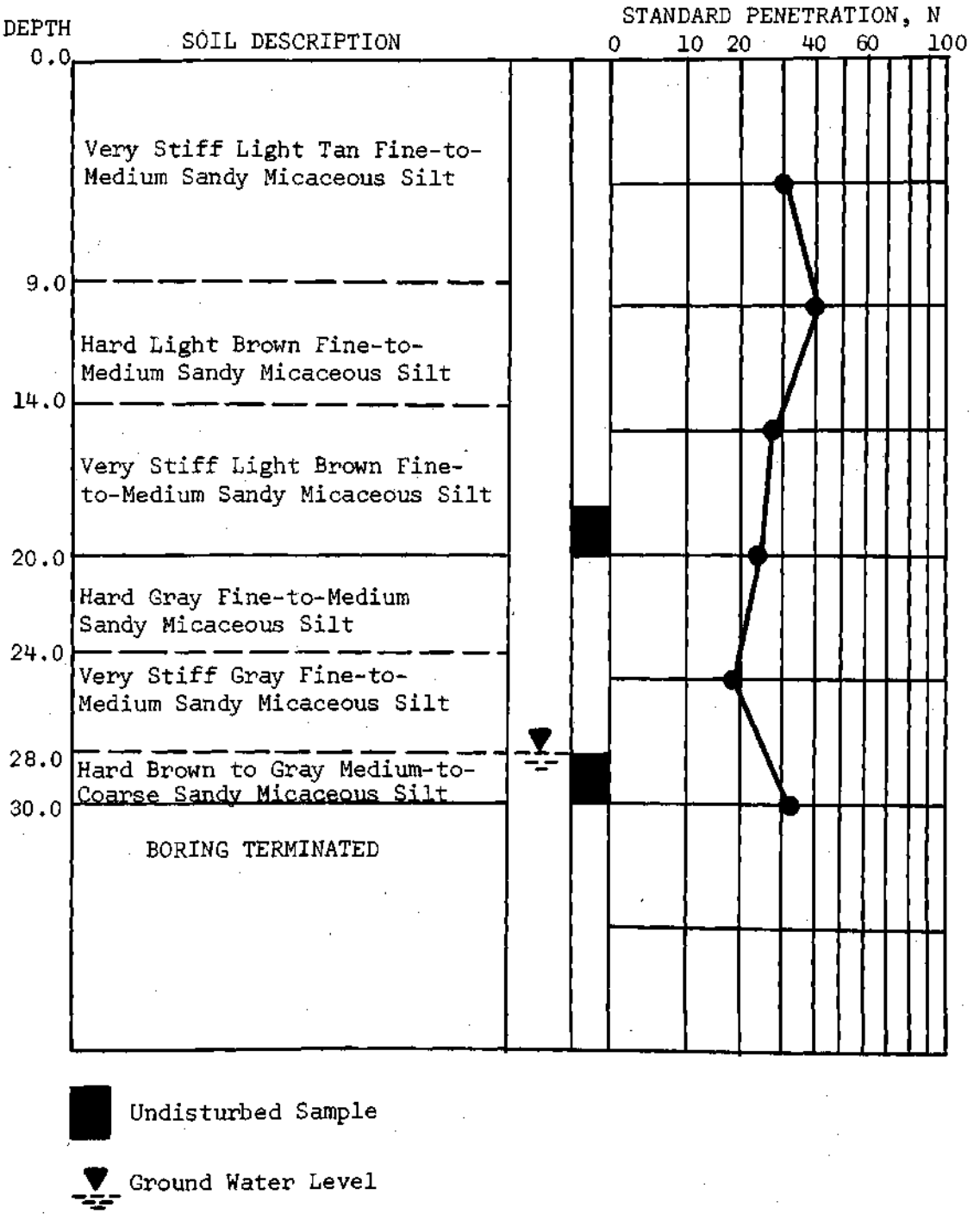

Figure 71. Soil Test Boring E

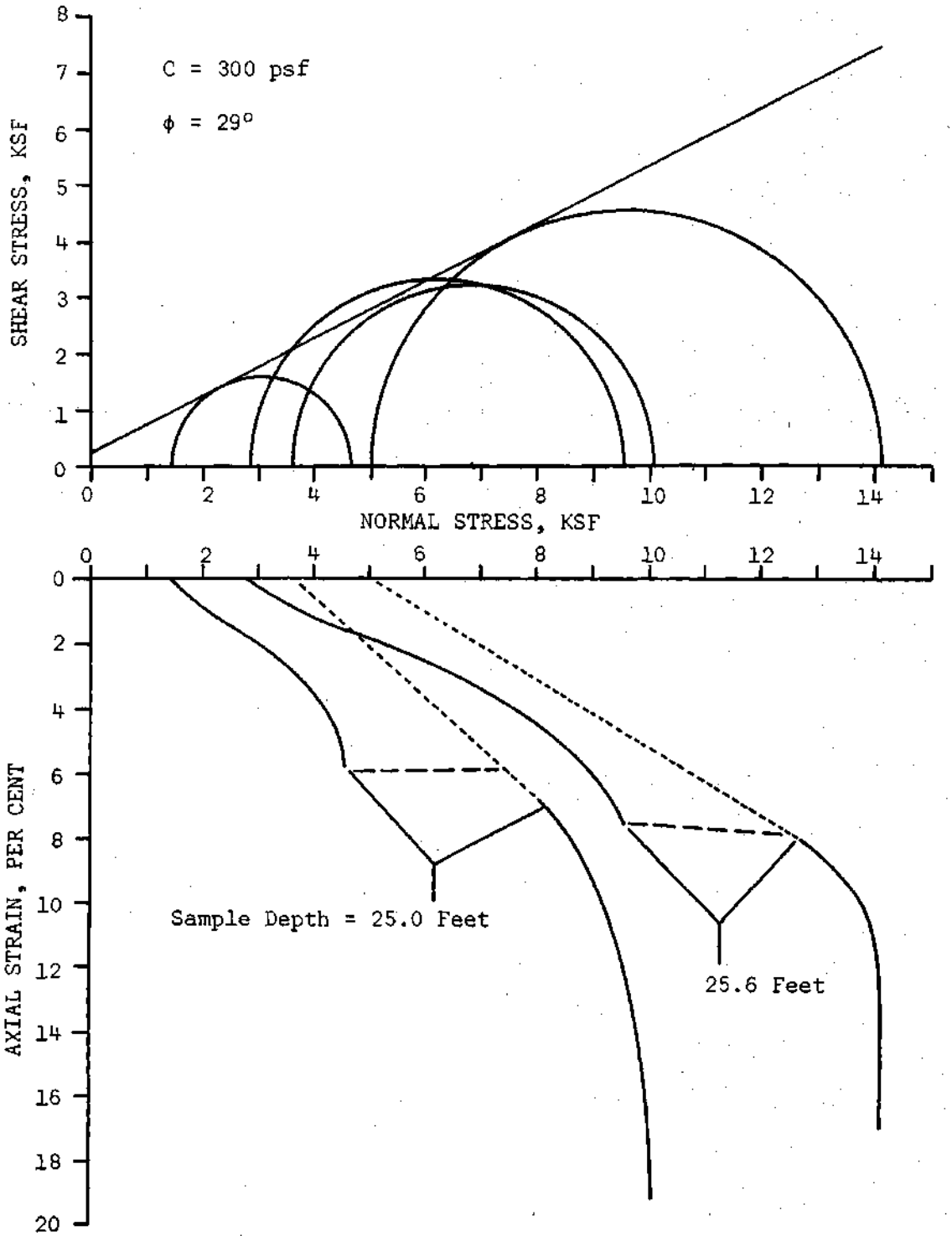

Figure 72. Results of Triaxial Shear Testing on Sample from Boring A at a Depth of 25 Feet

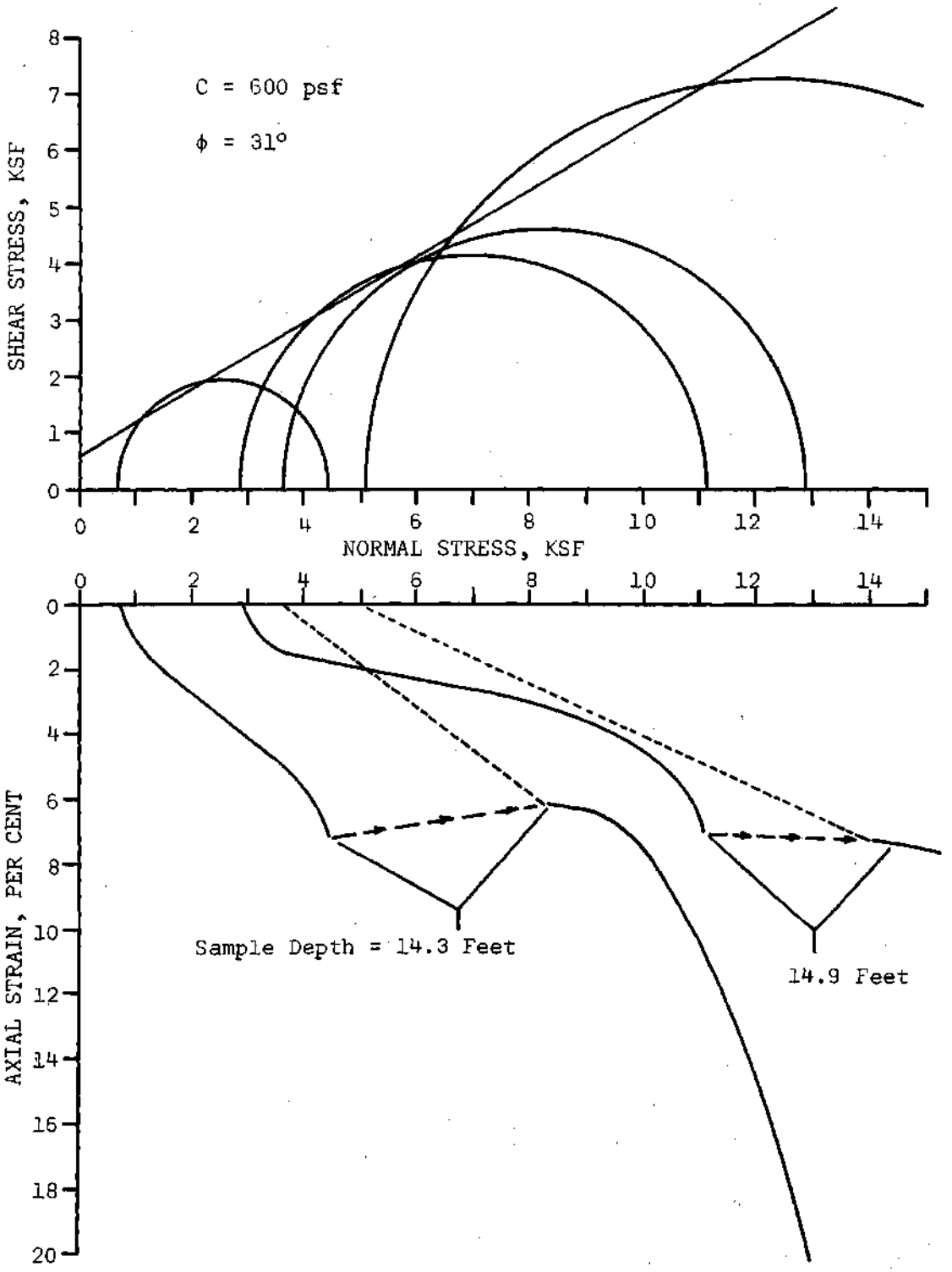

Figure 73. Results of Triaxial Shear Testing on Sample from Boring B at a Depth of 15 Feet

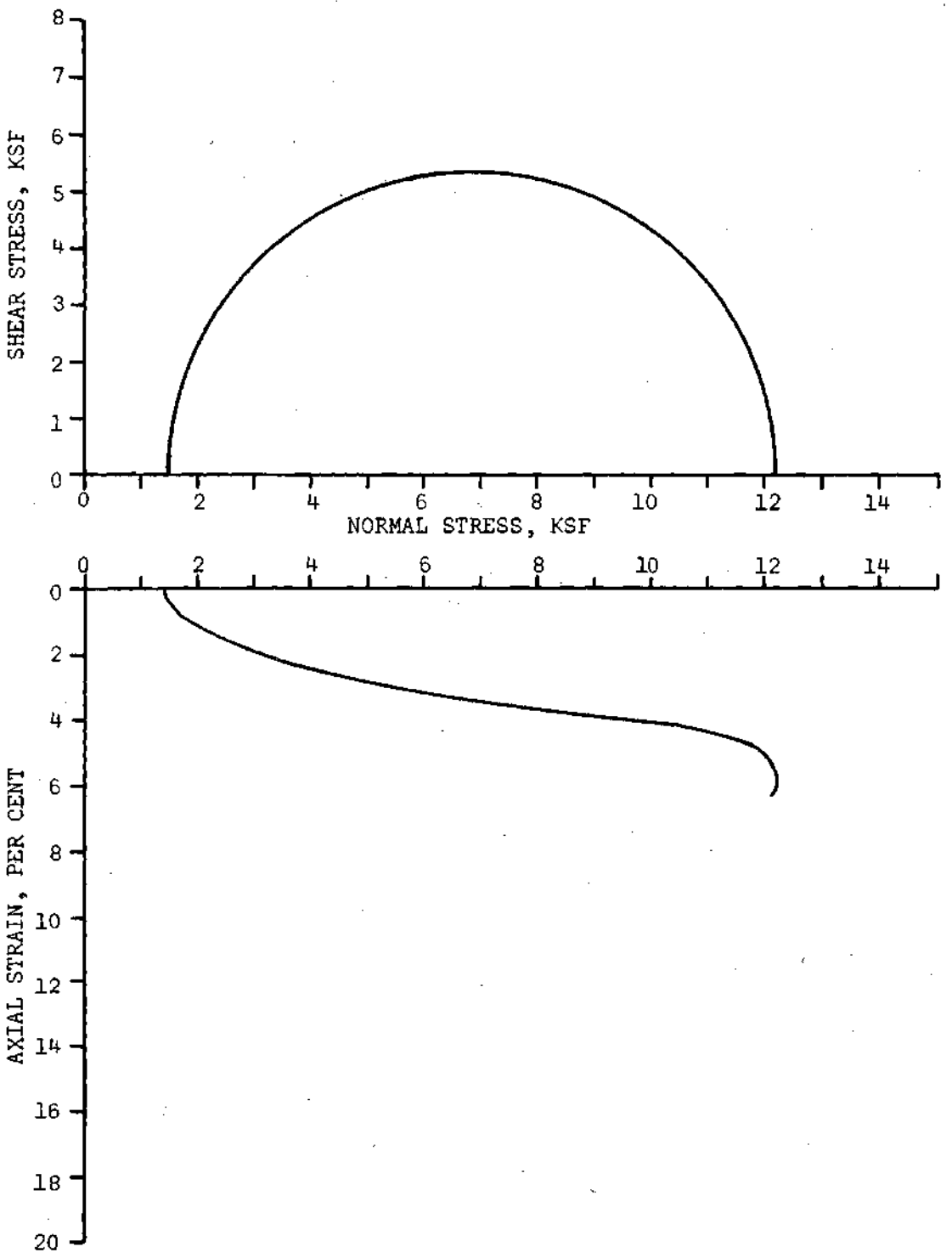

Figure 74. Results of Triaxial Shear Testing on Sample from Boring B at a Depth of 15.6 Feet

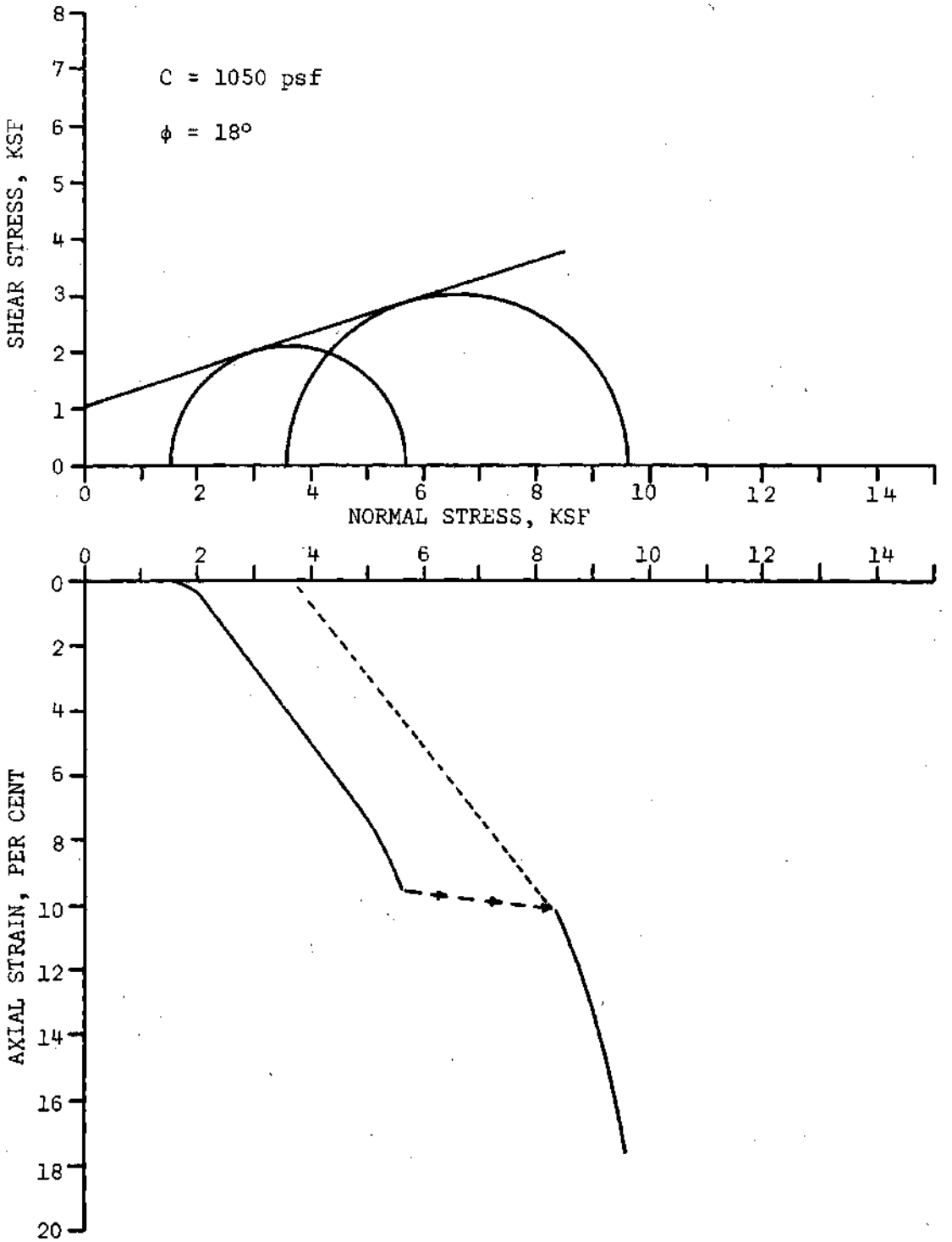

Figure 75. Results of Triaxial Shear Testing on Sample from Boring D at a Depth of 25.5 Feet

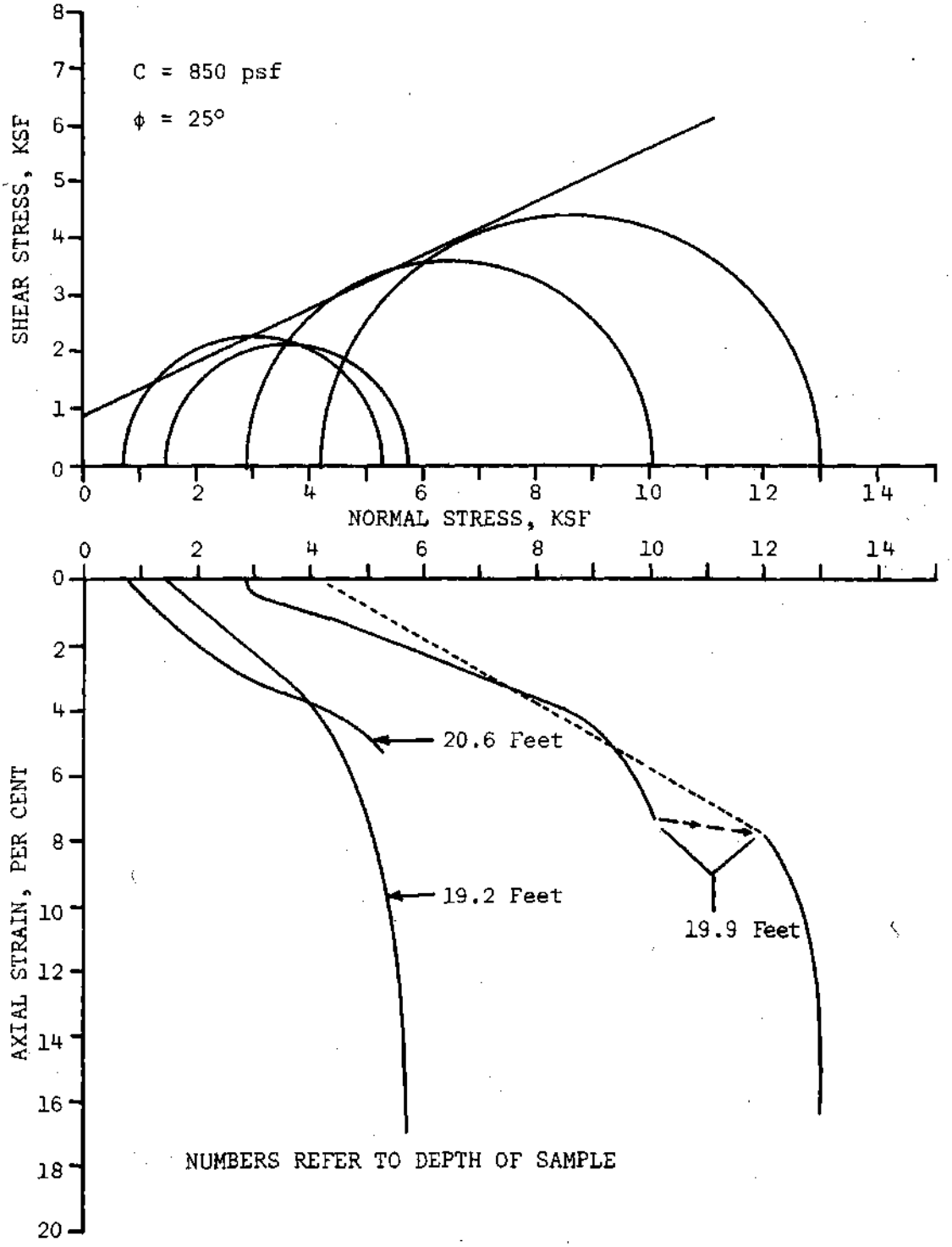

Figure 76. Results of Triaxial Shear Testing on Sample from Boring D at a Depth of 20 Feet

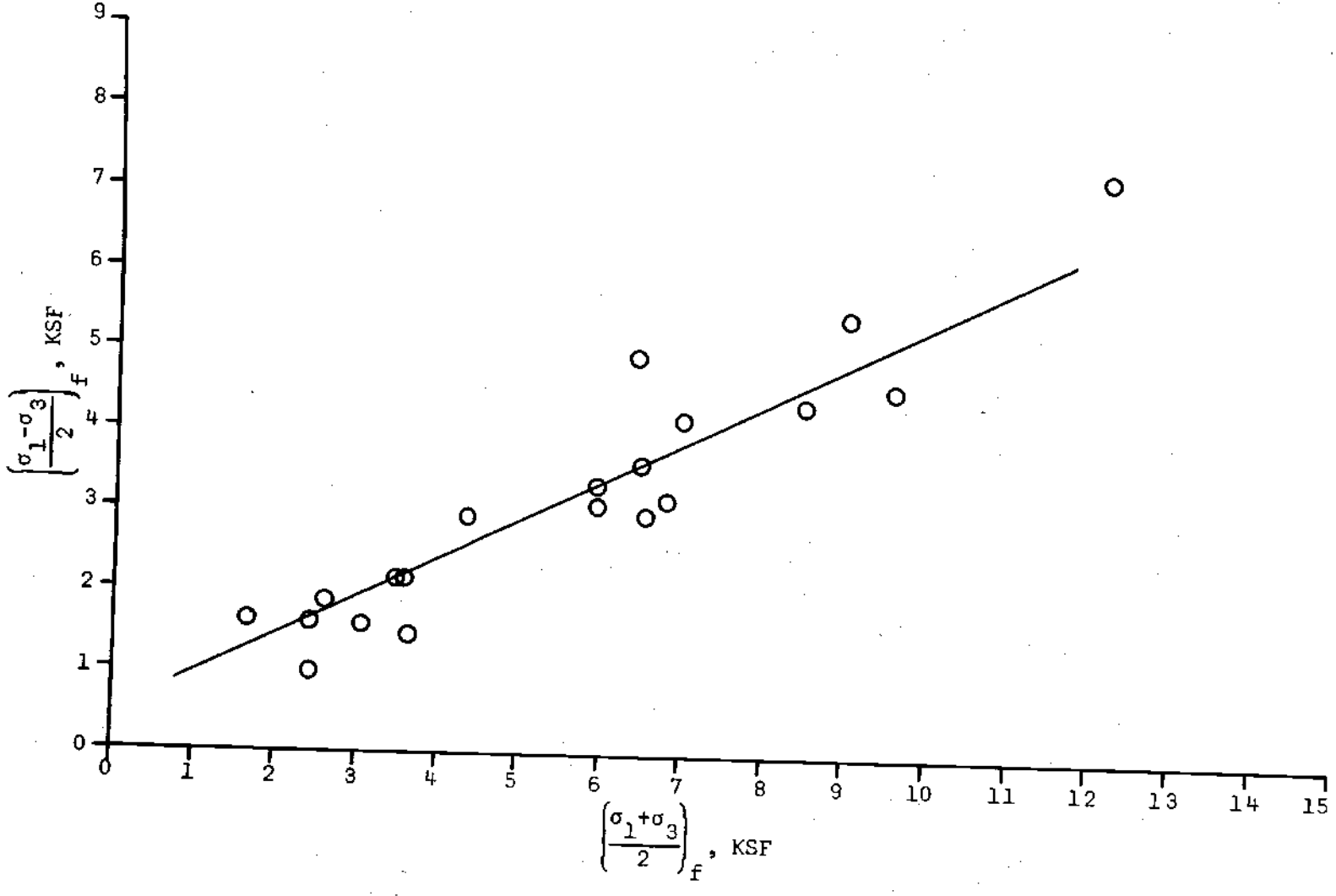

Figure 77. Summary of Results of Triaxial Shear Testing of Weathered Rock

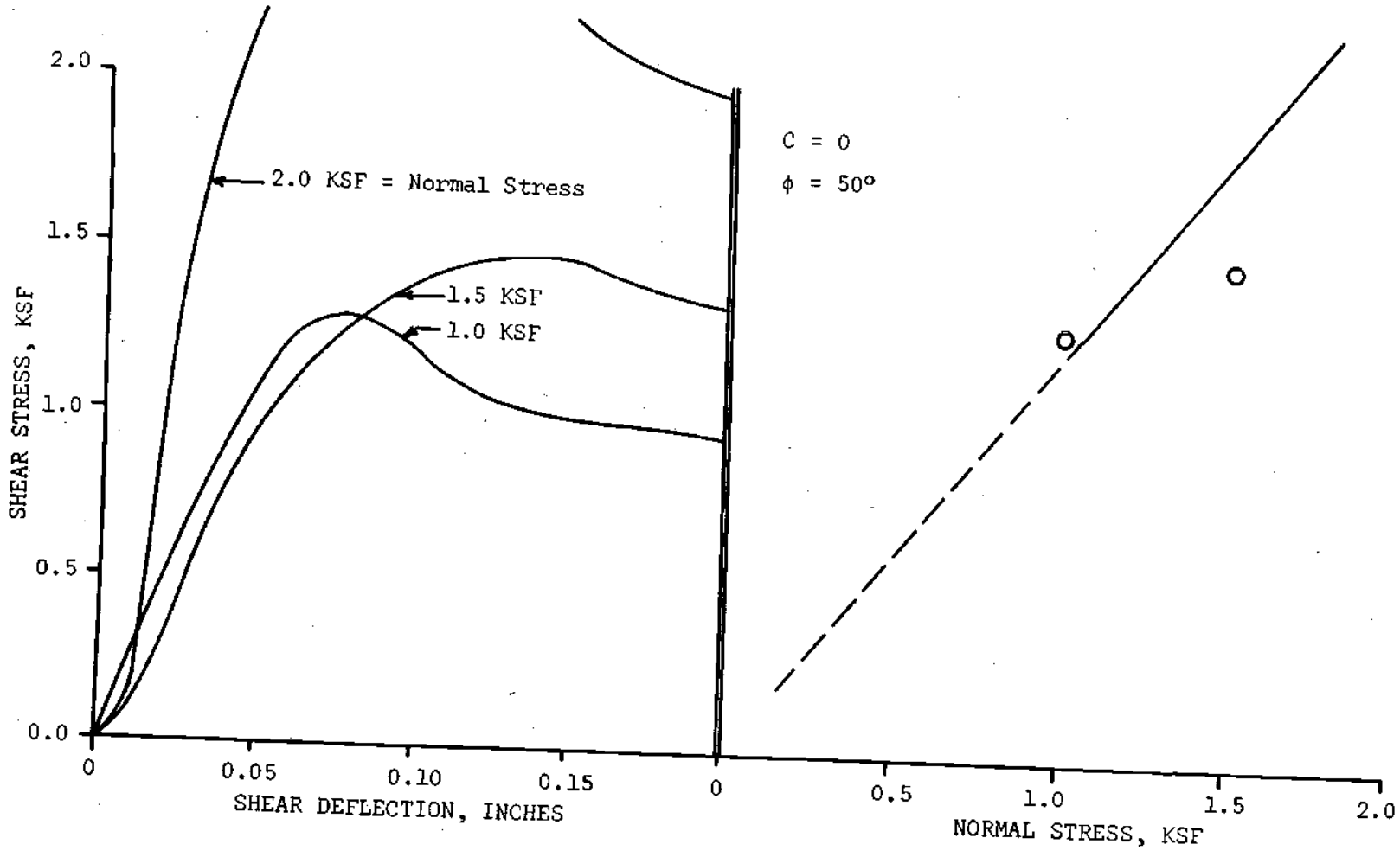

Figure 78. Results of Double Ring Shear Testing on Samples from Test Pier Two at a Depth of 15 Feet

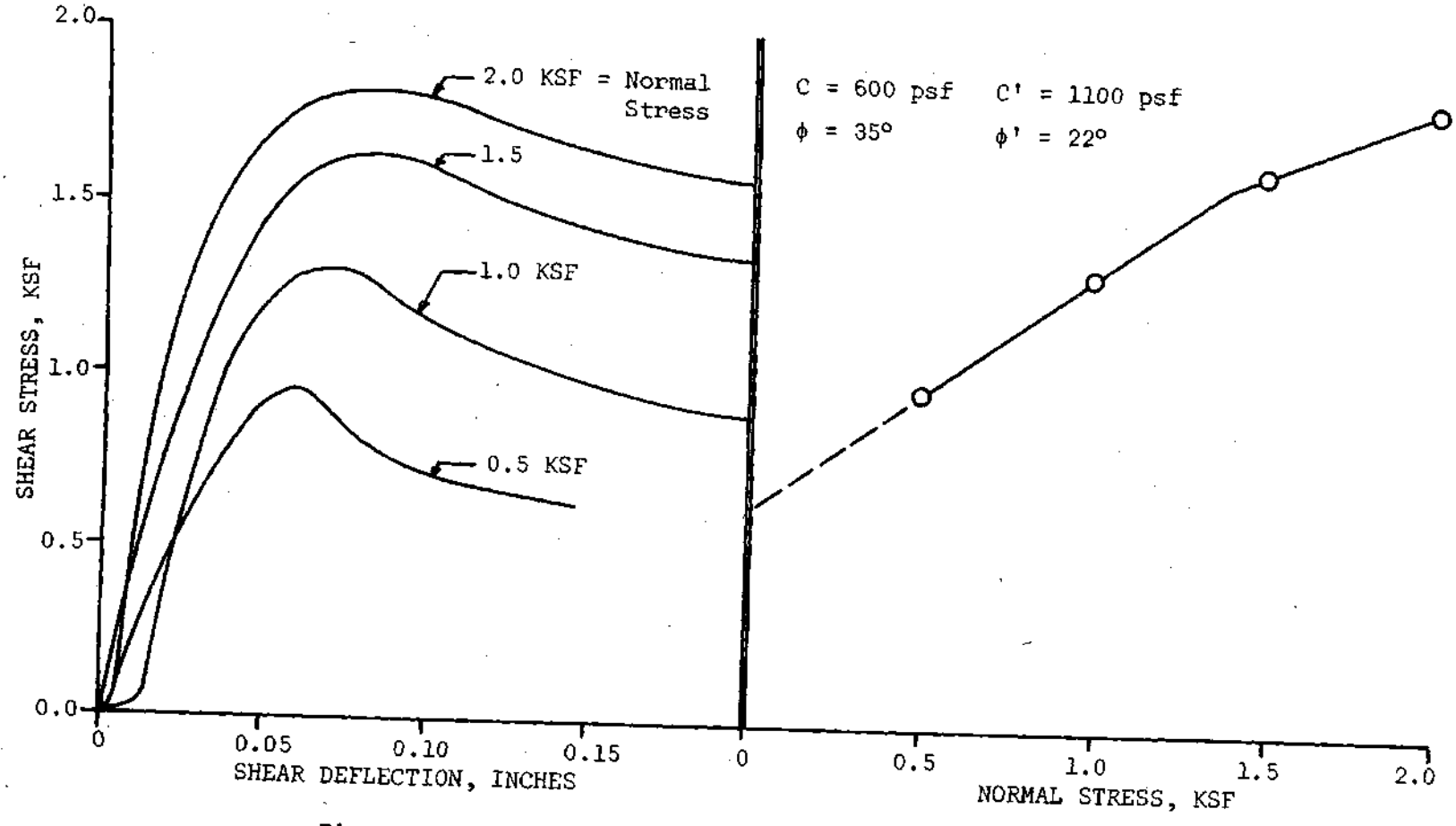

Figure 79. Results of Double Ring Shear Testing on Samples from Test Pier Three at a Depth of 22 Feet

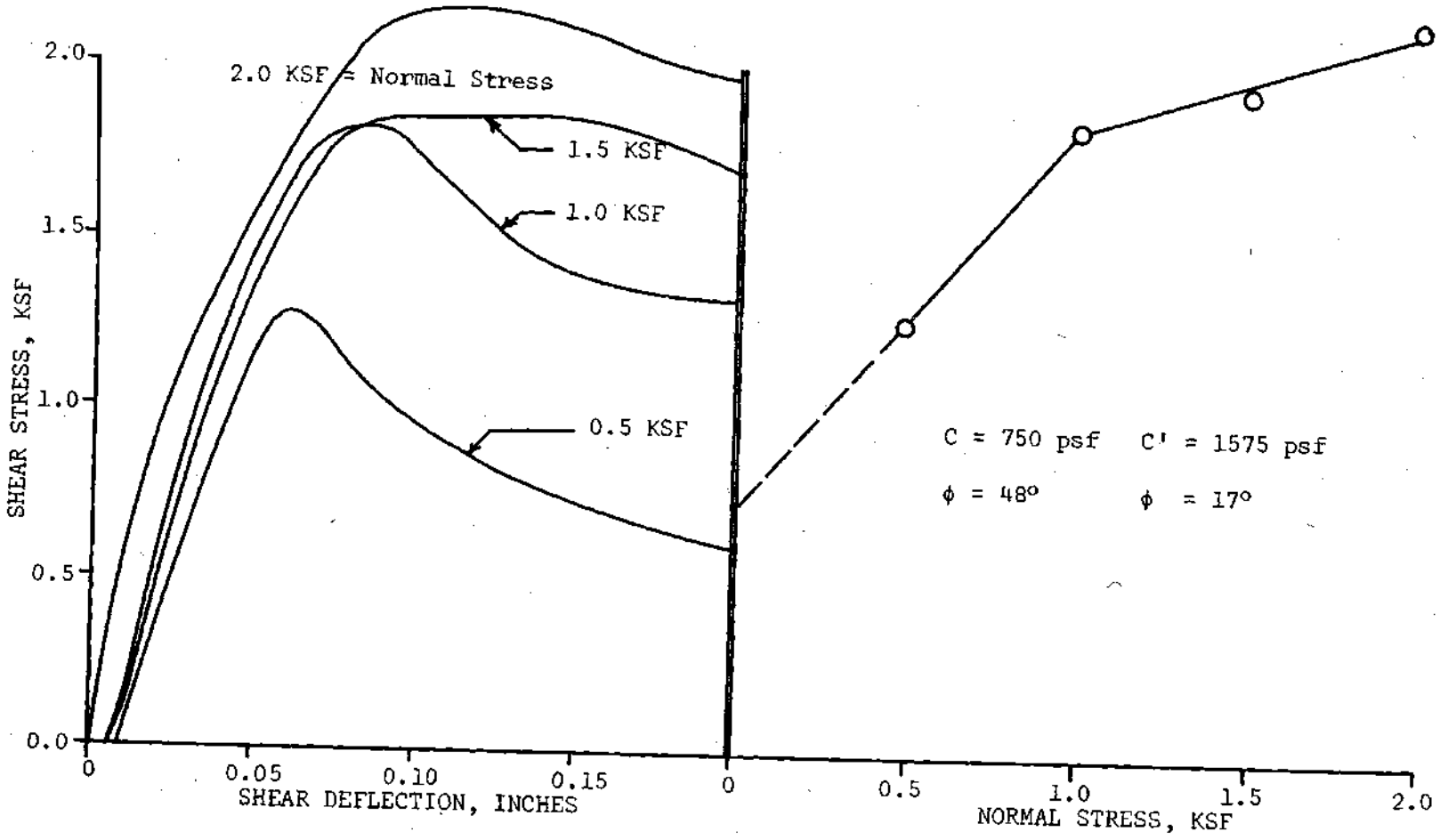

Figure 80. Results of Double Ring Shear Testing on Samples from Test Pier Four at a Depth of 22 Feet

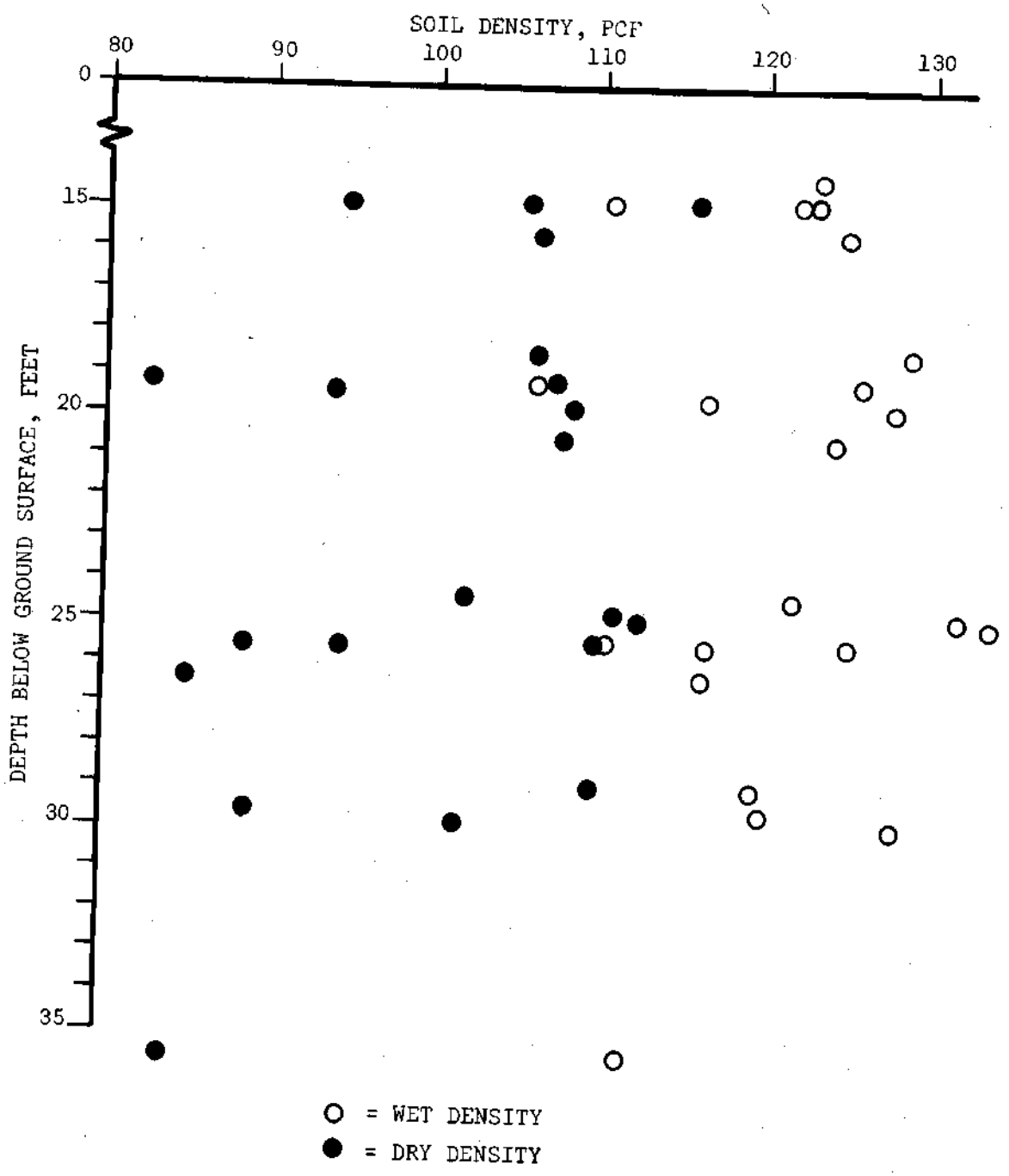

Figure 81. Profile of Soil Density Variation with Depth, Obtained from Undisturbed Soil Samples

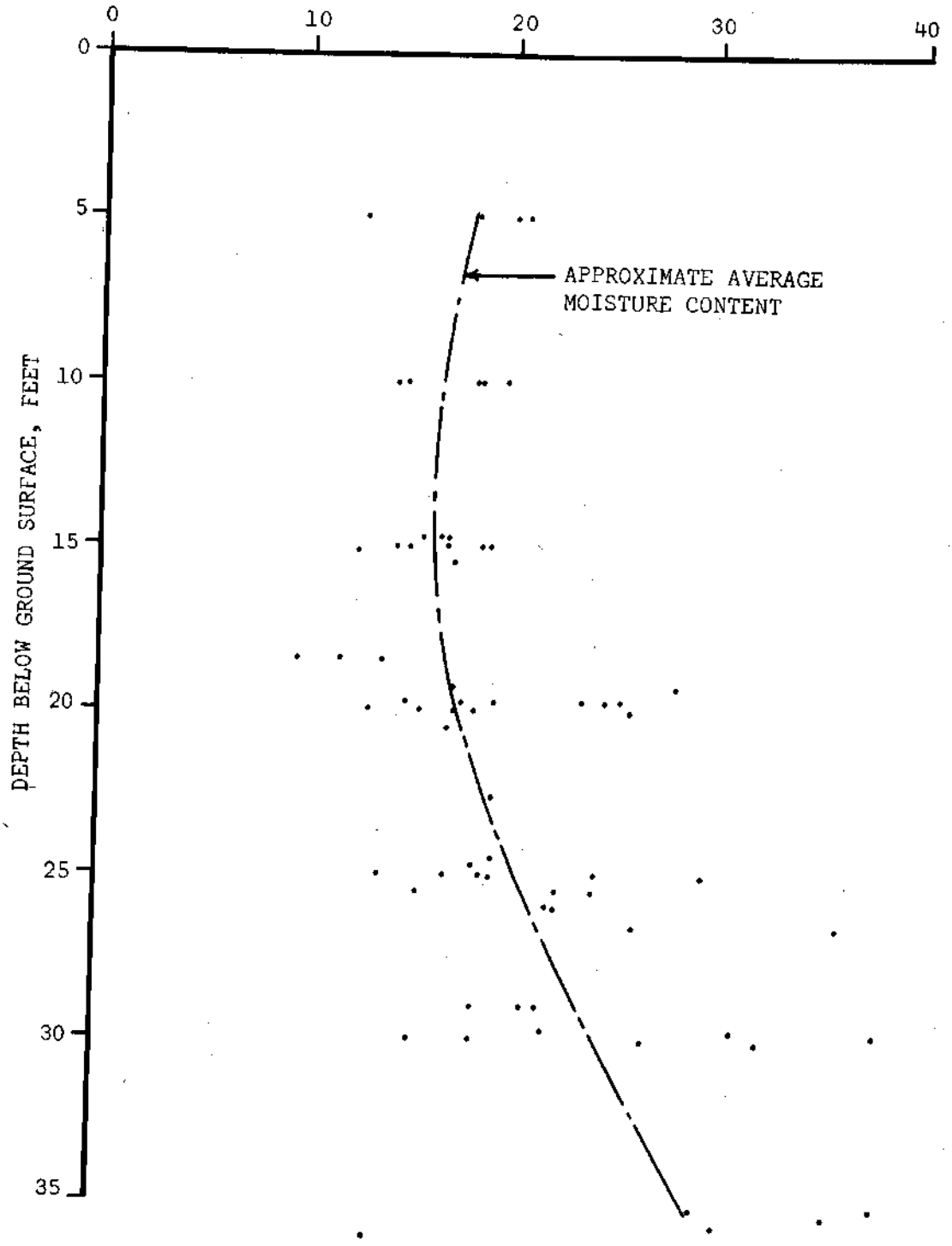

Figure 82. Profile of Moisture Content Variation with Depth Obtained from all Samples Obtained

APPENDIX B

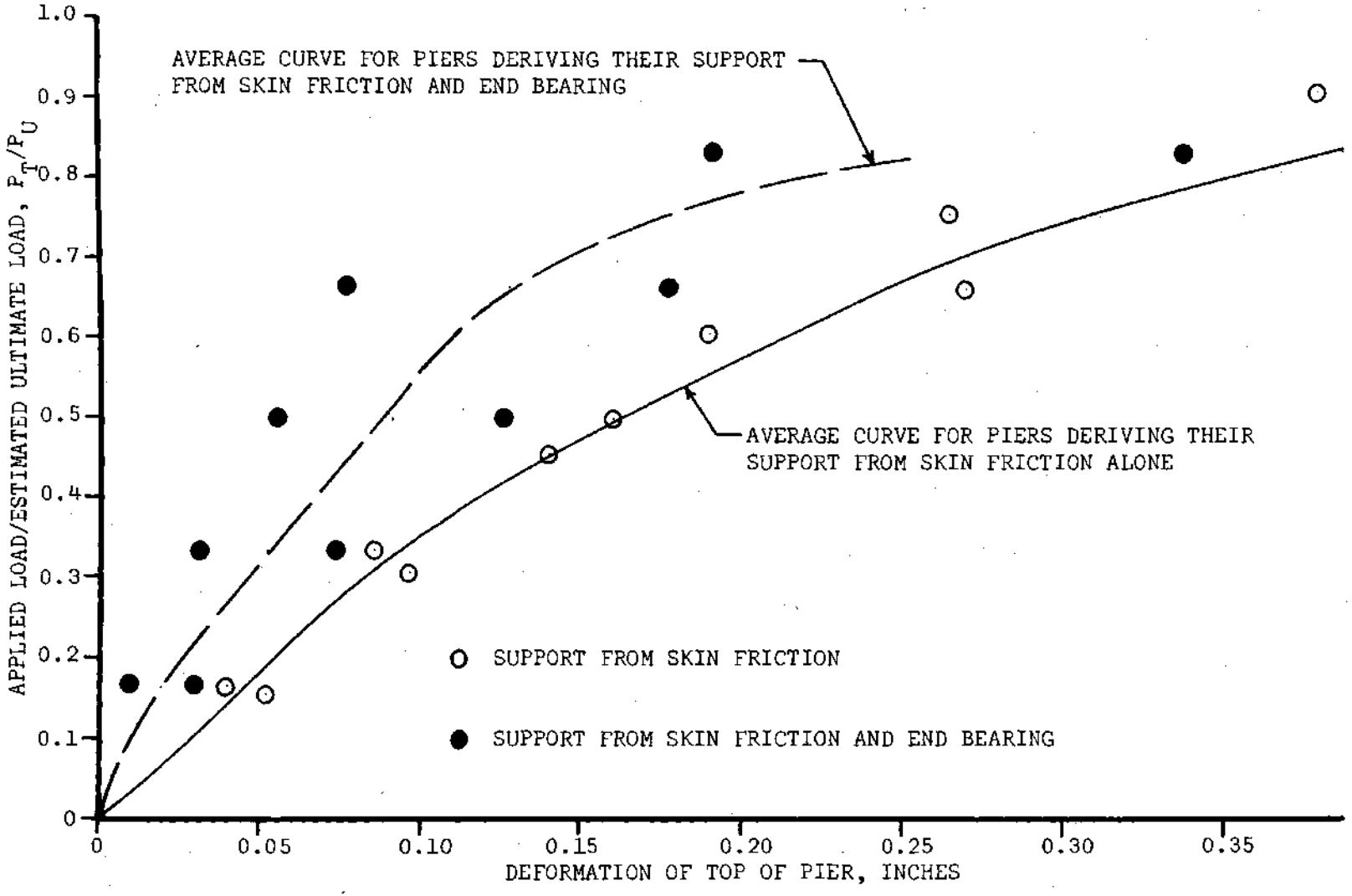

Figure 83. Fraction of Ultimate Load vs. Deformation of the Top of the Pier for Piers in Predominately Clayey Soils in California (From Private Records of Dames and Moore)

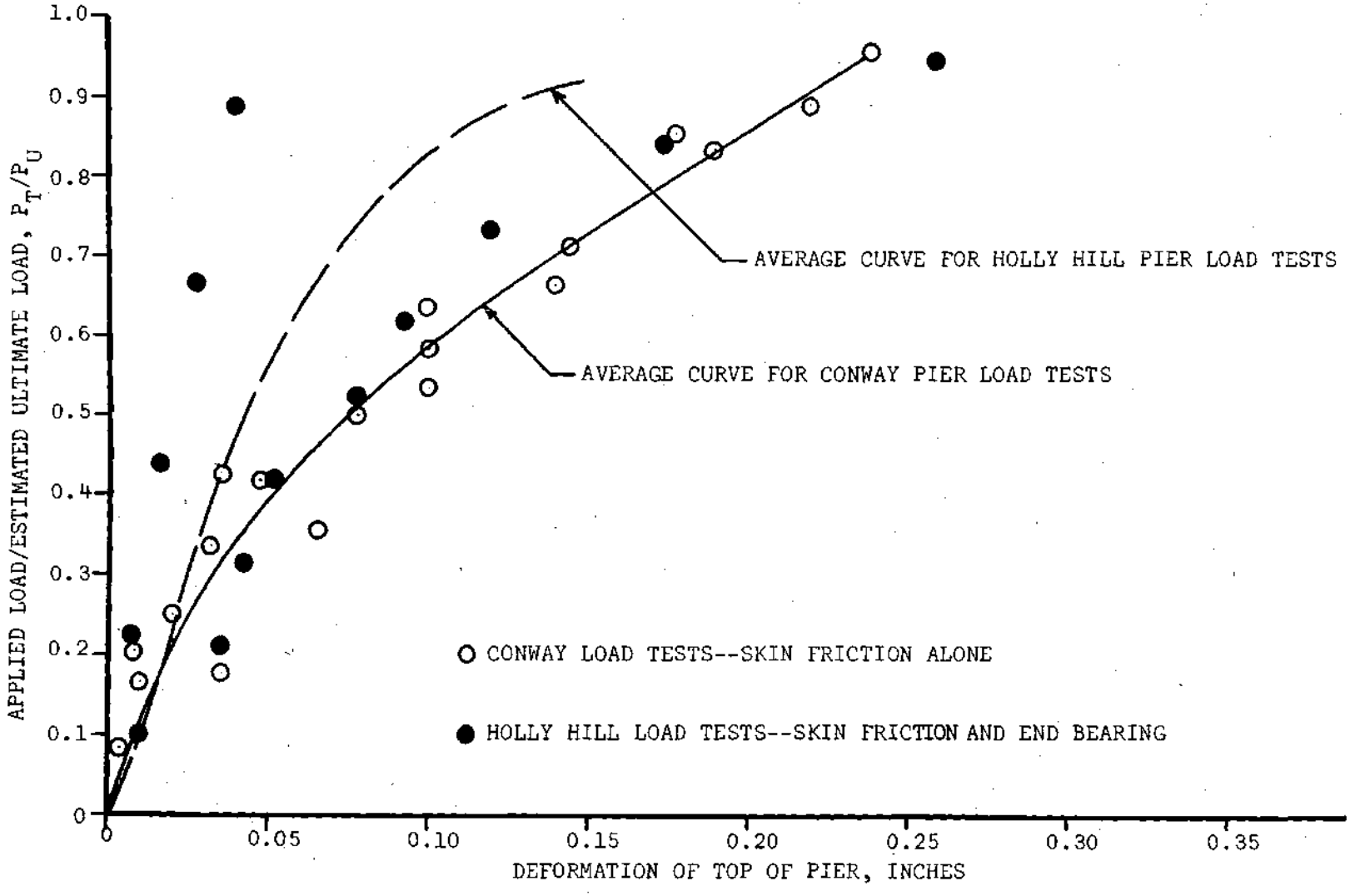

Figure 84. Fraction of Ultimate Load vs. Deformation of the Top of the Pier for Piers in Predominately Clayey Soils in South Carolina (From Private Records of McKinney Drilling Company)

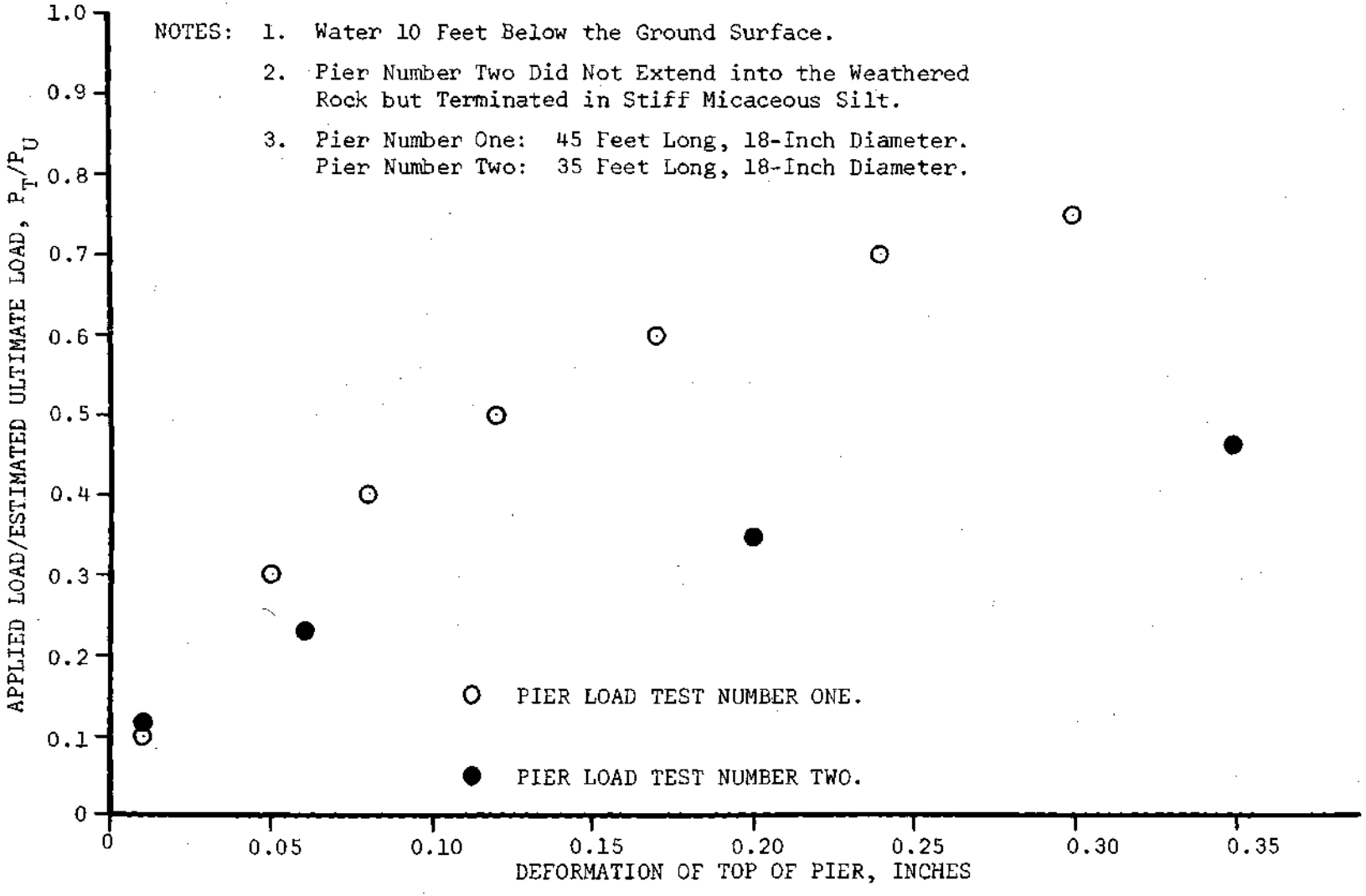

Figure 85. Fraction of Ultimate Load vs. Deformation of the Top of the Pier for Piers in Predominately Silty Soils and Weathered Rock in Atlanta, Georgia (From Private Records of McKinney Drilling Company)

APPENDIX C

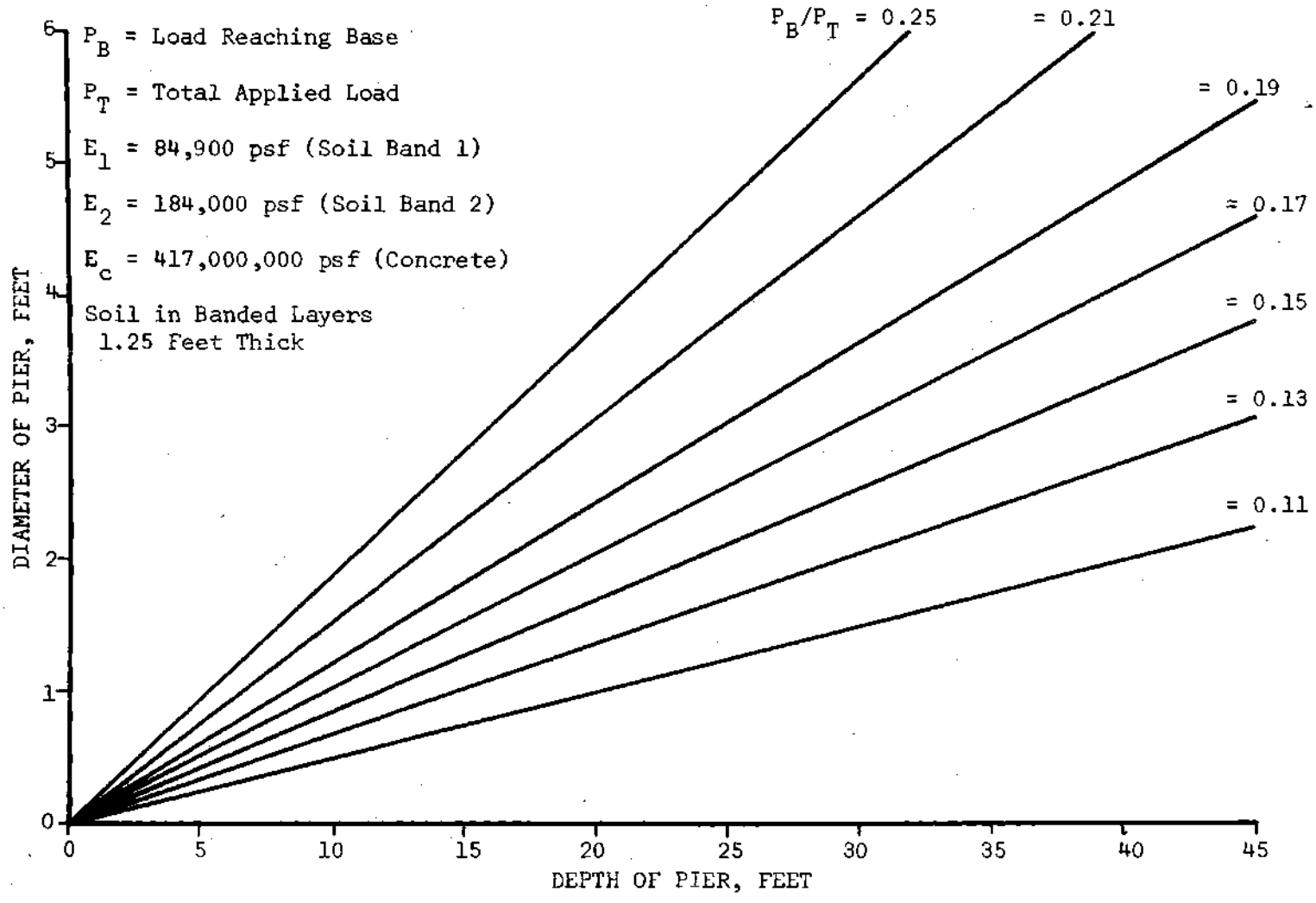

Figure 86. Ratio of the Load Reaching the Base of a Pier to the Applied Load for Various Depths and Diameters

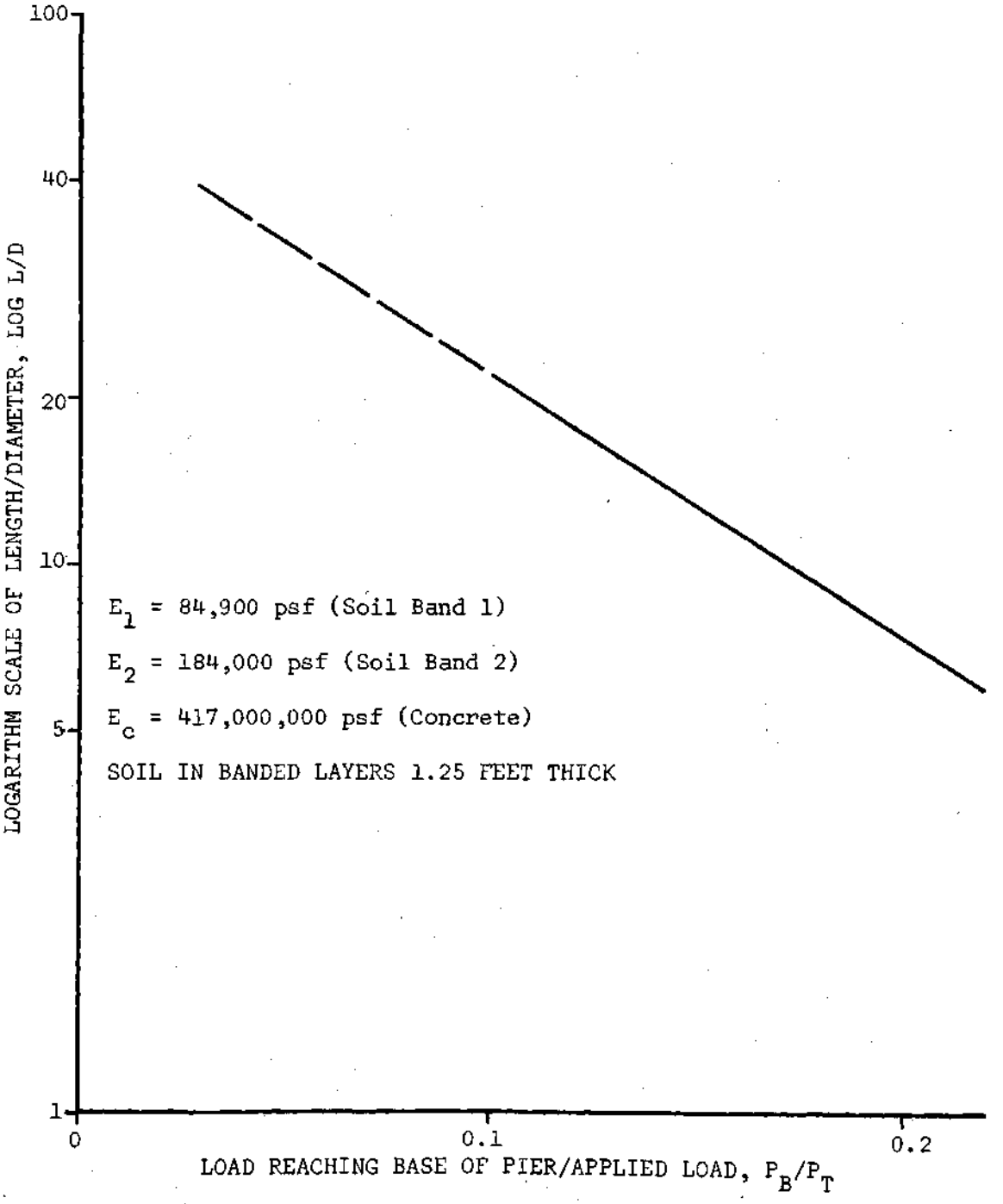

Figure 87. Ratio of the Load Reaching the Base of a Pier as a Function of the Length and Diameter of a Pier Embedded in an Elastic Media

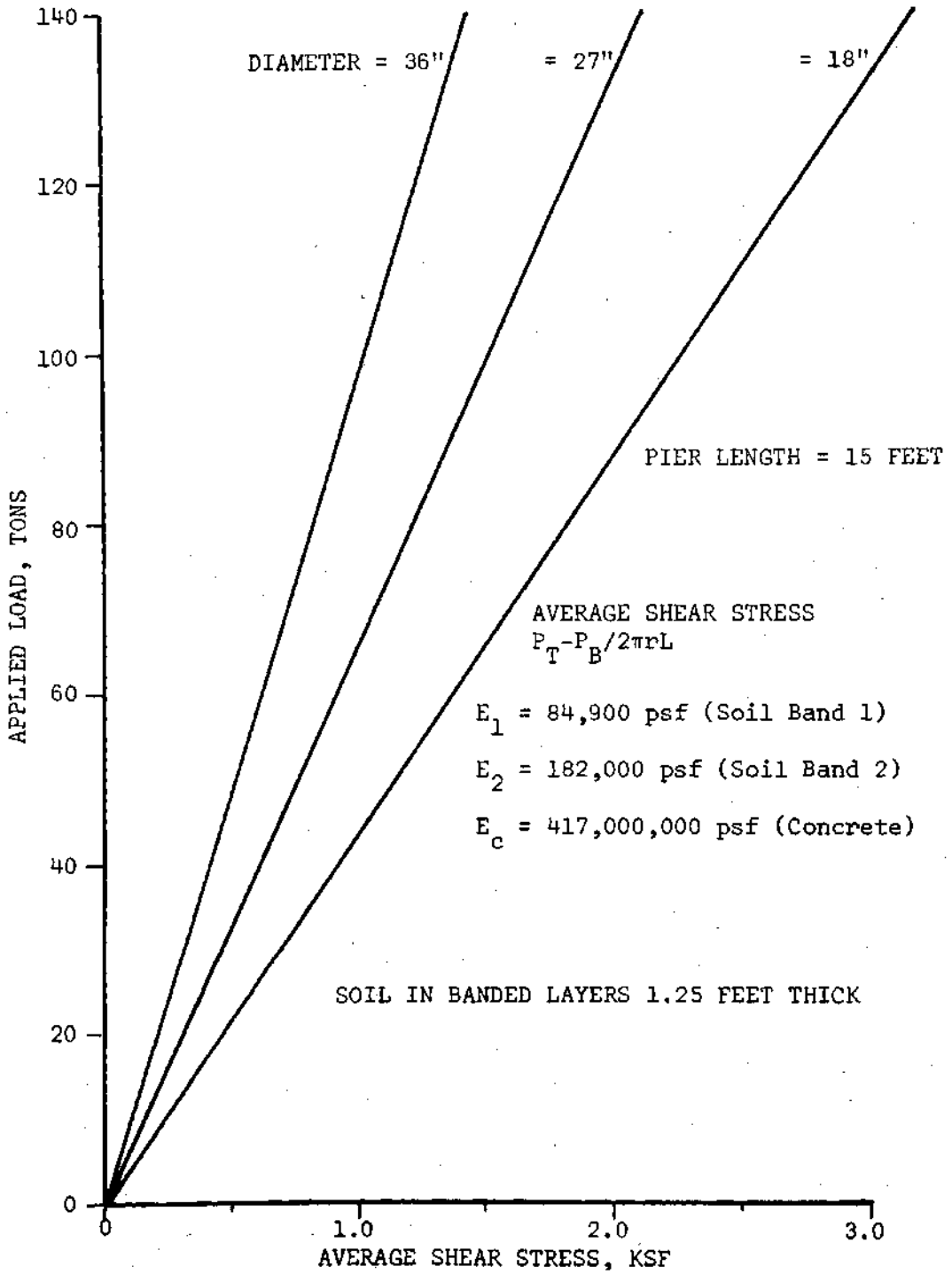

Figure 88. Average Shear Stress as a Function of Applied Load for a 15-Foot Long Pier in a Layered Elastic Soil

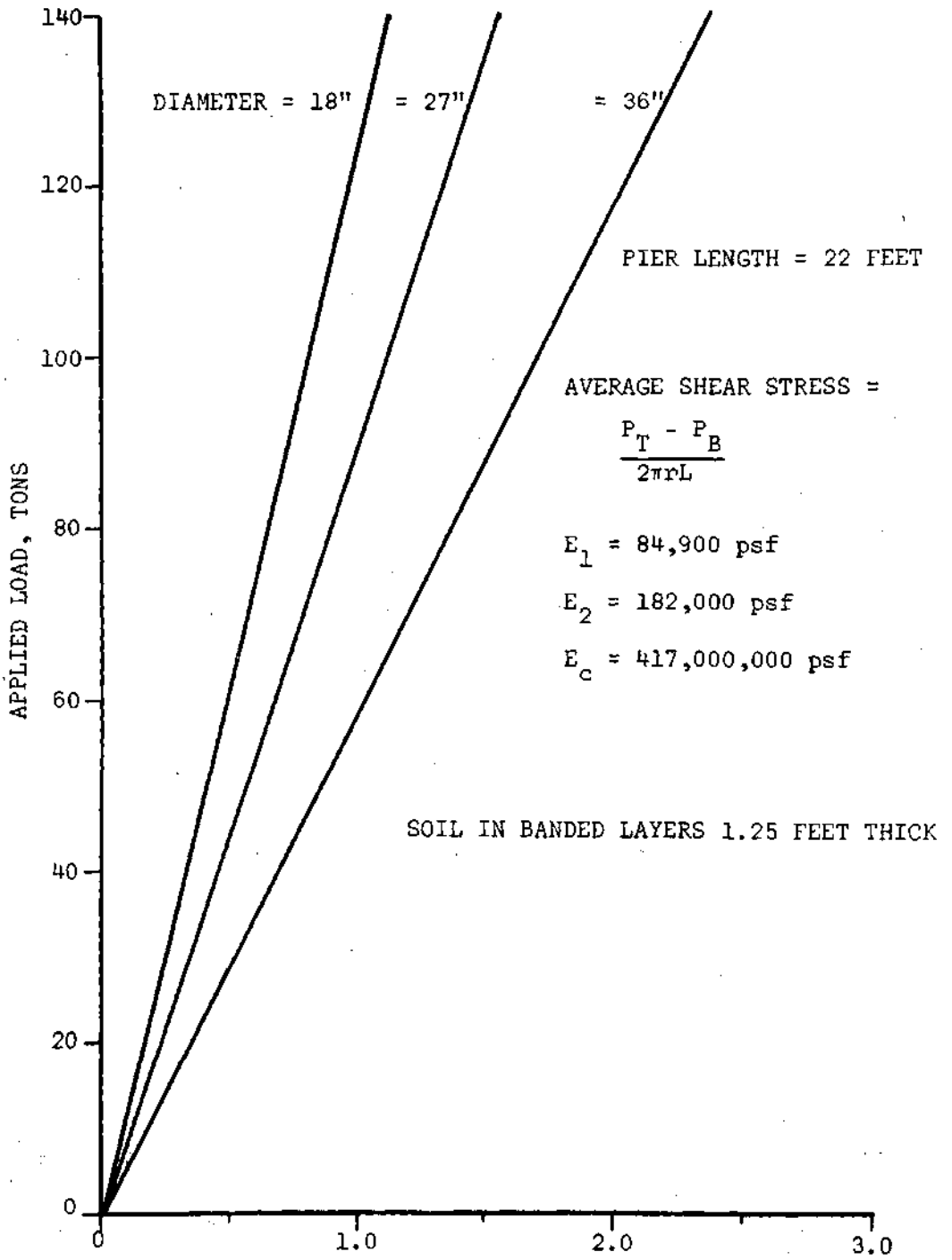

Figure 89. Average Shear Stress as a Function of Applied Load for a 22-Foot Long Pier in a Layered Elastic Soil

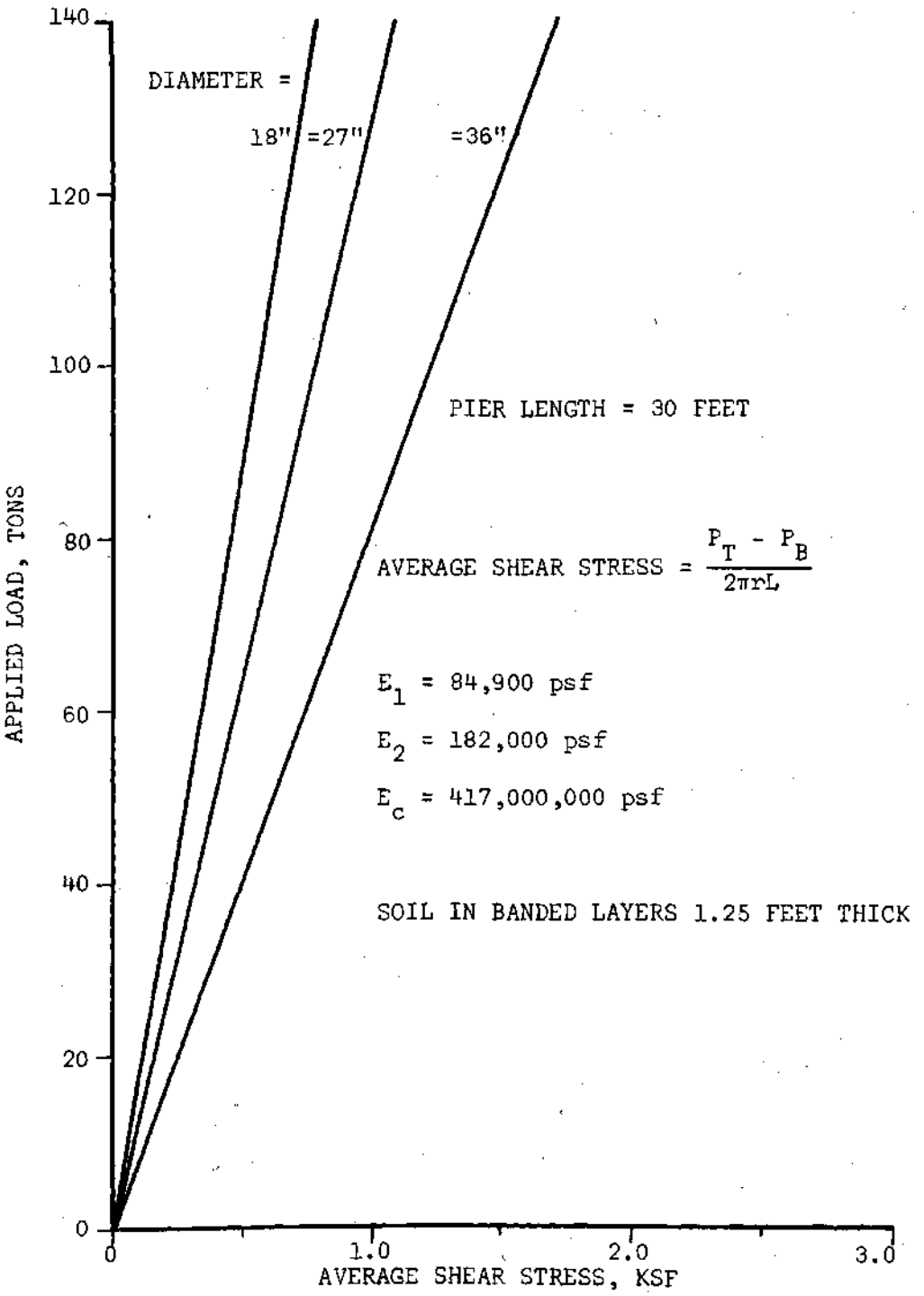

Figure 90. Average Shear Stress as a Function of Applied Load for a 30-Foot Long Pier in a Layered Elastic Soil

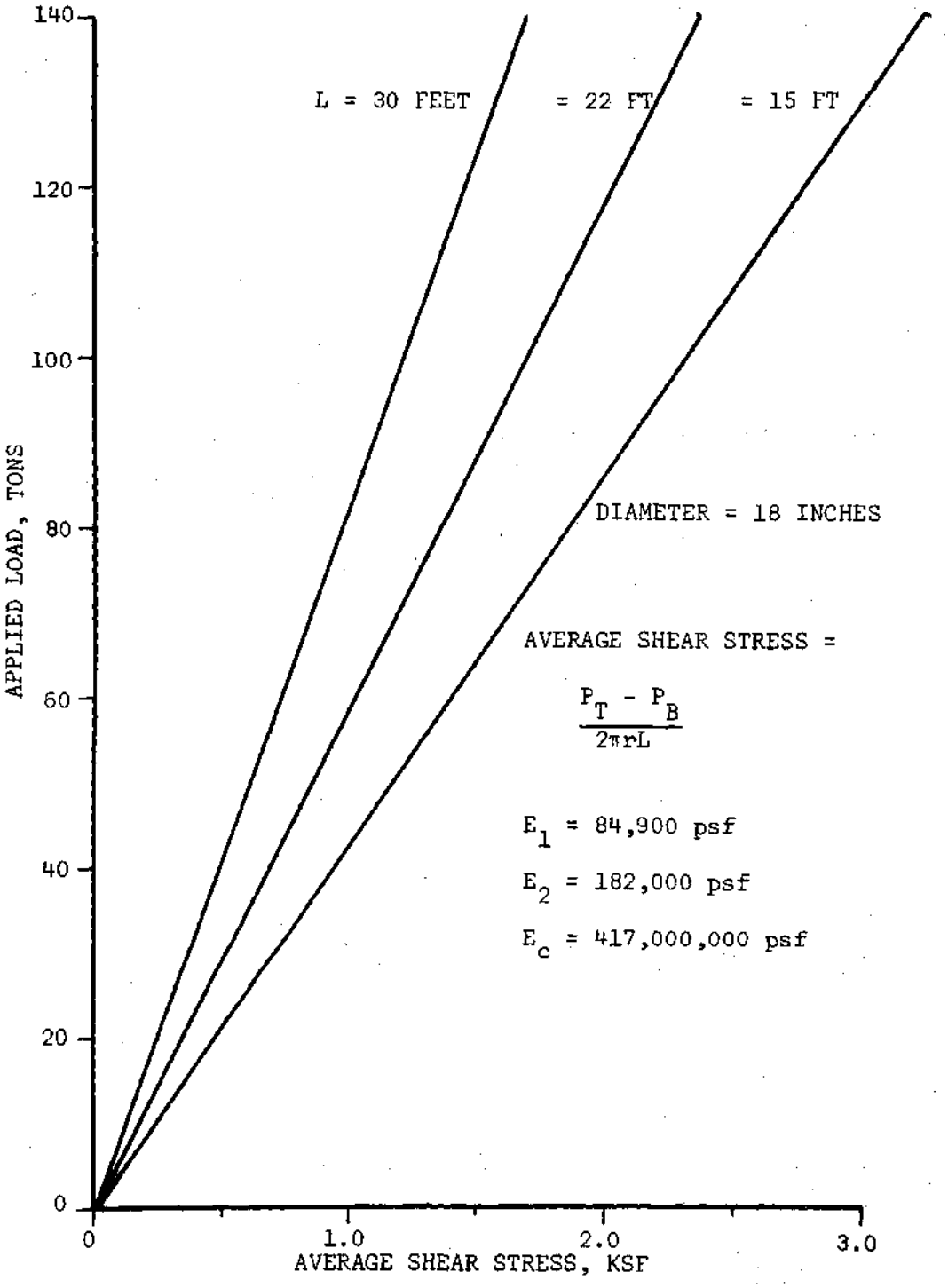

Figure 91. Average Shear Stress as a Function of Applied Load for an 18-Inch Diameter Pier in Layered Elastic Soil

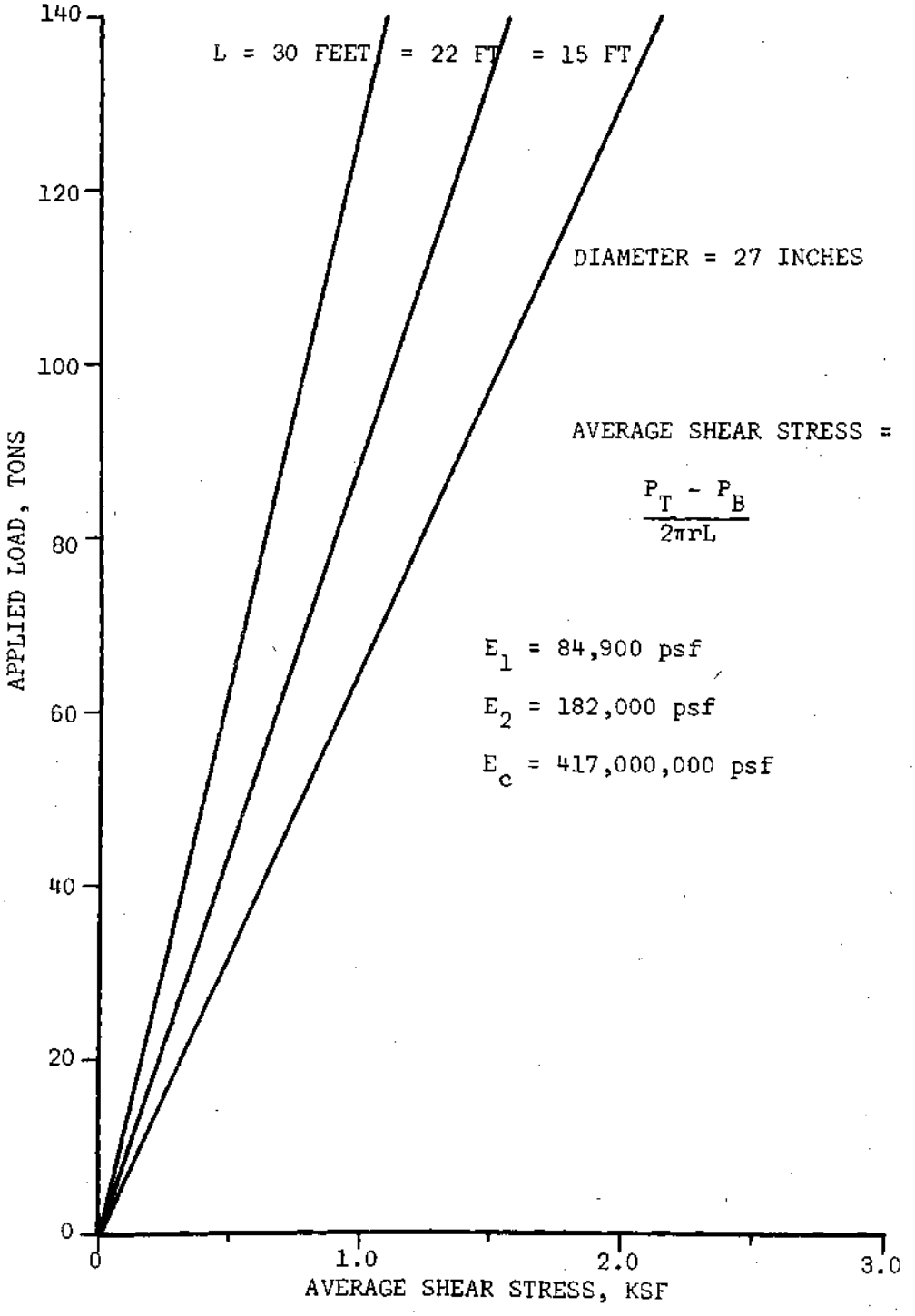

Figure 92. Average Shear Stress as a Function of Applied Load for a 27-Inch Diameter Pier in a Layered Elastic Soil

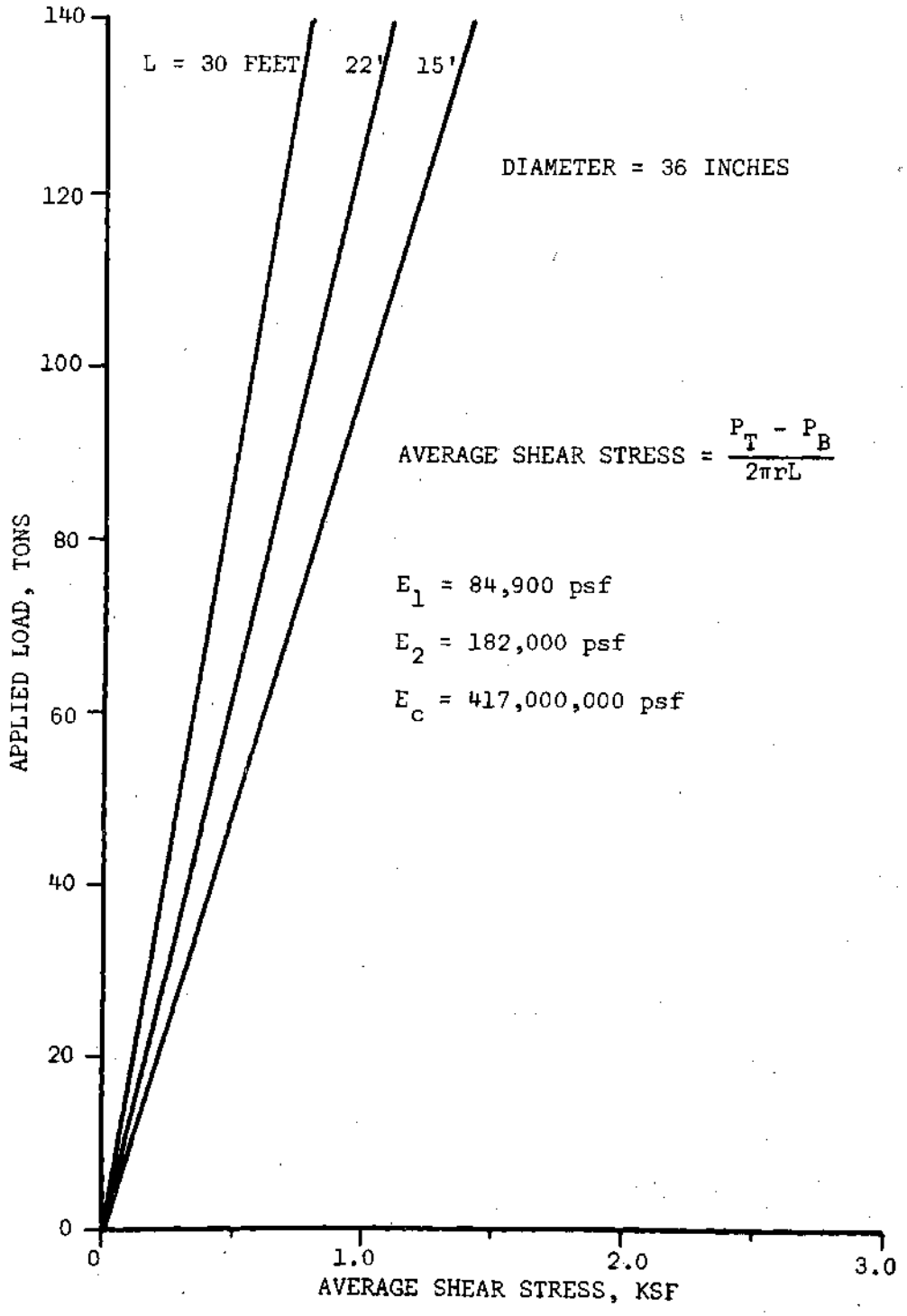

Figure 93. Average Shear Stress as a Function of Applied Load for a 36-Inch Diameter Pier in a Layered Elastic Soil

BIBLIOGRAPHY

BIBLIOGRAPHY

Literature Cited

1. Peck, R. B. "History of Building Foundations in Chicago," *Chicago Soil Mechanics Lecture Series,* Department of Civil Engineering, Illinois Institute of Technology, Chicago, Illinois, 1963, p. 1-1 to 1-56.

2. Osterberg, J. O. "Current Practice in Foundation Design," *Chicago Soil Mechanics Lecture Series,* Department of Civil Engineering, Illinois Institute of Technology, Chicago, Illinois, 1963, p. 6-1 to 6-40.

3. Mohr, H. A., "The GOW Caisson," *Journal of the Boston Society of Civil Engineers,* Vol. 54, No. 3, July, 1967, p. 149-194.

4. Gerwick, B. C., Jr. "Bell-Pier Construction, Recent Developments and Trends; Major Bridge Piers in Deep Water," *Journal of the American Concrete Institute,* October, 1965, p. 1281-1291.

5. Hunt, H. W. "Building Foundation Built as a Caisson for Port Storage in Stockholm," *Civil Engineering,* Vol. 35, January, 1965, p. 60-62.

6. "Caisson with Features of Bridge and Ship is Floating Gate to Enclose Big Dry Dock; Puget Sound Naval Shipyard, Bremerton," *Engineering News Record,* Vol. 165, August 4, 1960, p. 33.

7. "Sunshine Bridge Cantilevers Over the Mississippi at Donaldsonville, La.," *Engineering News Record,* Vol. 171, September 12, 1963, p. 28-30.

8. "Two Types of Caissons Support Tall Piers for Louisiana Bridge," *Engineering News Record,* Vol. 173, September 3, 1964, p. 28-29.

9. "Hineley Point Caisson," *Engineer,* Vol. 208, July 31, 1959, p. 37-38.

10. "Telescopic Caisson Lighthouse," *Engineer,* Vol. 208, September 11, 1959, p. 238-240.

11. "Caisson Sinking at Queenhill Bridge," *Engineer,* Vol. 208, October 23, 1959, p. 480-481.

12. "Caissons Dig Out a Seven Story Basement in Geneva," *Engineering News Record,* Vol. 167, July 6, 1961, p. 42-43.

13. "Five-Story Basement Sinks Below Grade: Nikkei Building, Tokyo," *Engineering News Record,* Vol. 169, December 6, 1962, p. 43.

14. Bozozuk, M. and Jarrett, P. M. "Instrumentation for Negative Skin Friction Studies on Long Piles in Marine Clay on the Autoroute Du Quebec," *Workshop Meeting of the International Bridge, Tunnell and Turnpike Association,* Montreal, Canada, November, 1956, p. 3.

15. White, R. E., "Pretest Tiebacks and Drilled-In Caissons," *Civil Engineering,* Vol. 33, No. 4, April, 1963, p. 36-38.

16. "Tie Back Wall Braces Building Excavation," *Construction Methods,* November, 1962, p. 117.

17. Both, W. S., "Tie Backs in Soil for Undistructed Deep Excavation," *Civil Engineering,* Vol. 39, No. 9, September, 1966, p. 46-49.

18. "Giant Spikes Halt Earth Movement in California," *Civil Engineering,* Vol. 28, January, 1958, p. 64.

19. Sowers, G. F. "Soil Problems in the Southern Piedmont Region," *Proceedings of The American Society of Civil Engineering,* Vol. 80, No. 416, March, 1954, p. 1.

20. Herrick, S. M. and LeGrand, H. E., *Geology and Ground-Water Resources of The Atlanta Area, Georgia,* Bulletin 55, Georgia Department of Mines, Mining and Geology, 1949.

21. Santee Portland Cement Company--Report of Drilled-In Caisson Load Tests at Holly Hill, South Carolina, Communications with McKinney Drilling Company.

22. Landmark Apartments, Atlanta, Georgia, Communications with McKinney Drilling Company.

23. Moore, W. W., "Golden Gateway; Foundation Design," *Civil Engineering,* Vol. 34, January, 1964, p. 33-35.

24. Persons, B. S., "Drilled Piles and Drilled and Belled Caissons as Building Foundations," *Convention of the American Society of Civil Engineers,* Jackson, Mississippi, February, 1957.

25. Burland, J. B., Butler, F. G., Dunkan, P., "The Behavior and Design of Large Diameter Bored Piles in Stiff Clay," *Symposium on Large Bored Piles,* London, England, 1966, p. 54.

26. Terzaghi, K., "Theoretical Soil Mechanics," John Wiley and Sons, Inc., New York, 1943.

27. "Symposium on Large Bored Piles," Institution of Civil Engineers, London, England, 1960.

28. "Symposium on Large Bored Piles," Institution of Civil Engineers, London, England, 1966.

29. Whitaker, T. and Cooke, R. W., "An Investigation of the Shaft and Base Resistances of Large Bored Piles in London Clay," *Symposium on Large Bored Piles,* 1966, p. 7.

30. Skempton, A. W., "Summing Up," *Symposium on Large Diameter Bored Piles,* 1966, p. 155.

31. Skempton, A. W., "Cast-In-Situ Bored Piles in London Clay," *Geotechnique,* Vol. 9, 1959, p. 153.

32. Gooder, H. Q. and Leonards, M. W., "Some Tests on Bored Piles in London Clay," *Geotechnique,* Vol. 4, 1954, p. 32.

33. Meyerhof, G. G. and Murdock, L. J., "An Investigation of the Bearing Capacity of Some Bored Piles in London Clay," *Geotechnique,* Vol. 3, 1954, p. 207.

34. Woodward, R. J., Londgren, R., and Biotano, J. D., "Pile Loading Tests in Stiff Clays," *Proceeding of the Fifth International Conference on Soil Mechanics and Foundation Engineering,* Vol. 2, 1961, p. 177.

35. Meyerhof, G. G., "The Ultimate Bearing Capacity of Foundations," *Geotechnique,* Vol. 2, 1951, p. 301.

36. DuBose, L. A., "Load Studies on Drilled Shafts," *Proceedings Highway Research Board,* Vol. 34, Washington, D. C., 1954, p. 152.

37. DuBose, L. A., "A Comprehensive Study of Factors Influencing the Load Carrying Capacity of Drilled and Cast-In-Place Concrete Piles," Part I, *Texas Transportation Institute,* College Station, Texas, July, 1956.

38. DuBose, L. A., "A Comprehensive Study of Factors Influencing the Load Carrying Capacities of Drilled and Cast-In-Place Concrete Piles," Part II, *Texas Transportation Institute,* College Station, Texas, October, 1956.

39. Mohan, D., Jain, G. S., and Kumar, V., "Load Bearing Capacity of Piles," *Geotechnique,* Vol. 13, March, 1963, p. 76.

40. Berezantzev, V. G., "Design of Deep Foundations," Proceedings of *The Sixth International Conference on Soil Mechanics and Foundation Engineering,* Vol. 2, Montreal, Canada, 1965, p. 234.

41. Vesic, A. S., *Bearing Capacity of Deep Foundations in Sand*, Highway Research Record No. 39, National Academy of Sciences, National Research Council, 1963, p. 112.

42. Vesic, A. S., "Investigations of Bearing Capacity of Piles in Sand," *Soil Mechanics Laboratory Publication No. 3, Duke University*, Durham, North Carolina, 1964.

43. Vesic, A. S., "Ultimate Loads and Settlements of Deep Foundations in Sand," *Soil Mechanics Laboratory Publication No. 6, Duke University*, Durham, North Carolina, 1967.

44. Young, D., "Stress Distribution Around a Rigid Column in a Consolidating Stratum," *Sixth Texas Conference on Soil Mechanics and Foundation Engineering*, University of Texas, Austin, Texas, 1943, p. 1.

45. Mindlin, R. D., "Force and Point in the Interior of a Semi-Infinite Solid," *Physic*, Vol. 7, May, 1936.

46. Henley, A. D., "Investigation of Side Shear Stress Transfer for Drilled in Foundation Shafts in Weak Soils," *Fifth Annual Symposium on Engineering Geology and Soils Engineering*, Pocatello, Idaho, 1967.

47. Walters, J. V. "The Bearing Capacity of Drilled Piers in Decomposed Rock," Unpublished Thesis for a Master of Science in Civil Engineering Degree, *Georgia Institute of Technology*, Atlanta, Georgia, 1958.

48. Sowers, G. B. and Sowers, G. F. *Introductory Soil Mechanics and Foundations*, The Macmillan Company, New York, 1953, p. 40.

49. Taylor, D. W. "A Triaxial Shear Investigation on a Partially Saturated Soil," *Triaxial Testing of Soils and Bituminous Mixtures*, ASTM STP 106, Philadelphia, 1951, p. 180.

50. Fleming, H. D. "Undrained Triaxial Compression Tests on a Decomposed Phyllite," *Australia-New Zealand Conference on Soil Mechanics and Foundation Engineering*, June, 1952, p. 112.

51. Lambe, T. W. *Soil Testing for Engineers*, John Wiley and Sons Inc., New York, 1951, p. 104 and 128.

52. D'Appolonia, E. and Hirbar, J. A. "Load Transfer in a Step-Taper Pile," *Journal of the Soil Mechanics and Foundations Division*, ASCE, Vol. 89, SM 6, November, 1963, p. 67.

53. D'Appolonia, E. and Romualidi, J. P., "Load Transfer in End Bearing Steel H-Piles," *Journal of the Soil Mechanics and Foundations Division,* ASCE, Vol. 89, SM 2, March, 1963, p. 1.

54. Broms, B. B. and Hellman, L. "End Bearing and Skin Friction of Piles," *Journal of the Soil Mechanics and Foundations Division,* ASCE, Vol. 94, SM 2, March, 1968, p. 421.

55. Shiver, D. F., "Lateral Pressures Against a Pile in Cohesionless Soil," Unpublished Thesis for a Master of Science Degree in Civil Engineering, Georgia Institute of Technology, Atlanta, Georgia, 1967.

56. Coyle, N. M. and Sulaiman, I. M., "Skin Friction for Steel Piles in Sand," *Journal of the Soil Mechanics and Foundations Division,* ASCE, Vol. 93, SM 6, November, 1967.

57. Crandall, L. L. "Electrical Resistance Strain Gages for Determining the Transfer of Load from Driven Piling to Soil," *Proceeding of the Second International Conference on Soil Mechanics and Foundations Engineering,* Vol. 4, Zurich, Switzerland, 1948, p. 122.

58. Seed, H. B. and Reese, L. C., "The Action of Soft Clay Along Friction Piles," *Transactions of the American Society of Civil Engineers,* Vol. 122, 1957, p. 731.

59. Reese, L. C. and Seed, H. B., "Pressure Distributions Along Friction Piles," *Proceedings of the American Society for Testing and Materials,* Vol. 55, 1955, p. 1156.

60. Worley, H. E. and Meyer, R. C., "Development of a Cell for the Installation of Electrical Strain Gages in Concrete," *Journal of the American Concrete Institute,* October, 1953, p. 121.

61. Thoma, E. C. and Schneebeli, R. E., "Method of Preparing SR4 Strain Gages for Embedment in Concrete," *Journal of the American Concrete Institute,* Vol. 24, No. 4, December, 1952, p. 305.

62. Druburgh, R. B., Peter, B. G. W., and Plewes, W. G., "Waterproofing Strain Gages on Reinforcing Bars in Concrete Exposed to the Sea," *Materials Research and Standards,* July, 1965, p. 350.

63. Thurman, A. G., "Computed Load Capacity and Movement of Friction and End Bearing Piles Embedded in Uniform and Stratified Soils," Ph.D. Thesis, Carnegie Institute of Technology, Pittsburgh, Pennsylvania.

64. Thurman, A. G. and D'Appolonia, "Computed Movement of Friction and End Bearing Piles Embedded in Uniform and Stratified Soils," *Proceeding of the Sixth International Conference on Soil Mechanics and Foundation Engineering,* Montreal, Canada, Vol. II, 1965, p. 323.

65. Mansur, C. I. and Focht, J. A., "Pile Loading Tests, Morganza Floodway Control Structure," *Transactions of the American Society of Civil Engineers,* Vol. 128, 1963, p. 555.

66. Coyle, H. M. and Reese, L. C. "Load Transfer in Axially Loaded Piles in Clay," *Journal of the Soil Mechanics and Foundations Division,* ASCE, Vol. 92, No. SM-2, March, 1966, p. 1.

67. Berezantzev, V., Kristoforov, V., and Golubkov, V. "Load Bearing Capacity and Deformation of Deep Foundations," *Proceedings of the Fifth International Conference on Soil Mechanics and Foundation Engineering,* Paris, France, Vol. II, 1961.

68. Broms, B. B., Discussion of Reference 69, *Journal of the Soil Mechanics and Foundations Division,* ASCE, Vol. 39, SM6, November, 1963, p. 125.

69. Norland, R. L., "Bearing Capacity of Piles in Cohesionless Soils," *Journal of the Soil Mechanics and Foundation Division,* ASCE, Vol. 89, SM3, May, 1963, p. 1.

70. Westergaard, H. M., "A Problem of Elasticity Suggested by a Problem in Soil Mechanics; A Soft Material Reinforced by Numerous Strong Horizontal Sheets in Mechanics of Solids," S. Timoshenko Sixtieth Anniversary Volume, MacMillan, New York, 1938.

71. Potyondy, J. G. "Skin Friction Between Various Soils and Construction Materials," *Geotechnique,* Vol. 11, p. 339.

72. Bishop, A. W., Henkel, D. J. *The Measurement of Soil Properties in the Triaxial Test,* 2nd Edition, Arnold, London, 1962.

73. Kerisel, J. L., "Vertical and Horizontal Bearing Capacity of Deep Foundations in Clay," *Symposium on Bearing Capacity and Settlement of Foundations,* Duke University, Durham, North Carolina, 1967, pp. 45-51.

74. Poulos, H. G., Davis, E. H., "The Settlement Behavior of Single Axially-Loaded Incompressible Piles and Piers, *Geotechnique,* Vol. XVIII, No. 3, September 1968, p. 351.

75. Barksdale, R. C., *Nonlinear Viscoelastic Analysis of Layered Systems,* Soil Mechanics Laboratory, Georgia Institute of Technology, June, 1969.

76. Vesic, A. S., "Tests on Instrumented Piles, Ogeechee River Site," *Journal of the Soil Mechanics and Foundations Division,* ASCE, Vol. 96, SM 2, March, 1970, p. 561.

VITA

Francis Xavier Watson was born in Flushing, New York, on November 18, 1943. Until graduation from Syosset High School in Syosset, Long Island, Francis Watson lived in New York. After high school he attended Worcester Polytechnic Institute in Worcester, Massachusetts, where he received his Bachelor of Science Degree in Civil Engineering in June, 1965. Upon completion of U. S. Navy Officer Candidate School in Newport, Rhode Island, he began his studies at Georgia Institute of Technology in Atlanta, Georgia. It is from this school that he received his MSCE in 1966 and Ph.D. in 1970.

From June, 1966, through November, 1968, Mr. Watson was employed by Law Engineering Testing Company in Atlanta, Georgia. Since November, 1968, he has been on active duty with the U. S. Navy as a Lieutenant in the CEC. Upon completion of a one-year tour of duty in Vietnam, he reported to the Public Works Center in San Diego, California, where he is presently assigned.